

ISSN 1854-6250

APEM
journal

Advances in Production Engineering & Management

Volume 17 | Number 3 | September 2022



University of Maribor

Published by CPE
apem-journal.org

Advances in Production Engineering & Management

Identification Statement

	ISSN 1854-6250 Abbreviated key title: Adv produc engineer manag Start year: 2006 ISSN 1855-6531 (on-line)
	Published quarterly by Chair of Production Engineering (CPE), University of Maribor Smetanova ulica 17, SI – 2000 Maribor, Slovenia, European Union (EU) Phone: 00386 2 2207522, Fax: 00386 2 2207990 Language of text: English APEM homepage: apem-journal.org University homepage: www.um.si

APEM Editorial

Editor-in-Chief

Miran Brezocnik

editor@apem-journal.org, info@apem-journal.org
University of Maribor, Faculty of Mechanical Engineering Smetanova ulica 17, SI – 2000 Maribor, Slovenia, EU

Desk Editor

Martina Meh

desk1@apem-journal.org

Janez Gotlih

desk2@apem-journal.org

Website Technical Editor

Lucija Brezocnik

desk3@apem-journal.org

Editorial Board Members

Eberhard Abele, Technical University of Darmstadt, Germany
Bojan Acko, University of Maribor, Slovenia
Joze Balic, University of Maribor, Slovenia
Agostino Bruzzone, University of Genoa, Italy
Borut Buchmeister, University of Maribor, Slovenia
Ludwig Cardon, Ghent University, Belgium
Nirupam Chakraborti, Indian Institute of Technology, Kharagpur, India
Edward Chlebus, Wroclaw University of Technology, Poland
Igor Drstvensek, University of Maribor, Slovenia
Illes Dudas, University of Miskolc, Hungary
Mirko Ficko, University of Maribor, Slovenia
Vlatka Hlupic, University of Westminster, UK
David Hui, University of New Orleans, USA
Pramod K. Jain, Indian Institute of Technology Roorkee, India
Isak Karabegović, University of Bihać, Bosnia and Herzegovina

Janez Kopac, University of Ljubljana, Slovenia
Qingliang Meng, Jiangsu University of Science and Technology, China
Lanndon A. Ocampo, Cebu Technological University, Philippines
Iztok Palcic, University of Maribor, Slovenia
Krsto Pandza, University of Leeds, UK
Andrej Polajnar, University of Maribor, Slovenia
Antonio Pouzada, University of Minho, Portugal
R. Venkata Rao, Sardar Vallabhbhai National Inst. of Technology, India
Rajiv Kumar Sharma, National Institute of Technology, India
Katica Simunovic, J. J. Strossmayer University of Osijek, Croatia
Daizhong Su, Nottingham Trent University, UK
Soemon Takakuwa, Nagoya University, Japan
Nikos Tsourveloudis, Technical University of Crete, Greece
Tomo Udiljak, University of Zagreb, Croatia
Ivica Veza, University of Split, Croatia



Subsidizer: The journal is subsidized by Slovenian Research Agency



Creative Commons Licence (CC): Content from published paper in the APEM journal may be used under the terms of the Creative Commons Attribution 4.0 International Licence (CC BY 4.0). Any further distribution of this work must maintain attribution to the author(s) and the title of the work, journal citation and DOI.

Statements and opinions expressed in the articles and communications are those of the individual contributors and not necessarily those of the editors or the publisher. No responsibility is accepted for the accuracy of information contained in the text, illustrations or advertisements. Chair of Production Engineering assumes no responsibility or liability for any damage or injury to persons or property arising from the use of any materials, instructions, methods or ideas contained herein.

Published by CPE, University of Maribor.

Advances in Production Engineering & Management is indexed and abstracted in the **WEB OF SCIENCE** (maintained by **Clarivate Analytics**): **Science Citation Index Expanded**, **Journal Citation Reports** – Science Edition, **Current Contents** – Engineering, Computing and Technology • **Scopus** (maintained by **Elsevier**) • **Inspec** • **EBSCO**: Academic Search Alumni Edition, Academic Search Complete, Academic Search Elite, Academic Search Premier, Engineering Source, Sales & Marketing Source, TOC Premier • **ProQuest**: CSA Engineering Research Database – Cambridge Scientific Abstracts, Materials Business File, Materials Research Database, Mechanical & Transportation Engineering Abstracts, ProQuest SciTech Collection • **TEMA (DOMA)** • The journal is listed in **Ulrich's** Periodicals Directory and **Cabell's** Directory



University of Maribor
Chair of Production Engineering (CPE)

Advances in Production Engineering & Management

Volume 17 | Number 3 | September 2022 | pp 259–396

Contents

Scope and topics	262
Financing and information sharing in capital-constrained supply chain Duan, H.W.; Wang, M.T.; Ye, Y.S.	263
Effect of printing parameters on the mechanical behaviour of the thermoplastic polymer processed by FDM technique: A research review Tripathy, C.R.; Sharma, R.K.; Rattan, V.K.	279
Evolutionary game analysis of company collaborative strategy in cloud manufacturing platform environment Xiao, M.; Tian, Z.Y.	295
Development of a flexible tooling system for sheet metal bending Stefanovska, E.; Pepelnjak, T.	311
A new approach for quality prediction and control of multistage production and manufacturing process based on Big Data analysis and Neural Networks Tian, S.; Zhang, Z.; Xie, X.; Yu, C.	326
Experimental determination of influences on a gauge block's stack length Lipus, L.C.; Acko, B.; Tompa, J.	339
Last-mile delivery optimization considering the demand of market distribution methods: A case studies using Adaptive Large Neighborhood Search algorithm Huang, Q.L.; Wang, W.J.; Liang, X.J.; Xu, L.; Niu, X.Y.; Yang, X.Y.	350
Modelling surface roughness in finish turning as a function of cutting tool geometry using the response surface method, Gaussian process regression and decision tree regression Vukelic, D.; Simunovic, K.; Kanovic, Z.; Saric, T.; Doroslovacki, K.; Prica, M.; Simunovic, G.	367
Multi-objective Intuitionistic Fuzzy Linear Programming model for optimization of industrial closed-loop supply chain network Kousar, S.; Batool, M.; Kousar, N.; Pamucar, D.; Ozbilge, E.; Tantay, B.	381
Calendar of events	394
Notes for contributors	395

Journal homepage: apem-journal.org

ISSN 1854-6250 (print)

ISSN 1855-6531 (on-line)

Published by CPE, University of Maribor.

Scope and topics

Advances in Production Engineering & Management (APEM journal) is an interdisciplinary refereed international academic journal published quarterly by the *Chair of Production Engineering* at the *University of Maribor*. The main goal of the *APEM journal* is to present original, high quality, theoretical and application-oriented research developments in all areas of production engineering and production management to a broad audience of academics and practitioners. In order to bridge the gap between theory and practice, applications based on advanced theory and case studies are particularly welcome. For theoretical papers, their originality and research contributions are the main factors in the evaluation process. General approaches, formalisms, algorithms or techniques should be illustrated with significant applications that demonstrate their applicability to real-world problems. Although the *APEM journal* main goal is to publish original research papers, review articles and professional papers are occasionally published.

Fields of interest include, but are not limited to:

Additive Manufacturing Processes	Machine Learning in Production
Advanced Production Technologies	Machine-to-Machine Economy
Artificial Intelligence in Production	Machine Tools
Assembly Systems	Machining Systems
Automation	Manufacturing Systems
Big Data in Production	Materials Science, Multidisciplinary
Block Chain in Manufacturing	Mechanical Engineering
Computer-Integrated Manufacturing	Mechatronics
Cutting and Forming Processes	Metrology in Production
Decision Support Systems	Modelling and Simulation
Deep Learning in Manufacturing	Numerical Techniques
Discrete Systems and Methodology	Operations Research
e-Manufacturing	Operations Planning, Scheduling and Control
Evolutionary Computation in Production	Optimisation Techniques
Fuzzy Systems	Project Management
Human Factor Engineering, Ergonomics	Quality Management
Industrial Engineering	Risk and Uncertainty
Industrial Processes	Self-Organizing Systems
Industrial Robotics	Smart Manufacturing
Intelligent Manufacturing Systems	Statistical Methods
Joining Processes	Supply Chain Management
Knowledge Management	Virtual Reality in Production
Logistics in Production	

Financing and information sharing in capital-constrained supply chain

Duan, H.W.^a, Wang, M.T.^a, Ye, Y.S.^{b,*}

^aXihua University, School of Management, Chengdu, Sichuan, P.R. China

^bSichuan University, Institute for Disaster Management and Reconstruction, Chengdu, Sichuan, P.R. China

ABSTRACT

This paper focuses on financing choices and information-sharing strategies in the capital-constrained supply chain. We model four scenarios with the capital constraints of the respective manufacturer and retailer using bank credit financing (BCF) and trade credit financing (TCF) approaches to address financing problems, and investigate the retailer's willingness to share demand forecasting information. We find that TCF is an equilibrium financing choice for a capital-constrained supply chain. However, when a capital-constrained member chooses TCF, sharing demand information over the supply chain becomes more difficult. The interactions between the choices of financing approach and information sharing based on the game equilibriums, as well as the conditions that encourage the well-funded member to offer TCF in the capital-constrained supply chains, have also been analytically explored and numerically verified. Additional managerial insights are provided for discussions.

ARTICLE INFO

Keywords:

Supply chain;
Capital constraint;
Information sharing;
Financing choice;
Game equilibrium

*Corresponding author:

moriye@scu.edu.cn
(Ye, Y.S.)

Article history:

Received 2 May 2022
Revised 27 July 2022
Accepted 10 Aug 2022



Content from this work may be used under the terms of the Creative Commons Attribution 4.0 International Licence (CC BY 4.0). Any further distribution of this work must maintain attribution to the author(s) and the title of the work, journal citation and DOI.

1. Introduction

Capital is the basic guarantee for smooth operations and management of supply chains, nevertheless, many enterprises are capital-constrained during startup phases [1]. According to Enterprise Surveys (World Bank Group, 2018), which encompass more than 135,000 enterprises in 139 countries, 53.6 % of the enterprises require a loan, and 26.5 % cited access to finance as a major restriction. Both the manufacturer and the retailer may face capital constraints. In March 2018, Peugeot Citroen immediately issued a supply disruption warning when noticed that up to 85 % of the major suppliers were facing financing difficulties. A total of 19 % of U.S. retailers closed their stores due to capital-constrained reasons in the first half of 2019, and more than 7,000 retail stores were finally closed. In 2020, the outbreak of the COVID-19 pandemic posed great challenges to the stability of the supply chain system and undermined the shortage of funds in the supply chain [2]. Many companies suffer from budget pressure had to close down a mass of their factories and stores. On March 23, 2020, Tesla temporarily suspended production at its two plants in New York and California. In May, the first major fashion retailer, J. Crew Group Inc. filed for bankruptcy, followed by Neiman Marcus, a luxury department store, and in

December, Debenhams, a British retail giant with more than 230 years of history, declared bankruptcy.

To ease the capital constraints, a firm may have access to more than one financing sources. Bank credit financing (BCF) is a common financing approaches provided by banks for firms to meet the financing requirements. In 2016, 20 % of China's small and medium-sized firms (SMEs) borrowed from banks [3], To increase the overall efficiency of the entire supply chain, large well-funded firms often provide trade credit financing (TCF) to the participants within the supply chain in practice. Ford Motor Credit Company LLC, a wholly-owned subsidiary of Ford Motor Company, offers wholesale loans to dealers to finance the purchase of vehicle inventory, as well as loans to dealers to finance working capital and enhancements to dealership facilities [4]. And Haier provides trade credit to its small partners to alleviate their financial strain [5]. However, the related research seem to have opposing opinions on whether capital-constrained buyers/retailers should adopt BCF or TCF. Through numerical research, Zhou and Groenevelt [6] contend that bank credit is better than trade credit. Whereas Kouvelis and Zhao [7] pointed out that if the retailer is provided an effectively constructed scheme, they would always choose supplier financing over bank financing. Jing *et al.* [8] demonstrate that TCF (BCF) is the unique financing equilibrium when production costs are below (above) a certain threshold, when both bank credit and trade credit are available.

Specifically, for the capital-constrained supply chain with the coexistence of bank and trade credits, demand uncertainty and information asymmetry should also be emphasized. Demand uncertainty would not only aggravate the internal difficulties of enterprises' operations but also exert external financing pressure on capital-constrained enterprises [9]. Internally, it necessitates greater financial investment in inventory management to prevent stock-outs, while externally, the uncertain sales revenue makes it harder for firms to maintain robust cash flow and may raise the risk of default, a critical factor for their lending agents or institutions in determining the interest rate. Wang *et al.* [1] have shown that increased demand uncertainty may prompt lenders to charge a higher interest rate, which would further impact the decisions and performance of supply chain participants in the lending market. Therefore, demand forecasting is important for capital-constrained enterprises because it is an effective way to reduce demand uncertainty [10]. If the retailer shares demand information with the upstream manufacturer, it would help the manufacturer improve the accuracy of demand forecasting. Thus, the problem would be whether the retailer decides to share private demand information with the upstream manufacturer in a capital-constrained supply chain. Given that both manufacturers and retailers may face increasing capital constraints, wherein the uncertain demand and asymmetric information further complicate the financing for the capital-constrained member, this paper addresses the following issues: How does a capital-constrained member make financing choices in the face of asymmetric demand information? Will the retailer share demand information when the capital-constrained member addresses the financing problem through BCF and TCF respectively? How will the information be shared with different financing choices? All the above-mentioned problems are key to capital-constrained supply chain management under information asymmetry.

However, while the theoretical studies on respective financing and information sharing are abundant, there is limited research focusing on supply chain management that considers both demand information asymmetry and capital constraints at an operational level. This paper shows the equilibrium choices of financing and information-sharing strategies for an information-asymmetric supply chain with either capital-constrained manufacturers or retailers. Based on the game equilibriums, the interactions between the above two strategies (i.e., financing vs. information sharing) are analysed, and the conditions that the well-funded member is willing to provide TCF are further discussed.

This paper contributes to the state-of-the-art research in three ways: First, we identify the financing choices, i.e., BCF or TCF, that the capital-constrained manufacturer/retailer prefers to take in the face of asymmetric demand information. We find that TCF is an equilibrium financing choice in both scenarios with capital constraints of manufacturer and retailer. Second, we further analyse the correlation between the choice of financing approach and information sharing.

Although the capital-constrained member's financing choice does not directly affect the retailer's information-sharing strategy, the value of information sharing has changed: when the capital-constrained member opts for TCF, the retailer is less willing to share demand information in case of losing profits. Third, we consider the bank deposit and loan rates for the choice of BCF in the construction of the game model and numerically analyse the ranges of deposit and loan rates that urge the well-funded member become willing to provide TCF.

The rest of the paper is organized as follows. Section 2 reviews the relevant literature and Section 3 introduces the model framework. In Section 4, the game model when capital-constrained manufacturer adopts BCF and TCF are built respectively, and the equilibrium solutions are discussed. And the game equilibriums of the model when capital-constrained retailer adopts BCF and TCF are analysed in Section 5. Based on the equilibrium results, the impact of the financing approach on the value of information sharing is explored in Section 6, and the willingness of the well-funded member to provide TCF in Section 7. Section 8 is the numerical study. The last section summarizes the conclusions and provides additional managerial insights for discussions.

2. Literature review

This is an interface study of operations management and finance in which the financing options in a capital-constrained supply chain are investigated. It is a typical practice for enterprises suffering capital constraint to establish alternate financing approaches with distinct decisional dynamics amongst supply chain participants. Numerous studies have investigated the selection of financing approaches in a capital-constrained supply chain when alternative capital sources are available [11-16], wherein a significant amount of research has shown the effect of demand uncertainty on the efficiency of BCF and TCF. Jing *et al.* [8] conclude that BCF should be used under high demand uncertainty to increase channel efficiency. Overall, TCF is more lucrative than BCF for the manufacturer provided manufacturing costs and demand fluctuation are modest but is less profitable otherwise. Based on this study, Chen *et al.* [17] further verify that TCF improves the efficiency of the channel compared with bank credit. The retailer shares the demand risk with the manufacturer under TCF, and the manufacturer's risk sharing effectively reduces the retailer's marginal cost, which causes the retailer to increase the order quantity. Increased inventory at the store improves anticipated product sales, hence increasing the manufacturer's earnings. They conclude that trade credit is the only financing equilibrium in wholesale price contracts. According to Zhao and Arnd [18], the retailer may select between two pre-shipment finance mechanisms (APD, advance payment discount; BPOF, buyer-backed purchase order financing) to alleviate the supplier's financial difficulties. They discover that the retailer chooses APD over BPOF until the marginal cost of financial hardship outweighs the value of the unit discount. They demonstrate that the financing equilibrium zone of APD grows with both the retailer's internal capital level and demand fluctuation. The decisional dynamics of a supply chain that includes a supplier and a capital-constrained retailer that selects between BCF and TCF are examined by Shi *et al.* [9] in relation to demand uncertainty reduction (DUR). They recommend that when DUR is high and wholesale price is exogenous and cheap, the retailers should take TCF. And retailers should only take TCF, when the wholesale price is determined endogenously, and both DUR and manufacturing costs are low.

Notably, the research described above has mostly focused on choosing a financing approach, and some of them have shown that reducing demand uncertainty would impact the efficacy of BCF and TCF. But all the above literature is conducted under information symmetry. None of them has examined the information-sharing decision of retailers in a capital-constrained supply chain. Information sharing decision, that is, whether to share information based on the self-interest of the information holder, is the core issue in the field of information sharing. In recent years, much study has been undertaken on the relationship between information sharing and supply chain operation decisions. Mishra *et al.* [19] demonstrate that in both make-to-order and make-to-stock situations, sharing the forecast unconditionally by the retailer is advantageous for the manufacturer but detrimental for the retailer. However, Li and Zhang [20] conclude that if

the level of demand uncertainty is moderate, the retailer has an incentive to voluntarily share the information manufacturer in the make-to-stock situations. Lai *et al.* [21] demonstrate that forecast sharing from the port can not only increase profitability for both partners, but also encourage investments in sustainability, even when the carrier is risk-averse in the marine supply chain. Liu *et al.* [22] investigate information sharing in a fresh-produce e-commerce supply chain in which the supplier provides freshness-keeping effort, and the e-tailer offers value-added services. They discover that information sharing is more likely to happen when the supplier is more cost-effective in investment in freshness-keeping or when the e-tailer is more effective in service investment. Li *et al.* [23] focus on a supply chain in which the manufacturer buys a component from the supplier who has private information on supply disruption risk. They discover that when the supplier's initial reliability is low in the pull regime, greater information transparency may be damaging to the manufacturer, but the high-type supplier might surprise provide a significant return under information asymmetry. Wang *et al.* [24] investigate information sharing in secondary supply chains in the presence of potential supplier intrusion and find that the degree of information sharing by retailers was not related to supplier intrusion. Liu *et al.* [25] study the information-sharing problem in a secondary supply chain consisting of two homogeneous manufacturers and a value-added retailer and find that when value-added services are cost-inefficient, the manufacturer's receipt of information shared by the retailer hurts its profit instead. Guan *et al.* [26] develop the information-sharing strategies for two competing supply chains and conclude that when one supply chain chooses an information-sharing strategy will affect the strategy choice of the other supply chain. Yan *et al.* [27] analyse the impact of blockchain technology on supply chain information coordination and conclude that blockchain technology can effectively reduce supply chain operating costs.

However, very few studies consider the effect of information sharing on the financing options of a capital-constrained supply chain, as far as we are aware. To take advantage of this research opportunity, this research seeks to analyse the equilibrium choices of financing approach and information-sharing strategy in a capital-constrained supply chain with the analysis of the interactions between financing channel choice and information-sharing decisions.

3. Model framework

Consider a capital-constrained supply chain consisting of a manufacturer (he) and a retailer(she) with asymmetric demand information. The manufacturer or the retailer facing capital constraints chooses between BCF and TCF when challenged with financing problems. BCF is a common financing approach whereby capital constraints are eased by bank loans, whereas TCF with capital-constrained manufacturer/retailer differs. When the manufacturer faces capital constraints, the retailer can offer TCF through advance payment. On the other hand, if the retailer is capital-constrained, TCF is provided via deferred payment from the manufacturer. Thus, it is important for the capital-constrained member to determine which financing approach should be adopted. The proximity to the customers facilitates the retailer to receive more accurate information about the market demand than the manufacturer does. It enables the retailer to determine whether to share the demand information with the manufacturer. This paper explores the equilibrium financing decision of the capital-constrained member and the equilibrium information-sharing decision of the retailer, as well as the interplay of the above two decisions.

The sequence of the game when manufacturer faces capital constraints is as follows. Before the selling season, the retailer decides whether to share the information, and the manufacturer decides whether to accept the information if retailer is willing to share. Then the manufacturer determines wholesale price w ($w > c$), and the retailer determines retail price p ($p > w$) and places the order. After receiving the order, the manufacturer begins production with per-unit production cost c if he has sufficient funds, otherwise, he resorts to TCF or BCF for financing. When production is completed, the manufacturer sells the products to the retailer at w and deposits profits into bank. During the selling season, the retailer sells products in the market at p , and also deposits the sales proceeds on zero deposit and withdrawal. At the end of the sales season, the manufacturer and retailer take back the principal and interest on the deposit, and

the manufacturer pays off the debt. If the retailer is capital-constrained, she pays for the product upon receipt by taking out a loan from the bank or at the end of the sale season through a deferred payment option offered by the manufacturer.

3.1 Demand function

The demand function is written as $D = a - bp + \varepsilon$, where a refers to the market size and b the demand elasticity of retail price. ε is the randomness of market demand, which is assumed to be normally distributed with a mean of 0 and a variance of σ^2 . We assume that the retailer has private demand forecasting information γ , i.e., $\gamma = \varepsilon + \delta$, where δ captures the noise in the forecast error, which is also normally distributed with a mean of 0 and a variance of σ_0^2 . According to the existing literature [19, 21], we denote $H = E[\varepsilon|\gamma] = \frac{\sigma^2\gamma}{\sigma_0^2 + \sigma^2}$ and $Var[\varepsilon|\gamma] = \frac{\sigma^2\sigma_0^2}{\sigma_0^2 + \sigma^2}$, where H refers to the market demand fluctuation.

3.2 Model assumptions

To facilitate the construction of the models, we have the following assumptions:

- (1) The capital-constrained member's initial capital is assumed to be zero.
- (2) No moral hazard exists. Both the manufacturer and retailer are creditworthy and the loan will be repaid at the conclusion of the sales period;
- (3) No bankruptcy risk happens. The supply chain system and the bank operate in good conditions in the game and there are no extreme changes in the market environment.
- (4) During the s season, the retailer deposits the sales revenue in the bank on a zero-deposit basis, disregarding the self-retaining non-deposit.

4. Manufacturer's choice with capital constraints

4.1 Analysis of trade credit financing

The retailer can ease the manufacturer's capital constraints by paying in advance, which is a typical type of TCF. The sequence of the game when a capital-constrained manufacturer adopts TCF is shown in Fig. 1.

When the retailer is not willing to share demand information, the manufacturer has to determine the wholesale price according to his private information. The expected profit functions of the manufacturer and the retailer can be described as follows:

$$E[\pi_{M1}^{MN}] = (1 + I_M)(w_1^{MN} - c)(a - bp_1^{MN} + E[\varepsilon]) \tag{1}$$

$$E[\pi_{R1}^{MN}] = [(1 + I_R)p_1^{MN} - w_1^{MN}](a - bp_1^{MN} + E[\varepsilon|\gamma]) \tag{2}$$

where I_M and I_R refer to the deposit rate of the manufacturer and the retailer. We express $I_M = (t_{pre} + t_{se})i_M$ and $I_R = t_{se}i_R$, wherein t_{pre} denotes the length of lead time, t_{se} the length of sales period, i_M the bank deposit rate and i_R the deposit rate for zero deposit and withdrawal.

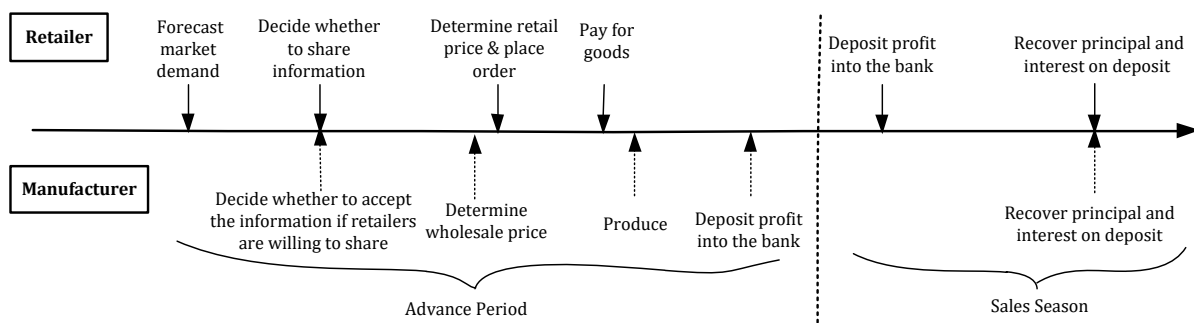


Fig. 1 The sequence of events with manufacturer's choice of TCF

When the retailer decides to share her private demand forecasting information, the manufacturer determines the wholesale price depending on the information shared by the retailer. The expected profit functions of the manufacturer and the retailer are written as:

$$E[\pi_{M1}^{MI}] = (1 + I_M)(w_1^{MI} - c)(a - bp_1^{MI} + E[\varepsilon|\gamma]) \tag{3}$$

$$E[\pi_{R1}^{MI}] = [(1 + I_R)p_1^{MI} - w_1^{MI}](a - bp_1^{MI} + E[\varepsilon|\gamma]). \tag{4}$$

By solving with back induction, we can get the equilibriums of the game with retailer's sharing or not sharing demand information as shown in Table 1.

Table 1 The game equilibriums with manufacturer's choice of TCF

	No information sharing	Information sharing
p_1^*	$p_1^{MN*} = \frac{(3a + 2H)(1 + I_R) + bc}{4b(1 + I_R)}$	$p_1^{MI*} = \frac{3(a + H)(1 + I_R) + bc}{4b(1 + I_R)}$
w_1^*	$w_1^{MN*} = \frac{a(1 + I_R) + bc}{2b}$	$w_1^{MI*} = \frac{(a + H)(1 + I_R) + bc}{2b}$
π_{R1}^*	$\pi_{R1}^{MN*} = A_1$	$\pi_{R1}^{MI*} = B_1$
π_{M1}^*	$\pi_{M1}^{MN*} = (1 + I_M)C_1 - \frac{H^2(1 + I_R)(1 + I_M)}{8b}$	$\pi_{M1}^{MI*} = 2(1 + I_M)B_1$
π_{SC1}^*	$\pi_{SC1}^{MN*} = A_1 + (1 + I_M)C_1 - \frac{H^2(1 + I_R)(1 + I_M)}{8b}$	$\pi_{SC1}^{MI*} = (3 + 2I_M)B_1$

Note: $A_1 = \frac{[(a+2H)(1+I_R)-bc]^2}{16b(1+I_R)}$, $B_1 = \frac{[(a+H)(1+I_R)-bc]^2}{16b(1+I_R)}$, $C_1 = \frac{[(a-H)(1+I_R)-bc]^2}{16b(1+I_R)}$. The deposit rate of the respective manufacturer and retailer and the bank loan rate is denoted as $I_M = (t_{pre} + t_{se})i_M$, $I_R = t_{se}i_R$ where t_{pre} , t_{se} , i_M , and i_R represent the length of lead time, the length of sales period, the bank deposit rate and the deposit rate for zero deposit and withdrawal respectively.

According to the game equilibriums, when the manufacturer faces capital constraints and adopts TCF, the optimal wholesale price is positively related to the retailer's deposit rate and deposit time regardless of whether she shares demand information. Inversely, the optimal retail price is negatively related to the retailer's deposit rate and deposit time. Both the optimal wholesale price and retail price are independent of the manufacturer's deposit rate and deposit time.

The retailers' profits are only positively related to the retailer's time deposit rate of small savings for lump-sum withdrawal over time, which is independent of the manufacturers' deposit rate and time. In contrast, the manufacturers' profits are positively correlated not only with both members' deposit rates and time but also with the retailer's time deposit rate of small savings for lump-sum withdrawal over time.

4.2 Analysis of bank credit financing

BCF refers to the financing channel where the manufacturer raises seed money from bank loans. The sequence of events when a capital-constrained manufacturer adopts BCF is shown in Fig. 2.

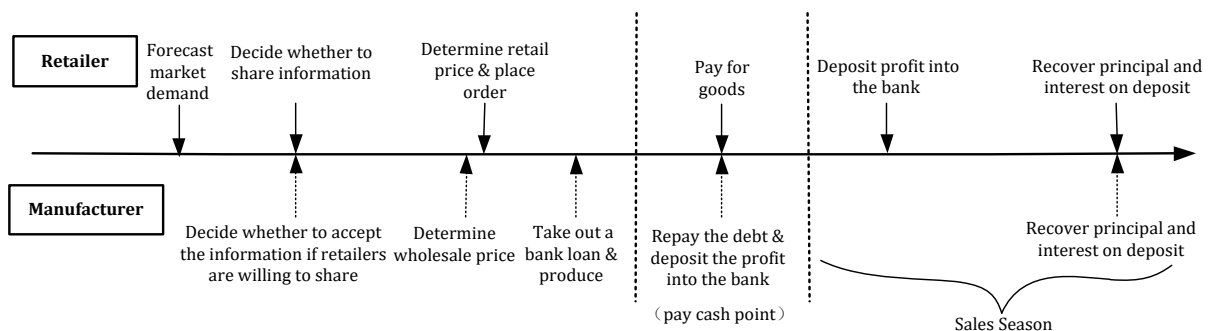


Fig. 2 The sequence of events with manufacturer's choice of BCF

When the retailer does not share demand information, the manufacturer can only determine the wholesale price based on his private information. The expected profit functions of the manufacturer and the retailer are as follows:

$$E[\pi_{M2}^{MN}] = [(1 + I_M)w_2^{MN} - (1 + I_M + J_M)c](a - bp_2^{MN} + E[\varepsilon]) \tag{5}$$

$$E[\pi_{R2}^{MN}] = [(1 + I_R)p_2^{MN} - w_2^{MN}](a - bp_2^{MN} + E[\varepsilon|\gamma]) \tag{6}$$

On the other hand, if the retailer shares her private demand forecasting information with the manufacturer, the wholesale price is chosen according to the information that is shared by retailer. The expected profit functions of the manufacturer and the retailer can be described as follows:

$$E[\pi_{M2}^{MI}] = [(1 + I_M)w_2^{MI} - (1 + I_M + J_M)c](a - bp_2^{MI} + E[\varepsilon|\gamma]) \tag{7}$$

$$E[\pi_{R2}^{MI}] = [(1 + I_R)p_2^{MI} - w_2^{MI}](a - bp_2^{MI} + E[\varepsilon|\gamma]) \tag{8}$$

By solving the above formulas, we derive the game equilibriums with alternative information-sharing decisions of the retailer, which is shown in Table 2.

Table 2 The game equilibriums with manufacturer’s choice of BCF

No information sharing		Information sharing
p_2^*	$p_2^{MN*} = \frac{(3a + 2H)(1 + I_M)(1 + I_R) + bc(1 + I_M + J_M)}{4b(1 + I_M)(1 + I_R)}$	$p_2^{MI*} = \frac{3(a + H)(1 + I_M)(1 + I_R) + bc(1 + I_M + J_M)}{4b(1 + I_M)(1 + I_R)}$
w_2^*	$w_2^{MN*} = \frac{a(1 + I_M)(1 + I_R) + bc(1 + I_M + J_M)}{2b(1 + I_M)}$	$w_2^{MI*} = \frac{(a + H)(1 + I_M)(1 + I_R) + bc(1 + I_M + J_M)}{2b(1 + I_M)}$
π_{R2}^*	$\pi_{R2}^{MN*} = A_2$	$\pi_{R2}^{MI*} = B_2$
π_{M2}^*	$\pi_{M2}^{MN*} = C_2 - \frac{H^2(1 + I_M)(1 + I_R)}{8b}$	$\pi_{M2}^{MI*} = 2(1 + I_M)B_2$
π_{SC2}^*	$\pi_{SC2}^{MN*} = A_2 + C_2 - \frac{H^2(1 + I_M)(1 + I_R)}{8b}$	$\pi_{SC2}^{MI*} = (3 + 2I_M)B_2$

Note: $A_2 = \frac{[(a+2H)(1+I_R)(1+I_M)-bc(1+I_M+J_M)]^2}{16b(1+I_R)(1+I_M)^2}$, $B_2 = \frac{[(a+H)(1+I_R)(1+I_M)-bc(1+I_M+J_M)]^2}{16b(1+I_R)(1+I_M)^2}$, $C_2 = \frac{[(a-H)(1+I_R)(1+I_M)-bc(1+I_M+J_M)]^2}{16b(1+I_R)(1+I_M)^2}$.

The deposit rate of the respective manufacturer and retailer and the bank loan rate is denoted as $I_M = t_{se}i_M$, $I_R = t_{se}i_R$ and $J_M = t_{pre}j_M$, where t_{pre} , t_{se} , i_M , i_R and j_M represent the length of lead time, the length of sales period, the bank deposit rate, the deposit rate for zero deposit and withdrawal and the bank loan rate respectively.

A comparison with the previous conclusions in Section 4.1 shows that when the manufacturer faces capital constraints and adopts BCF, both the optimal wholesale price and the optimal retail price are related to the manufacturer's bank deposit and loan interest rate, as well as the length of lead time and sales period. Meanwhile, the profits of both the retailer and manufacturer depend on the manufacturer's loan rate and the length of lead time. The rest of the conclusions are similar to those in the previous section.

4.3 Information sharing strategy with manufacturer's capital constraints

By comparing the game equilibriums in the scenarios with retailer’s sharing or not sharing demand information, we have the following analytical results for the information-sharing strategy when the manufacturer is capital-constrained.

Proposition 1: The retailer’s equilibrium information sharing strategy with the manufacturer’s capital constraints is given as:

(1) When the actual market demand fluctuates positively (i.e., $H > 0$), regardless of the capital-constrained manufacturer’s choice of TCF or BCF, the wholesale price and the retail price will both increase if the retailer shares demand information, i.e., $w_1^{MI*} > w_1^{MN*}$, $w_2^{MI*} > w_2^{MN*}$, $p_1^{MI*} > p_1^{MN*}$ and $p_2^{MI*} > p_2^{MN*}$. Meanwhile, the retailer's profit will decrease while the manufacturer’s profit grows, i.e., $\pi_{R1}^{MN*} > \pi_{R1}^{MI*}$, $\pi_{R2}^{MN*} > \pi_{R2}^{MI*}$, $\pi_{M1}^{MN*} < \pi_{M1}^{MI*}$ and $\pi_{M2}^{MN*} < \pi_{M2}^{MI*}$. Thus, it is not wise for the retailer to share demand information.

(2) When the actual market demand fluctuates negatively (i.e., $H < 0$), regardless of the capital-constrained manufacturer's choice of TCF or BCF, the wholesale price and the retail price will go down with the retailer's information sharing decision, i.e., $w_1^{MI*} < w_1^{MN*}$, $w_2^{MI*} < w_2^{MN*}$, $p_1^{MI*} < p_1^{MN*}$ and $p_2^{MI*} < p_2^{MN*}$. Meanwhile, the retailer's profit will be improved and the manufacturer's profit will decrease, i.e., $\pi_{R1}^{MN*} < \pi_{R1}^{MI*}$, $\pi_{R2}^{MN*} < \pi_{R2}^{MI*}$, $\pi_{M1}^{MN*} > \pi_{M1}^{MI*}$ and $\pi_{M2}^{MN*} > \pi_{M2}^{MI*}$. As a result, the manufacturer will not accept the offer of information sharing even if the retailer is willing to.

In conclusion, with positively fluctuating demand, the manufacturer may raise the wholesale price given the demand information shared by the retailer, which will exacerbate the double marginalization effect. It results in the retailer's no willingness of sharing demand information. In contrast, with negatively fluctuating demand, the demand information shared by the retailer may force the manufacturer to reduce the wholesale price. Even if it encourages the retailer to share demand information, the manufacturer will not accept it because his profit will be reduced. In summary, information sharing can't be realized in a supply chain with a capital-constrained manufacturer.

4.4 Manufacturer's financing choice with capital constraints

Given the game equilibriums of the capital-constrained manufacturer adopting TCF and BCF, we have the following analytical results for the equilibrium financing approach for the manufacturer.

Proposition 2: The profits of both the retailer and the manufacturer will be improved if the capital-constrained manufacturer chooses TCF, regardless of whether the retailer shares demand information or not, i.e., $\pi_{M1}^{MI*} > \pi_{M2}^{MI*}$, $\pi_{R1}^{MI*} > \pi_{R2}^{MI*}$, $\pi_{M1}^{MN*} > \pi_{M2}^{MN*}$ and $\pi_{R1}^{MN*} > \pi_{R2}^{MN*}$. Therefore, TCF is the equilibrium financing choice for the capital-constrained manufacturer.

5. Retailer's choice with capital constraints

5.1 Analysis of trade credit financing

The retailer's financing problem is possibly solved by deferred payment, which is a typical type of TCF provided by the manufacturer. The sequence of decisions when the capital-constrained retailer adopts TCF is shown in Fig. 3.

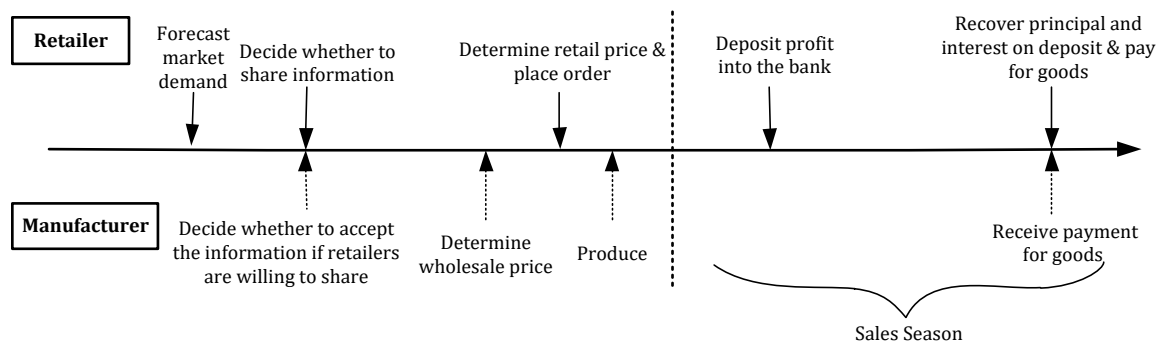


Fig. 3 The sequence of events with capital-constrained retailer's choice of TCF

For the retailer's decision not to share demand information, the manufacturer can only determine the wholesale price based on private information. The expected profit functions of the manufacturer and the retailer can be described as follows:

$$E[\pi_{M3}^{RN}] = (w_3^{RN} - c)(a - bp_3^{RN} + E[\varepsilon]) \tag{9}$$

$$E[\pi_{R3}^{RN}] = [(1 + I_R)p_3^{RN} - w_3^{RN}](a - bp_3^{RN} + E[\varepsilon|\gamma]) \tag{10}$$

When the retailer shares her private demand forecasting information, the manufacturer determines the wholesale price depending on the information shared by the retailer. The expected profit function of the manufacturer and the retailer are given as:

$$E[\pi_{M3}^{RI}] = (w_3^{RI} - c)(a - bp_3^{RI} + E[\varepsilon|\gamma]) \tag{11}$$

$$E[\pi_{R3}^{RI}] = [(1 + I_R)p_3^{RI} - w_3^{RI}](a - bp_3^{RI} + E[\varepsilon|\gamma]) \tag{12}$$

Solving with the back induction method, we show the game equilibriums when the retailer shares demand information or not in Table 3.

Table 3 The game equilibriums with capital-constrained retailer’s choice of TCF

	No information sharing	Information sharing
p_3^*	$p_3^{RN*} = \frac{(3a + 2H)(1 + I_R) + bc}{4b(1 + I_R)}$	$p_3^{RI*} = \frac{3(a + H)(1 + I_R) + bc}{4b(1 + I_R)}$
w_3^*	$w_3^{RN*} = \frac{a(1 + I_R) + bc}{2b}$	$w_3^{RI*} = \frac{(a + H)(1 + I_R) + bc}{2b}$
π_{R3}^*	$\pi_{R3}^{RN*} = A_3$	$\pi_{R3}^{RI*} = B_3$
π_{M3}^*	$\pi_{M3}^{RN*} = C_3 - \frac{H^2(1 + I_R)}{8b}$	$\pi_{M3}^{RI*} = 2B_3$
π_{SC3}^*	$\pi_{SC3}^{RN*} = A_3 + C_3 - \frac{H^2(1 + I_R)}{8b}$	$\pi_{SC3}^{RI*} = 3B_3$

Note: $A_3 = \frac{[(a+2H)(1+I_R)-bc]^2}{16b(1+I_R)}$, $B_3 = \frac{[(a+H)(1+I_R)-bc]^2}{16b(1+I_R)}$, $C_3 = \frac{[(a-H)(1+I_R)-bc]^2}{8b(1+I_R)}$. Denote $I_R = t_{se}i_R$ as the retailer’s deposits, where t_{se} refers to the length of sales period, i_R the deposit rate for zero deposit and withdrawal.

5.2 Analysis of bank credit financing

The retailer may also go for bank loans to deal with the financing problem. The sequence of decisions when the capital-constrained retailer adopts BCF is shown in Fig. 4.

Without information sharing from the retailer, the manufacturer chooses the wholesale price solely dependent on his private information. The expected profit functions of the manufacturer and the retailer are as follows:

$$E[\pi_{M4}^{RN}] = (1 + I_M)(w_4^{RN} - c)(a - bp_4^{RN} + E[\varepsilon]) \tag{13}$$

$$E[\pi_{R4}^{RN}] = [(1 + I_R)p_4^{RN} - (1 + J_R)w_4^{RN}](a - bp_4^{RN} + E[\varepsilon|\gamma]) \tag{14}$$

While the retailer decides to share, the manufacturer determines the wholesale price according to the information shared by the retailer. The expected profit functions of the manufacturer and the retailer are described as:

$$E[\pi_{M4}^{RI}] = (1 + I_M)(w_4^{RI} - c)(a - bp_4^{RI} + E[\varepsilon|\gamma]) \tag{15}$$

$$E[\pi_{R4}^{RI}] = [(1 + I_R)p_4^{RI} - (1 + J_R)w_4^{RI}](a - bp_4^{RI} + E[\varepsilon|\gamma]) \tag{16}$$

Thus, we have the game equilibriums when the retailer shares or does not share demand information, as summarized in Table 4.

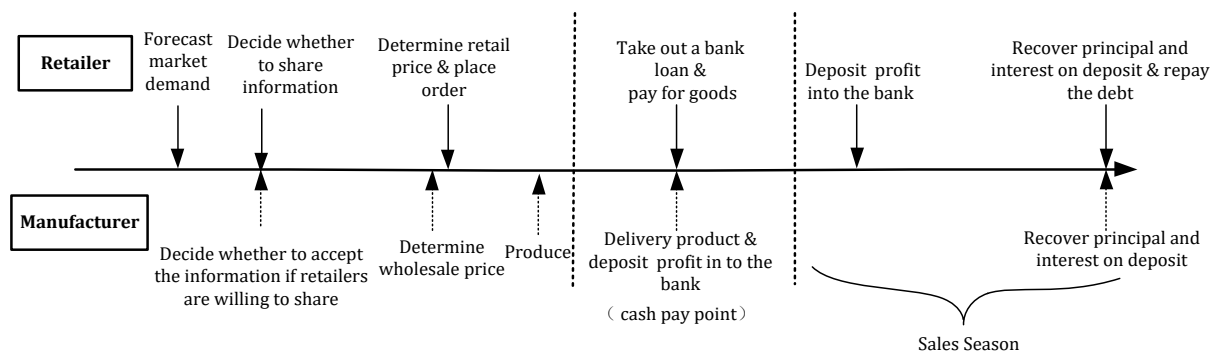


Fig. 4 The sequence of events with capital-constrained retailer’s choice of BCF

Table 4 The game equilibriums with capital-constrained retailer's choice of BCF

	No information sharing	Information sharing
p_4^*	$p_4^{RN*} = \frac{(3a + 2H)(1 + I_R) + bc(1 + J_R)}{4b(1 + I_R)}$	$p_4^{RI*} = \frac{3(a + H)(1 + I_R) + bc(1 + J_R)}{4b(1 + I_R)}$
w_4^*	$w_4^{RN*} = \frac{a(1 + I_R) + bc(1 + J_R)}{2b(1 + J_R)}$	$w_4^{RI*} = \frac{(a + H)(1 + I_R) + bc(1 + J_R)}{2b(1 + J_R)}$
π_{R4}^*	$\pi_{R4}^{RN*} = A_4$	$\pi_{R4}^{RI*} = B_4$
π_{M4}^*	$\pi_{M4}^{RN*} = (1 + I_M)C_4$	$\pi_{M4}^{RI*} = \frac{2(1 + I_M)}{(1 + J_R)} B_4$
π_{SC4}^*	$\pi_{SC4}^{RN*} = A_4 + (1 + I_M)C_4$	$\pi_{SC4}^{RI*} = \frac{(3 + 2I_M + J_R)}{(1 + J_R)} B_4$

Note: $A_4 = \frac{[(a+2H)(1+I_R)-bc(1+J_R)]^2}{16b(1+I_R)}$, $B_4 = \frac{[(a+H)(1+I_R)-bc(1+J_R)]^2}{16b(1+I_R)}$, $C_4 = \frac{[(a-H)(1+I_R)-bc(1+J_R)]^2-H^2(1+I_R)^2}{8b(1+I_R)(1+J_R)}$. The deposit rate of the respective manufacturer and retailer and the bank loan rate is denoted as $I_M = t_{se}i_M$, $I_R = t_{se}i_R$ and $J_M = t_{pre}j_M$, where t_{pre} , t_{se} , i_M , i_R and j_M represent the length of lead time, the length of sales period, the bank deposit rate, the deposit rate for zero deposit and withdrawal and the bank loan rate respectively.

5.3 Information sharing strategy with retailer's capital constraints

Comparing the game equilibriums obtained from Table 5 (i.e., information sharing vs. no information sharing), we have the following propositions with regard to the information-sharing strategy when the retailer faces capital constraints.

Proposition 3: The equilibrium information-sharing strategy in a supply chain with retailer's capital constraints is provided as follows:

(1) When the actual market demand fluctuates positively (i.e., $H > 0$), regardless of whether the financially constrained retailer takes TCF or BCF, the wholesale price and the retail price will be improved if the retailer shares demand information, i.e., $w_3^{RI*} > w_3^{RN*}$, $w_4^{RI*} > w_4^{RN*}$, $p_3^{RI*} > p_3^{RN*}$ and $p_4^{RI*} > p_4^{RN*}$. Meanwhile, the retailer's profit will decrease while the manufacturer's profit grows, i.e., $\pi_{R3}^{RN*} > \pi_{R3}^{RI*}$, $\pi_{R4}^{RN*} > \pi_{R4}^{RI*}$, $\pi_{M3}^{RN*} < \pi_{M3}^{RI*}$ and $\pi_{M4}^{RN*} < \pi_{M4}^{RI*}$. As a consequence, the retailer has no motives to share demand information.

(2) When the actual market demand fluctuates negatively (i.e., $H < 0$), regardless of whether the financially constrained retailer takes TCF or BCF, the wholesale price and the retail price will be reduced if the retailer shares demand information, i.e., $w_3^{RI*} < w_3^{RN*}$, $w_4^{RI*} < w_4^{RN*}$, $p_3^{RI*} < p_3^{RN*}$ and $p_4^{RI*} < p_4^{RN*}$. Meanwhile, the retailer's profit will increase while that of the manufacturer decreases, i.e., $\pi_{R3}^{RN*} < \pi_{R3}^{RI*}$, $\pi_{R4}^{RN*} < \pi_{R4}^{RI*}$, $\pi_{M3}^{RN*} > \pi_{M3}^{RI*}$ and $\pi_{M4}^{RN*} > \pi_{M4}^{RI*}$. Therefore, the manufacturer will choose not to accept the information-sharing offer even if the retailer has a willingness to share.

In conclusion, with positively fluctuating demand, the manufacturer may raise the wholesale price given the demand information shared by the retailer, which will exacerbate the double marginalization effect. It results in the retailer's no willingness of sharing demand information. In contrast, with negatively fluctuating demand, the demand information shared by the retailer may force the manufacturer to reduce the wholesale price. Even if it encourages the retailer to share demand information, the manufacturer will not accept it because his profit will be reduced.

In summary, information sharing can't be realized in a supply chain with a capital-constrained retailer.

5.4 Retailer's financing choice with capital constraints

Given the game equilibriums of the capital-constrained manufacturer's choice between TCF and BCF, we have the following analytical results for the equilibrium financing strategy when the retailer is capital-constrained.

Proposition 4: The profits of both the retailer and the manufacturer will be improved if the capital-constrained retailer chooses TCF, regardless of whether the retailer shares demand information or not, i.e., $\pi_{M3}^{RI*} > \pi_{M4}^{RI*}$, $\pi_{R3}^{RI*} > \pi_{R4}^{RI*}$, $\pi_{M3}^{RN*} > \pi_{M4}^{RN*}$ and $\pi_{R3}^{RN*} > \pi_{R4}^{RN*}$. Therefore, TCF is the equilibrium financing choice for the capital-constrained retailer. Because BCT increases the cost of retailer.

6. Impact of financing choice on the value of information sharing

According to Proposition 1 and Proposition 3, we conclude that it is not wise for the retailer to share demand forecasting information regardless of the capital-constrained member's financing choice (i.e., TCF vs. BCF). However, will the financing choice have an impact on the value of information sharing? Is information sharing beneficial to the whole supply chain? Can manufacturer incentivize the retailer to share demand forecasting information through unilateral payment? To answer the above questions, we conduct the value analysis of information sharing based on the game equilibriums for the capital-constrained member adopting TCF and BCF respectively to look at the impact of capital constraints and financing choices on the value of information sharing.

The value of information sharing to the manufacturer and retailer is denoted as v_{Mj}^i , v_{Rj}^i , and the value of information sharing to the supply chain as v_j . Then we have:

$$v_{Mj}^i = \pi_{Mj}^{iI*} - \pi_{Mj}^{iN*} \quad (17)$$

$$v_{Rj}^i = \pi_{Rj}^{iI*} - \pi_{Rj}^{iN*} \quad (18)$$

$$v_j = v_{Mj}^i + v_{Rj}^i \quad (19)$$

where $i = M, R$, $j = 1, 2, 3, 4$, M means the manufacturer faces capital constraints, R means the retailer faces capital constraints, 1 means the capital-constrained manufacturer adopts TCF, 2 means the capital-constrained manufacturer adopts BCF, 3 means the capital-constrained retailer adopts TCF, 4 means the capital-constrained retailer adopts BCF.

The value of information sharing calculated based on Eqs. 17 to 19, and the following results can be derived.

Result 1: When $H > 0$, the value of information sharing to the retailer is negative with $|v_{R1}^M| > |v_{R2}^M|$ and $|v_{R3}^R| > |v_{R4}^R|$, which suggests that the retailer loses more profit from sharing demand information so that she is less willing to share while TCF is used. When $H < 0$, the value of information sharing to the manufacturer is negative with $|v_{M1}^M| > |v_{M2}^M|$ and $|v_{M3}^R| > |v_{M4}^R|$, whereby the manufacturer suffers greater profit loss if he accepts the demand information shared by the retailer. Thus, the manufacturer becomes passive toward retailer's information sharing under TCF.

From Result 1, it is clear that information sharing is more difficult to achieve when the capital-constrained member adopts TCF, notwithstanding cost savings and efficiency improvements in financing.

Result 2: When TCF is adopted, the retailer's profit loss from sharing information is equal under capital constraints of alternative supply chain members, i.e., $v_{R1}^M = v_{R3}^R$. On the other hand, with BCF on condition that $1 + t_{se}i_M - \frac{t_{pre}j_R}{t_{se}j_R} > 0$, the retailer's profit loss from sharing information is higher under the manufacturer's capital constraints, whereas it would remain higher under the retailer's capital constraints if $1 + t_{se}i_M - \frac{t_{pre}j_R}{t_{se}j_R} < 0$.

From Result 2, what is interesting is that the capital constraint concern has zero effect on the value of information sharing to the retailer once TCF is used. However, this conclusion does not hold when the capital-constrained member prefers BCF.

Result 3: In a capital-constrained supply chain with either TCF or BCF being chosen, when the actual market demand fluctuates positively (i.e., $H > 0$), the value of information sharing to the supply chain remains positive, i.e., $v_1 > 0$, $v_2 > 0$, $v_3 > 0$, and $v_4 > 0$. At this point, information sharing can increase the overall profits of the supply chain. When the actual market demand fluctuates negatively (i.e., $H < 0$), the value of information sharing to the supply chain remains negative, i.e., $v_1 < 0$, $v_2 < 0$, $v_3 < 0$, and $v_4 < 0$. At this point, information sharing can't increase the overall profits of the supply chain.

When the actual market demand fluctuates positively, result 3 further verifies that information sharing brings benefits to the whole supply chain, which is expected to achieve through contract design such as a single-sided payment contract.

7. Well-funded member's willingness to offer trade credit financing

The above analysis concludes that TCF is an equilibrium financing choice for capital-constrained supply chains. However, the well-funded member's offering of TCF leads to his/her loss of the interest earned from depositing the fund in the bank. Thus, the well-funded member needs to trade off the gains and losses of providing TCF. In the following, we derive the conditions on which the well-funded member is willing to offer TCF with the respective capital-constrained manufacturer and retailer.

Result 4: Given the capital constraints for the manufacturer, if the retailer shares demand information, the condition that the retailer is willing to provide TCF is

$$\frac{bcj_M[2(a+H)W - bc(2 + 2t_{se}i_M + t_{pre}j_M)]}{2i_R[(a+H)^2W^2 - b^2c^2(1 + t_{se}i_M)^2]} > 1, \quad (20)$$

whereas if the retailer does not share demand information, the condition that the retailer is willing to provide TCF is

$$\frac{bcj_M[2(a+2H)W - bc(2 + 2t_{se}i_M + t_{pre}j_M)]}{2i_R[a(a+2H)W^2 - b^2c^2(1 + t_{se}i_M)^2 + 2HWbc(1 + t_{se}i_M)]} > 1, \quad (21)$$

where $W = (1 + t_{se}i_R)(1 + t_{se}i_M)$.

Result 5: Given the capital constraints for the retailer, if the retailer shares information, the conditions that the manufacturer is willing to provide TCF is

$$\frac{(1 + t_{se}j_R)(1 - t_{se}i_M)[N + Ht_{se}i_R]^2}{(1 + t_{se}i_M)[N + Ht_{se}i_R - bct_{se}j_R]^2} > 1, \quad (22)$$

whereas if the retailer does not share information, the conditions that the manufacturer is willing to provide TCF is,

$$\frac{(1 + t_{se}j_R)(1 - t_{se}i_M)\{N^2 - 2HN\}}{(1 + t_{se}i_M)\{[N - bct_{se}j_R]^2 - 2H(1 + t_{se}i_R)[N - bct_{se}j_R]\}} > 1, \quad (23)$$

where $N = a(1 + t_{se}i_R) - bc$.

We observe that the willingness of the well-funded member to provide internal financing to the capital-constrained member is related to the demand fluctuation type and the deposit and loan rates for the respective manufacturer and retailer. In the following section, we will derive the varying ranges of j_M , i_R , and H for retailer's willingness to offer TCF, and the ranges of j_R , i_M and H for manufacturer's willingness to offer TCF using numerical analysis.

8. Numerical analysis

In this section, we first numerically verify the relevant conclusions, and then we analyse the willingness of the well-funded member to provide TCF. Parameters are set as follows: $a = 130, b = 1, c = 10, H \in (-40, 40), i_R = 0.1, i_M = 0.1, j_M = 0.15, j_R = 0.15,$ and $t_{se} = t_{pre} = 1.$

8.1 Impact of financing choices on the value of information sharing

The impacts of the financing choices on the value of information to the manufacturer and the retailer are depicted in Fig. 5 and Fig. 6. The x-axis represents market demand fluctuation in Fig. 5 and Fig. 6. The y-axis represents the profit of retailer in Fig. 5, and y-axis represents the profit of manufacturer in Fig. 6. From Fig. 5, the absolute value of information sharing to the retailer adopting TCF is greater than that adopting BCF. When $H > 0,$ the value of information sharing to the retailer is negative, where the retailer suffers greater profit loss adopting TCF and becomes more reluctant to share demand information. When $H < 0,$ the value of information sharing to the retailer is positive, which suggests that the retailer enjoys improved profits adopting TCF and is more willing to share demand information. The conclusions are independent of the takers of capital constraints in the supply chain. As shown in Fig. 6, the value of information sharing to the manufacturer is positive when $H > 0,$ which indicates that the manufacturer gains more from information sharing while adopting TCF. When $H < 0,$ the conclusion is the opposite. The arithmetic analysis is consistent with the conclusions from Result 1.

In summary, we numerically verify that sharing information benefits the manufacturer rather than the retailer when the actual market demand fluctuates positively, and vice versa if the actual market demand fluctuates negatively, which is irrelevant with the takers of capital constraints in the supply chain. In particular, when TCF is adopted, it should be also noted that the capital-constrained member's financing choice may exert a more numerically significant effect on the value of information.

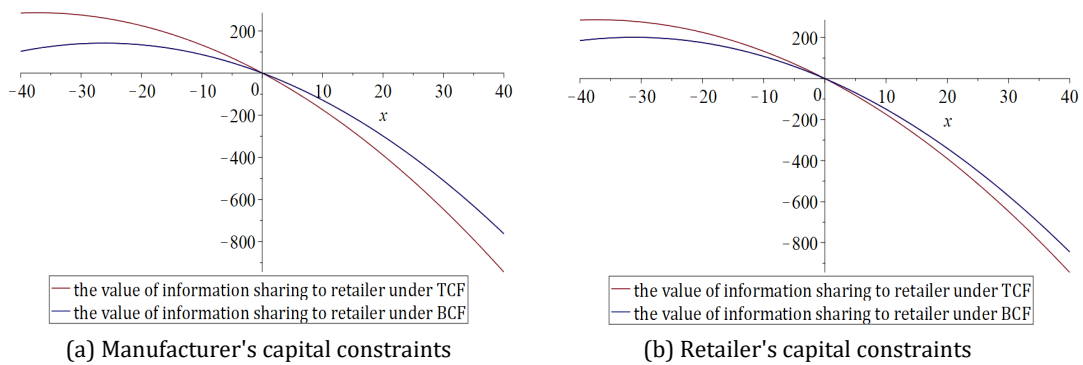


Fig. 5 Impact of financing choices on the value of information sharing to retailer

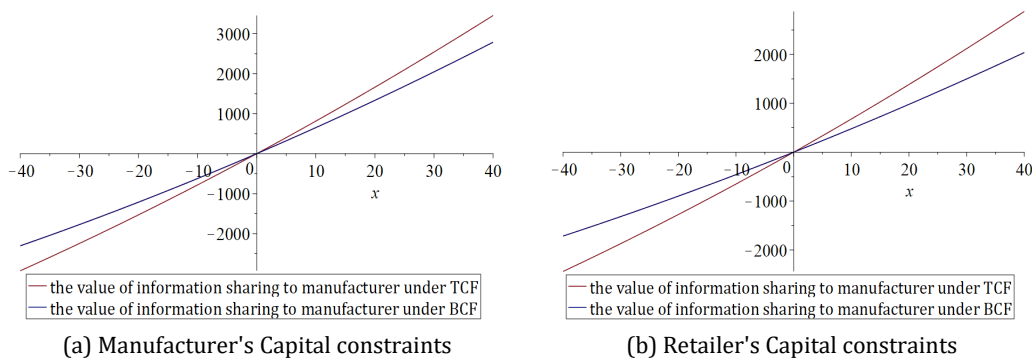


Fig. 6 Impact of financing choices on the value of information sharing to manufacturer

8.2 Willingness analysis of well-funded member to provide trade credit financing

Firstly, we capture the conditions for the retailer's willingness to offer TCF to the capital-constrained manufacturer, as shown in Fig. 7. Assume that $H = 10$, the x-axis represents the retailer's deposit rate and the y-axis is the manufacturer's loan rate. The vertical axis gives M (i.e., $M = \pi_{R1}^{MI*} - \pi_{R2}^{MI*} - w_1^{MI*}(a - bp_1^{MI*} + H)t_{pre}i_R$), which indicates the difference between the incremental revenue and reduced interest income when the retailer provides TCF. Specifically, $M > 0$ means that the retailer is willing to offer TCF, while $M < 0$ indicates that the retailer is reluctant to offer TCF.

With information sharing from the retailer, the impact of the loan rate and deposit rate on the retailer's willingness to provide TCF is shown in Fig. 7(a). We observe that the varying range of the rates that encourage the retailer to offer TCF satisfies $x \in [0.16, 1], y \in [0.01, 0.06]$. When the retailer chooses not to share demand information, the impact of the loan rate and the deposit rate on the retailer's willingness to provide TCF is depicted in Fig. 7(b), wherein the varying range of the rates that encourages the retailer to offer TCF locate within $x \in [0.15, 1]$ and $y \in [0.01, 0.06]$.

Then, we capture the conditions for the manufacturer's willingness to offer TCF to the capital-constrained retailer in Fig. 8. Likewise, the x-axis denotes the manufacturer's deposit rate and the y-axis the retailer's loan rate. With the retailer's information sharing, the condition that allows the manufacturer to accept delayed payment (i.e., offer TCP) is given as $x \in [0, 0.4], y \in [0.01, 1]$, whereas the counterpart condition without the retailer's information sharing satisfies $x \in [0, 0.41], y \in [0, 1]$.

According to our numerical analysis, we show that the deposit rate of the well-funded member that allows for offering TCF varies much lower for the manufacturer than for the retailer, while the varying condition of the bank loan rate that encourages the capital-constrained member to choose TCF is much laxer for the manufacturer than for the retailer. It may suggest that TCF is possible to be a popular financing approach if the manufacturer is capital-constrained. Moreover, the impacts of the retailer's information sharing decisions on the varying ranges of the rates are very slight, regardless of the capital constraint of either the manufacturer or the retailer.

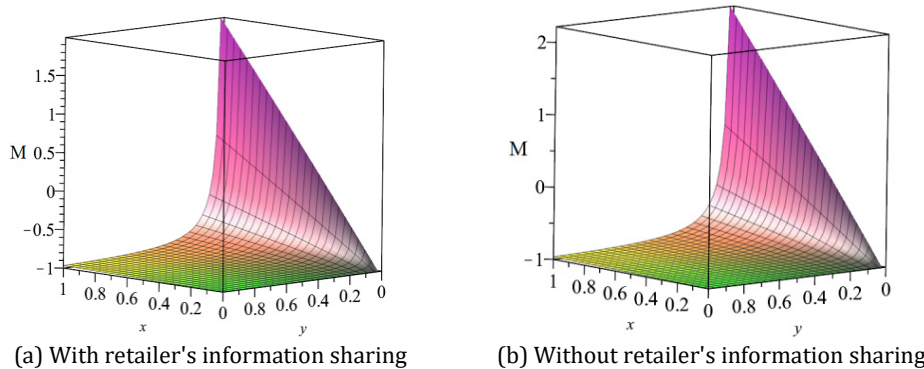


Fig. 7 The conditions for the retailer's willingness to offer TCF to the capital-constrained manufacturer

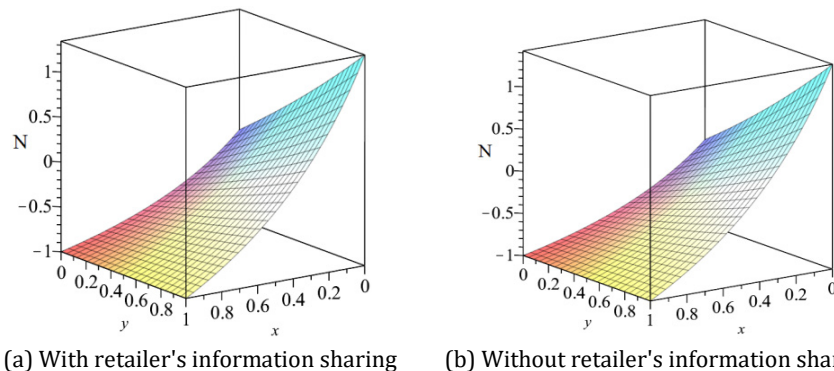


Fig. 8 The conditions for the manufacturer's willingness to offer TCF to the capital-constrained retailer

9. Conclusion

We model four scenarios of the capital-constrained supply chain using BCF and TCF to address financing problems, with the consideration of the retailer's decisions on sharing demand information or not. We derive the equilibrium financing and information-sharing strategies with the capital constraints of the manufacturer and the retailer respectively and find that TCF is an equilibrium financing choice for a capital-constrained supply chain. The retailer has no willingness to share demand forecasting information if the actual demand fluctuates positively, whereas she prefers to share when the actual demand fluctuates negatively but the manufacturer is reluctant to accept in case of profit loss.

By comparing the equilibriums of the game, we further analyse the interactions between the financing and information-sharing strategies and provide useful managerial insights. First, when a capital-constrained member chooses TCF, it becomes more difficult to share demand information over the supply chain. Second, when the capital-constrained member, either manufacturer or retailer, adopts TCF, the value of information sharing to the retailer would not change; however, this conclusion does not hold if BCF is used in the capital-constrained supply chain. Third, sharing demand information over the supply chain is always beneficial to the system, whereby the contract design, such as a single-sided payment contract, should be emphasized to facilitate information sharing. Finally, we provide the conditions that encourage the well-funded member to offer TCF in the capital-constrained supply chain. Given the benefits that TCF brings to the reduction of financing costs and the improvement of financing efficiency, we suggest that capital-constrained companies should respond to financial crises through TCF. To improve demand forecasting information sharing over the supply chain, the design of incentive mechanisms in capital-constrained supply chains is necessary and imperative. This will be one of the future directions of our research. In addition, this paper assumes that there is no insolvency risk for capital-constrained firms, which deserves a further understanding in the future research of capital-constrained supply chains. Also, it should be emphasized that the concerns of international crises, such as wars, pandemics and lack of raw materials, become an urgent and imperative topic in today's capital-constrained supply chains, which needs more targeted modelling and discussion in our extension studies.

References

- [1] Wang, F., Yang, X., Zhuo, X., Xiong, M. (2019). Joint logistics and financial services by a 3PL firm: Effects of risk preference and demand volatility, *Transportation Research Part E: Logistics and Transportation Review*, Vol. 130, 312-328, doi: [10.1016/j.tre.2019.09.006](https://doi.org/10.1016/j.tre.2019.09.006).
- [2] Duan, W., Ma, H., Xu, D.S. (2021). Analysis of the impact of COVID-19 on the coupling of the material flow and capital flow in a closed-loop supply chain, *Advances in Production Engineering & Management*, Vol. 16, No. 1, 5-22, doi: [10.14743/apem2021.1.381](https://doi.org/10.14743/apem2021.1.381).
- [3] SME Finance Forum. China MSME finance report 2016, from <https://www.smefinanceforum.org/post/china-msme-finance-report-2016>, accessed March 25, 2022.
- [4] Hua, S., Liu, J., Cheng, T.C.E., Zhai, X. (2019). Financing and ordering strategies for a supply chain under the option contract, *International Journal of Production Economics*, Vol. 208, 100-121, doi: [10.1016/j.ijpe.2018.10.008](https://doi.org/10.1016/j.ijpe.2018.10.008).
- [5] Jin, W., Zhang, Q., Luo, J. (2019). Non-collaborative and collaborative financing in a bilateral supply chain with capital constraints, *Omega*, Vol. 88, 210-222, doi: [10.1016/j.omega.2018.04.001](https://doi.org/10.1016/j.omega.2018.04.001).
- [6] Zhou, J., Groenevelt, H. (2007). *Impacts of financial collaboration in a three-party supply chain*, Working paper, The Simon School, University of Rochester, New York, USA.
- [7] Kouvelis, P., Zhao, W. (2012). Financing the newsvendor: Supplier vs. bank, and the structure of optimal trade credit contracts, *Operations Research*, Vol. 60, No. 3, 566-580, doi: [10.1287/opre.1120.1040](https://doi.org/10.1287/opre.1120.1040).
- [8] Jing, B., Chen, X., Cai, G. (2012). Equilibrium financing in a distribution channel with capital constraint, *Production and Operations Management*, Vol. 21, No. 6, 1090-1101, doi: [10.1111/j.1937-5956.2012.01328.x](https://doi.org/10.1111/j.1937-5956.2012.01328.x).
- [9] Shi, J., Li, Q., Chu, L.K., Shi, Y. (2021). Effects of demand uncertainty reduction on the selection of financing approach in a capital-constrained supply chain, *Transportation Research Part E: Logistics and Transportation Review*, Vol. 148, Article No. 102266, doi: [10.1016/j.tre.2021.102266](https://doi.org/10.1016/j.tre.2021.102266).
- [10] Li, L., Zhang, H. (2008). Confidentiality and information sharing in supply chain coordination, *Management Science*, Vol. 54, No. 8, 1467-1481, doi: [10.1287/mnsc.1070.0851](https://doi.org/10.1287/mnsc.1070.0851).
- [11] Yan, X., Wang, Y. (2014). A newsvendor model with capital constraint and demand forecast update, *International Journal of Production Research*, Vol. 52, No. 17, 5021-5040, doi: [10.1080/00207543.2014.894261](https://doi.org/10.1080/00207543.2014.894261).

- [12] Cao, E., Du, L., Ruan, J. (2019). Financing preferences and performance for an emission-dependent supply chain: Supplier vs. bank, *International Journal of Production Economics*, Vol. 208, 383-399, doi: [10.1016/j.ijpe.2018.08.001](https://doi.org/10.1016/j.ijpe.2018.08.001).
- [13] Zhen, X., Shi, D., Li, Y., Zhang, C. (2020). Manufacturer's financing strategy in a dual-channel supply chain: Third-party platform, bank, and retailer credit financing, *Transportation Research Part E: Logistics and Transportation Review*, Vol. 133, Article No. 101820, doi: [10.1016/j.tre.2019.101820](https://doi.org/10.1016/j.tre.2019.101820).
- [14] Shen, B., Wang, X., Cao, Y., Li, Q. (2020). Financing decisions in supply chains with a capital-constrained manufacturer: Competition and risk, *International Transactions in Operational Research*, Vol. 27, No. 5, 2422-2448, doi: [10.1111/itor.12670](https://doi.org/10.1111/itor.12670).
- [15] Shi, J., Guo, J., Du, Q., Lin, F., Lai, K.K., Cheng, T.C.E. (2020). Optimal financing mode selection for a capital-constrained retailer under an implicit bankruptcy cost, *International Journal of Production Economics*, Vol. 228, Article No. 107657, doi: [10.1016/j.ijpe.2020.107657](https://doi.org/10.1016/j.ijpe.2020.107657).
- [16] Yang, H., Zhuo, W., Shao, L., Talluri, S. (2021). Mean-variance analysis of wholesale price contracts with a capital-constrained retailer: Trade credit financing vs. bank credit financing, *European Journal of Operational Research*, Vol. 294, No. 2, 525-542, doi: [10.1016/j.ejor.2021.01.042](https://doi.org/10.1016/j.ejor.2021.01.042).
- [17] Chen, X. (2015). A model of trade credit in a capital-constrained distribution channel, *International Journal of Production Economics*, Vol. 159, 347-357, doi: [10.1016/j.ijpe.2014.05.001](https://doi.org/10.1016/j.ijpe.2014.05.001).
- [18] Zhao, L., Huchzermeier, A. (2019). Managing supplier financial distress with advance payment discount and purchase order financing, *Omega*, Vol. 88, 77-90, doi: [10.1016/j.omega.2018.10.019](https://doi.org/10.1016/j.omega.2018.10.019).
- [19] Mishra, B.K., Raghunathan, S., Yue, X. (2009). Demand forecast sharing in supply chains, *Production and Operations Management*, Vol. 18, No. 2, 152-166, doi: [10.1111/j.1937-5956.2009.01013.x](https://doi.org/10.1111/j.1937-5956.2009.01013.x).
- [20] Li, T., Zhang, H. (2015). Information sharing in a supply chain with a make-to-stock manufacturer, *Omega*, Vol. 50, 115-125, doi: [10.1016/j.omega.2014.08.001](https://doi.org/10.1016/j.omega.2014.08.001).
- [21] Lai, X., Tao, Y., Wang, F., Zou, Z. (2019). Sustainability investment in maritime supply chain with risk behavior and information sharing, *International Journal of Production Economics*, Vol. 218, 16-29, doi: [10.1016/j.ijpe.2019.02.021](https://doi.org/10.1016/j.ijpe.2019.02.021).
- [22] Liu, M., Dan, B., Zhang, S., Ma, S. (2020). Information sharing in an E-tailing supply chain for fresh produce with freshness-keeping effort and value-added service, *European Journal of Operational Research*, Vol. 290, No. 2, 572-584, doi: [10.1016/j.ejor.2020.08.026](https://doi.org/10.1016/j.ejor.2020.08.026).
- [23] Li, G., Liu, M., Bian, Y., Sethi, S.P. (2020). Guarding against disruption risk by contracting under information asymmetry, *Decision Sciences*, Vol. 51, No. 6, 1521-1559, doi: [10.1111/decis.12437](https://doi.org/10.1111/decis.12437).
- [24] Wang, J., Zhuo, W. (2020). Strategic information sharing in a supply chain under potential supplier encroachment, *Computers & Industrial Engineering*, Vol. 150, Article No. 106880, doi: [10.1016/j.cie.2020.106880](https://doi.org/10.1016/j.cie.2020.106880).
- [25] Liu, M., Zhao, Y., Huang, R., Perera, S. (2021). Vertical value-added cost information sharing in a supply chain, *Annals of Operations Research*, Vol. 2021, 1-34, doi: [10.1007/s10479-021-04021-3](https://doi.org/10.1007/s10479-021-04021-3).
- [26] Guan, Z., Zhang, X., Zhou, M., Dan, Y. (2020). Demand information sharing in competing supply chains with manufacturer-provided service, *International Journal of Production Economics*, Vol. 220, Article No. 107450, doi: [10.1016/j.ijpe.2019.07.023](https://doi.org/10.1016/j.ijpe.2019.07.023).
- [27] Yan, K., Cui, L., Zhang, H., Liu, S., Zuo, M. (2022). Supply chain information coordination based on blockchain technology: A comparative study with the traditional approach, *Advances in Production Engineering & Management*. Vol. 17, No. 1, 5-15, doi: [10.14743/apem2022.1.417](https://doi.org/10.14743/apem2022.1.417).

Effect of printing parameters on the mechanical behaviour of the thermoplastic polymer processed by FDM technique: A research review

Tripathy, C.R.^{a,*}, Sharma, R.K.^b, Rattan, V.K.^a

^aGNA University, Phagwara, Punjab, India

^bNational Institute of Technology, Hamirpur, India

ABSTRACT

Fused deposition modelling (FDM) is an additive-based manufacturing technique used by various industries due to its effectiveness & ability to make complicated geometries possible. This technique requires sufficient knowledge about the process and its parameters including their effect on the component's mechanical characteristics. Thus, it is crucial to review the available articles on this topic not only to identify the practical and useful aspects, limitations, and process variables but also to understand how the results of the literature are relevant to be used for real applications and further studies. A systematic literature review is carried out based on the type of 3D printing materials. The printing parameters which influence the mechanical characteristics of the FDM specimens are discussed based on the results presented in the literature. From the present study, it has been found that the process variables such as orientation, raster angle, raster width, layer height, and contours directly affect the quality of the 3D-printed parts. It has also been found that the effect of these process variables also varies with the type of thermoplastic materials. The present article will help researchers to select FDM processed material and appropriate process variables for further research.

ARTICLE INFO

Keywords:

3D printing;
Additive manufacturing;
Fused deposition modeling (FDM);
Process parameters;
Mechanical properties;
Thermoplastic polymer;
Review study

**Corresponding author:*
chittatripathy@rediffmail.com
(Tripathy, C.R.)

Article history:

Received 13 May 2022
Revised 14 August 2022
Accepted 12 September 2022



Content from this work may be used under the terms of the Creative Commons Attribution 4.0 International License (CC BY 4.0). Any further distribution of this work must maintain attribution to the author(s) and the title of the work, journal citation and DOI.

1. Introduction

Plastic manufacturing is one of the cutting-edge market that produces plastic components at a low price and least time [1]. There are many processes available to manufacture plastic components like injection moulding, Blow moulding, etc. These processes are beneficial for large volume production as mould development for a specific component is quite costly. In contrast, other techniques are also available which are cheaper for low volume production, such as fused deposition modelling (FDM) or fused filament fabrication (FFF) [2]. FDM uses 3D CAD data for creating a physical model with the help of CAD softwares and 3D printing machines. This technique rapidly transfers design ideas into functional prototypes from the regular CAD model. It builds the product with complex geometry and is hard to be fabricated using conventional manufacturing techniques at low costs. It uses a 3D scanner for an existing product and CAD software for a new product to generate virtual CAD model and build physical products using different AM technologies.

These technologies are used in various manufacturing sectors like defence, aerospace, medical, art and design for customization and rapid production [3-5].

Additive manufacturing is a modern manufacturing technique to create components by depositing materials layer by layer using a virtual model developed in CAD. In this process, the CAD model is exported into stereolithographic (*.stl) format, which defines the entire model into a series of 2D cross-sections. The converted file is then transferred to any of the AM machines for creating the physical part [6, 7] with more accuracy, stability, and durability. Additive manufacturing is generally designated as (ISO/ASTM standard 52900:2021 [1]).

- Stereolithography (SLA): The final product is generated with the help of an ultraviolet laser inside a vat of resin. This method uses light-sensitive polymers, whose limited availability limits the application of this technique. Though, it provides a better surface finish and lesser raw material wastage.
- Selective laser sintering (SLS): This process uses powder as raw material which is melted and fused with the help of a laser beam. The fused powder is then stacked layer upon layer to form the part based on CAD data. The performance of the components sintered through SLS process is significantly affected by the quality of powder used.
- Polyjet 3D printing (PJP): This technology uses a variety of printing materials. In the dentistry and medical field, patient anatomy can be better understood by printing the model using this technique.
- Inkjet 3D printing (IJP): This technique uses the liquid formed of polymer solution to build parts layer by layer. It is economically good for printing the part using a variety of materials.
- Laminated object manufacturing (LOM): it uses material sheets to fabricate components layer by layer with the help of a laser, which cut the sheets as per the requirement. The layer of the sheet is combined using adhesives, and the part is fabricated by repeating the steps.
- Multi-Jet-Printing (MJP): In this technique, a thin solid layer of ceramic or metallic powder is created by spraying a liquid binder through a nozzle. In order to have higher strength the fabricated part is sintered in the furnace.
- Colour-Jet Printing (CJP): This technique is frequently used in medical applications due to its ability to print coloured products. In this technique, powder and binder are used as core material and resin respectively. The powder is spread over a platform with the help of a roller to form a layer and then the binder is sprayed through a printing head jet over each layer at a point specified by CAD software to form the final product.
- Fused Deposition Modelling (FDM): This technique is based on the extrusion method, in which, the thermoplastic material is melted through heating and deposited layer by layer over a printer bed to fabricate a model.

These techniques vary according to the building layers and based on the materials type that can be used for part fabrication. Among the available additive manufacturing technology, the FDM process is best to manufacture thermoplastic components due to its low initial investment, less material wastage, simplicity of the process, and easy availability of 3D printing software [8].

2. The FDM technique

The brief layout of FDM technique is graphically represented in Fig. 1. In this process, the part is modelled using CAD software and converted to STL format. Almost all CAD software can generate this format and sent it to RPT software to check the defects in the model [9]. In the FDM process, wire of polymer is liquified and extruded along a precise toolpath creating the shape of each layer. The system extrudes both build material and temporal support material with the help of nozzles mounted on the extruder [10]. The movement of the extruder head is controlled through the motor, and the low temperature of the printing bed allows the deposited material to solidify very fast [11]. The system repeats the step until the part is finalized. After completion of the process, parts are moved out of the machine bed and support material is removed using a different technique.

In the fused deposition modelling process, as described above, two forms of materials are used. One is to build the physical model, and another is for generating a support structure.

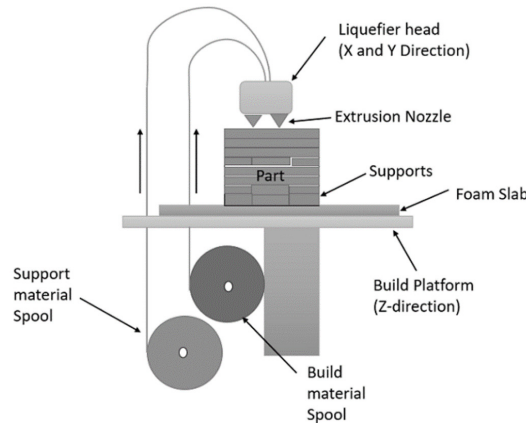


Fig. 1 Simplified layout for FDM process

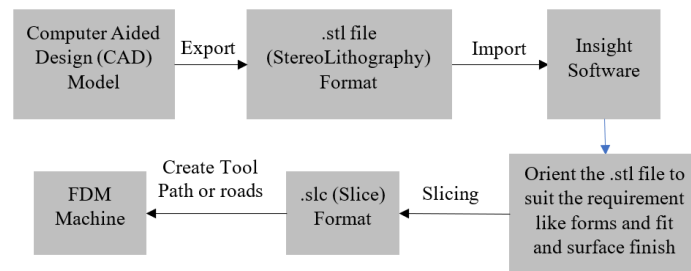


Fig. 2 Fused deposition modelling process flow diagram

This process produces low stiffness products of thermoplastic polymer material. ABS and PLA polymers are compatible and cheap; therefore, it is widely used with 3D printers. Recently, NASA designed a space exploration vehicle for transporting humans to Mars with almost 70 FDM parts onboard such as vents, ducts, etc. [15]. An ability of functional efficiency under a cryogenic environment made PLA and ABS to be used for the fabrication of the rover.

The performance of PLA is quite well under low temperatures and has also been used in the medical field [16]. However, the low toughness characteristic of PLA made it to use with the composition of ABS [17]. ABS found its wide application in automobile sectors [18]. For complete understanding of the FDM process, one has to perform many trials, although many researchers have investigated the mechanical behaviour of FDM built components and found that those are affected by various process variables/parameters.

All these parameters are represented through the fishbone diagram shown in Fig. 3. The present work is focused on identifying how these variables affect the 3D printed part quality.

The selection of appropriate process parameters has made FDM a complicated manufacturing process. Understanding the selection of these parameters is quite difficult [19, 20].

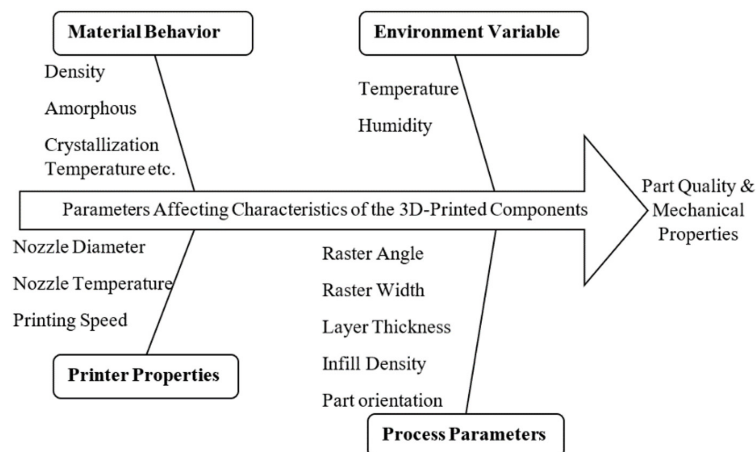


Fig. 3 Parameters/variables affecting FDM part quality

3. A research review and discussion

3.1 FDM process parameters

The mechanical behaviour of FDM based parts is affected by various process parameters like infill-density, pattern (via honeycomb, rectilinear, concentric), raster-width, layer thickness (h), temperature, extruder speed, the air-gap in the same layer or between the layers, raster-angle (via 0° , 45° and 90°), nozzle diameter, build-orientation (via on-edge, upright, and Flat), etc [21, 22]. The different process variables affecting the mechanical characteristics of the part are described as follows.

- Layer thickness: when a material is extruded from the tip of the nozzle to form a layer, the height of that layer along a vertical direction is termed layer height or thickness (Fig. 5). The layer height value is always lower than the diameter of the nozzle tip [22]. The selection of layer thickness is based on:
 - The diameter of nozzle tip [19]
 - The material [19]
- Build-orientation: It is the alignment of the built component within the printing bed along X-axis (Flat), Y-axis (Up-right), or Z-axis (On-edge) of the 3D printing machine [19, 23] Build-orientation of the part is shown in Fig. 4.

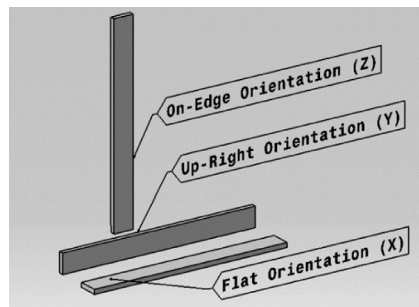


Fig. 4 Build-orientation of the Component

- Raster-angle: It is the inclination of extruded material with the X-axis of a printing bed (Fig. 5). This angle ranges from 0° to 90° [19, 23].
- Air-gap: The free space between two successive beads on the same layer of the 3D printed part is termed as air-gap [19, 23] (Fig. 5).
- Build-style: Build-style is the way rasters are filled to build the part. The build-style of any component defines its density. The parts can be fabricated with three different Build-styles [19].
 - Solid normal: This build-style completely fills the interior of the part and provides a strong interior.
 - Sparse: This Build-style leaves the gap while material deposition uses a unidirectional raster thereby minimizing the material consumption and part-build time.
 - Sparse double dense: This build-style uses a crosshatch raster pattern, which reduces material consumption and part-build time.
- Support-style: It helps to prevent the collapsing of components during fabrication by extending the surface of the model [19]. It can be provided in four different ways.
 - Basic: it is the default support-style, which provides support to all the part features using small support raster curves.
 - Sparse: Compared to basic support, it utilizes less amount of material, which reduces the support material consumption.
 - Surround: It is used for all the parts to fill the small features or small components.
 - Break-away: It's equivalent to "Sparse," except it has separate blocks that are easier to remove compared to the other three types of support styles.

- Extrusion temperature: It is the temperature with which the polymeric filaments are treated within the nozzles prior it extruded. Its value varies with the type of material and printing speed [23].
- Print Speed: It is the movement of nozzle tip along the printing bed plane for fabrication of the part [23].
- Nozzle diameter: It is defined as the diameter of the nozzle tip of the extruder [24]
- Infill pattern: It is defined as the pattern in which extrusion of material takes place to fill the internal zone of a 3D printed part. Some of the widely used infill patterns are cross, linear infill, diamond, and honeycomb [23]. Honeycomb infill pattern has the capacity to resist a higher load compared to others [24].
- Raster/bead width: It is the beads size that are extruded on the printing bed to create rasters. The raster width for depositing any material is selected based on the diameter of the nozzle tip mounted on the extruder head [23, 19] (Fig. 5).
- Infill-density: The infill-density reflects the internal structure solidity of the fabricated component. Unlike the external structure of the part, Inside, the structure isn't always solid; it can be sparse, with a variety of shapes, sizes, and infill patterns [23, 24].
- Contour Number: Number of outer solid layers surrounding internal structure of the 3D printed component [19]. This process variable can also be referred to as perimeter (Fig. 5).
- Contour width/Perimeter width: It is defined as the thickness of each contour/perimeter measured horizontally [19] as shown in Fig. 5.
- Contour to contour air-gap: The free space between two successive perimeters [19] as shown in Fig. 5.

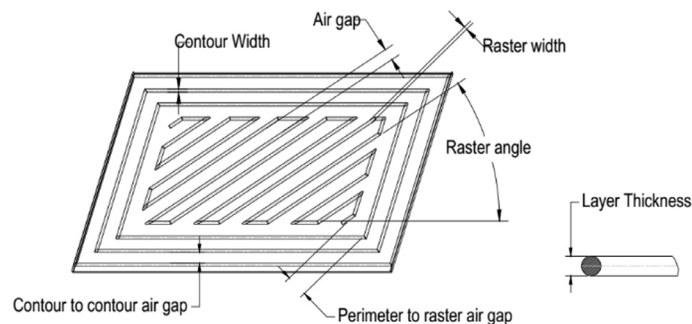


Fig. 5 FDM Tool path parameters

3.2 Influence of process parameters on mechanical behaviour of parts

It is mandatory to investigate the influence of FDM printing variables on part characteristics, since, the influence of layer height on the part characteristics with flat orientation-built components is vague [25]. Some researchers reported that an increase of layer height causes decrease in mechanical behaviour [26-28]. Whereas Abbott *et al.* [29] reported the opposite behaviour. Wu *et al.* [30] found that, for P-E-E-K, an increase of layer height from 200 μm to 300 μm increased the bending, compressive, and tensile strength but a further increase of layer thickness causes a decrease in these properties. Samples fabricated with the lower speed along with lower layer height have higher tensile strength [31].

Rouf *et al.* [32] investigated the impact of various process variables on the mechanical behaviour of the component, and it was found that along with the strength of the component the process parameter also affects tribological properties [33-35]. Bhosle *et al.* [36] analysed the Impact of layer height, Printing speed, and infill percentage on tensile strength, printing time, and surface finish. From the analysis, it was found that layer height and infill percentage are highly contributing to the surface roughness and strength [37-38] of the build parts. The author suggested keeping layer height lower to improve the performance of FDM for surface roughness and tensile strength. Kaur *et al.* [13] analysed the impact of printing variables on the tribological behaviour of ABS polymer. The authors found that FDM process parameters not only improve strength but also improve surface finish and tribological behaviour. These improvements are obtained through optimization of the process variables as well as the addition of material to the raw polymer.

Kumar and Ranjan [39] analysed the effect of bed temperature, infill percentage, and outer perimeter on the elongation behaviour of Nylon 6. The authors found that at 100 infill percentage, 60° C bed temperature, and four contour numbers provide maximum elongation in the component and thereby increase the tensile strength. They also found that infill percentage was more significant followed by bed temperature and outer perimeter.

Patil *et al.* [14] optimized some of the input variables viz. infill percentage, infill pattern, print speed, and layer thickness using multi-objective optimization for achieving better surface roughness, printing time, and filament length consumed for PLA. They reported the best response after the optimum setting of the parameters to the triangular pattern with 70 % infill, 100 mm/h printing speed, and 0.2 mm layer height.

Casavola *et al.* [20] explored the influence of raster orientation on the residual stresses that occur in FDM-fabricated ABS material parts due to the sudden change in temperature during processing. The authors concluded that components fabricated at a $\pm 30^\circ$ raster orientation is the worst configuration because the component exhibited higher residual stress, whereas the part fabricated with $\pm 45^\circ$ was the best configuration with the lowest residual stress.

Chacon *et al.* [40] analysed the impact of layer height, build direction, and feed-rate on the flexural and tensile behaviour of PLA specimens. The authors found that with an increase of layer height the mechanical properties decreased for flat oriented built specimens. However, for on-edge built orientation, the flexural strength was found lower at low layer height. On the contrary, for upright built orientation, specimens with high layer thickness possessed higher mechanical properties.

Shubham *et al.* [41] analysed the impact of layer height on impact, hardness, and tensile characteristics of ABS samples. The authors reported that Izod impact and tensile strength increased with the reduction of layer height. Whereas, the hardness value was first decreased and then increased with the increase of layer height. Later on, Shubham *et al.* [42] optimised the various printing parameters (viz. infill percentage, nozzle temperature, and layer height) by reporting the dynamic mechanical characteristics of ABS built components. The authors found the highest storage modulus at higher values of printing parameters. They also found that the impact of layer height and percentage of infill on dynamic mechanical behaviour was most significant, whereas the impact of nozzle temperature was low.

Daminabo *et al.* [43] gave an overview of AM techniques. The authors focused on FDM technique due to its cost efficiency, scalability, and ability to process a variety of materials. They suggested the use of biodegradable, bio-based, and eco-friendly materials having the capability of multi-functionality for future research and development. Ramesh and Paneerselvam [44] analysed the effect of various input variables like print speed, layer height, and infill percentage on the mechanical behaviour of fabricated nylon samples. Through the analysis, the authors found that parts printed with 100 infill percent exhibit optimum (max) flexural strength, Shore-D hardness, and UTS. This is due to the fact that 100 % infill don't have pores and therefore, the sample strength increased. The infill percent was found to have the highest impact on the mechanical behaviour of the fabricated components. Complete filling of the material eliminates the space caused for the crack growth of the sample. The layer height of 0.1 mm has affected the mechanical characteristics like impact, tensile and flexural strength. However, maximum Shore-D hardness was found at 0.3 mm layer height. The selected parameter of print speed didn't have a effective influence on the mechanical behaviour however, low speed causes heat-affected zones and higher speed causes the wrapping defect. The authors have suggested extending this work through the use of fillers in the nylon matrix and evaluating and comparing the related properties with pure material.

Pazhamannil *et al.* [45] assessed the effect of various process variables on the UTS of PLA component using the Taguchi technique. The values of UTS were predicted using an artificial neural network. The authors found that the tensile strength of the specimens increases at reduced layer height due to improved inter-layer bonding at reduced layer thickness. They also found the higher tensile strength with increased nozzle temperature due to quick growth of the neck caused by long-duration intermolecular diffusion across the interface. The authors concluded that infill speed did not influence the tensile property of the component significantly. Therefore, one can

alter the infill speed without affecting the strength of the component. In order to get better tensile properties, one should keep a high nozzle temperature with a low layer height.

Yadav *et al.* [46] analysed the impact of printing variables like material density, layer height, and extrusion temperature on the tensile behaviour of different materials like ABS, PETG, and their different compositions. The analysis showed that extrusion temperature was found more dominant factor for the tensile strength compared to other considered parameters. The maximum tensile strength for PETG material was found at an extrusion temperature of 225 °C and 0.1 mm layer height. The authors suggested analysing the influence of other printing variables using the ANFIS model, or other models can also be developed to analyse these parameters.

Gebisa and Lemu [47] carried out a study to analyse the tensile behaviour of ULTEM-9085 material using the design of an experiment by varying some of the printing variables. The authors considered five printing variables viz. raster-angle, raster-width, air-gap, contour width, and contour number and found only the raster-angle to have a substantial influence on the tensile behaviour of the material. They suggested doing the flexural and impact test to analyse the parameters. Wankhede *et al.* [48] analysed the influence of the printing variables viz. support-style, layer height, and infill percentage on the build-time and surface roughness of part made of ABS material. The authors performed the experiment using Taguchi's L8 Orthogonal Array. The significant behaviour of the parameters was presented using the Analysis of Variance (ANOVA) technique. From ANOVA results, they found that the layer height has a more dominant effect on surface roughness and build-time among all the process parameters considered.

Solomon *et al.* [49] reviewed the development of the various samples and input parameter optimisation for the FDM technique. Through this review, the authors found that layer thickness or layer height was considered to be more significant factor in evaluating the part quality. It was also observed that the raster orientation dominates in evaluating the mechanical behaviour of the fabricated component. They also found that much work has been done on the printing variables and their optimisation; still, many unknown factors affect the part quality and process efficiency that need to be explored and suggested exploring more material as filament.

Vicente *et al.* [50] analysed the influence of two input variables, i.e., density and pattern of the infill, on the mechanical characteristics of ABS components. Through the experiment, 5 % variation in maximum tensile strength was observed with variation of infill pattern. This variation was significantly improved by varying the infill-density. Maximum tensile strength was observed for the component fabricated with rectilinear pattern and 100 infill percentage. The authors have reported that if the density is kept constant, then the honeycomb pattern exhibits a better tensile strength.

Rajpurohit and Dave [51] highlighted the impact of input variables like layer thickness, raster-width, and raster-angle on the material characteristics of 3D printed PLA material. The authors chose tensile strength to analyse the mechanical behaviour of the fabricated component. They used the Taguchi method to optimise the process variables and also used the ANOVA tool to predict the significant process variables. Based on the experimental results, they observed the maximum tensile at a raster-angle of 45°, and it was also observed that tensile strength increases with increase of layer height. Among the selected parameters, raster-width was found to be the most significant process variable affecting strength.

Dawoud *et al.* [52] compared FDM and injection moulding techniques by analysing the mechanical behaviour of ABS material. The authors explored the potential of the FDM technique by varying the parameters like raster angle and gap. They varied the raster angle of odd as well as even layers. Through the investigation, they found the raster gap as a significant input for FDM, where denser components equivalent to moulded parts can be fabricated using a negative gap of -0.05 mm. It was also observed that the flexural and tensile strength of the FDM component fabricated with +45° raster-angle of even layer, -45° raster-angle of odd layer, and gap of -0.05 was able to attain 86 % and 91 % respectively of the moulded parts strength respectively. The FDM technique showed the dimensional accuracy acceptable and found within the specified range of size. Further, raster angle and gap did not find to be affecting the dimensional preciseness of the component.

Wang *et al.* [53] analysed the impact of input variables on the mechanical behaviour of 3D printed PEEK material. The authors reported the impact of process parameters like the layer height, printing speed, and printing temperature on the microstructure, mechanical characteristics, and surface quality of the fabricated component. Through the analysis, they found that components possessed maximum density, along with improved surface quality and reduced internal defects when printed with a small printing layer height of 0.1 mm, a higher printing temperature of 440 °C, and a printing speed of 20 mm/s. Though the author considered some of the input parameters, the effect of other parameters still needs to be investigated like density, pattern, line direction, overlap percentage of infill, the diameter of nozzle and filament, the flow of filament, orientation of rasters, print direction, enable print cooling, UV Light, etc. The authors only focused on analysing the tensile characteristics and density of the part whereas, the other parameters like flexural strength, impact strength, etc. need to be analysed.

Kaplun *et al.* [54] explored the impact of raster patterns and print orientation on the mechanical behaviour of 3D-printed 9085 and Antero 840CN03 (PEKK) for their potential use in aerospace and defence-grade polymers. Through the analysis, the authors found that the mechanical strength of PEKK was higher than ULTEM 9085. They concluded that raster angle and pattern both play a major role to enhance the mechanical characteristics of FDM parts.

Sheoran and Kumar [12] reviewed the literature on the optimisation of FDM parameters and found that limitations in physical parameters, like availability of nozzle diameter and some specific values of layer height, restrict the integration of DOE and optimisation techniques. Thus, this limitation has to be addressed by coupling statistical DOE tools and modern optimisation techniques. Consequently, a newer mathematical modelling approach needs to be developed.

Kumar *et al.* [55] presented the influence of print orientation and fill density on flexural and tensile strength for a standard ASA material. The authors have followed ASTM standards to fabricate and test the specimen. Through the testing, the tensile strength was reported with 52.2 MPa when printed with Z-90 print orientation and 100 % fill density. The results were compared with injection moulded components and were found with higher tensile strength. Whereas, components fabricated with Y-90 print orientation and 25 % fill density exhibit high flexural strength of 65.7 MPa.

Szykiedans *et al.* [56] explored the mechanical behaviour of 3D printed PET-G. The authors only focused on tensile strength and elastic modulus. The author found variation in tensile modulus due to the presence of air-gap in the print structure

Durgashyam *et al.* [57] perceived the impact of printing variables on tensile and flexural properties of PET-G material fabricated using the FDM technique. They considered the process parameters like infill-density, feed-rate, and layer height to analyse their effectiveness. They found that the components with lower layer height and feed-rate and with higher infill-density have shown good tensile properties. In contrast, the material showed good flexural strength at minimum layer height, a lesser percentile of infill-density, and a moderate feed-rate. Through, this work authors concluded that among layer height, infill-density, and feed-rate, the significance of layer height is much higher compared to other process parameters.

Gebisa and Lemu [58] investigated the impact of FDM processing variables on the flexural strength of ULTEM 9085 considering five processing variables viz. air-gap, raster-angle, raster-width, contour width, and contour number. They found that raster-angle and raster-width have influenced the flexural property of the material to a larger extent.

Mohamed *et al.* [59] analysed the impact of printing variables on the dynamic mechanical characteristics of PC-ABS components fabricated using the FDM method. Through this analysis, they showed that air-gap, contour number, and layer height have the highest influence on the mechanical characteristics of the part. The authors also varied layer thickness, raster angle, air gap, build orientation, and road width to analyse the dynamic and cyclic conditions of 3D printed parts [60]. The authors used same material as before to optimise the parameters with a combination of artificial neural network and fractional factorial design. They found that dynamic modulus of elasticity increases with increase of layer thickness; whereas reverse trend was found with increase of other parameters.

Ahn *et al.* [61] analysed the impact of bead width, raster orientation, model temperature, air-gap, and material colour on the compressive and tensile behaviour of ABS parts fabricated using the FDM method. Their analysis showed that the mechanical behaviour of the fabricated components was found to be anisotropic and parameter-dependent. They also revealed that raster orientation and air-gap have an impact on the mechanical characteristics of the part.

Deng *et al.* [62] studied the optimisation of the mechanical behaviour of P-E-E-K in terms of printing variables. The authors considered layer height, printing speed, filling ratio, and extrusion temperature to analyse the tensile characteristics of the component. They revealed the optimum mechanical characteristics that can be obtained for the process parameters with a set of filling ratio at 40 %, printing speed at 60 mm/s, layer height at 0.2 mm, and extrusion temperature at 370 °C.

Onwubolu and Rayegani [63] looked at the impact of raster-angle, width, orientation, air-gap, and layer height on the tensile behaviour of ABS components fabricated using the FDM technique. Their study revealed that the optimal process variables that could enhance the tensile behaviour of the component are increased raster-angle, minimum raster-width, minimum layer height, and negative air-gap. It has also been observed that for zero-part orientation, maximum tensile strength is obtained.

Bagsik *et al.* [64] reported the impact of build direction on the compressive and tensile behaviour of ULTEM-9085-part build with FDM technology. The authors showed that the build-direction of the edge exhibits the highest tensile strength among all build directions, i.e., edge, upright and flat. Their investigation also revealed that compressive strength was maximum for the part built along upright-direction.

Bagsik and Schöppner [65] also explored the influence of other process variables like raster-to-perimeter and raster-to-raster air-gap, build-orientation, raster-angle, and raster-width. The tensile behaviour of the same material fabricated using FDM technology. Their study revealed that for all build directions with a negative raster air-gap, the tensile strength was highest. They also revealed that thicker filament can enhance the tensile behaviour for both build directions, i.e., edge and upright. However, the tensile behaviour for the components fabricated with build-orientation flat can be enhanced by using a thinner filament.

Motaparti *et al.* [66] analysed the impact of printing variables on the compressive nature of 3D-printed ULTEM-9085 component. The authors considered three process variables, like, build-orientation, raster-angle, and air-gap. They concluded that the compressive strength of the component gets affected by raster-angle and build-orientation.

Motaparti *et al.* [67] also highlighted the influence of the process variables like air-gap, raster-angle, and printing direction on the flexural behaviour of ULTEM 9085 fabricated using the FDM process with Build-styles of sparse and solid. Their analysis uncovered that the build-orientation of vertical or on-edge could provide higher flexural yield strength compared to other build directions.

Masood *et al.* [68] presented the impact of the airgap, raster-angle, and raster-width on the tensile strength of Polycarbonate (PC) polymer. The authors found the highest tensile strength of the selected material on a process parameter setting as in air-gap type of solid normal, raster-width of 0.6064 mm and raster-angle of 45°.

Gorski *et al.* [69] presented the impact of part orientation on tensile, bending, and impact strength of the part fabricated by ABS. The result showed that with a change in the orientation, the values of strength increased due to a change in macroscopic material behaviour.

Durgun and Ertan [70] explored the influence of part orientation and raster-angle on surface roughness, tensile and flexural characteristics. Through the result, the authors suggested that the part orientation has the highest influence on the product quality and mechanical properties of the part compared to the raster-angle. The result also showed that surface roughness has a close relationship with mechanical behaviour.

Ognzan *et al.* [71] explored the influence of deposition angle, layer height, and infill on the flexural strength of FDM samples fabricated using PLA material. The results showed that layer height has a dominant effect on flexural strength compared to the other two parameters. Table 1 shows an overview of the various process parameters for different polymers.

Table 1 Some published work on FDM process parameters

Ref.	Mat.	Input parameters	Remarks
Al-Ghamdi [72]	ABS	Fill density, Layer thickness, Shell thickness, Feed-rate,	Specific mass was not affected by feed-rate. The specific time and energy both decrease with the decrease of layer height and infill-density and by increasing feed-rate.
Garzon-Hernandez <i>et al.</i> [73]	ABS	Layer height, Number of layers, Raster orientation,	Maximum stress and higher elastic modulus were found for lower layer thickness and longitudinal raster direction. low mechanical property with an increased number of layers.
Pramanik <i>et al.</i> [74]	ABS	Printing, Speed, Extruder temperature, Fill density, Bed temperature, Layer height	Extruder temperature and print speed were found to be the most dominant parameters of surface roughness followed by the layer thickness and infill-density.
Galeja <i>et al.</i> [75]	ABS	Raster-angle (Fill angle)	With an increase in raster-angle, the strength of the component reduces. However, maximum strength is obtained at a raster-angle of 55°.
Divyathej <i>et al.</i> [76]	ABS	Layer height	Injection-moulded part exhibits higher tensile properties, and low layer thickness showed better mechanical properties among FDM printed samples. FDM specimens showed excellent flexural strength compared to moulded ones, and 0.15 mm layer thickness gave optimum flexural strength. 0.2 mm layer thickness showed the most preferable compressive strength. The surface finish of moulded samples was found to be better than FDM.
Kuznetsov <i>et al.</i> [77]	PLA	Nozzle diameter, Printing speed, Layer thickness	The Layer height has affected the intra-layer cohesion to a greater extent. An increase in layer height reduces the part strength for all nozzle diameters.
Rodríguez-Panes <i>et al.</i> [78]	ABS, PLA	Layer height, Infill density, Part orientation	The results for ABS showed a lower variation compared to PLA. The infill percentage has a higher influence on the mechanical characteristics of the part, although this effect is higher in PLA compared to ABS. The specimens fabricated using PLA having higher tensile strength than ABS due to their more rigid nature.
Arif <i>et al.</i> [79]	PEEK	Part orientation	The part orientation H-0° was found to be best for tensile, flexural, and fracture toughness, followed by H-90° and V-90°.
Rinaldi <i>et al.</i> [80]	PEEK	Infill density, Part orientation	The mechanical properties of FDM and injection moulded samples were found same for 100 % infill printed in the X-Y plane, whereas, samples printed in the Z direction were found to be extremely brittle with premature failures. Low mechanical properties were found in the samples fabricated with a low infill percentage.
Mishra <i>et al.</i> [81]	ABS	Contour number, Layer thickness, Raster-width, Part orientation, Raster angle and air-gap	Flexural strength was increased with increase of external perimeter (Contour). The failure also shifted from the edge to the centre. Anisotropy of the specimen was also reduced at 30° raster angle.
Samykano [82]	PLA	Fill percentage, Raster angle and layer height	Infill percentage significantly influenced the tensile strength out of selected input parameters.
Mendricky and Fris [83]	PLA	Layer height, Extruded line width, Top layer thickness, Number of walls, Infill percent, Infill pattern, Print speed, Part orientation etc.	Top layer height, Shape of the top layer, and print speed were found most influencing the roughness at the top of the fabricated part. Overall layer height, part orientation, and wall printing speed were found to be dominating for wall roughness.

The effect of main process variables on the mechanical behaviour are presented in Table 2. The table also consists of most frequently used optimisation techniques. It is also observed that Taguchi and ANOVA based method is most often used for almost all the parameters. However, machine learning methods based on ANN and fuzzy is implemented with few parameters. The ANN and fuzzy based optimisation methods have proved to be more accurate in providing optimal set of parameters value.

Table 2 The effect of the main process variables on the mechanical behaviour

Process parameters	Influence on the mechanical behaviour	Optimisation technique used
Raster angle	Tensile strength, Flexural strength, Impact strength, Surface roughness, Dimensional accuracy	Taguchi method [19, 84], Gray relation analysis [84], ANOVA [84], Fuzzy Logic [85, 86], Artificial Neural Network (ANN), GA
Layer thickness	Tensile strength, Flexural strength, Impact strength, Hardness, Compressive strength, Dimensional accuracy, Surface roughness	Taguchi method [84], Hybrid particle swarm, Bacterial forage optimization, Artificial Neural Network (ANN), Gray relation analysis [84], ANOVA [84], Fuzzy logic [85, 86]
Raster width	Elasticity, Tensile strength, Flexural strength, Impact strength, Dimensional accuracy	Taguchi method [84], ANOVA [84], Artificial Neural Network (ANN), Fuzzy logic [85, 86]
Contour number	Elasticity, Tensile strength, Impact strength, Flexural strength, Impact strength, Dimensional accuracy	Taguchi method, ANOVA, Regression analysis [88]
Infill density	Flexural strength, Tensile strength, % Elongation	RSM, ANOVA, Taguchi method [89], GA, GA-ANN, GA-ANFIS [90]
Infill pattern	Surface roughness, Hardness, Flexural Modulus, Tensile strength	Taguchi method, ANOVA, Regression analysis [87]
Build orientation	Tensile strength, Flexural strength, Fracture toughness	Fuzzy Logic [85, 86], ANOVA [84], Regression analysis, Taguchi method [84]
Air gap	Tensile strength, Flexural strength, Impact strength,	ANOVA [84], Regression analysis, Taguchi method [84], Fuzzy logic [85, 86]
Support style	Tensile strength, Dimension accuracy, Surface roughness	ANOVA along with gray relational analysis, Taguchi method [91]

4. Challenges and future scope

From the above discussion, it has been found that the process variables influence the quality of the FDM product to a great extent. Manufacturers and users are mainly concerned with the mechanical characteristics of the component like tensile strength, compressive strength, yield strength, flexural strength, impact strength, hardness, dimensional accuracy, production time, surface roughness, and durability. Therefore, researchers are investigating the most significant process parameter to enhance the mechanical characteristic of the component. However, there are still no unique significant parameters found for all materials, parts, and mechanical properties. There is always a need to adjust most of the parameters to meet the required part quality. After all these parameter adjustments, porosity remains within the FDM fabricated component because of its layering approach. The presence of porosity within the components fabricated through the FDM technique leads to having lower mechanical properties compared to the injection-moulded components. To enhance the mechanical behaviour and quality of these components, it is necessary to develop the relationship between printing variables and material characteristics through mathematical modelling approaches.

From the literature review, it has been found that various printing variables (parameters) influence the quality of the component fabricated using the FDM technique. Hence, it is required to identify the critical parameters and determine their optimum values to improve the quality of the component. However, there are very few authors who have developed the relationships of the process variables with the mechanical behaviour and part quality, which is not enough for all types of FDM processed materials.

Many authors have analysed the influence of FDM process variables on PLA, ABS, ULTEM 9085, PETG, Nylon-6 built parts. However, very few authors have reported on other FDM processed materials, both in terms of FDM process optimisation and material characterization. Therefore, it is necessary to fabricate and identify the significant process parameters for other FDM processed materials like ASA, PEEK, PEKK, PET-G, and nylon-12.

As far as material behaviour is concerned, most authors have reported on the optimisation of the printing input variables for enhancing the material characteristics of the parts fabricated using the FDM technique. However, very few authors have worked on the optimisation technique of FDM printing input variables for chemical, dynamic mechanical characteristics, chemical resistance, UV resistance and thermal of the parts printed using the FDM technique. Therefore, the impact of process variables on these factors needs to be investigated.

The impact of printing variables on surface roughness, dimensional accuracy, impact, flexural, compressive, and tensile strength have been studied thoroughly by the authors. However, the other types of material properties like stress-strain behaviour at high-strain-rate loading conditions, porosity, product and process cost, vibration, production time, creep, and hardness need to be studied. The researchers should also work on the application of new optimisation techniques integrated with DOE, modelling techniques, and new statistical designs in the future, and identify the optimum setting of printing variables, and should also test the functionality of parts fabricated using the FDM technique.

Environmental factors like relative humidity and temperature also affect the part quality. These factors may affect the surface quality and the dimensional accuracy of the FDM processed parts of materials like ABS, PLA, nylon-12, etc. Therefore, it is necessary to determine the optimal sets of humidity and temperature for FDM processed materials.

The process of FDM machines is restricted by some physical constraints and has an impact on the setting of the optimum values of process variables, which must be addressed in future research. Among these constraints, the most crucial is the layer thickness whose value depends on the nozzle diameter; therefore, the user cannot select the layer thickness values other than specified values for that particular machine. The second constraint is imposed on nozzle diameter, which has a specified range of raster-width. In these conditions, the user cannot use any arbitrary values other than those defined by their range. These constraints complicate the optimisation of the FDM process variables and their selection on the machine for fabricating the component. Therefore, it is difficult to solve FDM process-related problems using traditional DOE techniques. Thus, the development of new mathematical modelling and optimisation approach is required for solving the constraints-related problems for the selection of optimum values of process variables beyond the specified range and also make it possible and feasible for practical applications.

5. Conclusion

This work presents the various process parameters of fused deposition modelling-based additive manufacturing technique and their effect on mechanical characteristics of 3D-Printed components made of different thermoplastic materials. Through this study, it has been found that many researchers have worked on ABS, ABS+, PLA, ULTEM 9085; however, there exists future scope to analyse the influence of FDM process variables on the mechanical behaviour of other thermoplastic materials like ASA, PET-G, PEEK, and PEKK, etc.

The present study also identified that printing process parameters have their roles and influence. Among all the process parameters, layer height has the highest influence on surface finish, build time, and strength of the component. Maximum strength is obtained with a rectilinear pattern, 100 % infill-density, and increased layer thickness. Raster width, raster angle, and contour numbers also affect the mechanical property of the component. It has also been found that most of the researchers analysed the influence on tensile and flexural properties; however, very few researchers have analysed the effect on impact strength. Overall, the parameters like part orientation, layer height, raster-angle, raster width, and contours directly affect the quality of the 3D-printed part.

From the investigation, the input variables which affect the mechanical behaviour of the part can be set with most significant (layer height, raster-angle, and raster-width), significant (contour width and contour number) and least significant (air-gap). Although many authors have suggested a minus air-gap for enhancing the mechanical characteristics of the component, it was observed that minus air-gap has some drawbacks. Its effect can differ based on the thermoplastic used for

processing. Although FDM process saves time and cost for low volume production, whereas, mechanical behaviour of its product doesn't exceed injection moulded product. Hence, one should investigate other methods to improvise the properties of FDM products. Here, an effort is made to help researchers toward the selection of FDM processed material and variables for further research.

References

- [1] Marwah, O.M.F., Darsani, A., Johar, M.A., Rosden, A.A., Mohamad, E.J., Shaari, M.F., Haq, R.H.A., Amin, A.M. (2017). Evaluation of injection molding process parameters for manufacturing polyethylene terephthalate, *MATEC Web of Conferences*, Vol. 135, 1-10, doi: [10.1051/mateconf/201713500037](https://doi.org/10.1051/mateconf/201713500037).
- [2] Meekers, I., Refalo, P., Rochman, A. (2018). Analysis of process parameters affecting energy consumption in plastic injection moulding, *Procedia CIRP*, Vol. 69, 342-347, doi: [10.1016/j.procir.2017.11.042](https://doi.org/10.1016/j.procir.2017.11.042).
- [3] Ganeshkar, J., Kamble, D. (2014). Design and manufacturing of plastic injection mould, *Pertanika Journal of Science and Technology Supplement*, Vol. 2, No. 5, 439-442.
- [4] Knezovic, N., Dolsak, B. (2018). In-process non-destructive ultrasonic testing application during wire plus arc additive manufacturing, *Advances in Production Engineering & Management*, Vol. 13, No. 2, 158-168, doi: [10.14743/apem2018.2.281](https://doi.org/10.14743/apem2018.2.281).
- [5] Patalas-Maliszewska, J., Topczak, M. (2021). A new management approach based on additive manufacturing technologies and Industry 4.0 requirements, *Advances in Production Engineering & Management*, Vol. 16, No. 1, 125-135, doi: [10.14743/apem2021.1.389](https://doi.org/10.14743/apem2021.1.389).
- [6] Javaid, M., Haleem, A. (2019). Current status and applications of additive manufacturing in dentistry: A literature-based review, *Journal of Oral Biology and Craniofacial Research*, Vol. 9, No. 3, 179-185, doi: [10.1016/j.jobcr.2019.04.004](https://doi.org/10.1016/j.jobcr.2019.04.004).
- [7] Sari, T., Güleş, H.K., Yiğitöl, B. (2020). Awareness and readiness of Industry 4.0: The case of Turkish manufacturing industry, *Advances in Production Engineering & Management*, Vol. 15, No. 1, 57-68, doi: [10.14743/apem2020.1.349](https://doi.org/10.14743/apem2020.1.349).
- [8] Song, Y., Li, Y., Song, W., Yee, K., Lee, K.-Y., Tagarielli, V.L. (2017). Measurements of the mechanical response of unidirectional 3D-printed PLA, *Materials & Design*, Vol. 123, 154-164, doi: [10.1016/j.matdes.2017.03.051](https://doi.org/10.1016/j.matdes.2017.03.051).
- [9] Tak, A., Ingavale, P., Khopatkar, C., Bhure, S., Barve, V., Rajurkar, A. (2015). Effect of 3D printing parameters on dimensional accuracy & shrinkage on printed parts, In: *Proceedings of National Conference on Modeling, Optimization and Control - NCMOC - 2015*, Pune, Maharashtra, India.
- [10] Pham, D.T., Dimov, S.S. (2012). *Rapid manufacturing: The technologies and applications of rapid prototyping and rapid tooling*, Springer, London, United Kingdom.
- [11] Shofner, M.L., Lozano, K., Rodríguez-Macías F.J., Barrera, E.V. (2003). Nanofiber-reinforced polymers prepared by fused deposition modeling, *Journal of Applied Polymer Science*, Vol. 89, No. 11, 3081-3090, doi: [10.1002/app.12496](https://doi.org/10.1002/app.12496).
- [12] Sheoran, A.J., Kumar, H. (2020). Fused deposition modeling process parameters optimization and effect on mechanical properties and part quality: Review and reflection on present research, *Materials Today Proceedings*, Vol. 21, Part 3, 1659-1672, doi: [10.1016/j.matpr.2019.11.296](https://doi.org/10.1016/j.matpr.2019.11.296).
- [13] Kaur, G., Singari, R.M., Kumar, H. (2022). A review of fused filament fabrication (FFF): Process parameters and their impact on the tribological behavior of polymers (ABS), *Materials Today Proceedings*, Vol. 51, Part 1, 854-860, doi: [10.1016/j.MATPR.2021.06.274](https://doi.org/10.1016/j.MATPR.2021.06.274).
- [14] Patil, P., Singh, D., Raykar, S.J., Bhamu, J. (2021). Multi-objective optimization of process parameters of Fused Deposition Modeling (FDM) for printing Polylactic Acid (PLA) polymer components, *Materials Today Proceedings*, Vol. 45, Part 6, 4880-4885, doi: [10.1016/j.matpr.2021.01.353](https://doi.org/10.1016/j.matpr.2021.01.353).
- [15] Ortiz-Acosta, D., Moore, T. (2019). Functional 3D printed polymeric materials, In: Sahu, D. (ed.), *Functional Materials*, IntechOpen, London, United Kingdom, doi: [10.5772/intechopen.80686](https://doi.org/10.5772/intechopen.80686).
- [16] Hamad, K., Kaseem, M., Yang, H.W., Deri, F., Ko, Y.G. (2015). Properties and medical applications of polylactic acid: A review, *Express Polymer Letters*, Vol. 9, No. 5, 435-455, doi: [10.3144/expresspolymlett.2015.42](https://doi.org/10.3144/expresspolymlett.2015.42).
- [17] Jo, M.Y., Ryu, Y.J., Ko, J.H., Yoon, J.-S. (2012). Effects of compatibilizers on the mechanical properties of ABS/PLA composites, *Journal of Applied Polymer Science*, Vol. 125, No. 2, 231-238, doi: [10.1002/app.36732](https://doi.org/10.1002/app.36732).
- [18] Raj, S.A., Muthukumar, E., Jayakrishna, K. (2018). A case study of 3D printed PLA and its mechanical properties, *Materials Today Proceedings*, Vol. 5, No. 5, Part 2, 11219-11226, doi: [10.1016/j.matpr.2018.01.146](https://doi.org/10.1016/j.matpr.2018.01.146).
- [19] Mohamed, O.A., Masood, S.H., Bhowmik, J.L. (2015). Optimization of fused deposition modeling process parameters: A review of current research and future prospects, *Advances in Manufacturing*, Vol. 3, 42-53, doi: [10.1007/s40436-014-0097-7](https://doi.org/10.1007/s40436-014-0097-7).
- [20] Casavola, C., Cazzato, A., Moramarco, V., Pappalettera, G. (2017). Residual stress measurement in Fused Deposition Modelling parts, *Polymer Testing*, Vol. 58, 249-255, doi: [10.1016/j.polymertesting.2017.01.003](https://doi.org/10.1016/j.polymertesting.2017.01.003).
- [21] Hossain, M.S., Ramos, J., Espalin, D., Perez, M., Wicker, R. (2013). Improving tensile mechanical properties of FDM-manufactured specimens via modifying build parameters, In: *2013 International Solid Freeform Fabrication Symposium*, University of Texas at Austin, 380-392.
- [22] Sood, A.K., Ohdar, R.K., Mahapatra, S.S. (2010). Parametric appraisal of fused deposition modelling process using the grey Taguchi method, *Proceedings of the Institution of Mechanical Engineers, Part B: Journal of Engineering Manufacture*, Vol. 224, No. 1, 135-145, doi: [10.1243/09544054JEM1565](https://doi.org/10.1243/09544054JEM1565).

- [23] Dey, A., Yodo, N. (2019). A systematic survey of FDM process parameter optimization and their influence on part characteristics, *Journal of Manufacturing and Materials Processing*, Vol. 3, No. 3, Article No. 64, [doi: 10.3390/jmmp3030064](https://doi.org/10.3390/jmmp3030064).
- [24] Moradi, M., Meiabadi, S., Kaplan, A. (2019). 3D printed parts with honeycomb internal pattern by Fused Deposition Modelling; Experimental characterization and production optimization, *Metals and Materials International*, Vol. 25, 1312-1325, [doi: 10.1007/s12540-019-00272-9](https://doi.org/10.1007/s12540-019-00272-9).
- [25] Rankouhi, B., Javadpour, S., Delfanian, F., Letcher, T. (2016). Failure analysis and mechanical characterization of 3D printed ABS with respect to layer thickness and orientation, *Journal of Failure Analysis and Prevention*, Vol. 16, No. 3, 467-481, [doi: 10.1007/s11668-016-0113-2](https://doi.org/10.1007/s11668-016-0113-2).
- [26] Selva Priya, M., Naresh, K., Jayaganthan, R., Velmurugan, R. (2019). A comparative study between in-house 3D printed and injection molded ABS and PLA polymers for low-frequency applications, *Materials Research Express*, Vol. 6, No. 8, Article No. 085345, [doi: 10.1088/2053-1591/ab2776](https://doi.org/10.1088/2053-1591/ab2776).
- [27] Vaezi, M., Chua, C.K. (2011). Effects of layer thickness and binder saturation level parameters on 3D printing process, *International Journal of Advanced Manufacturing Technology*, Vol. 53, No. 1-4, 275-284, [doi: 10.1007/s00170-010-2821-1](https://doi.org/10.1007/s00170-010-2821-1).
- [28] Noori, H. (2019). Interlayer fracture energy of 3D-printed PLA material, *International Journal of Advanced Manufacturing Technology*, Vol. 101, 1959-1965, [doi: 10.1007/s00170-018-3031-5](https://doi.org/10.1007/s00170-018-3031-5).
- [29] Abbott, A.C., Tandon, G.P., Bradford, R.L., Koerner, H., Baur, J.W. (2018). Process-structure-property effects on ABS bond strength in fused filament fabrication, *Additive Manufacturing*, Vol. 19, 29-38, [doi: 10.1016/j.addma.2017.11.002](https://doi.org/10.1016/j.addma.2017.11.002).
- [30] Wu, W., Geng, P., Li, G., Zhao, D., Zhang, H., Zhao, J. (2015). Influence of layer thickness and raster-angle on the mechanical properties of 3D-printed PEEK and a comparative mechanical study between PEEK and ABS, *Materials*, Vol. 8, No. 9, 5834-5846, [doi: 10.3390/ma8095271](https://doi.org/10.3390/ma8095271).
- [31] Bin Sukindar, N.A., Bin Mohd Ariffin, M.K.A., Bin Baharudin, B.T.H.T., Binti Jaafar, C.N.A., Bin Ismail, M.I.S. (2017). Analysis on the impact process parameters on tensile strength using 3d printer repetier-host software, *ARPN Journal of Engineering and Applied Sciences*, Vol. 12, No. 10, 3341-3346.
- [32] Rouf, S., Raina, A., Irfan Ul Haq, M., Naveed, N., Jeganmohan, S., Farzana Kichloo, A. (2022). 3D printed parts and mechanical properties: Influencing parameters, sustainability aspects, global market scenario, challenges and applications, *Advanced Industrial and Engineering Polymer Research*, Vol. 5, No. 3, 143-158, [doi: 10.1016/I.AIEPR.2022.02.001](https://doi.org/10.1016/I.AIEPR.2022.02.001).
- [33] Roy, R., Mukhopadhyay, A. (2021). Tribological studies of 3D printed ABS and PLA plastic parts, *Materials Today Proceedings*, Vol. 41, Part 4, 856-862, [doi: 10.1016/j.matpr.2020.09.235](https://doi.org/10.1016/j.matpr.2020.09.235).
- [34] Norani, M.N.M., Abdollah, M.F.B., Abdullah, M.I.H.C., Amiruddin, H., Ramli, F.R., Tamaldin, N. (2021). 3D printing parameters of acrylonitrile butadiene styrene polymer for friction and wear analysis using response surface methodology, *Proceedings of the Institution of Mechanical Engineers, Part J: Journal of Engineering Tribology*, Vol. 235, No. 2, 468-477, [doi: 10.1177/1350650120925601](https://doi.org/10.1177/1350650120925601).
- [35] Dangnan, F., Espejo, C., Liskiewicz, T., Gester, M., Neville, A. (2020). Friction and wear of additive manufactured polymers in dry contact, *Journal of Manufacturing Processes*, Vol. 59, 238-247, [doi: 10.1016/j.jmapro.2020.09.051](https://doi.org/10.1016/j.jmapro.2020.09.051).
- [36] Bhosale, V., Gaikwad, P., Dhere, S., Sutar, C., Raykar, S.J. (2022). Analysis of process parameters of 3D printing for surface finish, printing time and tensile strength, *Materials Today Proceedings*, Vol. 59, Part 1, 841-846, [doi: 10.1016/I.MATPR.2022.01.210](https://doi.org/10.1016/I.MATPR.2022.01.210).
- [37] Raj Mohan, R., Venkatraman, R., Raghuraman, S. (2021). Experimental analysis on density, micro-hardness, surface roughness and processing time of Acrylonitrile Butadiene Styrene (ABS) through Fused Deposition Modeling (FDM) using Box Behnken Design (BBD), *Materials Today Communications*, Vol. 27, Article No. 102353, [doi: 10.1016/j.mtcomm.2021.102353](https://doi.org/10.1016/j.mtcomm.2021.102353).
- [38] Khan, M.S., Mishra, S.B. (2019). Minimizing surface roughness of ABS-FDM build parts: An experimental approach, *Materials Today Proceedings*, Vol. 26, Part 2, 1557-1566, [doi: 10.1016/j.matpr.2020.02.320](https://doi.org/10.1016/j.matpr.2020.02.320).
- [39] Kumar, R., Ranjan, N. (2021). Influences of infill percentage, bed temperature and outer perimeters on elongation of 3D printed nylon 6, *Materials Today Proceedings*, Vol. 48, Part 5, 1661-1665, [doi: 10.1016/j.matpr.2021.09.529](https://doi.org/10.1016/j.matpr.2021.09.529).
- [40] Chacón, J.M., Caminero, M.A., García-Plaza, E., Núñez, P.J. (2017). Additive manufacturing of PLA structures using fused deposition modelling: Effect of process parameters on mechanical properties and their optimal selection, *Materials & Design*, Vol. 124, 143-157, [doi: 10.1016/j.matdes.2017.03.065](https://doi.org/10.1016/j.matdes.2017.03.065).
- [41] Shubham, P., Sikidar, A., Chand, T. (2016). The influence of layer thickness on mechanical properties of the 3D printed ABS polymer by fused deposition modeling, *Key Engineering Materials*, Vol. 706, 63-67, [doi: 10.4028/www.scientific.net/KEM.706.63](https://doi.org/10.4028/www.scientific.net/KEM.706.63).
- [42] Shubham, P., Aggarwal, C., Joshi, S. (2018). Optimization of process parameter to improve dynamic mechanical properties of 3D printed ABS polymer using Taguchi method, *International Journal of Mechanical and Production Engineering*, Vol. 6, No. 6, 2321-2071.
- [43] Daminabo, S.C., Goel, S., Grammatikos, S.A., Nezhad, H.Y., Thakur, V.K. (2020). Fused deposition modeling-based additive manufacturing (3D printing): Techniques for polymer material systems, *Materials Today Chemistry*, Vol. 16, Article No. 100248, [doi: 10.1016/j.mtchem.2020.100248](https://doi.org/10.1016/j.mtchem.2020.100248).
- [44] Ramesh, M., Panneerselvam, K. (2020). Mechanical investigation and optimization of parameter selection for Nylon material processed by FDM, *Materials Today Proceedings*, Vol. 46, Part 19, 9303-9307, [doi: 10.1016/j.matpr.2020.02.697](https://doi.org/10.1016/j.matpr.2020.02.697).

- [45] Pazhamannil, R.V., Govindan, P., Sooraj, P. (2020). Prediction of the tensile strength of polylactic acid fused deposition models using artificial neural network technique, *Materials Today Proceedings*, Vol. 46, Part 19, 9187-9193, [doi: 10.1016/j.matpr.2020.01.199](https://doi.org/10.1016/j.matpr.2020.01.199).
- [46] Yadav, D., Chhabra, D., Gupta, R.K., Phogat, A., Ahlawat, A. (2020). Modeling and analysis of significant process parameters of FDM 3D printer using ANFIS, *Materials Today Proceedings*, Vol. 21, Part 3, 1592-1604, [doi: 10.1016/j.matpr.2019.11.227](https://doi.org/10.1016/j.matpr.2019.11.227).
- [47] Gebisa, A.W., Lemu, H.G. (2019). Influence of 3D printing FDM process parameters on tensile property of ULTEM 9085, *Procedia Manufacturing*, Vol. 30, 331-338, [doi: 10.1016/j.promfg.2019.02.047](https://doi.org/10.1016/j.promfg.2019.02.047).
- [48] Wankhede, V., Jagetiya, D., Joshi, A., Chaudhari, R. (2019). Experimental investigation of FDM process parameters using Taguchi analysis, *Materials Today Proceedings*, Vol. 27, Part 3, 2117-2120, [doi: 10.1016/j.matpr.2019.09.078](https://doi.org/10.1016/j.matpr.2019.09.078).
- [49] Solomon, I.J., Sevvel, P., Gunasekaran, J. (2021). A review on the various processing parameters in FDM, *Materials Today Proceedings*, Vol. 37, Part 2, 509-514, [doi: 10.1016/j.matpr.2020.05.484](https://doi.org/10.1016/j.matpr.2020.05.484).
- [50] Fernandez-Vicente, M., Calle, W., Ferrandiz, S., Conejero, A. (2016). Effect of infill parameters on tensile mechanical behavior in desktop 3D printing, *3D Printing and Additive Manufacturing*, Vol. 3, No. 3, 183-192, [doi: 10.1089/3dp.2015.0036](https://doi.org/10.1089/3dp.2015.0036).
- [51] Rajpurohit, S.R., Dave, H.K. (2018). Effect of process parameters on tensile strength of FDM printed PLA part, *Rapid Prototyping Journal*, Vol. 24, No. 8, 1317-1324, [doi: 10.1108/RPJ-06-2017-0134](https://doi.org/10.1108/RPJ-06-2017-0134).
- [52] Dawoud, M., Taha, I., Ebeid, S.J. (2016). Mechanical behaviour of ABS: An experimental study using FDM and injection moulding techniques, *Journal of Manufacturing Processes*, Vol. 21, 39-45, [doi: 10.1016/j.jmapro.2015.11.002](https://doi.org/10.1016/j.jmapro.2015.11.002).
- [53] Wang, P., Zou, B., Xiao, H., Ding, S., Huang, C. (2019). Effects of printing parameters of fused deposition modeling on mechanical properties, surface quality, and microstructure of PEEK, *Journal of Materials Processing Technology*, Vol. 271, 62-74, [doi: 10.1016/j.jmatprotec.2019.03.016](https://doi.org/10.1016/j.jmatprotec.2019.03.016).
- [54] Kaplun, B.W., Zhou, R., Jones, K.W., Dunn, M.L., Yakacki, C.M. (2020). Influence of orientation on mechanical properties for high-performance fused filament fabricated ultem 9085 and electro-statically dissipative polyetherketoneketone, *Additive Manufacturing*, Vol. 36, Article No. 101527, [doi: 10.1016/j.addma.2020.101527](https://doi.org/10.1016/j.addma.2020.101527).
- [55] Raam Kumar, S., Sridhar, S., Venkatraman, R., Venkatesan, M. (2020). Polymer additive manufacturing of ASA structure: Influence of printing parameters on mechanical properties, *Materials Today Proceedings*, Vol. 39, Part 4, 1316-1319, [doi: 10.1016/j.matpr.2020.04.500](https://doi.org/10.1016/j.matpr.2020.04.500).
- [56] Szykiedans, K., Credo, W., Osiński, D. (2017). Selected mechanical properties of PETG 3-D prints, *Procedia Engineering*, Vol. 177, 455-461, [doi: 10.1016/j.proeng.2017.02.245](https://doi.org/10.1016/j.proeng.2017.02.245).
- [57] Durgashyam, K., Indra Reddy, M., Balakrishna, A., Satyanarayana, K. (2019). Experimental investigation on mechanical properties of PETG material processed by fused deposition modeling method, *Materials Today Proceedings*, Vol. 18, Part 6, 2052-2059, [doi: 10.1016/j.matpr.2019.06.082](https://doi.org/10.1016/j.matpr.2019.06.082).
- [58] Gebisa, A.W., Lemu, H.G. (2018). Investigating effects of fused-deposition modeling (FDM) processing parameters on flexural properties of ULTEM 9085 using designed experiment, *Materials*, Vol. 11, No. 4, Article No. 500, [doi: 10.3390/ma11040500](https://doi.org/10.3390/ma11040500).
- [59] Mohamed, O.A., Masood, S.H., Bhowmik, J.L., Nikzad, M., Azadmanjiri, J. (2016). Effect of process parameters on dynamic mechanical performance of FDM PC/ABS printed parts through design of experiment, *Journal of Materials Engineering and Performance*, Vol. 25, 2922-2935, [doi: 10.1007/s11665-016-2157-6](https://doi.org/10.1007/s11665-016-2157-6).
- [60] Mohamed Omar, A., Masood Syed, H., Bhowmik Jahar, L. (2016). Investigation of dynamic elastic deformation of parts processed by fused deposition modeling additive manufacturing, *Advances in Production Engineering & Management*, Vol. 13, No. 3, 227-238, [doi: 10.14743/apem2016.3.223](https://doi.org/10.14743/apem2016.3.223).
- [61] Ahn, S.-H., Montero, M., Odell, D., Roundy, S., Wright, P.K. (2002). Anisotropic material properties of fused deposition modeling ABS, *Rapid Prototyping Journal*, Vol. 8, No. 4, 248-257, [doi: 10.1108/13552540210441166](https://doi.org/10.1108/13552540210441166).
- [62] Deng, X., Zeng, Z., Peng, B., Yan, S., Ke, W. (2018). Mechanical properties optimization of poly-ether-ether-ketone via fused deposition modeling, *Materials*, Vol. 11, No. 2, Article No. 216, [doi: 10.3390/ma11020216](https://doi.org/10.3390/ma11020216).
- [63] Onwubolu, G.C., Rayegani, F. (2014). Characterization, and optimization of mechanical properties of ABS parts manufactured by the fused deposition modelling process, *International Journal of Manufacturing Engineering*, Vol. 2014, Article ID 598531, [doi: 10.1155/2014/598531](https://doi.org/10.1155/2014/598531).
- [64] Bagsik, A., Schöppner, V., Klemp, E. (2010). FDM part quality manufactured with Ultem* 9085. In: *Proceedings of the 14th International Scientific Conference on Polymeric Materials*, Halle (Saale), Germany, 307-315.
- [65] Bagsik, A., Schöppner, V. (2011). Mechanical properties of fused deposition modeling parts manufactured with Ultem 9085, In: *Proceedings of ANTEC 2011: 69th Annual Technical Conference of the Society of Plastics Engineers*, Boston, USA, 1294-1298.
- [66] Motaparti, K.P., Taylor, G., Leu, M.C., Chandrashekhara, K., Castle, J., Matlack, M. (2016). Effects of build parameters on compression properties for ULTEM 9085 parts by fused deposition modeling, In: *Proceedings of the 27th Annual International Solid Freeform Fabrication Symposium - An Additive Manufacturing Conference, SFF 2016*, Austin, USA, 964-977.
- [67] Motaparti, K.P., Taylor, G., Leu, M.C., Chandrashekhara, K., Castle, J., Matlack, M. (2017). Experimental investigation of effects of build parameters on flexural properties in fused deposition modeling parts, *Virtual and Physical Prototyping*, Vol. 12, No. 3, 207-220, [doi: 10.1080/17452759.2017.1314117](https://doi.org/10.1080/17452759.2017.1314117).
- [68] Masood, S.H., Mau, K., Song, W.Q. (2010). Tensile properties of processed FDM polycarbonate material, *Materials Science Forum*, Vol. 654-656, 2556-2559, [doi: 10.4028/www.scientific.net/MSF.654-656.2556](https://doi.org/10.4028/www.scientific.net/MSF.654-656.2556).

- [69] Górski, F., Wichniarek, R., Kuczko, W., Zawadzki, P., Buń, P. (2015). Strength of ABS parts produced by fused deposition modelling technology – A critical orientation problem, *Advances in Science and Technology Research Journal*, Vol. 9, No. 26, 12-19, doi: [10.12913/22998624/2359](https://doi.org/10.12913/22998624/2359).
- [70] Durgun, I., Ertan, R. (2014). Experimental investigation of FDM process for improvement of mechanical properties and production cost, *Rapid Prototyping Journal*, Vol. 20, No. 3, 228-235, doi: [10.1108/RPJ-10-2012-0091](https://doi.org/10.1108/RPJ-10-2012-0091).
- [71] Lužanin, O., Movrin, D., Plančak, M. (2014). Effect of layer thickness, deposition angle, and infill on maximum flexural force in FDM-built specimens, *Journal for Technology of Plasticity*, Vol. 39, No. 1, 49-58.
- [72] Al-Ghamdi, K.A. (2019). Sustainable FDM additive manufacturing of ABS components with emphasis on energy minimized and time efficient lightweight construction, *International Journal of Lightweight Materials and Manufacture*, Vol. 2, No. 4, 338-345, doi: [10.1016/j.ijlmm.2019.05.004](https://doi.org/10.1016/j.ijlmm.2019.05.004).
- [73] Garzon-Hernandez, S., Garcia-Gonzalez, D., Jérusalem, A., Arias, A. (2020). Design of FDM 3D printed polymers: An experimental-modeling methodology for the prediction of mechanical properties, *Materials & Design*, Vol. 188, Article No. 108414, doi: [10.1016/j.matdes.2019.108414](https://doi.org/10.1016/j.matdes.2019.108414).
- [74] Pramanik, D., Mandal, A., Kuar, A.S. (2020). An experimental investigation on improvement of surface roughness of ABS on fused deposition modelling process, *Materials Today Proceedings*, Vol. 26, Part 2, 860-863, doi: [10.1016/j.matpr.2020.01.054](https://doi.org/10.1016/j.matpr.2020.01.054).
- [75] Galeja, M., Hejna, A., Kosmela, P., Kulawik, A. (2020). Static and dynamic mechanical properties of 3D printed ABS as a function of raster angle, *Materials*, Vol. 13, No. 2, Article No. 297, doi: [10.3390/ma13020297](https://doi.org/10.3390/ma13020297).
- [76] Divyathej, M.V., Varun, M., Rajeev, P. (2016). Analysis of mechanical behavior of 3D printed ABS parts by experiments, *International Journal of Scientific & Engineering Research*, Vol. 7, No. 3, 116-124.
- [77] Kuznetsov, V.E., Solonin, A.N., Urzhumtsev, O.D., Schilling, R., Tavitov, A.G. (2018). Strength of PLA components fabricated with fused deposition technology using a desktop 3D printer as a function of geometrical parameters of the process, *Polymers*, Vol. 10, No. 3, Article No. 313, doi: [10.3390/polym10030313](https://doi.org/10.3390/polym10030313).
- [78] Rodríguez-Panes, A., Claver, J., Camacho, A.M. (2018). The influence of manufacturing parameters on the mechanical behaviour of PLA and ABS pieces manufactured by FDM: A comparative analysis, *Materials*, Vol. 11, No. 8, Article No. 1333, doi: [10.3390/ma11081333](https://doi.org/10.3390/ma11081333).
- [79] Arif, M.F., Kumar, S., Varadarajan, K.M., Cantwell, W.J. (2018). Performance of biocompatible PEEK processed by fused deposition additive manufacturing, *Materials & Design*, Vol. 146, 249-259, doi: [10.1016/j.matdes.2018.03.015](https://doi.org/10.1016/j.matdes.2018.03.015).
- [80] Rinaldi, M., Ghidini, T., Cecchini, F., Brandao, A., Nanni, F. (2018). Additive layer manufacturing of poly (ether ether ketone) via FDM, *Composites Part B: Engineering*, Vol. 145, 162-172, doi: [10.1016/j.compositesb.2018.03.029](https://doi.org/10.1016/j.compositesb.2018.03.029).
- [81] Mishra, S.B., Malik, R., Mahapatra, S.S. (2017). Effect of external perimeter on flexural strength of FDM build parts, *Arabian Journal for Science and Engineering*, Vol. 42, 4587-4595, doi: [10.1007/s13369-017-2598-8](https://doi.org/10.1007/s13369-017-2598-8).
- [82] Samykano, M. (2021). Mechanical property and prediction model for FDM-3D printed polylactic acid (PLA), *Arabian Journal for Science and Engineering*, Vol. 46, 7875-7892, doi: [10.1007/s13369-021-05617-4](https://doi.org/10.1007/s13369-021-05617-4).
- [83] Mendricky, R., Fris, D. (2020). Analysis of the accuracy and the surface roughness of FDM/FFF technology and optimization of process parameters, *Tehnički Vjesnik – Technical Gazette*, Vol. 27, No. 4, 1166-1173, doi: [10.17559/TV-20190320142210](https://doi.org/10.17559/TV-20190320142210).
- [84] Liu, X., Zhang, M., Li, S., Si, L., Peng, J., Hu, Y. (2017). Mechanical property parametric appraisal of fused deposition modeling parts based on the gray Taguchi method, *International Journal of Advanced Manufacturing Technology*, Vol. 89, 2387-2397, doi: [10.1007/s00170-016-9263-3](https://doi.org/10.1007/s00170-016-9263-3).
- [85] Srivastava, M., Rathee, S., Maheshwari, S., Kundra, T.K. (2018). Multi-objective optimisation of fused deposition modelling process parameters using RSM and fuzzy logic for build time and support material, *International Journal of Rapid Manufacturing*, Vol. 7, No. 1, 25-42, doi: [10.1504/ijrapidm.2018.089727](https://doi.org/10.1504/ijrapidm.2018.089727).
- [86] Sahu, R.K., Mahapatra, S.S., Sood, A.K. (2013) A study on dimensional accuracy of fused deposition modeling (FDM) processed parts using fuzzy logic, *Journal for Manufacturing Science & Production*, Vol. 13, No. 3, 183-197, doi: [10.1515/jmsp-2013-0010](https://doi.org/10.1515/jmsp-2013-0010).
- [87] Raju, M., Gupta, M.K., Bhanot, N., Sharma, V.S. (2019). A hybrid PSO-BFO evolutionary algorithm for optimization of fused deposition modelling process parameters, *Journal of Intelligent Manufacturing*, Vol. 30, 2743-2758, doi: [10.1007/s10845-018-1420-0](https://doi.org/10.1007/s10845-018-1420-0).
- [88] Zaman, U.K.U., Boesch, E., Siadat, A., Rivette, M., Baqai, A.A. (2019). Impact of fused deposition modeling (FDM) process parameters on strength of built parts using Taguchi's design of experiments, *International Journal of Advanced Manufacturing Technology*, Vol 101, 1215-1226, doi: [10.1007/s00170-018-3014-6](https://doi.org/10.1007/s00170-018-3014-6).
- [89] Torres, J., Coteló, J., Karl, J., Gordon, A.P. (2015). Mechanical property optimization of FDM PLA in shear with multiple objectives, *Journal of The Minerals, Metals & Materials Society*, Vol. 67, 1183-1193, doi: [10.1007/s11837-015-1367-y](https://doi.org/10.1007/s11837-015-1367-y).
- [90] Deshwal, S., Kumar, A., Chhabra, D. (2020). Exercising hybrid statistical tools GA-RSM, GA-ANN and GA-ANFIS to optimize FDM process parameters for tensile strength improvement, *CIRP Journal of Manufacturing Science and Technology*, Vol. 31, 189-199, doi: [10.1016/j.cirpj.2020.05.009](https://doi.org/10.1016/j.cirpj.2020.05.009).
- [91] Wang, C.C., Lin, T.-W., Hu, S.-S. (2007). Optimizing the rapid prototyping process by integrating the Taguchi method with the gray relational analysis, *Rapid Prototyping Journal*, Vol 13, No. 5, 304-315, doi: [10.1108/13552540710824814](https://doi.org/10.1108/13552540710824814).

Evolutionary game analysis of company collaborative strategy in cloud manufacturing platform environment

Xiao, M.^{a,*}, Tian, Z.Y.^a

^aShenyang University of Technology, School of Management, Shenyang, P.R. China

ABSTRACT

The collaboration between manufacturing companies and demand companies is the focus of effective operation of cloud manufacturing platform. The evolutionary game model of manufacturing company, demand company and cloud platform was established, and the strategy stability of the three parties was analyzed in this paper. Based on Lyapunov discrimination method, the equilibrium points of the system were explored, and the simulation was applied to analyze the influence of key factors in the evolution process by MATLAB2021a. The results show that: (1) The evolution of company collaborative cooperation strategies in the cloud platform environment is staged; (2) The collaborative subsidy to the manufacturing company and the demand company by the cloud platform, the collaborative effort degree of the manufacturing company and the demand company, the value-added profits of the manufacturing company, the penalties and profits of the manufacturing company's speculation behavior, the loss of information leakage of demand company, and the government's subsidy for cloud platform supervision are important factors that affect the strategies of each subject; (3) The establishment of the cloud platform supervision mechanism can promote collaboration between the manufacturing company and the demand company. The results of the study can provide a beneficial strategic decision guidance for the development of the cloud manufacturing platform.

ARTICLE INFO

Keywords:
Cloud manufacturing platform;
Manufacturing company;
Collaborative cooperation;
Evolutionary game;
Simulation;
MATLAB programming platform

**Corresponding author:*
mengxiao@sut.edu.cn
(Xiao, M.)

Article history:
Received 15 March 2022
Revised 17 August 2022
Accepted 29 August 2022



Content from this work may be used under the terms of the Creative Commons Attribution 4.0 International License (CC BY 4.0). Any further distribution of this work must maintain attribution to the author(s) and the title of the work, journal citation and DOI.

1. Introduction

With the integration of Internet of Things and Internet of services with manufacturing, the production systems of the fourth industrial revolution are undergoing renovation [1]. The cloud manufacturing is becoming a service-oriented manufacturing mode for the development of advanced manufacturing [2]. With the good communication channels and expanded communication fields, the cloud manufacturing platform transforms the companies on the platform from a relatively closed self-centered and self-organization system to an open innovation system with cooperation, which is an effective implementation of the strategy of "Internet + Manufacturing". In the cloud platform, capacity sharing changes the traditional manufacturing mode, breaks the balance of the original production system, and transforms the roles of companies and users from the traditional separation mode of producer and consumer to the co-creators of products, improving the technical performance and reducing the purchase price [3]. The relationship between supplier and demander has changed from simple value exchange to value co-creation.

Shared manufacturing based on the cloud platform has attracted the attention of relevant scholars and industrialists [4], but the development of cloud platform is still in the exploratory stage, and how to develop cloud manufacturing platform is still a common concern of platform

operators and users. However, in the process of cloud platform application, some problems restricting companies' cloud adoption are gradually exposed [5]. While company collaboration is facilitated, large-scale resource sharing implemented in cloud platforms may widen the credibility gap [6]. In the process of cooperation, the situation of "free-riding" in which one partner only benefits and does not invest often occurs [7]. This reduces the effectiveness of the cloud platform to create value for companies and is not conducive to the promotion of shared innovative ideas in the system, which requires certain supervision. Facing the market environment in which the scale of companies entering the cloud platform is gradually expanding, it is necessary to make an in-depth analysis on the strategies to promote the collaborative cooperation of companies in the cloud platform.

Therefore, from the perspective of cooperation and supervision of the cloud platform, this study systematically analyzes the promotion effect of the subsidy and penalty mechanism of the cloud platform and the efforts of manufacturing company and demand company on company collaboration with the evolutionary game method, which can provide some guidance for the prosperous sharing economy and the healthy development of cloud manufacturing platform.

2. Literature review

The existing researches on cloud platform mainly focus on the business model of cloud platform, the relationship between the supply and the demand in cloud platform and the supervision of cloud platform.

The cloud platform integrates sharing with the internet, expanding small-scale sharing based on strong ties to large-scale sharing based on weak ties. Therefore, the sharing based on the cloud platform breaks through the traditional sharing behavior and becomes a more macroeconomic sharing. In the sharing economy, the cloud platform plays the role of digital media to match supply and demand. Some scholars have proposed that platform services based on the network environment will gradually become the mainstream mode of the modern service industry. Compared with traditional business mode, cloud platforms can assist buyers and sellers to match and connect faster, provide a more economical mode to increase customer value, create competitive advantage and transform business processes to increase industry profits [8], which is more consistent with the concept of sustainable development. The cloud manufacturing can realize customization and modularization of resources in the cloud platform [9], and the multi-user-oriented manufacturing service distribution [2]. Many scholars have discussed the mode of cloud manufacturing. Woo *et al.* [10] believed that intelligent cloud manufacturing platform can improve the utilization efficiency of resources in platform network sharing and provide manufacturing services on demand. Barenji *et al.* [11] found that various departments in the platform can use joint design to achieve effective communication across regions and reach perfect cooperative target by using the method of the case study. Zhang *et al.* [12] proposed that the machine system based on cloud platform can customize the architecture of intelligent manufacturing of products. Li *et al.* [13] thought that industrial robots were the service objects of the internet platform deriving from the industrial mode of "government procurement and leasing". Xu *et al.* [14] and Wu and Zhang [15] proposed the design scheme of the comprehensive platform for information services provided by supply chain participants based on the ethereum block-chain for intelligent manufacturing. Xiao *et al.* [16] suggested a service resource matching method by combining the characteristics of manufacturing service task on cloud platform, such as relevance, synergy and diversity. The construction and mode of cloud manufacturing platforms have attracted more and more scholars' attention.

Based on big data and artificial intelligence, the digital cloud platform focuses on the resource sharing of bilateral participants and is an effective carrier to achieve value creation of resource sharing service system. In the cloud platform, the main subject of supply and demand can give full play to the effective utilization of resources [17], form complementary advantages, reduce energy consumption [18], and play a guiding role in innovation. The services of cloud platforms have the characteristics of network externality, and integration, functionality and derivation of scientific and technological resources [19]. The researches on cloud platforms have found that

the network effects generated by cloud platforms improve the competitive advantages and profits of the platforms [20], and the active cooperation of service providers can create higher benefits for both parties. Upgrading of manufacturing networks through the cloud platform has become the mode adopted by many manufacturing companies, which is also the reason that drives them to join the cloud manufacturing platform [21]. At the same time, product design, manufacturing network [22], competitive pressures, manager's influence, compatibility and applicability all play the critical roles in the cloud platform operation [9]. Collaboration is the key to the success of cloud platforms [23]. Ren *et al.* [24] suggested the service composition method because of synergies in allusion to social synergy characteristics of manufacturing services, and described five relationships of service networks. Company collaboration in the cloud platform is a complex system engineering [25]. How to effectively promote this synergistic relationship is still in the exploratory stage.

While the cloud manufacturing platform brings many conveniences to the development of the manufacturing industry, it also produces certain negative effects. For example, intelligent manufacturing requires the sharing of data and information, which not only leads to the risk of information exchange [26], but also brings issues such as the security of cloud platform data and information [11] and the complexity of trust relationships between cooperating subjects [27], making it difficult to ensure the credibility and responsibility of cross-company production activities [28]. Some scholars have proposed that the complexity of service upgrade would initiate cognitive bias behavior of organizational participants to jeopardize the accomplish of serviceization within the organization [29]. With the increase in the number of cloud manufacturing platform products, platform services focus more on communication and coordination between service providers and consumers, while incentive and punishment mechanisms are not well established [30]. All these make it difficult for platform supervision to promote its healthy development. Scholars have realized the necessity of effective monitoring of cloud platforms [30], and proposed some monitoring methods such as consensus mechanism of service capability proof [5]. Even if the existing supervision methods are not perfect and need to be further explored, it has been recognized by scholars that company coordination still needs to be managed, which the platform is responsible for [31, 32], and one of the autonomous cycles of the platform is believed to allow self-supervision of the coordination process [33].

3. Model building

3.1 Model description and assumption

In cloud manufacturing environment, a variety of manufacturing resources are organized by the platform to enhance the competitiveness of supply chain and realizes on-demand matching between resource demanders and suppliers based on unified management and operation, and finally completes the full life cycle of manufacturing. In this study, a collaborative cooperation multi-agent game model of cloud platform, manufacturing company and demand company is constructed. The logical relationship of the subjects in cloud manufacturing platform is shown in Fig. 1.

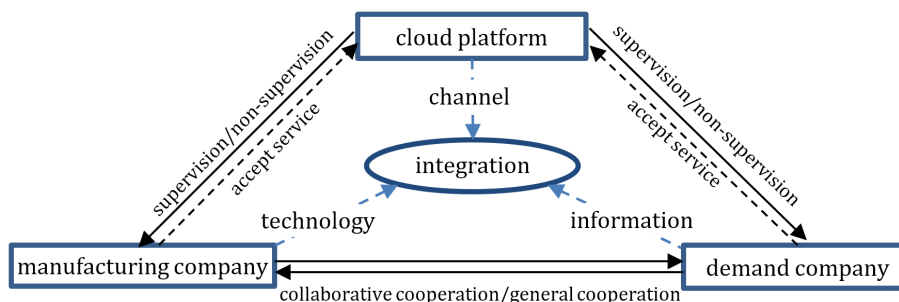


Fig. 1 Logical relationship of game model in the cloud platform environment

For the purpose of studying behavioral strategies of three-party game subjects of cloud platform, manufacturing company and demand company, the following assumptions are proposed.

Assumption 1: There are three participants in the evolutionary game model, namely the cloud platform, the manufacturing company and the demand company, and they take the maximization of their respective benefits as the goal in decision-making. Due to the characteristics of bounded rational subjects, each subject achieves the optimal strategy with keeping learning in the process and adjusts the strategy based on the strategic choice of the other parties and their benefits. The game process is repeated and dynamic. The proportion of manufacturing company collaborative cooperation is indicated as x , and the proportion of general cooperation is indicated as $1 - x$; the proportion of demand company collaborative cooperation is indicated as y , and the proportion of general cooperation is indicated as $1 - y$; the proportion of cloud platform supervision is indicated as z , and the proportion of non-supervision is indicated as $1 - z$; where $0 \leq x \leq 1, 0 \leq y \leq 1, 0 \leq z \leq 1$.

Assumption 2: The government actively promotes cloud manufacturing platform, and will subsidize platform supervision and the collaborative cooperation behavior of manufacturing company and demand company. The payoff of the normal operation of the cloud platform without supervision is E . When implementing the supervision of companies on the platform, the regulatory cost of cloud platform is C_p , and government subsidy for the cloud platform is S_p . If both manufacturing company and demand company choose the collaborative cooperation strategy, it will bring the value-added benefits F_p to the cloud platform.

Assumption 3: When cloud platform chooses the supervision strategy, if manufacturing company or the demand company chooses to collaboratively cooperate, the degree of collaborative effort of the manufacturing company is set as α ($0 < \alpha \leq 1$), and the degree of collaborative effort of the demand company is set as β ($0 < \beta \leq 1$). The cloud platform provides subsidies to manufacturing company and demand company on behalf of the government, and the subsidies are proportional to the effort of the company, denoted as αS_M and βS_C respectively.

Assumption 4: When both manufacturing company and demand company choose to collaborative cooperation, they can obtain value-added collaborative profits. The value-added profit of collaborative cooperation of manufacturing company is W_M , and that of demand company is W_C . The amount of the collaborative cooperation profit is proportional to the effort of the company, and the value-added collaborative profits of manufacturing company is αW_M and the value-added collaborative profits of demand company is βW_C .

Assumption 5: When the manufacturing company chooses collaborative cooperation and the demand company chooses general cooperation, due to the hardware upgrades carried out by the manufacturing company, even if the demand company does not collaborate cooperate with it, the manufacturing company will have a certain additional profit T . The value-added profit of the manufacturing company is proportional to its effort, so it can be described as αT . At this time, the demand company cannot obtain additional profits.

Assumption 6: When the manufacturing company chooses general cooperation and the demand company chooses collaborative cooperation, because of collaboratively cooperating by providing information, the information leakage loss of the demand company may occur, denoted as V . The loss of demand company is proportional to its collaborative effort, and the loss amount is expressed as βV . At this time, the general cooperation as "free-rider" behavior can bring the speculative profit Q to the manufacturing company, and the amount of the speculative profit is proportional to the effort of the demand company, which is expressed as βQ . The punishment mechanism in cooperation can effectively curb the occurrence of "free-rider" behavior. Therefore, the manufacturing company should be punished with the penalty to compensate the collaborative cooperation of the demand company, which is expressed as L_M .

Assumption 7: When both manufacturing company and demand company choose general cooperation, the parties can only obtain the payoffs of general cooperation, which are expressed as R_M and R_C respectively.

On the basis of the above descriptions and assumptions, the strategy game payoff matrix of the three-party is acquired, as illustrated in Table 1.

Table 1 Payoff matrix of three-party subjects

Strategy choice	Demand company	Cloud platform	
		Supervision (z)	Non-supervision (1 - z)
Manufacturing company	Collaborative cooperation (y)	$\alpha W_M + \alpha S_M + R_M$	$\alpha W_M + R_M$
		$\beta W_C + \beta S_C + R_C$	$\beta W_C + R_C$
	General cooperation (1 - y)	$E - C_P + S_P + F_P - \alpha S_M - \beta S_C$	$E + F_P$
		$\alpha S_M + R_M + \alpha T$	$R_M + \alpha T$
	Collaborative cooperation (y)	R_C	R_C
		$E - C_P + S_P - \alpha S_M$	E
General cooperation (1 - x)	Collaborative cooperation (y)	$R_M - L_M + \beta Q$	$R_M + \beta Q$
	General cooperation (1 - y)	$\beta W_C + R_C - \beta V + L_M$	$R_C - \beta V$
		$E - C_P + S_P - \beta S_C$	E
		R_M	R_M
		R_C	R_C
		$E - C_P + S_P$	E

3.2 Model analysis

The stability and evolution path of three subjects strategies are explored by the stability theory of differential equations, and two conditions should be satisfied for the stable point of replication dynamic equation: $F(x) = 0$, and $\frac{dF(x)}{dx} < 0$.

Replication dynamic analysis of manufacturing company strategy

The expected payoff of manufacturing company carrying out collaborative cooperation strategy is set as U_{11} , and the expected payoff of manufacturing company carrying out general cooperation strategy is set as U_{12} , which are defined as follows:

$$U_{11} = yz(\alpha W_M + \alpha S_M + R_M) + (1 - y)z(\alpha S_M + R_M + \alpha T) + y(1 - z)(\alpha W_M + R_M) + (1 - y)(1 - z)(R_M + \alpha T) \tag{1}$$

$$U_{12} = yz(R_M - L_M + \beta Q) + (1 - y)zR_M + y(1 - z)R_M + (1 - y)(1 - z)R_M \tag{2}$$

$$U_1 = xU_{11} + (1 - x)U_{12} \tag{3}$$

The replication dynamic equation of manufacturing company strategy is as follows:

$$F(x) = \frac{dx}{dt} = x(U_{11} - U_1) = x(1 - x)(U_{11} - U_{12}) = x(1 - x)(y(\alpha W_M - \alpha T - \beta Q) + z\alpha S_M + yzL_M + \alpha T) \tag{4}$$

$$F'(x) = \frac{dF(x)}{dx} = (1 - 2x)(y(\alpha W_M - \alpha T - \beta Q) + z\alpha S_M + yzL_M + \alpha T) \tag{5}$$

Assume $W(z) = y(\alpha W_M - \alpha T - \beta Q) + z\alpha S_M + yzL_M + \alpha T$, when $z_0 = \frac{(y-1)\alpha T - y(\alpha W_M - \beta Q)}{\alpha S_M + yL_M}$, proposition 1 is established.

Proposition 1: when $0 < z < z_0 < 1$, the evolutionary stable state of x tends to 0, the stable strategy of the manufacturing company is general cooperation. When $0 < z_0 < z < 1$, the evolutionary stable state of x tends to 1, the stable strategy of the manufacturing company is collaborative cooperation.

Proof: $W(z)$ increases monotonically over the interval. When $z = z_0$, $W(z) = 0$, $F(x) = 0$, and $F'_x(x) = 0$, so $x \in [0,1]$ is in the stable state, and there is no fixed stable strategy in the interval; When $0 < z < z_0 < 1$, $W(z) < 0$, $F_x(0) = 0$, and $F'_x(0) < 0$, so $x = 0$ has stability; When $0 < z_0 < z < 1$, $W(z) > 0$, $F_x(1) = 0$, and $F'_x(1) < 0$, so $x = 1$ has stability.

The phase diagram of the manufacturing company strategy choice is obtained according to the above analysis, as illustrated in Fig. 2.

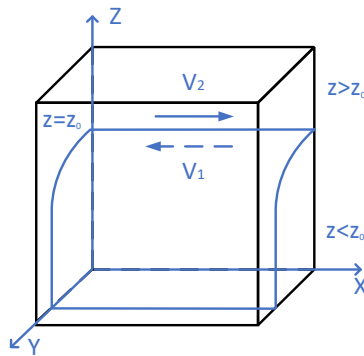


Fig. 2 Phase diagram of the manufacturing company strategy choice

Inference 1: When the values of S_M , W_M , L_M and T raise while other parameters keep constant, manufacturing company will approach collaborative cooperation strategy. In common, when the values of β and Q raise, manufacturing company will approach general cooperation strategy.

Proof: Since $z_0 = \frac{(y-1)\alpha T - y(\alpha W_M - \beta Q)}{\alpha S_M + y L_M}$, the value of z_0 will fall with the raising of the values of S_M , W_M , L_M and T , and the volume of V_2 changes inversely with the value of z_0 . The enlarge of V_2 shows that the manufacturing company is more inclined to the cooperative cooperation strategy. The value of z_0 will raise with the raising of the values of β and Q , and the volume of V_1 changes the same as the value of z_0 . The enlarge of V_1 shows that the manufacturing company is more inclined to the general strategy. It presents that the proportion of manufacturing company choosing collaborative cooperation is directly proportional to the subsidies for the collaborative cooperation of the manufacturing company, the value-added profits of the manufacturing company when the two sides collaborative cooperate, the speculative penalty of the general cooperation and the additional profit of collaborative cooperation of the manufacturing company, and inversely proportional to the degree of collaborative effort of the demand company and the speculative profit of the general cooperation of the manufacturing company.

Replication dynamic analysis of the demand company strategy

The expected payoff of demand company carrying out collaborative cooperation strategy is set as U_{21} , and the expected payoff of demand company carrying out general cooperation strategy is set as U_{22} , which are defined as follows:

$$U_{21} = xz(\beta W_C + \beta S_C + R_C) + x(1 - z)(\beta W_C + R_C) + (1 - x)z(\beta W_C + R_C - \beta V + L_M) + (1 - x)(1 - z)(R_C - \beta V) \tag{6}$$

$$U_{22} = xzR_C + x(1 - z)R_C + (1 - x)zR_C + (1 - x)(1 - z)R_C \tag{7}$$

$$U_2 = yU_{21} + (1 - y)U_{22} \tag{8}$$

The replication dynamic equation of demand company strategy is as follows:

$$F(y) = \frac{dy}{dt} = y(U_{21} - U_2) = y(1 - y)(U_{21} - U_{22}) = y(1 - y)(x(\beta W_C + \beta V) + z\beta S_C - \beta V + (1 - x)zL_M) \tag{9}$$

$$F'(y) = \frac{dF(y)}{dy} = (1 - 2y)(x(\beta W_C + \beta V) + z\beta S_C - \beta V + (1 - x)zL_M) \tag{10}$$

Assume $W(x) = x(\beta W_C + \beta V) + z\beta S_C - \beta V + (1 - x)zL_M$, when $x_0 = \frac{\beta V - z\beta S_C - zL_M}{\beta W_C + \beta V - zL_M}$, proposition 2 is established.

Proposition 2: When $0 < x < x_0 < 1$, the evolutionary stable point state of y tends to 0, the stable strategy of the demand company is general cooperation. When $0 < x_0 < x < 1$, the evolutionary stable state of y tends to 1, the stable strategy of the demand company is collaborative cooperation.

Proof: $W(x)$ increases monotonically over the interval. When $x = x_0$, $W(x) = 0$, $F(y) = 0$, and $F'_y(y) = 0$, so $y \in [0,1]$ is in the stable state, and there is no fixed stable strategy in the interval; When $0 < x < x_0 < 1$, $W(x) < 0$, $F_y(0) = 0$, and $F'_y(0) < 0$, so $y = 0$ has stability; When $0 < x_0 < x < 1$, $W(x) > 0$, $F_y(1) = 0$, and $F'_y(1) < 0$, so $y = 1$ has stability.

The phase diagram of the demand company strategy choice is obtained according to the above analysis, as illustrated in Fig. 3.

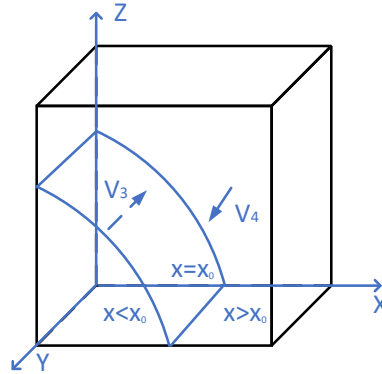


Fig. 3 Phase diagram of the demand company strategy choice

Inference 2: When the values of W_C , S_C and L_M raise while other parameters keep constant, the demand company will approach collaborative cooperation strategy. In common, when the value of V raises, the demand company will approach general cooperation strategy.

Proof: Since $x_0 = \frac{\beta V - z\beta S_C - zL_M}{\beta W_C + \beta V - zL_M}$, the value of x_0 will fall with the raising of the values of S_C , W_C and L_M , and the volume of V_4 changes inversely with the value of x_0 . The enlarge of V_4 shows that the demand company is more inclined to the collaborative cooperation strategy. The value of x_0 will raise with the raising of the value of V , and the volume of V_3 changes the same as the value of x_0 . The enlarge of V_3 shows that the demand company is more inclined to the general cooperation strategy. It presents that the proportion of demand company implementing collaborative cooperation is directly proportional to the subsidies for the collaborative cooperation of the demand company, the value-added profits of the demand company when the two sides collaborative cooperate, and the speculative penalty for the general cooperation of the manufacturing company, inversely proportional to the loss of information leakage of the collaborative cooperation of the demand company.

Replication dynamic stability analysis of the cloud platform strategy

The expected payoff of cloud platform carrying out supervision strategy is set as U_{31} , and the expected payoff of cloud platform carrying out non-supervision strategy is set as U_{32} , which are defined as follows:

$$U_{31} = xy(E - C_P + S_P + F_P - \alpha S_M - \beta S_C) + x(1 - y)(E - C_P + S_P - \alpha S_M) + (1 - x)y(E - C_P + S_P - \beta S_C) + (1 - x)(1 - y)(E - C_P + S_P) \quad (11)$$

$$U_{32} = xy(E + F_P) + x(1 - y)E + (1 - x)yE + (1 - x)(1 - y)E \quad (12)$$

$$U_3 = zU_{31} + (1 - z)U_{32} \quad (13)$$

The replication dynamic equation of cloud platform strategy is as follows:

$$F(z) = \frac{dz}{dt} = z(U_{31} - U_3) = z(1 - z)(U_{31} - U_{32}) = z(1 - z)(S_P - y\beta S_C - x\alpha S_M - C_P) \quad (14)$$

$$F'(z) = \frac{dF(z)}{dz} = (1 - 2z)(S_P - y\beta S_C - x\alpha S_M - C_P) \quad (15)$$

Assume $W(y) = S_P - y\beta S_C - x\alpha S_M - C_P$, when $y_0 = \frac{S_P - x\alpha S_M - C_P}{\beta S_C}$, proposition 3 is established.

Proposition 3: when $0 < y < y_0 < 1$, the evolutionary stable state of z tends to 1, the stable strategy of the cloud platform is supervision. When $0 < y_0 < y < 1$, the evolutionary stable state of z tends to 0, the stable strategy of the cloud platform is non-supervision.

Proof: $W(y)$ decreases monotonically over the interval. When $y = y_0$, $W(y) = 0$, $F(z) = 0$, and $F'_z(z) = 0$, so $z \in [0,1]$ is in the stable state, and there is no fixed stable strategy in the interval; When $0 < y < y_0 < 1$, $W(y) > 0$, $F_z(1) = 0$, and $F'_z(1) < 0$, so $z = 1$ has stability; When $0 < y_0 < y < 1$, $W(y) < 0$, $F_z(0) = 0$, and $F'_z(0) < 0$, so $z = 0$ has stability.

The phase diagram of the cloud platform strategy choice is obtained according to the above analysis, as illustrated in Fig. 4.

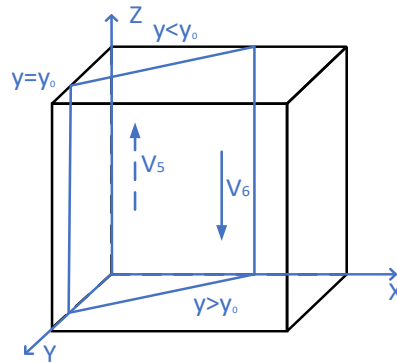


Fig. 4 Phase diagram of the cloud platform strategy choice

Inference 3: When the value of S_P raises while other parameters keep constant, the cloud platform will approach supervision strategy. In common, when the values of α , β , S_C , S_M and C_P raise, the cloud platform will approach non-supervision strategy.

Proof: Since $y_0 = \frac{S_P - x\alpha S_M - C_P}{\beta S_C}$, the value of y_0 will raise with the raising of the value of S_P , and the volume of V_5 changes the same as the value of y_0 . The enlarge of V_5 shows that the cloud platform is more inclined to supervision strategy. The value of y_0 will fall with the raising of the values of α , β , S_C , S_M and C_P , and the volume of V_6 changes inversely with the value of y_0 . The enlarge of V_6 shows that the cloud platform is more inclined to non-supervision strategy increases. It presents that the proportion of cloud platform implementing collaborative cooperation is directly proportional to the government subsidy for the supervision of the cloud platform, and inversely proportional to the degree of collaborative effort of the manufacturing company and the demand company, the subsidies provided by the cloud platform for the collaborative cooperation of the manufacturing company and the demand company and the regulatory cost of the cloud platform.

4. Results and discussion

4.1 Strategy stability analysis of the strategies in evolutionary games

In order to analyze the asymptotic stability of the strategies in evolutionary games, according to Lyapunov method, the eigenvalues of the Jacobian matrix are determined based on the replication dynamic equation of the subject. When the eigenvalues are negative, the equilibrium point is asymptotically stable. The Jacobian matrix of the replication dynamic system is expressed as Eq. 16. The eigenvalues of Jacobian matrix are indicated in Appendix A.

$$J = \begin{bmatrix} F'_x(x) & F'_y(x) & F'_z(x) \\ F'_x(y) & F'_y(y) & F'_z(y) \\ F'_x(z) & F'_y(z) & F'_z(z) \end{bmatrix} \tag{16}$$

The system equilibrium points of three-party evolutionary game are inditacted in Table 2.

Table 2 Strategy stability analysis of evolutionary game system

Equilibrium point	Eigenvalue	Symbol	Stability
E1(0,0,0)	$\alpha T, -\beta V, S_P - C_P$	(+, -, X)	unstable
E2(0,0,1)	$\alpha S_M + \alpha T, \beta S_C - \beta V + L_M, -(S_P - C_P)$	(+, X, X)	unstable
E3(0,1,0)	$\alpha W_M - \beta Q, \beta V, S_P - \beta S_C - C_P$	(X, +, X)	unstable
E4(1,0,0)	$-\alpha T, \beta W_C, S_P - \alpha S_M - C_P$	(-, +, X)	unstable
E5(0,1,1)	$\alpha W_M + \alpha S_M + L_M - \beta Q, -(\beta S_C + L_M - \beta V), -(S_P - \beta S_C - C_P)$	(X, X, X)	ESS in condition I
E6(1,0,1)	$-(\alpha S_M + \alpha T), \beta W_C + \beta S_C, -(S_P - \alpha S_M - C_P)$	(-, +, X)	unstable
E7(1,1,0)	$-(\alpha W_M - \beta Q), -\beta W_C, S_P - \beta S_C - \alpha S_M - C_P$	(X, -, X)	ESS in condition III
E8(1,1,1)	$-(\alpha W_M - \beta Q + \alpha S_M + L_M), -(\beta W_C + \beta S_C), -(S_P - \beta S_C - \alpha S_M - C_P)$	(X, -, X)	ESS in condition II

Note: X denotes uncertain of symbol, ESS denotes the evolutionary stable strategy.
 Condition I: $\alpha(S_M + W_M) < \beta Q - L_M, \beta S_C + L_M > \beta V, S_P > \beta S_C + C_P$
 Condition II: $\alpha(S_M + W_M) > \beta Q - L_M, S_P > \beta S_C + \alpha S_M + C_P$
 Condition III: $\alpha W_M > \beta Q, S_P < \beta S_C + \alpha S_M + C_P$

When $\alpha(S_M + W_M) < \beta Q - L_M, \beta S_C + L_M > \beta V, S_P > \beta S_C + C_P$, if the difference between the speculative profit and the speculative penalty when the manufacturing company chooses general cooperation is more than the sum of the additional profit of the collaborative cooperation and the cooperative subsidy of the cloud platform, then the manufacturing company tends to choose the general cooperation strategy. When the sum of the platform subsidy for the demand company and the speculative punishment of the manufacturing company is more than the information leakage risk loss of the demand company, then the demand company tends to choose the collaborative cooperation strategy. If the government's subsidy for cloud platform supervision is more than the sum of the cloud platform regulatory cost and the subsidy for the demand company, the cloud platform tends to choose supervision strategy. As a result, the stable evolution strategy of the three-party subjects is E5(general cooperation, collaborative cooperation, supervision).

When $\alpha(S_M + W_M) > \beta Q - L_M$ and $S_P > \beta S_C + \alpha S_M + C_P$, on the basis of condition I, if the sum of the synergistic subsidy and synergistic benefit of the manufacturing company is more than the difference between the speculative profit and the speculative penalty of the manufacturing company, the manufacturing company tends to choose the collaborative cooperation. If the government's subsidies for cloud platform supervision are still more than the sum of the regulatory costs of cloud platform and the subsidies for manufacturing company and demand company, the cloud platform will continue to choose the supervision strategy. When the manufacturing company chooses collaborative collaboration and the cloud platform chooses supervision, the value-added profits of the demand company's collaborative cooperation are greater, so the collaborative cooperation strategies are chosen. Therefore, the stable evolution strategy of the three-party subjects is E8 (collaborative cooperation, collaborative cooperation, supervision).

When $\alpha W_M > \beta Q$, and $S_P < \beta S_C + \alpha S_M + C_P$, on the basis of condition II, if the manufacturing company and the demand company improve their collaborative efforts, the sum of the regulatory cost and the subsidies for the manufacturing company and demand company of the cloud platform is more than the government's subsidies for cloud platform supervision, the cloud platform tends to non-supervision strategy. If the value-added profits of the manufacturing company's collaborative cooperation are more than the profits of the manufacturing company's speculative behavior, the value-added profits of the demand company are larger, and the manufacturing company and the demand company also tend to adopt the collaborative cooperation strategy. Therefore, the stable evolution strategy of the three-party subjects is E7 (collaborative cooperation, collaborative cooperation, non-supervision).

4.2 Numerical simulation analysis

To test strategic stability of three-party evolutionary game, the model parameters are assigned values based on the real situation, and MATLAB2021a is used for numerical simulation.

Equilibrium steady state of the model

When condition I is met, the model parameters are assigned as followings: $C_P = 30, S_P = 50, W_M = 30, S_M = 20, \alpha = 0.1, Q = 25, T = 15, L_M = 5, W_C = 30, S_C = 20, \beta = 0.5, V = 26$; when condition II is

met, $S_M = 40$, $\alpha = 0.2$, and other parameters are the same with condition I; when condition III is met, $\alpha = 0.6$, $\beta = 0.6$, $S_C = 40$, and other parameters are the same with condition II. The evolution results of the data simulation over time are shown in Fig. 5.

According to Fig. 5, in the early stage of the establishment of the cloud platform, the profits of collaborative cooperation are less than the speculative profits of general cooperation for the manufacturing company. Therefore, driven by the interests, the manufacturing company will gradually stabilize in the general cooperation strategy. When the manufacturing company generally cooperates, if the government's supervision subsidy is more than the supervision investment for the cloud platform, the cloud platform will stabilize in the supervision strategy. So the evolutionary game system will be stable in the strategy combination E5 (0,1,1). As the supervision mechanism of the cloud platform is gradually established, with the increase of subsidies obtained by manufacturing company for collaborative cooperation, the level of collaborative effort of company will increase, and manufacturing company will be stable in collaborative cooperation strategy, so the evolutionary game system is stable in the strategy combination E8 (1,1,1). In the improvement stage of cloud platform, with the increase of collaborative subsidies for the demand company, the degree of collaborative effort between manufacturing company and demand company is further increased, the proportion of cloud platform supervision is reduced, and finally stabilized in the non-supervision strategy, so the evolutionary game system will be stable in the strategy combination E7 (1,1,0). This means that as long as both the manufacturing company and the demand company have a long-term development concept and can recognize the benefits brought by collaboration, the cloud platform can make the two parties collaborate without supervision.

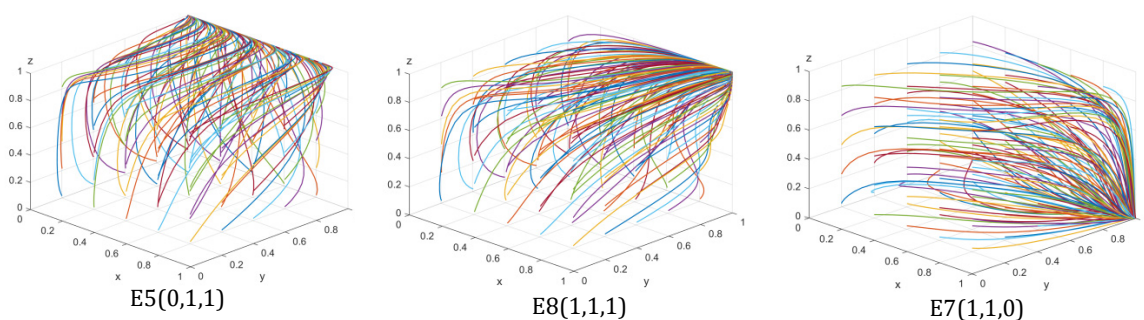


Fig. 5 System evolution stability at equilibrium points

The influence of the subsidies and the value-added profits for the collaborative cooperation of the manufacturing company

On the basis of condition I, if $S_M = \{20, 30, 50, 60\}$, and the simulation results of three-party evolutionary game are indicated in Fig. 6a. If $W_M = \{30, 45, 60, 80\}$, the simulation results of the three-party evolutionary game are indicated in Fig. 6b.

According to Fig. 6a, with the raising of the subsidy of cloud platform for manufacturing company, the proportion of the manufacturing company to choose collaborative cooperation increases. The strategy of the manufacturing company will shift from general cooperation to collaborative cooperation, and the critical value of changing the strategy is $S_M = 45$. Due to the change of manufacturing company's strategy, the evolution strategy combination will change from E5 (general cooperation, collaborative cooperation, supervision) to E8 (collaborative cooperation, collaborative cooperation, supervision). According to Fig. 6b, with the increase of the value-added profits of manufacturing company in collaborative cooperation, the proportion of manufacturing company choosing collaborative cooperation increases. The strategy of the manufacturing company will shift from general cooperation to collaborative cooperation, and the critical value for changing the strategy is $W_M = 55$. Due to the change of manufacturing company's strategy, the evolution strategy combination will change from E5 (general cooperation, collaborative cooperation, supervision) to E8 (collaborative cooperation, collaborative cooperation, supervision).

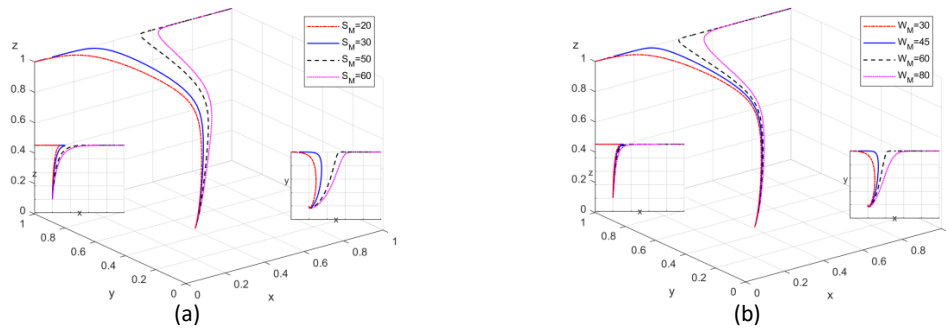


Fig. 6 Influence of the subsidies and the value-added profits for the collaborative cooperation of manufacturing company on strategy evolution

The influence of the degree of collaborative effort of the manufacturing company and the demand company

On the basis of condition I, if $\alpha = \{0.10, 0.13, 0.20, 0.35, 0.55, 0.65\}$, and the simulation results of three-party evolutionary game are indicated in Fig. 7a. If $\beta = \{0.2, 0.3, 0.41, 0.5, 0.85, 0.95\}$, the simulation results of three-party evolutionary game are indicated in Fig. 7b.

According to Fig. 7a, with the increase of the collaborative efforts of the manufacturing company, three evolutionary stable states may appear in the system. The critical value of changing the strategy of manufacturing company is $\alpha_1 = 0.15$, and the critical value of changing the strategy of the cloud platform is $\alpha_2 = 0.5$. When $0.15 < \alpha < 0.5$, the proportion of the manufacturing company choosing collaborative cooperation increases with the increase of α . The strategy of the manufacturing company will shift from general cooperation to collaborative cooperation, the evolution strategy combination will change from E5 (general cooperation, collaborative cooperation, supervision) to E8 (collaborative cooperation, collaborative cooperation, supervision). When $\alpha > 0.5$, the proportion of the cloud platform choosing supervision decreases with the increase of α . The strategy of the cloud platform will change from supervision to non-supervision, and the evolution strategy combination will change from E8 (collaborative cooperation, collaborative cooperation, supervision) to E7 (collaborative cooperation, collaborative cooperation, non-supervision).

According to Fig. 7b, with the change of the degree of collaborative effort of the demand company, two evolutionary stable states and an unstable state may appear in the system. The critical value of changing the strategy of manufacturing company is $\beta_1 = 0.4$, and the critical value of changing the strategy of demand company is $\beta_2 = 0.83$. When $0.4 < \beta < 0.83$, the proportion of manufacturing company choosing collaborative cooperation increases with the increase of β . The strategy of the manufacturing company will change from general cooperation to collaborative cooperation, and the evolution strategy combination will change from E5 (general cooperation, collaborative cooperation, supervision) to E8 (collaborative cooperation, collaborative cooperation, supervision). When $\beta > 0.83$, the proportion of the demand company will decrease with the increase of β . The strategy of the demand company will tend to the unstable state, and the evolution strategy combination will be also in an unstable state.

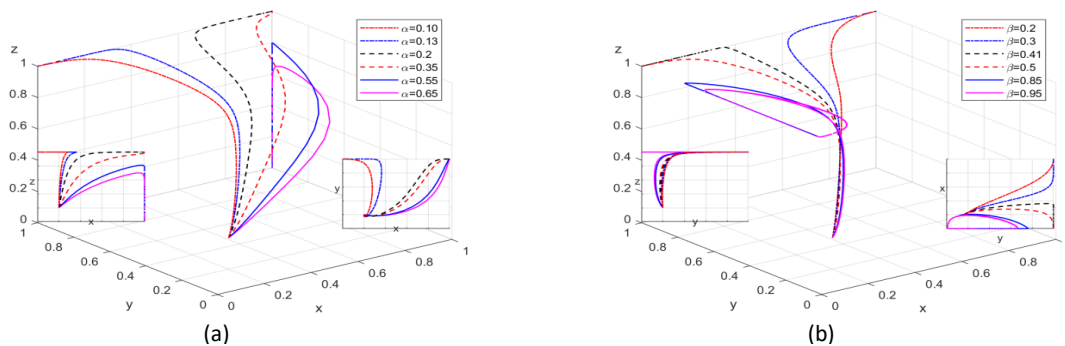


Fig. 7 The influence of the degree of collaborative effort of the manufacturing company and demand company on strategy evolution

The influence of the speculative penalty and profit of the general cooperation of the manufacturing company

On the basis of condition I, if $L_M = \{5, 7, 10, 15\}$, and the simulation results of three-party evolutionary game are indicated in Fig. 8a. If $Q = \{10, 15, 21, 25\}$, the simulation results of three-party evolutionary game are indicated in Fig. 8b.

According to Fig. 8a, with the increase of the speculative penalty of manufacturing company, the proportion of manufacturing company to choose collaborative cooperation increases. The strategy of the manufacturing company will shift from general cooperation to collaborative cooperation, and the critical value of changing the strategy is $L_M = 7.5$. Due to the change of manufacturing company's strategy, the evolution strategy combination will change from E5 (general cooperation, collaborative cooperation, supervision) to E8 (collaborative cooperation, collaborative cooperation, supervision). According to Fig. 8b, with the decrease of the speculative profits of manufacturing company, the proportion of manufacturing company to choose collaborative cooperation increases. The strategy of the manufacturing company will shift from general cooperation to collaborative cooperation, and the critical value of changing the strategy is $Q = 20$. Due to the change of manufacturing company's strategy, the evolution strategy combination will change from E5 (general cooperation, collaborative cooperation, supervision) to E8 (collaborative cooperation, collaborative cooperation, supervision).

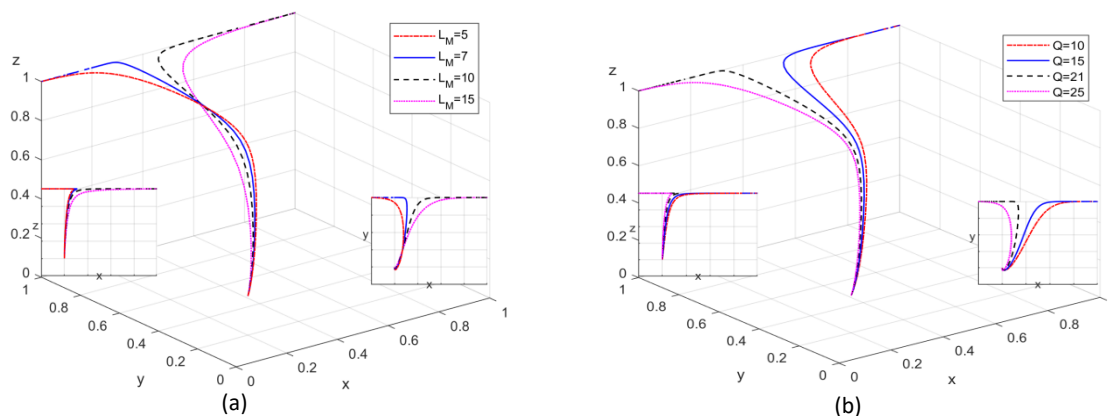


Fig. 8 The influence of the speculative penalty and profit of the general cooperation of the manufacturing company on strategy evolution

The influence of the loss of information leakage and the subsidies for the collaborative cooperation of the demand company

On the basis of condition II, if $V = \{15, 26, 40, 60\}$, and the simulation results of three-party evolutionary game are indicated in Fig. 9a. If $S_C = \{10, 20, 30, 35\}$, the simulation results of three-party evolutionary game are indicated in Fig. 9b.

According to Fig. 9a, with the increase of the information leakage loss of demand company, the proportion of manufacturing company to choose collaborative cooperation increases, the proportion of cloud platform to choose supervision increases, and the proportion of demand company to choose collaborative cooperation decreases. The evolution strategy combination will tend to E8 (collaborative cooperation, collaborative cooperation, supervision). According to Fig. 9b, the strategies of the cloud platform and the manufacturing company will be affected by the collaborative subsidies of the demand company. The critical value of changing the strategy is $S_C = 24$. When $S_C < 24$, with the increase of collaborative subsidies of demand company, the proportion of manufacturing company and demand company to choose collaborative cooperation increases, and the proportion of cloud platform to choose supervision increases. The evolution strategy combination will tend to E8 (collaborative cooperation, collaborative cooperation, supervision). When $S_C > 24$, with the increase of collaborative subsidies of demand company, the proportion of cloud platform supervision and the manufacturing company collaborative cooperation decreases, the cloud platform and the manufacturing company cannot evolve to a stable state, and the system cannot evolve to a stable state.

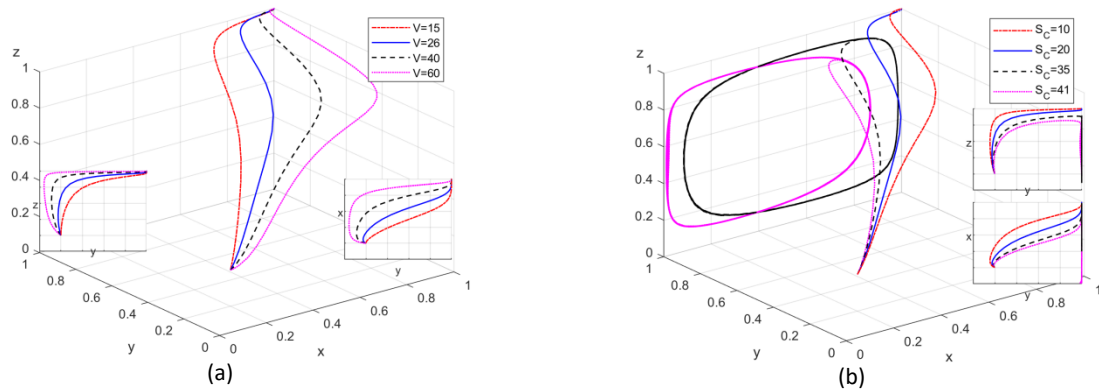


Fig. 9 The influence of the loss of information leakage and the subsidies for the collaborative cooperation of the demand company on strategy evolution

The influence of the government subsidy for the cloud platform supervision

On the basis of condition III, if $S_p = \{50, 70, 80, 90\}$, and the simulation results of three-party evolutionary game are indicated in Fig. 10.

According to Fig. 10, when the government subsidies for cloud platform supervision decrease, the proportion of the platform to choose supervising decreases. The strategy of the cloud platform will shift from supervision to non-supervision, and the critical value of changing the strategy is $S_p = 78$. Due to the change of cloud platform's strategy, the evolution strategy combination will change from E8 (collaborative cooperation, collaborative cooperation, supervision) to E7 (collaborative cooperation, collaborative cooperation, non-supervision).

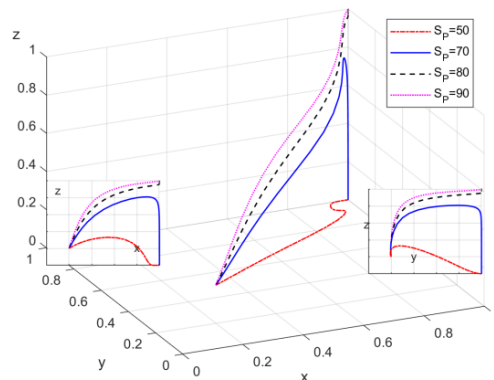


Fig. 10 The influence of the government subsidy for the cloud platform supervision on strategy evolution

5. Conclusion

This study constructed a three-party collaborative evolutionary game model with the cloud platform, the manufacturing company and the demand company, and the main conclusions are as follows:

- The strategy combination evolution of company collaborative cooperation in the cloud platform environment is staged. In the initial stage of cloud platform, since the manufacturing company can obtain free-riding profits in the process of cooperation, it tends to general cooperation strategy. However, with the support of platform subsidies, reward and punishment, the demand company can obtain better profits by sharing information and inclined to choose collaborative cooperation, and the platform tends to supervision due to government subsidies, so the system will be stable in the strategy combination of E5 (general cooperation, collaborative cooperation, supervision). With the increase of penalty costs and synergy profits of manufacturing company, the manufacturing company also tends to choose collaborative cooperation. Therefore, in the mid stage of cloud plat-

form, the system will be stable in the strategy combination of E8(collaborative cooperation, collaborative cooperation, supervision) depending on the supervision measures of the platform. When the cloud platform runs smoothly, manufacturing company and demand company can take advantage of the platform to integrate resources, the degree of company collaborative effort gradually increases, and the platform tends to implement non-supervision strategy. The platform has reached mature stage, in which the spontaneous collaboration of manufacturing company and demand company can form the effective operation of the cloud platform.

- The collaborative subsidy to manufacturing company, the value-added profit of the manufacturing company, the degree of collaborative effort of the manufacturing company and the demand company, and the penalty and profits of the manufacturing company's speculation are the important factors that affect the cooperation strategy of the manufacturing company. By appropriately increasing the subsidy to manufacturing company, the value-added profit of manufacturing company, the penalty for free-riding speculation of manufacturing company, and reducing the speculative profit of manufacturing company, and promoting the degree of collaborative effort of manufacturing company, the strategy of the manufacturing company will be changed from general cooperation to collaborative cooperation.
- The collaborative subsidy to demand company, the degree of collaborative efforts of demand company, the loss of information leakage of demand company, and the speculation penalty of manufacturing company are important factors that affect the cooperation strategy of demand company. With the increase of collaborative subsidy of demand company, the appropriate improvement of the level of collaborative efforts of demand company, the reduction of information leakage loss of demand company and the increase of speculative penalty of manufacturing company, the proportion of demand company to collaborative cooperation increases, and demand company gradually stabilizes in collaborative cooperation strategy.
- The degree of collaborative efforts of manufacturing company and demand company and the government's subsidy for cloud platform supervision are important factors that affect the platform supervision strategy. When the degrees of collaborative effort of manufacturing company and demand company are low, raising the government's regulatory subsidy for cloud platform can gradually increase the proportion of cloud platform supervision and cloud platform stabilize in the supervision strategy. However, as the degrees of collaborative efforts of manufacturing company and demand company increase, and the government's subsidy for cloud platform supervision reduces, the strategy of cloud platform can be changed from supervision to non-supervision.

Acknowledgement

This study was financially supported by 2023 LiaoNing Provincial Federation Social Science Circles Project (2023lslybkt-095), Social Science Planning Fund of Liaoning Province (L19BGL029), Social Science Planning Fund of Liaoning Province (L22AJY012), 2022 Shenyang Science and Technology Innovation Think Tank Decision-making Consulting Project (No.52), Key Project Fund of Scientific Research of Shenyang University of Technology (No.ZDZRGD2020041).

References

- [1] Gerrikagoitia, J.K., Unamuno, G., Urkia, E., Serna, A. (2019). Digital manufacturing platforms in the Industry 4.0 from private and public perspectives, *Applied Sciences*, Vol. 9, No. 14, Article No. 2934, doi: [10.3390/app9142934](https://doi.org/10.3390/app9142934).
- [2] Wang, T., Li, C., Yuan, Y., Liu, J., Adeleke, I.B. (2019). An evolutionary game approach for manufacturing service allocation management in cloud manufacturing, *Computers & Industrial Engineering*, Vol. 133, 231-240, doi: [10.1016/j.cie.2019.05.005](https://doi.org/10.1016/j.cie.2019.05.005).
- [3] Gnoni, M.G., Bragatto, P.A., Milazzo, M.F., Setola, R. (2020). Integrating IoT technologies for an "intelligent" safety management in the process industry, *Procedia Manufacturing*, Vol. 42, 511-515, doi: [10.1016/j.promfg.2020.02.040](https://doi.org/10.1016/j.promfg.2020.02.040).

- [4] Sahu, A.K., Sahu, A.K., Sahu, N.K. (2020). A review on the research growth of Industry 4.0: IIoT business architectures benchmarking, *International Journal of Business Analytics*, Vol. 7, No. 1, 77-97, doi: [10.4018/IJBAN.2020010105](https://doi.org/10.4018/IJBAN.2020010105).
- [5] Zhang, Y., Zhang, L., Liu, Y., Luo, X. (2021). Proof of service power: A blockchain consensus for cloud manufacturing, *Journal of Manufacturing Systems*, Vol. 59, 1-11, doi: [10.1016/j.jmsy.2021.01.006](https://doi.org/10.1016/j.jmsy.2021.01.006).
- [6] Yu, C., Jiang, X., Yu, S., Yang, C. (2020). Blockchain-based shared manufacturing in support of cyber physical systems: Concept, framework, and operation, *Robotics and Computer-Integrated Manufacturing*, Vol. 64, Article No. 101931, doi: [10.1016/j.rcim.2019.101931](https://doi.org/10.1016/j.rcim.2019.101931).
- [7] Hu, Y.L., Han, Q.L. (2021). Evolutionary game analysis on value co-creation of product service system, *Management Review*, Vol. 33, No. 6, 242-254, doi: [10.14120/j.cnki.cn11-5057/f.2021.06.021](https://doi.org/10.14120/j.cnki.cn11-5057/f.2021.06.021).
- [8] Kumar, A.S., Iyer, E. (2019). An industrial IoT in engineering and manufacturing industries–Benefits and challenges, *International Journal of Mechanical and Production Engineering Research and Development*, Vol. 9, No. 2, 151-160, doi: [10.24247/ijmperdapr201914](https://doi.org/10.24247/ijmperdapr201914).
- [9] Aziz, M.H., Qamar, S., Khasawneh, M.T., Saha, C. (2020). Cloud manufacturing: A myth or future of global manufacturing, *Journal of Manufacturing Technology Management*, Vol. 31, No. 7, 1325-1350, doi: [10.1108/jmtm-10-2019-0379](https://doi.org/10.1108/jmtm-10-2019-0379).
- [10] Woo, J., Shin, S.-J., Seo, W., Meilanitasari, P. (2018). Developing a big data analytics platform for manufacturing systems: Architecture, method, and implementation, *International Journal of Advanced Manufacturing Technology*, Vol. 99, 2193-2217, doi: [10.1007/s00170-018-2416-9](https://doi.org/10.1007/s00170-018-2416-9).
- [11] Barenji, A.V., Guo, H., Wang, Y., Li, Z., Rong, Y. (2021). Toward blockchain and fog computing collaborative design and manufacturing platform: Support customer view, *Robotics and Computer-Integrated Manufacturing*, Vol. 67, Article No. 102043, doi: [10.1016/j.rcim.2020.102043](https://doi.org/10.1016/j.rcim.2020.102043).
- [12] Zhang, Z., Wang, X., Zhu, X., Cao, Q., Tao, F. (2019). Cloud manufacturing paradigm with ubiquitous robotic system for product customization, *Robotics and Computer-Integrated Manufacturing*, Vol. 60, 12-22, doi: [10.1016/j.rcim.2019.05.015](https://doi.org/10.1016/j.rcim.2019.05.015).
- [13] Li, P., Cheng, Y., Song, W., Tao, F. (2020). Manufacturing services collaboration: Connotation, framework, key technologies, and research issues, *International Journal of Advanced Manufacturing Technology*, Vol. 110, 2573-2589, doi: [10.1007/s00170-020-06042-x](https://doi.org/10.1007/s00170-020-06042-x).
- [14] Xu, Z., Zhang, J., Song, Z., Liu, Y., Li, J., Zhou, J. (2021). A scheme for intelligent blockchain-based manufacturing industry supply chain management, *Computing*, Vol. 103, 1771-1790, doi: [10.1007/s00607-020-00880-z](https://doi.org/10.1007/s00607-020-00880-z).
- [15] Wu, Y., Zhang, Y. (2022). An integrated framework for blockchain-enabled supply chain trust management towards smart manufacturing, *Advanced Engineering Informatics*, Vol. 51, Article No. 101522, doi: [10.1016/j.aei.2021.101522](https://doi.org/10.1016/j.aei.2021.101522).
- [16] Xiao, Y., Li, C., Song, L., Yang, J., Su, J. (2021). A multidimensional information fusion-based matching decision method for manufacturing service resource, *IEEE Access*, Vol. 9, 39839-39851, doi: [10.1109/access.2021.3063277](https://doi.org/10.1109/access.2021.3063277).
- [17] Xu, W., Sun, H.Y., Awaga, A.L., Yan, Y., Cui, Y.J. (2022). Optimization approaches for solving production scheduling problem: A brief overview and a case study for hybrid flow shop using genetic algorithms, *Advances in Production Engineering & Management*, Vol. 17, No. 1, 45-56, doi: [10.14743/apem2022.1.420](https://doi.org/10.14743/apem2022.1.420).
- [18] Zhang, L., Yan, Y., Xu, W., Sun, J., Zhang, Y. (2022). Carbon emission calculation and influencing factor analysis based on industrial big data in the “double carbon” era, *Computational Intelligence and Neuroscience*, Vol. 2022, Article ID 2815940, doi: [10.1155/2022/2815940](https://doi.org/10.1155/2022/2815940).
- [19] García, K., Mendoza, S., Decouchant, D., Brézillon, P. (2018). Facilitating resource sharing and selection in ubiquitous multi-user environments, *Information Systems Frontiers*, Vol. 20, 1075-1095, doi: [10.1007/s10796-016-9708-0](https://doi.org/10.1007/s10796-016-9708-0).
- [20] Wang, H.Q., Li, J., Li, Y. (2019). Research on the evolution mechanism of platform-based science and technology resource sharing service paradigm, *China Soft Science*, No. 11, 153-165, doi: [10.3969/j.issn.1002-9753.2019.11.015](https://doi.org/10.3969/j.issn.1002-9753.2019.11.015).
- [21] Meng, F.S., Zhao, G., Xu, Y. (2019). Research on intelligent transformation and upgrading evolution game of high-end equipment manufacturing enterprises based on digitalization, *Scientific Management Research*, Vol. 37, No. 5, 89-97, doi: [10.19445/j.cnki.15-1103/g3.2019.05.015](https://doi.org/10.19445/j.cnki.15-1103/g3.2019.05.015).
- [22] Lampón, J.F., Frigant, V., Cabanelas, P. (2019). Determinants in the adoption of new automobile modular platforms: What lies behind their success?, *Journal of Manufacturing Technology Management*, Vol. 30, No. 4, 707-728, doi: [10.1108/jmtm-07-2018-0214](https://doi.org/10.1108/jmtm-07-2018-0214).
- [23] Meng, Z., Wu, Z., Gray, J. (2020). Architecting ubiquitous communication and collaborative-automation-based machine network systems for flexible manufacturing, *IEEE Systems Journal*, Vol. 14, No. 1, 113-123, doi: [10.1109/JSYST.2019.2918542](https://doi.org/10.1109/JSYST.2019.2918542).
- [24] Ren, M., Ren, L., Jain, H. (2018). Manufacturing service composition model based on synergy effect: A social network analysis approach, *Applied Soft Computing*, Vol. 70, 288-300, doi: [10.1016/j.asoc.2018.05.039](https://doi.org/10.1016/j.asoc.2018.05.039).
- [25] Ayala, N.F., Gerstlberger, W., Frank, A.G. (2019). Managing servitization in product companies: The moderating role of service suppliers, *International Journal of Operations & Production Management*, Vol. 39, No. 1, 43-74, doi: [10.1108/IJOPM-08-2017-0484](https://doi.org/10.1108/IJOPM-08-2017-0484).
- [26] Assaqty, M.I.S., Gao, Y., Hu, X., Ning, Z., Leung, V.C.M., Wen, Q., Chen, Y. (2020). Private-blockchain-based industrial IoT for material and product tracking in smart manufacturing, *IEEE Network*, Vol. 34, No. 5, 91-97, doi: [10.1109/MNET.011.1900537](https://doi.org/10.1109/MNET.011.1900537).

- [27] Wang, J., Yang, B., Zhai, L. (2022). Tripartite evolutionary game analysis of trust relationship between enterprises in a cloud manufacturing environment: A service composition perspective, *Discrete Dynamics in Nature and Society*, Vol. 2022, Article ID 6922627, doi: [10.1155/2022/6922627](https://doi.org/10.1155/2022/6922627).
- [28] Leng, J., Liu, J., Jiang, P. (2019). Blockchain models for cyber-credits of social manufacturing, In: Jiang P. (ed.), *Social Manufacturing: Fundamentals and Applications*, Springer, Cham, Switzerland, 197-217, doi: [10.1007/978-3-319-72986-2_9](https://doi.org/10.1007/978-3-319-72986-2_9).
- [29] Kapoor, K., Bigdeli, A.Z., Schroeder, A., Baines, T. (2021). A platform ecosystem view of servitization in manufacturing, *Technovation*, Article No. 102248, doi: [10.1016/j.technovation.2021.102248](https://doi.org/10.1016/j.technovation.2021.102248).
- [30] Tan, W., Zhu, H., Tan, J., Zhao, Y., Xu, L.D., Guo, K. (2021). A novel service level agreement model using blockchain and smart contract for cloud manufacturing in Industry 4.0, *Enterprise Information Systems*, Vol. 2021, No. 9, 1-26, doi: [10.1080/17517575.2021.1939426](https://doi.org/10.1080/17517575.2021.1939426).
- [31] Breunig, D.A., Stock, D., Bauernhansl, T. (2020). Requirements and concept for a modular and state-oriented control device architecture, *Procedia Manufacturing*, Vol. 42, 281-287, doi: [10.1016/j.promfg.2020.02.096](https://doi.org/10.1016/j.promfg.2020.02.096).
- [32] Wang, B., Wang, P., Tu, Y. (2021). Customer satisfaction service match and service quality-based blockchain cloud manufacturing, *International Journal of Production Economics*, Vol. 240, Article No. 108220, doi: [10.1016/j.ijpe.2021.108220](https://doi.org/10.1016/j.ijpe.2021.108220).
- [33] Sánchez, M., Exposito, E., Aguilar, J. (2020). Implementing self-* autonomic properties in self-coordinated manufacturing processes for the Industry 4.0 context, *Computers in Industry*, Vol. 121, Article No. 103247, doi: [10.1016/j.compind.2020.103247](https://doi.org/10.1016/j.compind.2020.103247).

Appendix A

Jacobian matrix of replicated dynamical systems:

$$J = \begin{bmatrix} (1-2x)(y(\alpha W_M - \alpha T - \beta Q) + z\alpha S_M + yzL_M + \alpha T) & x(1-x)(\alpha W_M - \alpha T - \beta Q + zL_M) & x(1-x)(\alpha S_M + yL_M) \\ y(1-y)(\beta W_C + \beta V - zL_M) & (1-2y)(x(\beta W_C + \beta V) + z\beta S_C - \beta V + (1-x)zL_M) & y(1-y)(\beta S_C + (1-x)L_M) \\ z(1-z)(-\alpha S_M) & z(1-z)(-\beta S_C) & (1-2z)(S_P - y\beta S_C - x\alpha S_M - C_P) \end{bmatrix}$$

Development of a flexible tooling system for sheet metal bending

Stefanovska, E.^a, Pepelnjak, T.^{a,*}

^aUniversity of Ljubljana, Faculty of Mechanical Engineering, Slovenia

ABSTRACT

This article presents the design and development of a flexible tooling system for sheet metal bending. The flexible tooling system aims to reduce manufacturing disturbances and increase the efficiency of the forming process. First and foremost, the structural behaviour of the sheet metal is investigated using the finite element method for the numerical simulation of the three-point bending process. The analysis' findings enabled the prediction of component reaction to loads, which are essential for the further optimization and enhancement of the tooling system's flexibility. At the initial stage of the development phase, SolidWorks, the computer-aided design software, is utilized to visualise the flexible tooling system and improve the tooling connectivity design. Furthermore, the prototype is developed by integrating mechanical and electrical components, such as the Arduino Mega microcontroller, stepper motors, and digital stepper drivers. Automation is achieved by programming the Arduino microcontroller board and controlling the stepper motors' movement to ensure precise displacement and speed control of the forming tools. The tooling system's major qualities are its high flexibility, achieved through the implementation of two moveable support cylinders and the possibility of being further upgraded to a closed-loop forming system. The higher level of automation and optimization of the sheet metal bending process can lead to improved processing efficiency and help achieve the desired formed products with higher quality and the required geometric tolerance. It is expected that the development of a flexible tooling system will find widespread application in sheet metal bending processes, resulting in reduced material costs, rapid equipment set-up and higher processing repeatability.

ARTICLE INFO

Keywords:

Sheet metal forming;
Finite element analysis (FEM);
Computer-aided design (CAD);
Flexible tooling system;
Cyber-physical systems;
Smart manufacturing;
Industry 4.0;
Digital twin

*Corresponding author:

tomaz.pepelnjak@fs.uni-lj.si
(Pepelnjak, T.)

Article history:

Received 25 January 2022
Revised 17 September 2022
Accepted 21 September 2022



Content from this work may be used under the terms of the Creative Commons Attribution 4.0 International Licence (CC BY 4.0). Any further distribution of this work must maintain attribution to the author(s) and the title of the work, journal citation and DOI.

1. Introduction

Sheet metal forming processes are manufacturing processes used to deform the sheet metal plastically into desired shapes. Sheet metal forming is widely used as a mass production processing technology due to its high processing speed and low processing cost compared to other methods [1]. Metal forming processes are an important field of research since the modern industry constantly aims for advanced processing performance and product quality control [2]. For minimizing production costs and achieving desired product quality, the determination of optimal process parameters, such as tool and workpiece geometrical data, material properties, contact conditions, and other technological parameters is of critical importance [3, 4]. Complicated physical phenomena, such as tool elastic deformations, sheet metal's material non-linearities, springback occurrence caused by material elastic recovery, and dynamic friction situations, impact output product quality [5]. Better output results can be obtained by studying the relative performance of a material in a given application and considering all the influential parameters that occur throughout the

forming process. The parameters of the process, including acting stresses, strains, and temperature fields, as well as local conditions of the microstructure (e.g., damage, grain size, structural composition) and the surface (e.g., lubricant layer thickness, surface micro-geometry), are used to describe the process and its limits [6]. Finite element simulation is essential for evaluating the material response to different influential parameters, further reducing forming process uncertainties and eliminating any deviations of the finished part from the initial design [7]. Optimizing all the process parameters and controlling the process limits can be extremely challenging, though it can improve the performance of the forming process used for the manufacturing of parts with a more accurate final geometry. Applying methods for modelling, simulation and optimization of production processes leads to the generation of new and better manufacturing solutions and to the optimization of process parameters [8].

Industries have developed various advanced technologies that can contribute to the creation of autonomous operational systems and process enhancements [9]. Effective implementation of Industry 4.0 technologies [10] offers more efficient and higher-quality production processes, as well as enabling predictive and preventative maintenance, resulting in reduced downtime and decreased long-term operational costs. The advanced connectivity of the embedded systems allows collecting and exchanging real-time information to identify, locate, track, monitor, and optimize the production processes [11, 12]. This allows for improved product quality, efficiency, and flexibility in producing customized items on a wide scale while reducing resource consumption [13, 14]. Sensors that monitor the part during the manufacturing process, actuators with sufficient flexibility and adaptability to allow modifications in response to changing process conditions, and model development with sufficient speed and efficiency to allow operation under changing process conditions are just a few of the features that can be implemented to improve the sheet metal forming processes [15]. Fig. 1 shows a closed-loop concept of metal forming control system that uses multiple sensors to monitor and optimize the metal forming process.

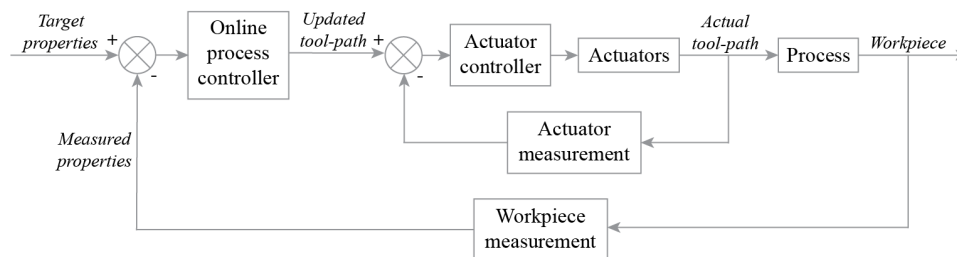


Fig. 1 A system diagram for closed-loop control of sheet metal forming process [15]

1.1 Fundamentals of sheet metal bending process

The production of high-precision sheet metal components is extremely important in the automotive, electronics, and housing-utensil industries [16]. The stability of the forming process is affected by a variety of structural properties, process disturbances, and complex parameter correlations. Therefore, manufacturers must constantly evaluate their strategies and search for new methods to improve process efficiency and achieve the desired product quality. One of the most frequent forming processes used in the manufacturing of sheet metal components is bending [17]. In sheet metal bending, plastic deformation occurs when the specimen undergoes permanent deformation or a non-reversible change in shape in response to applied loads. The formability of sheet metals, which refers to the material's capability to undergo plastic deformation to a specific shape while meeting quality requirements, is primarily influenced by the general mechanical properties, including the thickness and anisotropic features of the materials [18]. Dai *et al.* emphasize that during the design stage of the bending process, specific sheet material characteristics must be considered (i.e., Young's modulus, yield stress, the ratio of yield stress to ultimate tensile stress, initial anisotropy yielding criterion, and the microstructure of the material) [19]. FEM is the main technique for predicting sheet metal forming processes and determining the distribution of stresses and strains in the material, forming forces, and possible locations of defects in advance [20, 21]. For the successful application of the FEM to predict springback, it is necessary to know and understand the influence of numerical parameters on simulation results. In the metal forming

process, the bending force has to be determined so that the sheet metal can undergo plastic deformation and the desired shape can be achieved. Nevertheless, after the forming force is released, the material partially returns to its original shape due to its elastic recovery, which is known as springback [22]. Springback is expressed as the difference in dimension between the fully loaded and the unloaded configuration [23]. As a result, the springback must be considered in the metal forming process, since it decreases the bent angle of the sheet metal by a few degrees. The springback significantly influences the dimensional accuracy of the bent sheet metal; therefore, controlling and minimizing this challenging phenomenon can improve the bending process's accuracy.

1.2 Optimization of sheet metal forming processes

The fourth industrial revolution influences sheet metal forming operations with modifications, including enhanced manufacturing productivity, increased product quality, decreased technological difficulties for adapting the equipment, and reduced processing time. By developing and integrating sensing technologies for the visualization and monitoring of the forming process, production control (e.g., quality verification and traceability of the parameters) can be enhanced [24]. The expansion of smart manufacturing is enabled by innovative technologies that improve the cyber-physical systems (CPS) for better communication, process control, decision-making, and problem-solving capabilities [25]. Medić *et al.* [26] investigated the contribution of advanced digital technologies offering the greatest benefits to the Industry 4.0 production, considering the real-time monitoring of manufacturing processes as one of the key elements. In smart manufacturing, the digital twin (DT) technique is utilized to simulate physical entities, predicting their performance and behaviour under various scenarios [27]. The digital twin establishes the mapping and interaction between the physical and digital worlds, delivering specific information and presenting all of the influencing factors, thereby providing comprehensive technical guarantee and optimization capabilities [28]. In the event of an unplanned change or shutdown, the digital twin simulates numerous possibilities and delivers the optimal solution in real-time, allowing the real system to be constantly improved through a feedback loop. In the simulated environment, the DT of a real manufacturing activity can show, evaluate, and improve the process. The digital twin allows for process parameter identification, monitoring, and prediction, as well as comparison of the digital equivalent of the process to its recorded parameters obtained from the measured data from the physical environment. The digital twin's decision-making abilities can enable modification of the formed part's geometry by timely responding to predictions of potential process uncertainties that may occur during the forming process and by controlling the forming tool actuators to react fast to the instructions. The accuracy of the forming process, the quality of the finished product, and the processing efficiency can continuously improve with the implementation of the digital twin.

Developing appropriate sensors for monitoring the material flow during the sheet metal forming processes is extremely challenging. Fig. 3 depicts an example of applicable technology using a contact-based material flow measurement sensor known as a rolling ball sensor [29]. The mechanical transmission of the sheet metal's plane movement onto the rolling ball serves as the foundation for this sensor. The rotating motion of the ball is transmitted to two perpendicularly positioned measuring rollers. Each measuring roller has a slotted running wheel that runs inside a photoelectric barrier and converts rotation to electrical impulses without contact. With this sensor technique, the material flow direction, velocity, and path may all be monitored independently in two orthogonal directions.

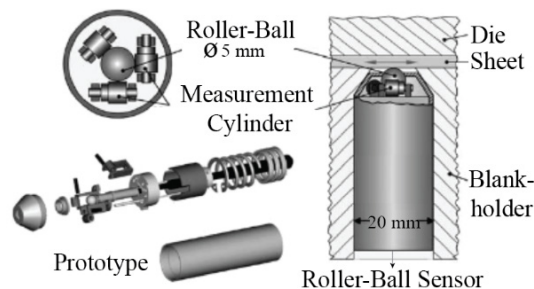


Fig. 3 Roller-ball sensor for material flow measurement [29]

Sah *et al.* [30] created a draw-in sensor based on the mutual inductance concept, as shown in Fig. 4. Current is stimulated in the first coil, causing electromotive force or induced voltages in the secondary coil. When metal is present close to the coils, the degree of mutual inductance varies; thus, the produced signal in the secondary coil reflects how much of the coil is covered up, providing a measure for the material draw-in amount. When monitoring the material draw-in of stamping processes, the contactless sensor eliminates the difficulties of conventional sensing. For example, when measuring material draw-in in stamping operations using standard sensing techniques, the edge wrinkle may cause loss of contact and difficulties in detecting the displacement.

Groche *et al.* [31] presented sensor fasteners that allow mechanical connections between the parts to be monitored for analysing forces and operational loads. To gather combined force and torque information in diverse regions, the sensor unit must be able to deliver and receive loads in all directions of space. The sensor fastener shown in Fig. 5 integrates a sensor component into an empty load-carrying model in the shape of a bolt. Simplified sensors are connected to the surface of the sensor body. To meet its functional requirements, the module incorporates an axial preload. A tensile load would otherwise cause the connected components to separate and interrupt the force transmission. In the sensor set-up, three strain gauges are placed on three sides of a rectangular cross-section. Individual axial forces and bending torques may be calculated by analysing each signal provided by the strain gauge. As a result, the novel concept enables a mechanical connection between the forming tools and the machine, as well as monitoring of operating loads.

Hinchy *et al.* [32] developed a physical manufacturing testbed that bends metal into V-brackets alongside a digital twin counterpart consisting of the three elements: machine, product, and process. Finite element modelling is utilized in the digital twin to forecast product outcomes and estimate product stress throughout the bending process. As shown in Fig. 6, the bending machine moves a V-press relative to a static V-die with a pair of high-torque stepper motors, while a load cell measures load throughout the bending process. An Internet of Things (IoT) [33] enabled microcontroller is used to control the system; it is capable of wirelessly transferring sensor data. A database of product attributes, such as material type, material qualities, product geometry, and product status, form the product's digital twin. The digital twin can be used to secure the expected results in metal forming operations, for example, the desired final bend angle. The digital twin concept contributes meaningfully to the metal forming process by predicting and optimizing the operation through the implementation of cyber-physical systems.

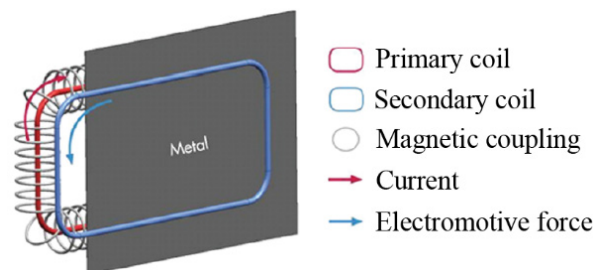


Fig. 4 Draw-in sensor based on the mutual inductance concept [30]

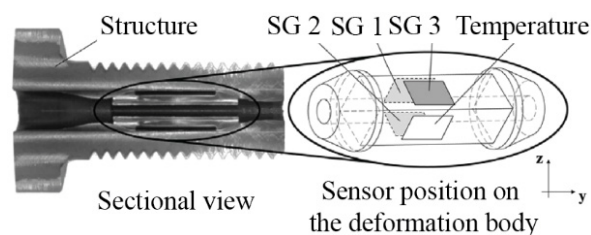


Fig. 5 Configuration of the sensor fastener [31]

Haag *et al.* [34] developed a digital twin concept for a bending beam test bench to prove that the digital representation of an individual product can play an integral role in a fully digitalized product life cycle. Fig. 7 presents the entire set-up of the digital twin system. The digital twin primarily includes the bending beam’s precise computer-aided design (CAD). The following steps include a combination of finite element technique simulations to reflect the complete test bench accurately in a virtual environment. An architecture based on the message-queuing telemetry transport (MQTT) protocol links the physical and digital twins. As parameters, either the resulting force on the beam or the ultimate displacement of the beam is entered into the system. Furthermore, the parameters are sent to the broker, who sends them to the physical twin, which then goes to the predetermined position until the movement or force is obtained, and then checks the other variables. The variable is then returned to the broker, who passes it along to the digital twin and IoT network. The digital twin starts an automated FEM analysis with the real force or movement values. Via the broker, the estimated findings are also sent back to the IoT platform, where they may be evaluated to the physical outputs. The objective is to automatically produce the digital twin and establish the network connection with its physical twin to make the concept applicable to a wide variety of devices.

By analysing data from prior research work in sheet metal forming, the set of scientific concepts and technologies being recently employed to improve the forming processes’ quality have been identified. This article proposes a novel perspective of increasing the flexibility of the three-point bending process by developing an innovative tooling system. The employment of two moveable support cylinders in addition to the forming punch that conducts the bending operation improves the configuration of the forming tools, resulting in higher efficiency and reduced forming time. The device is designed to provide greater opportunities for further optimization of the bending process and the capacity to be upgraded to a closed-loop forming system.

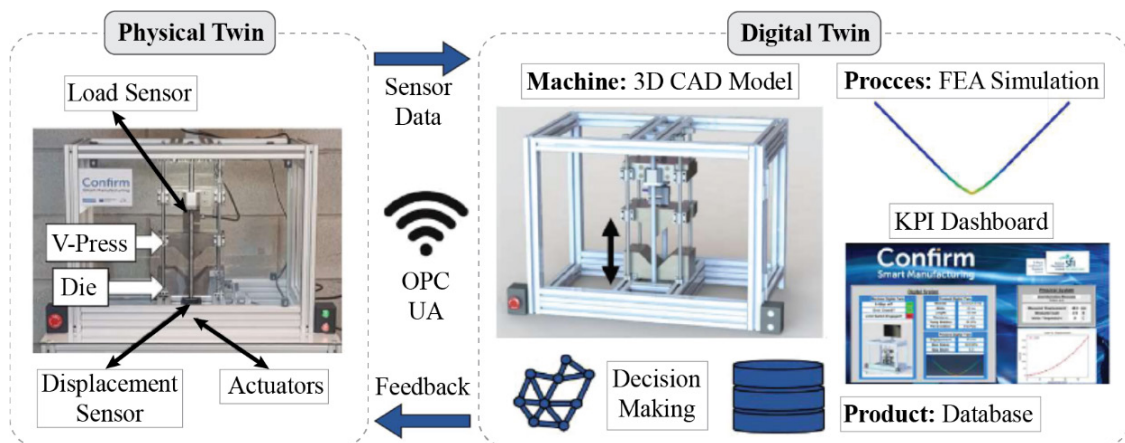


Fig. 6 Integration of physical and digital bending system [32]

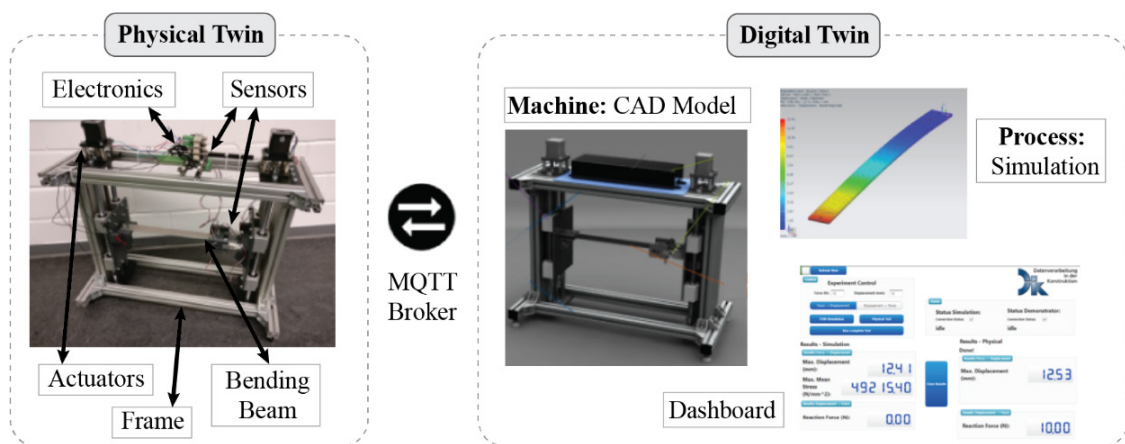


Fig. 7 Digital twin concept for bending beam test bench [34]

In the presented article, Section 1 reviewed the literature on topics relevant to the research undertaken, including introductory definitions related to the bending processes and the material properties of sheet metals. Also, the impact of Industry 4.0 on sheet metal forming operations, as well as several techniques for improving forming processes, were discussed. Furthermore, Section 2 describes the implemented methods using finite element analysis and computer-aided design for the visualization of the flexible tooling system. Section 3 presents the obtained results from the numerical simulations and the developed prototype of the flexible tooling system for sheet metal bending. Section 4 reviews the major findings in this article and offers recommendations for further research related to this study.

2. Materials and methods

This section describes the flexible tooling system set-up in detail, as well as the methods utilized to obtain the desired results. Fig. 8 illustrates the set-up of the three-point bending system and the overbending technique used in this investigation. The direction of the arrows indicates the movement of the forming tools that perform the sheet metal bending process. The three moveable forming tools exert force on the sheet metal, causing it to bend until the desired final shape is achieved. The overbending technique is used to obtain the desired bent angle by angularly bending the sheet metal over the specified angle and achieving the chosen final shape after the occurrence of springback.

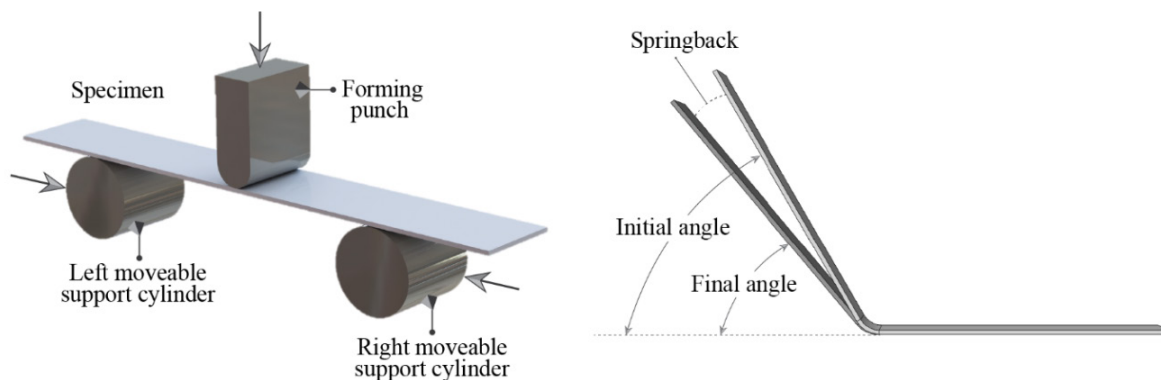


Fig. 8 Set-up of the three-point bending system and springback phenomenon

2.1 Finite element analysis

In the performed study, the initial findings of the three-point bending tests with flexible supports are obtained with a numerical simulation using the finite element software Abaqus. The goal of the numerical simulations was to determine the optimal process parameters for achieving a 90° bent angle of the specimen after springback. The model consists of sheet metal, forming punch and two support cylinders with precisely defined dimensions. The material properties, the design of the forming tool, the processing conditions and the tool wear are factors that influence the quality of the product, and their prediction is of great importance [35]. The thickness and material type of the sheet metal, as well as the radius of the forming tools, were the main parameters considered in the simulation. The sheet metal has a length of 140 mm, a width of 20 mm, and a thickness of 1 mm. The forming punch has a radius of 5 mm, while the moveable support cylinders have a radius of 10 mm.

Geometry information and a set of material behaviour rules are contained in each of the created parts in the Abaqus simulation. Homogeneous, solid sections are used to define the section properties of the sheet metal. The specified material type is steel DC04 according to DIN EN 10130 standard [36]. The material's mass density is 7.8×10^{-9} tonne/mm³, Young's modulus is 210,000 MPa, and Poisson's ratio is 0.3. The selected type of interaction is the surface-to-surface contact, which describes the contact between the sheet metal as a deformable surface and the forming tools as rigid surfaces. Considering the different surface roughness, the general contact with a Coulomb friction coefficient equal to 0.15 was selected for the interaction between the sheet metal

and the forming tools. The boundary conditions are then used to specify the loading and interaction between the sheet metal's surface and the forming tools, guaranteeing that the sheet metal deforms appropriately. The appropriate selection of finite element formulation, element size, and the number of integration points through the sheet metal's thickness is critical for the analysis's accuracy and prediction of the sheet metal's behaviour. Fig. 9 shows the variable number of elements in different regions over the sheet's metal thickness. An increased number of 5 elements through the thickness of the sheet metal is used in the region where it undergoes elasto-plastic deformation and comes into contact with the forming tools. The meshed specimen consists of a total number of 11,088 nodes and 8,700 elements. The elements consist of 1,800 linear hexahedral elements of type C3D8R and 6,900 linear hexahedral elements of type C3D8I. Considering the symmetry conditions, only a quarter of the sheet metal needs to be modelled. The FEM is simplified as a result, and the computing time is reduced. The symmetry boundary conditions are applied to the highlighted surfaces of the sheet metal, as shown in Fig. 9.

During the loading phase, the forming tools move with a velocity of 30 mm/s in both vertical and horizontal directions. The displacement of the forming punch, s_p , and the displacement of the support cylinders, s_c , is different in each FEM simulation, as shown in Table 1. Depending on the displacement and the velocity of the forming tools, the time of forming punch, t_p , the time of support cylinders, t_c , and the total forming time, t_{tot} , required for completing the bending process have different values.

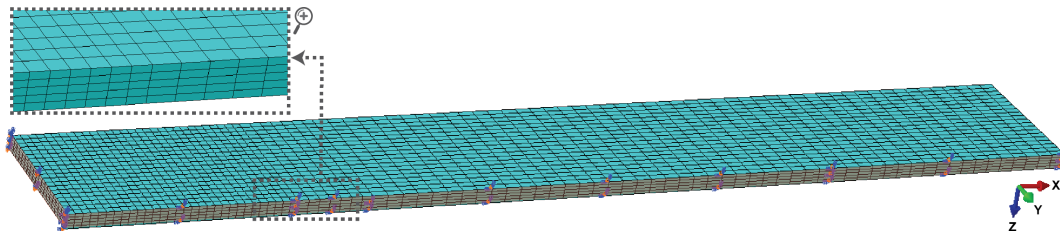


Fig. 9 Symmetry boundary conditions and assigned mesh on the sheet metal for the three-point bending analysis

Table 1 Combination of process parameters used in the three-point bending FEM simulations

No.	s_p (mm)	s_c (mm)	t_p (s)	t_c (s)	t_{tot} (s)
1	14	30	0.46	1	1
2	15	30	0.5	1	1
3	15.65	30	0.52	1	1
4	16	30	0.53	1	1
5	17	30	0.56	1	1
6	22.5	20	0.75	0.67	0.75
7	23.5	20	0.78	0.67	0.78
8	24.08	20	0.8	0.67	0.80
9	25.5	20	0.85	0.67	0.85
10	26.5	20	0.88	0.67	0.88
11	34	10	1.13	0.33	1.13
12	35	10	1.16	0.33	1.16
13	37	10	1.23	0.33	1.23
14	37.47	10	1.24	0.33	1.24
15	38	10	1.26	0.33	1.26
16	48	0	1.6	0	1.6
17	49	0	1.63	0	1.63
18	49.68	0	1.65	0	1.65
19	50	0	1.66	0	1.66
20	51	0	1.7	0	1.7

2.2 Computer-aided design

The three-point bending system is designed using the computer-aided design program SolidWorks, which involves sketching and adding dimensions to specify the geometry and position of all the components. The horizontal plate at the bottom supports the two vertical plates on which the linear systems are mounted. One linear system consists of two forming tools for supporting and bending the sheet metal in a horizontal direction, whereas the second linear system only has

one forming tool for bending the sheet metal in a vertical direction. The connected stepper motors enable the moving and positioning of the forming tools fixed on the linear systems. The sheet metal is inserted underneath the forming punch and on the movable support cylinders. The three-dimensional (3D) model of the bending device with the linear systems that perform the bending of the sheet metal in the vertical and horizontal direction is shown in Fig. 10.

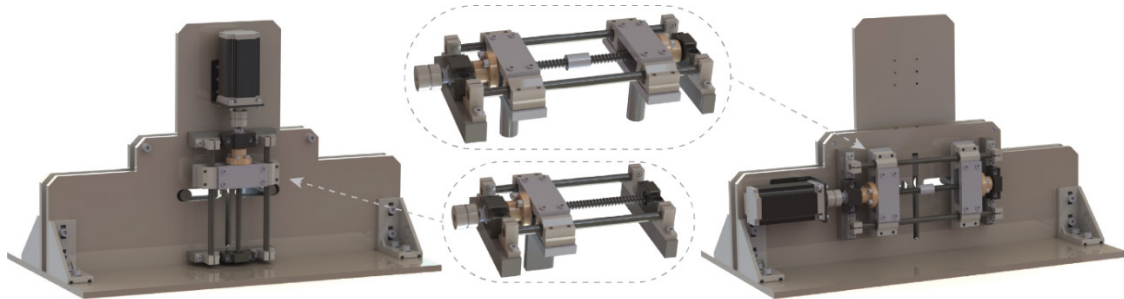


Fig. 10 3D model of the bending device with the vertical and horizontal linear systems

3. Results and discussion

This section presents the obtained results of the numerical approach and a comparative analysis for evaluating the findings' reliability. The finite element analysis was utilized to simulate the three-point bending process numerically. The findings of the numerical simulations were used to determine all specifications and requirements for the prototype development of the flexible tooling system.

3.1 Numerical simulation results

The influence of the process parameters on the sheet metal bending operation was studied by comparing the numerical results of 20 FEM simulations. The numerical simulations were conducted to identify the appropriate combination of process parameters for obtaining a 90° bent angle of the specimen after springback. The following influential process parameters were analyzed: bending angle before springback, α_1 , bending angle after springback, α_2 , angle difference before and after springback, $\Delta\alpha$, the maximum forming force of the forming punch, F_p , the maximum forming force of the support cylinders, F_c , displacement of the forming punch, s_p , displacement of the support cylinders, s_c , and total forming time required for completing the bending process, t_{tot} .

In the first set of numerical simulations, the range of the forming punch displacement is from 14 mm to 17 mm, and the displacement of the support cylinders is 30 mm. The second set has a range of forming punch displacement from 22.5 mm to 26.5 mm, and the displacement of the support cylinders is 20 mm. In the third set, the range of the forming punch displacement is from 34 mm to 38 mm, and the displacement of the support cylinders is 10 mm. In the fourth set, the support cylinders are fixed in their initial position, and the distance between them is 106 mm, whereas the range of the forming punch displacement is from 48 mm to 51 mm. Fig. 11 presents the various bending angle after springback, α_2 , obtained for different combinations of the forming tools' displacement. It can be seen that the bending angle after springback, α_2 , increases linearly by increasing the displacement of the forming punch, s_p . The desired bending angle after springback is 90° ±0.05° when the displacement of the forming punch is 15.65 mm, 24.08 mm, 37.47 mm, 49.68 mm, and the displacement of the support cylinders is 30 mm, 20 mm, 10 mm, 0 mm respectively.

Fig. 12 shows the relationship of the angle difference before and after springback, $\Delta\alpha$, and the bending angle after springback, α_2 . The numerical data show that when the forming force is released, the sheet metal returns towards its original shape by a few degrees due to the effect of springback. The overbending method is utilized to acquire the required bent angle by angularly bending the sheet metal over the specified angle and achieving the chosen final shape after the occurrence of springback.

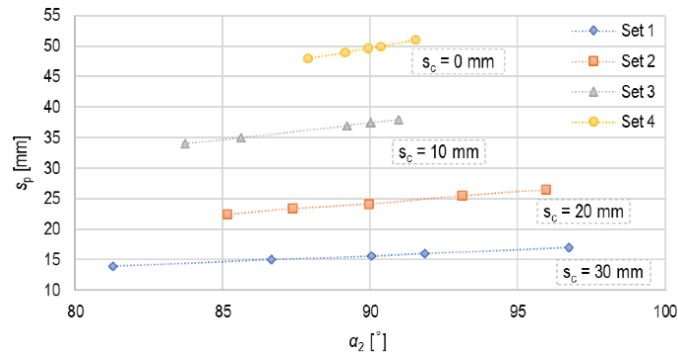


Fig. 11 Displacement of the forming punch, s_p , versus bending angle after springback, α_2 , for different displacement of the support cylinders, s_c

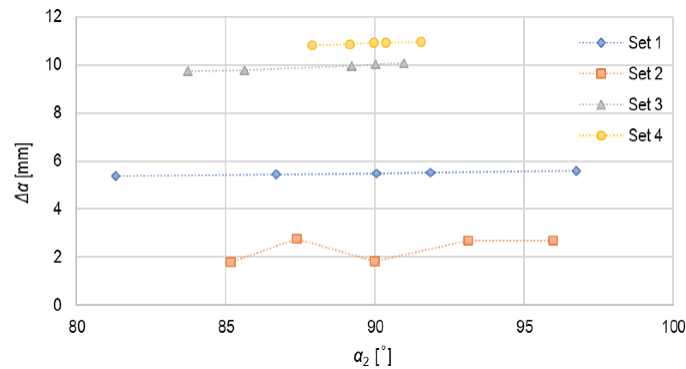


Fig. 12 The relationship of the angle difference before and after springback, $\Delta\alpha$, and the bending angle after springback, α_2

The total forming time, t_{tot} , is the sum of the time of forming punch, t_p , and the time of support cylinders, t_c , required for completing the bending process. During the loading phase of each numerical simulation, the forming tools move with a velocity of 30 mm/s in both vertical and horizontal directions. Fig. 13 presents the total forming time, t_{tot} , required to obtain the various bending angles after springback, α_2 . In addition to the forming punch that performs the bending operation, two moveable support cylinders are employed in the sets with numbers 1, 2, and 3.

In the fourth set, the support cylinders are fixed in their initial position, and only the forming punch is moveable, resulting in a significantly longer total forming time necessary to complete the bending operation. In the first set, the range of the forming punch displacement is from 14 mm to 17 mm, while the displacement of the support cylinders is 30 mm in each of the numerical simulations. As a result, the support cylinders need longer time than the forming punch to reach the specified displacement, equal to the total forming time, t_{tot} , of 1 s. It can be concluded that a reduction of the total forming time can be achieved by implementing two moveable support cylinders in addition to the forming punch that performs the bending operation simultaneously. By reducing forming time, continuous quality improvements and better production efficiency can be achieved.

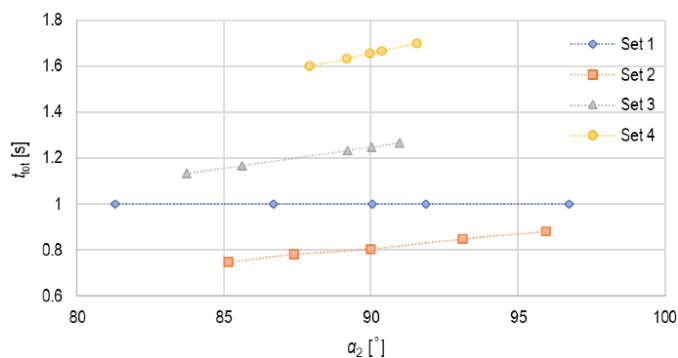


Fig. 13 Total forming time, t_{tot} , required for obtaining different bending angles after springback, α_2

The four cases of the FEM simulations for which the desired bending angle after springback is $90^\circ \pm 0.05^\circ$ are presented in Table 2. Fig. 14 shows the forming force evolution for different displacements of the forming tools in the cases when the bending angle after springback is $90^\circ \pm 0.05^\circ$. The solid section of the curve represents the forming tools' movement, while the dotted section of the curve shows the condition in which the forming punch has already reached the specified displacement and the moveable support cylinders are still performing the bending process (Fig. 14a), or vice versa (Fig. 14b). During the sheet metal bending operation, force is applied on the specimen in the vertical direction by the forming punch and in the horizontal direction by the support cylinders. The amount of maximum forming force required to achieve a 90° bending angle after springback has been determined. Furthermore, knowing the maximum forming force contributes to improving the design of the flexible tooling system by selecting the stepper motors with the relevant key specifications. Additionally, the forming force required to bend the sheet metal is considered to be twice as large when selecting the stepper motor used to position two movable support cylinders.

Table 2 Variety of cases in which the bending angle after springback is $90^\circ \pm 0.05^\circ$

Case	s_p (mm)	s_c (mm)	t_p (s)	t_c (s)	t_{tot} (s)	α_1 ($^\circ$)	α_2 ($^\circ$)	$\Delta\alpha$ ($^\circ$)	F_p (N)	F_c (N)
1	15.65	30	0.52	1	1	95.53	90.04	5.49	157.69	53.89
2	24.08	20	0.8	0.66	0.8	91.82	89.98	1.84	87.79	33.28
3	37.47	10	1.25	0.33	1.25	100.04	90.01	10.03	65.93	21.78
4	49.68	0	1.66	0	1.66	100.86	89.95	10.91	50.83	16.25

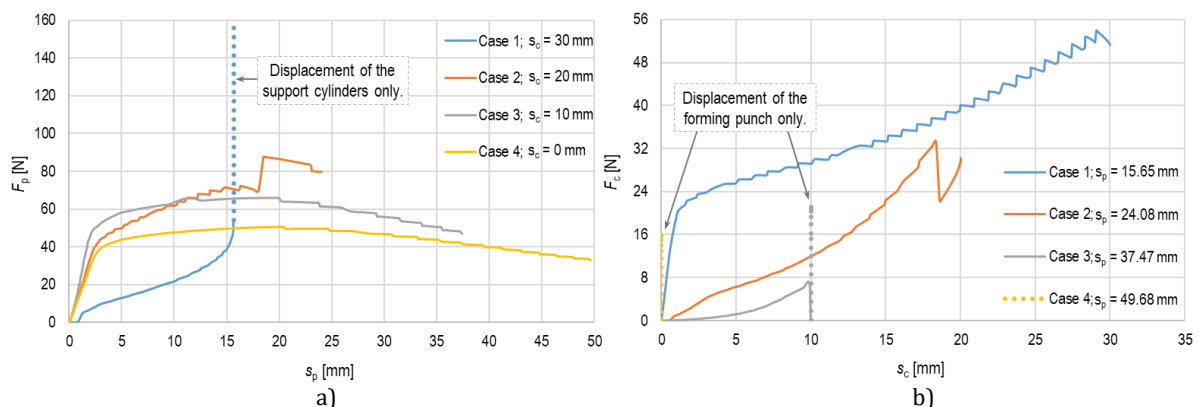


Fig. 14 Forming force evolution in the cases in which the bending angle after springback is $90^\circ \pm 0.05^\circ$:
a) force of the forming punch, F_p , versus displacement of the forming punch, s_p ;
b) force of the support cylinders, F_c , versus displacement of the support cylinders, s_c

Fig. 15 shows the relationship between the angle difference before and after springback, $\Delta\alpha$, and the total forming time, t_{tot} , in the cases in which the bending angle after springback is $90^\circ \pm 0.05^\circ$. Analysis was carried out to evaluate the angle difference before and after springback throughout the simulations to define the appropriate process parameters for reducing springback and achieving the necessary final geometry of the part. The best process parameters that minimize the springback were identified in the second case by comparing the simulations' results in which the bending angle after springback is $90^\circ \pm 0.05^\circ$. Springback is a critical challenge in metal forming, although by predicting and minimizing it using FEM simulations, it is feasible to improve the accuracy of the produced parts. Furthermore, ideal results are determined in the second case for the shortest time required to finish the bending process and obtain a bending angle of $90^\circ \pm 0.05^\circ$ degrees after springback.

By comparing the results obtained from the FEM simulations, the impact of various process parameters on the sheet metal bending operation is investigated. The second case in Table 3 has the process parameters of the optimal three-point bending FEM simulation. The specimen is bent to the required shape at a bending angle after springback of $90^\circ \pm 0.05^\circ$ degrees. The simulated bending angle before springback is 91.82° , and the bending angle after springback is 89.98° , thus resulting in 1.84° of springback.

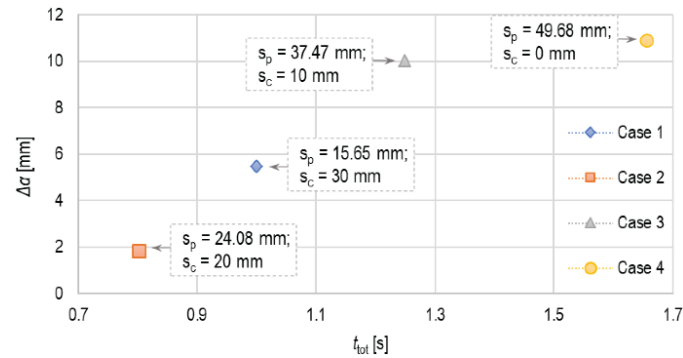


Fig. 15 The relationship of the angle difference before and after springback, $\Delta\alpha$, and the total forming time, t_{tot} , when the bending angle after springback is $90^\circ \pm 0.05^\circ$

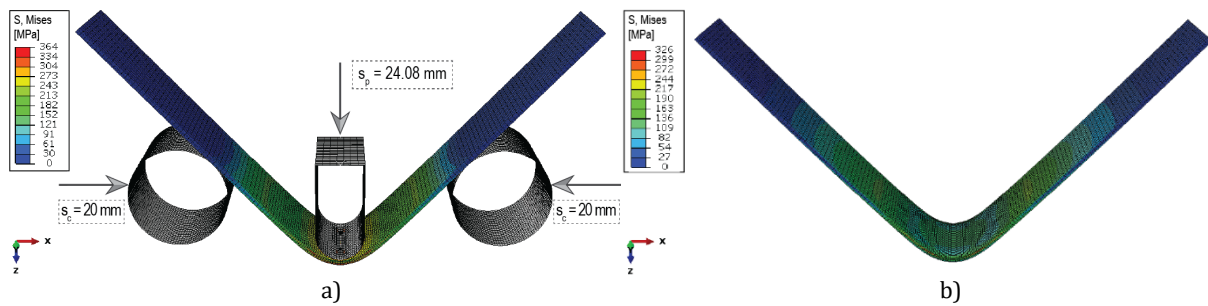


Fig. 16 Visualization of the three-point bending model: a) loading step; b) unloading step

The forming punch that bends the sheet metal in a vertical direction has a specified displacement of 24.08 mm and a maximum reaction force with a value of 87.79 N. The moveable support cylinders that bend the sheet metal horizontally from the left and right sides have a specified displacement of 20 mm and a maximum horizontal reaction force of 33.28 N. The total time required for the forming tools to reach the specified displacement for obtaining the desired bending angle after springback is 0.8 seconds. The sheet metal's behaviour at loading and unloading steps in the Abaqus simulation is shown in Fig. 16.

The numerical simulation results enabled the optimization of geometrical properties of the sheet metal, reduction of springback effect, and selection of the most dependable process parameters that are utilized as a reference for the design of the flexible tooling system. The obtained results show which process parameters are suitable for achieving the required 90° bent angle of the specimen after springback. It has been concluded that the flexibility of the three-point bending process is increased by the implementation of two moveable support cylinders in addition to the forming punch that performs the bending process. The appropriate forming tools' displacement and velocity during the bending process are identified to reduce processing time and increase process productivity. The computed maximum response force required for the forming tools to bend the sheet metal contributes to the comprehensive selection of stepper motors for a better design of the flexible tooling system for sheet metal bending.

3.2 Prototype development

The developed prototype of the bending device represents a preliminary version of a flexible tooling system for sheet metal bending, as shown in Fig. 17. The findings of the numerical simulations and the computer-aided design of the 3D model for the flexible tooling system were used to determine all specifications and requirements for the prototype development. The numerical simulations contributed to the identification of the optimal process parameters necessary for the production of sheet metal components with the desired shape. Furthermore, the 3D model's design enabled the visualization of the tooling system and the correct integration of the hardware and software components for effective system control. The prototype is created by integrating mechanical and electrical components, including Arduino Mega microcontroller, Nema 23 stepper motors, and digital stepper drivers. The stepper motors' movement is controlled by programming

the Arduino microcontroller board to provide accurate displacement and regulate the speed of the forming tools. The Nema 23 stepper motors are driven by DM542T digital stepper drivers, which use logical inputs to pulse the motors and are suitable for their voltage and current requirements. To adjust the position of the motor shaft, the micro-stepping technique is used, which may enhance resolution and significantly increase motion stability [37]. Micro-stepping allows the stepper drivers to position the Nema 23 stepper motor shaft accurately by generating a step angle as small as 0.014° (25,600 steps per revolution). In addition, a switching power supply model S-350-24 is utilized in the prototype. The open-source Arduino Software – Integrated Development Environment (IDE) is used to write the code and upload it to the Arduino Mega 2560 microcontroller. The wiring connection of the Arduino microcontroller, the power supply, and the Nema 23 stepper motors with their micro-stepping drivers is shown in Fig. 17.

The prototype's functionality was evaluated after the development phase, and the bending method was successfully completed. To conduct an accurate comparison of numerical and experimental data, several areas for future improvement of the currently developed flexible tooling system have been identified. Closed-loop automation, which enables improved process control, and the use of appropriate sensors allowing real-time monitoring of the bending angle throughout the bending operation, are the most significant advancements.

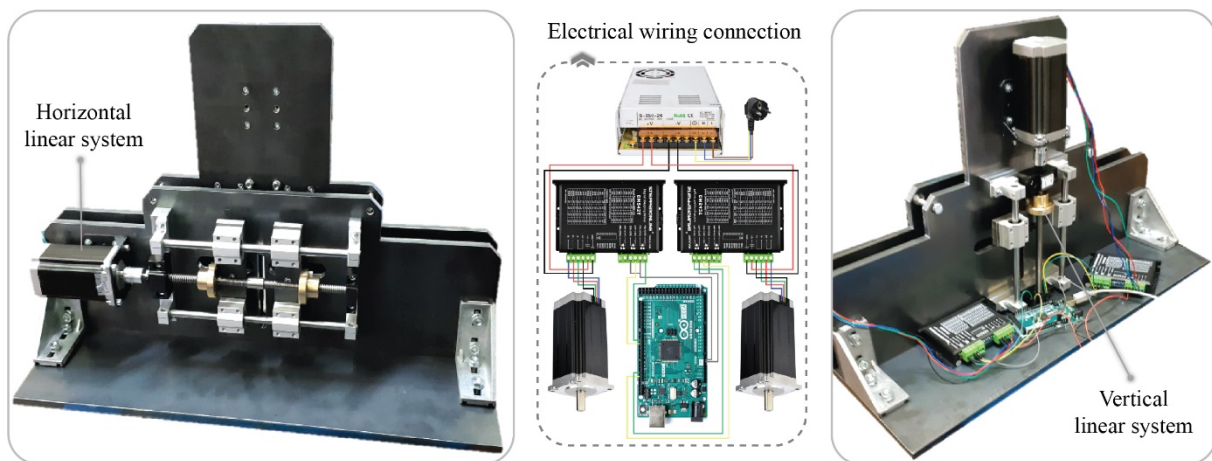


Fig. 17 Developed prototype of the flexible tooling system for sheet metal bending

4. Conclusion

Sheet metal bending processes are of crucial importance because they are widely applied for the manufacturing of various products, the majority of which are used in the automotive and aerospace industries. Since industrial requirements are rapidly increasing, the development of new methods for optimizing the bending process of sheet metals is in great demand. As a result, traditional metal forming tools are continuously being upgraded with novel technologies that can capture important data to improve the forming process. In this study, a novel flexible tooling system for optimizing process parameters and enhancing the sheet metal bending operation was developed.

The acquired results from the final element analysis contributed to the determination of the set-up and the geometry of the forming tools that are essential for obtaining the desired final shape of the bent sheet metal. The impact of various process parameters is evaluated by comparing simulation results, and the optimal three-point bending FEM simulation is selected. The most significant findings obtained from the performed numerical analysis are:

- The performed finite element analysis enabled the accurate prediction of the springback, which is 1.84° in the optimal three-point bending simulation.
- In addition to the forming punch that performs the bending process at the shortest production time with a displacement in a range from 22.5 mm to 26.5 mm, the innovative implementation of the moveable support cylinders with a displacement of 20 mm resulted in

greater flexibility of the bending process.

- The generated results indicate that the appropriate forming tools' displacement for obtaining the desired bending angle of $90^\circ \pm 0.05^\circ$ is 24.08 mm for the forming punch and 20 mm for the support cylinders.
- The determination of optimal displacement for the forming punch and the moveable support cylinders that move with a velocity of 30 mm/s during the bending process provided a reduction of processing time and improvement of process productivity for 48%, compared to the traditional three-point bending only with a movable forming punch.
- The applied overbending technique helps to eliminate the effect of springback occurrence by angularly bending the sheet metal for 1.84° over the required angle and achieving the desired angle of 89.98° after the forming force is released.
- The calculated maximum vertical force of 87.79 N and maximum horizontal force of 33.28 N required for the forming tools to bend the sheet metal aided in the selection of stepper motors for the design of the flexible sheet metal bending tooling system.

By predicting the influence of different process parameters using the numerical method, the essential data are acquired and incorporated into the design of a flexible tooling system for sheet metal bending. The following are the key characteristics of the developed flexible tooling system:

- Operating as an automated system capable of adjusting the forming tools' position and precisely controlling the bending process.
- Production of bent sheet metal parts with high quality and accuracy.
- Performance of continuous, well-structured, and rule-based forming operations.
- Run with high stability and dependability, reducing the occurrence of failures.
- The ability to bend sheet metals at various angles and thickness levels.

The expected results and the scientific contributions of the proposed research are focused to cover the most important, original, and innovative aspects of the following fields:

- Developed flexible tooling system for sheet metal bending that does not yet exist. The flexible tooling system aims to increase the efficiency of the forming process and reduce manufacturing disturbances.
- Significantly improved processing speed compared to the traditional three-point bending only with a movable forming punch, which is achieved by the innovative implementation of the moveable support cylinders.
- Designed flexible tooling system for sheet metal bending that has the potential for further implementation of sensors and upgrade of the controlling algorithm that can be utilized to process and analyse signals in real time. Those processed data will enable the prediction of potential deviations in bending process parameters that impact the final quality of the formed product and support the corresponding reaction of the actuators connected to the forming tools to eliminate potential errors.

Several areas can be recommended for potential improvement of the currently developed flexible tooling system, such as:

- Closed-loop automation that will enable advanced control of the forming process variables to the desired outcome without the need of human assistance.
- Implementation of appropriate sensors that will allow real-time measurement of the bending angle during the bending operation.
- Improvement of the currently developed flexible tooling system that will establish a connection between the FEM tools and the physical system for smooth data transfer between the cyber-physical system enabling online process monitoring and control.

Acknowledgement

The authors acknowledge the financial support of research core funding No. P2-0248 and Young Researcher Ema Stefanovska from the Slovenian Research Agency.

References

- [1] Tsuruya, T., Danseko, M., Sasaki, K., Honda, S., Takeda, R. (2019). Forming state recognition in deep drawing process with machine learning, *Journal of Advanced Mechanical Design, Systems and Manufacturing*, Vol. 13, No. 3, 1-3, doi: [10.1299/jamdsm.2019jamdsm0066](https://doi.org/10.1299/jamdsm.2019jamdsm0066).
- [2] Al-Tamimi, A., Darvizeh, R., Davey, K. (2018). Experimental investigation into finite similitude for metal forming processes, *Journal of Materials Processing Technology*, Vol. 262, 622-637, doi: [10.1016/j.jmatprotec.2018.07.028](https://doi.org/10.1016/j.jmatprotec.2018.07.028).
- [3] Puchlerska, S., Žaba, K., Pyzik, J., Pieja, T., Trzepieciński, T. (2021). Statistical analysis and optimisation of data for the design and evaluation of the shear spinning process, *Materials*, Vol. 14, No. 20, Article No. 6099, doi: [10.3390/ma14206099](https://doi.org/10.3390/ma14206099).
- [4] Zhao, X., Liu, Y., Hua, L., Mao, H. (2020). Structural analysis and size optimization of a fine-blanking press frame based on sensitivity analysis, *Strojniški Vestnik – Journal of Mechanical Engineering*, Vol. 66, No. 6, 408-417, doi: [10.5545/sv-jme.2020.6564](https://doi.org/10.5545/sv-jme.2020.6564).
- [5] Tatipala, S., Pilthammar, J., Sigvant, M., Wall, J., Johansson, C.M. (2018). Introductory study of sheet metal forming simulations to evaluate process robustness, *IOP Conference Series: Materials Science and Engineering*, Vol. 418, Article No. 012111, doi: [10.1088/1757-899X/418/1/012111](https://doi.org/10.1088/1757-899X/418/1/012111).
- [6] Volk, W., Groche, P., Brosius, A., Ghiotti, A., Kinsey, B.L., Liewald, M., Madej, L., Min, J., Yanagimoto, J. (2019). Models and modelling for process limits in metal forming, *CIRP Annals*, Vol. 68, No. 2, 775-798, doi: [10.1016/j.cirp.2019.05.007](https://doi.org/10.1016/j.cirp.2019.05.007).
- [7] Satošek, R., Valeš, M., Pepelnjak, T. (2019). Study of influential parameters of the sphere indentation used for the control function of material properties in forming operations, *Strojniški vestnik – Journal of Mechanical Engineering*, Vol. 65, No. 10, 585-598, doi: [10.5545/sv-jme.2019.6312](https://doi.org/10.5545/sv-jme.2019.6312).
- [8] Savkovic, B., Kovac, P., Rodic, D., Strbac, B., Klančnik, S. (2020). Comparison of artificial neural network, fuzzy logic and genetic algorithm for cutting temperature and surface roughness prediction during the face milling process, *Advances in Production Engineering & Management*, Vol. 15, No. 2, 137-150, doi: [10.14743/apem2020.2.354](https://doi.org/10.14743/apem2020.2.354).
- [9] Spaič, O., Krivokapić, Z., Kramar, D. (2020). Development of family of artificial neural networks for the prediction of cutting tool condition, *Advances in Production Engineering & Management*, Vol. 15, No. 2, 164-178, doi: [10.14743/apem2020.2.356](https://doi.org/10.14743/apem2020.2.356).
- [10] Ačko, B., Weber, H., Hutzschenreuter, D., Smith, I. (2020). Communication and validation of metrological smart data in IoT-networks, *Advances in Production Engineering & Management*, Vol. 15, No. 1, 107-117, doi: [10.14743/apem2020.1.353](https://doi.org/10.14743/apem2020.1.353).
- [11] Rojko, A. (2017). Industry 4.0 concept: Background and overview, *International Journal of Interactive Mobile Technologies*, Vol. 11, No. 5, 77-90, doi: [10.3991/ijim.v11i5.7072](https://doi.org/10.3991/ijim.v11i5.7072).
- [12] Buň, P., Grajewski, D., Górski, F. (2021). Using augmented reality devices for remote support in manufacturing: A case study and analysis, *Advances in Production Engineering & Management*, Vol. 16, No. 4, 418-430, doi: [10.14743/apem2021.4.410](https://doi.org/10.14743/apem2021.4.410).
- [13] Lopes De Sousa Jabbour, A.B., Jabbour, C.J.C., Foropon, C., Godinho Filho, M. (2018). When titans meet – Can Industry 4.0 revolutionise the environmentally-sustainable manufacturing wave? The role of critical success factors, *Technological Forecasting and Social Change*, Vol. 132, 18-25, doi: [10.1016/j.techfore.2018.01.017](https://doi.org/10.1016/j.techfore.2018.01.017).
- [14] Rosin, F., Forget, P., Lamouri, S., Pellerin, R. (2021). Impact of Industry 4.0 on decision-making in an operational context, *Advances in Production Engineering & Management*, Vol. 16, No. 4, 500-514, doi: [10.14743/apem2021.4.416](https://doi.org/10.14743/apem2021.4.416).
- [15] Polyblank, J.A., Allwood, J.M., Duncan, S.R. (2014). Closed-loop control of product properties in metal forming: A review and prospectus, *Journal of Materials Processing Technology*, Vol. 214, No. 11, 2333-2348, doi: [10.1016/j.jmatprotec.2014.04.014](https://doi.org/10.1016/j.jmatprotec.2014.04.014).
- [16] Thipprakmas, S., Phanitwong, W. (2011). Process parameter design of spring-back and spring-go in V-bending process using Taguchi technique, *Materials & Design*, Vol. 32, No. 8-9, 4430-4436, doi: [10.1016/j.matdes.2011.03.069](https://doi.org/10.1016/j.matdes.2011.03.069).
- [17] Liu, J.G., Fu, M.W., Lu, J., Chan, W.L. (2011). Influence of size effect on the springback of sheet metal foils in micro-bending, *Computational Materials Science*, Vol. 50, No. 9, 2604-2614, doi: [10.1016/j.commatsci.2011.04.002](https://doi.org/10.1016/j.commatsci.2011.04.002).
- [18] Kacar, I., Ozturk, F., Toros, S., Kılıç, S. (2020). Prediction of strain limits via the Marciniak-Kuczynski model and a novel semi-empirical forming limit diagram model for dual-phase DP600 advanced high strength steel, *Strojniški Vestnik – Journal of Mechanical Engineering*, Vol. 66, No. 10, 602-612, doi: [10.5545/sv-jme.2020.6755](https://doi.org/10.5545/sv-jme.2020.6755).
- [19] Dai, H.-L., Jiang, H.-J., Dai, T., Xu, W.-L., Luo, A.-H. (2017). Investigation on the influence of damage to springback of U-shape HSLA steel plates, *Journal of Alloys and Compounds*, Vol. 708, 575-586, doi: [10.1016/j.jallcom.2017.02.270](https://doi.org/10.1016/j.jallcom.2017.02.270).
- [20] Trzepieciński, T., Lemu, H.G. (2017). Effect of computational parameters on springback prediction by numerical simulation. *Metals*, Vol. 7, No. 9, Article No. 380, doi: [10.3390/met7090380](https://doi.org/10.3390/met7090380).
- [21] Szávai, S., Kovács, S., Bézi, Z., Kozak, D. (2021). Coupled numerical method for rolling contact fatigue analysis, *Tehnički Vjesnik – Technical Gazette*, Vol. 28, No. 5, 1560-1567, doi: [10.17559/TV-20201117124940](https://doi.org/10.17559/TV-20201117124940).

- [22] Sulaiman, S., Ariffin, M.K.A.M., Lai, S.Y. (2012). Springback behaviour in sheet metal forming for automotive door, *AASRI Procedia*, Vol. 3, 224-229, doi: [10.1016/j.aasri.2012.11.037](https://doi.org/10.1016/j.aasri.2012.11.037).
- [23] Panthi, S.K., Ramakrishnan, N., Ahmed, M., Singh, S.S., Goel, M.D. (2010). Finite element analysis of sheet metal bending process to predict the springback, *Materials & Design*, Vol. 31, No. 2, 657-662, doi: [10.1016/j.matdes.2009.08.022](https://doi.org/10.1016/j.matdes.2009.08.022).
- [24] Yang, M. (2019). Sensing technologies for metal forming, *Sensors and Materials*, Vol. 31, No. 10, 3121-3128, doi: [10.18494/SAM.2019.2399](https://doi.org/10.18494/SAM.2019.2399).
- [25] Herakovič, N., Zupan, H., Pipan, M., Protner, J., Šimic, M. (2019). Distributed manufacturing systems with digital agents, *Strojniški Vestnik – Journal of Mechanical Engineering*, Vol. 65, No. 11-12, 650-657, doi: [10.5545/sv-jme.2019.6331](https://doi.org/10.5545/sv-jme.2019.6331).
- [26] Medić, N., Anišić, Z., Lalić, B., Marjanović, U., Brezocnik, M. (2019). Hybrid fuzzy multi-attribute decision making model for evaluation of advanced digital technologies in manufacturing: Industry 4.0 perspective, *Advances in Production Engineering & Management*, Vol. 14, No. 4, 483-493, doi: [10.14743/apem2019.4.343](https://doi.org/10.14743/apem2019.4.343).
- [27] Qi, Q., Tao, F. (2018). Digital twin and big data towards smart manufacturing and Industry 4.0: 360 degree comparison, *IEEE Access*, Vol. 6, 3585-3593, doi: [10.1109/ACCESS.2018.2793265](https://doi.org/10.1109/ACCESS.2018.2793265).
- [28] Li, Y., Li, L. (2020). Enhancing the optimization of the selection of a product service system scheme: A digital twin-driven framework, *Strojniški Vestnik – Journal of Mechanical Engineering*, Vol. 66, No. 9, 534-543, doi: [10.5545/sv-jme.2020.6621](https://doi.org/10.5545/sv-jme.2020.6621).
- [29] Doege, E., Seidel, H.-J., Griesbach, B., Yun, J.-W. (2002). Contactless on-line measurement of material flow for closed loop control of deep drawing, *Journal of Materials Processing Technology*, Vol. 130-131, 95-99, doi: [10.1016/S0924-0136\(02\)00763-X](https://doi.org/10.1016/S0924-0136(02)00763-X).
- [30] Sah, S., Mahayotsanun, N., Peshkin, M., Cao, J., Gao, R.X. (2016). Pressure and draw-in maps for stamping process monitoring, *Journal of Manufacturing Science and Engineering*, Vol. 138, No. 9, Article No. 091005, doi: [10.1115/1.4033039](https://doi.org/10.1115/1.4033039).
- [31] Groche, P., Brenneis, M. (2014). Manufacturing and use of novel sensoric fasteners for monitoring forming processes, *Measurement*, Vol. 53, 136-144, doi: [10.1016/j.measurement.2014.03.042](https://doi.org/10.1016/j.measurement.2014.03.042).
- [32] Hinchy, E.P., Carcagno, C., O'Dowd, N.P., McCarthy, C.T. (2020). Using finite element analysis to develop a digital twin of a manufacturing bending operation, *Procedia CIRP*, Vol. 93, 568-574, doi: [10.1016/j.procir.2020.03.031](https://doi.org/10.1016/j.procir.2020.03.031).
- [33] Chen, L., Ye, Z., Jin, S. (2021). A security, privacy and trust methodology for IIoT, *Tehnički Vjesnik – Technical Gazette*, Vol. 28, No. 3, 898-906, doi: [10.17559/TV-20210122095638](https://doi.org/10.17559/TV-20210122095638).
- [34] Haag, S., Anderl, R. (2018). Digital twin – Proof of concept, *Manufacturing Letters*, Vol. 15, Part B, 64-66, doi: [10.1016/j.mfglet.2018.02.006](https://doi.org/10.1016/j.mfglet.2018.02.006).
- [35] Gomah, M., Demiral, M. (2020). An experimental and numerical investigation of an improved shearing process with different punch characteristics, *Strojniški Vestnik – Journal of Mechanical Engineering*, Vol. 66, No. 6, 375-384, doi: [10.5545/sv-jme.2020.6583](https://doi.org/10.5545/sv-jme.2020.6583).
- [36] DIN EN 10130 (2007). *Cold rolled low carbon steel flat products for cold forming – Technical delivery conditions*, DIN Deutsches Institut für Normung e. V., Berlin, Germany.
- [37] Kim, W., Shin, D., Lee, Y., Chung, C.C. (2016). Simplified torque modulated microstepping for position control of permanent magnet stepper motors, *Mechatronics*, Vol. 35, 162-172, doi: [10.1016/j.mechatronics.2016.02.002](https://doi.org/10.1016/j.mechatronics.2016.02.002).

A new approach for quality prediction and control of multistage production and manufacturing process based on Big Data analysis and Neural Networks

Tian, S.^a, Zhang, Z.^b, Xie, X.^{b,*}, Yu, C.^c

^aSchool of Basic Sciences, Shandong Institute of Petroleum and Chemical Technology, Dongying, P.R. China

^bBeijing Jiaotong University, School of Economics and Management, Beijing, P.R. China

^cSchool of Information and Electronics, Beijing Institute of Technology, Beijing, P.R. China

ABSTRACT

As consumers care more and more about product quality, it is important to mine the deep correlations between production and manufacturing parameters and the evaluation of product quality through the analysis of industrial big data. The existing research of product quality prediction faces several major problems: the lack of diverse quality features, the poor tractability of abnormal parameters, the strong nonlinearity of parameters, the obvious sequential property of data, and the severe time lag of data. To solve these problems, this paper explores the quality prediction and control of multistage MP process (MPMP) based on big data analysis. Firstly, the prediction strategy and flow were specified for MPMP product quality prediction, and the features were extracted from MPMP product quality. After that, the MPMP product quality features were described in multiple dimensions, the attention mechanism was introduced to the prediction process. In addition, the recurrent neural network was improved, and an MPMP product quality prediction model was established on bidirectional long short-term memory (BiLSTM) network. Our model was compared with AdaBoost and XGBoost through experiments. The effectiveness of our model was demonstrated by the results of the appearance quality PQ1, and the area under the curve (AUC) for each process parameter. In general, our model is superior to other algorithms in the accuracy, mean accuracy, and precision of product quality prediction.

ARTICLE INFO

Keywords:

Big data analysis;
Multistage production and manufacturing process (MPMP);
Quality prediction;
Machine learning;
Artificial neural network;
Recurrent neural network;
Bidirectional long short-term memory (BiLSTM)

*Corresponding author:

xxie@bjtu.edu.cn
(Xie, X.)

Article history:

Received 9 May 2022
Revised 16 August 2022
Accepted 20 August 2022



Content from this work may be used under the terms of the Creative Commons Attribution 4.0 International Licence (CC BY 4.0). Any further distribution of this work must maintain attribution to the author(s) and the title of the work, journal citation and DOI.

1. Introduction

With the continuous advancement of manufacturing intelligence, the new generation information technology (IT) has been deeply integrated with intelligent, automated production technology, providing an important driver of the industrial transformation of modern manufacturing [1-7]. As products become increasingly personalized, customized, and complex, the production and manufacturing (MP) process tends to cover multiple stages, and the consumers care more and more about product quality [8-14].

The manufacturing Internet of things (IoT) collects and stores the changing parameter data of the MP process, forming the industrial big data [15-22]. Through big data analysis, it is possible to reveal the deep connections between the parameters and the evaluation of product quality,

providing support to the optimization of manufacturing technology and the prediction of product quality in modern manufacturing.

In modern industries, information has been fully shared between production machines, smart subsystems, and mobile devices through advanced network technology [23, 24]. Ren *et al.* [25] proposed a soft measuring method for product quality prediction based on semi-supervised deep parallel factorization-machine (deepFM). Specifically, the process variables were discretized through data blocking; the deepFM was improved to extract quality information from different components, and obtain both high- and low-dimensional features. To solve the lack of process data and the strong nonlinearity and multiscale property of new intermittent processes, Chu *et al.* [26] presented a product quality prediction approach based on multi-scale kernel JYMKPLS (Joint-Y multi-scale kernel partial least squares) transfer learning. The merits of transfer learning and multiscale kernel learning were fully inherited by their approach. In addition, Lughofer *et al.* designed the strategies for online update and data removal of the model, aiming to adapt the transfer model continuous to new batch processes. Lughofer *et al.* [27] suggested that, in modern manufacturing facilities, high-quality production can be guaranteed through two basic stages. The first stage is to recognize the possible problems of product quality early on. The second stage is to take proper responses to the recognized problems. On this basis, Hao *et al.* put forward a holistic method to continuously implement the two stages under the prediction and maintenance framework of online production system, constructed a data-driven prediction model based on product quality standard, and realized the cyclic technological optimization in support of multistage functions. Hao *et al.* [28] developed an interaction model, which uses a linear model to characterize the influence of old production techniques and machines over quality degradation, and employs a random differential equation to capture the factors affecting quality degradation. Based on multiphase support vector regression (SVR), Zheng and Pan [29] proposed a soft measurement model for online quality prediction of liquid product concentration, and proved that the model is more efficient than the reported technologies. Melhem *et al.* [30] monitored the real-time quality of electronic products through the autocorrelation multivariate process, and came up with an online product quality prediction method, which forecasts the quality of products based on the correlations between product quality measurements in different steps.

The existing research of product quality prediction faces several major problems: the lack of diverse quality features, the poor tractability of abnormal parameters, the strong nonlinearity of parameters, the obvious sequential property of data, and the severe time lag of data. To solve these problems, this paper explores the quality prediction and control of multistage MP process (MPMP) based on big data analysis. Section 2 specifies the prediction strategy and flow for MPMP product quality prediction. Section 3 introduces recursion to the principal component analysis (PCA) based on kernel functions, and extracts the features of MPMP product quality. Section 4 describes the MPMP product quality features in multiple dimensions, and incorporates the attention mechanism to prediction process. In addition, the recurrent neural network was improved, and an MPMP product quality prediction model was established on bidirectional long short-term memory (BiLSTM) network. Our model was compared with AdaBoost and XGBoost through experiments. The effectiveness of our model was demonstrated by the results of the appearance quality $PQ1$, and the area under the curve (AUC) for each process parameter.

2. Quality prediction framework

Fig. 1 shows the MPMP product quality prediction strategy. Wireless sensing, industrial IoT, and big data analysis are adopted to capture and store the PM states and production technology parameters in different MP stages, aiming to facilitate the big data analysis. Fig. 2 shows the flow of MPMP product quality prediction. The specific steps of the prediction are as follows.

Firstly, the historical MPMP data are combined with the data on manufacturing technology, MP experience, and abnormal product quality into a real-time MPMP and product quality database. Next, the MPMP product quality is monitored in real time, referring to the product quality indices. After that, the MPMP data in the current stage and previous stages are mined through

big data analysis. On this basis, a product quality prediction model is established, and a strategy is developed to optimize abnormal production technology parameters.

The data from the historical MP and product quality database are preprocessed before being used to predict whether the product is qualified, update the product quality rule library, and optimize the abnormal production technology parameters.

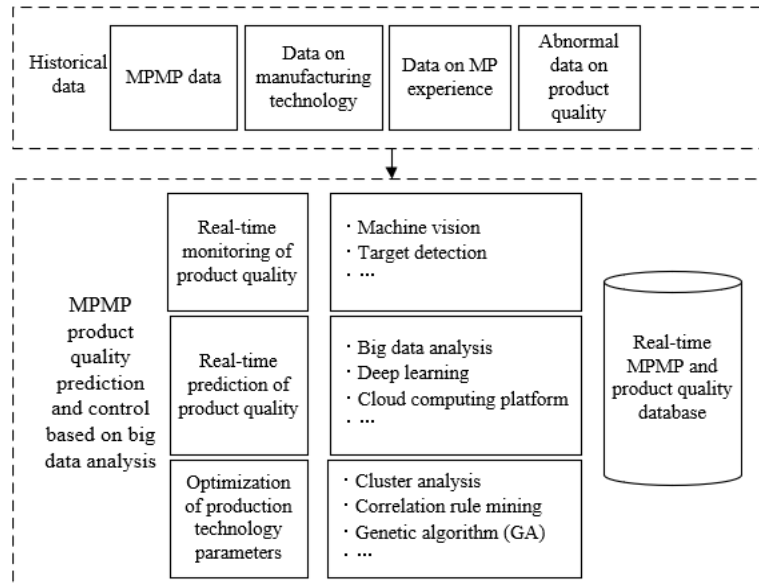


Fig. 1 MPMP product quality prediction strategy

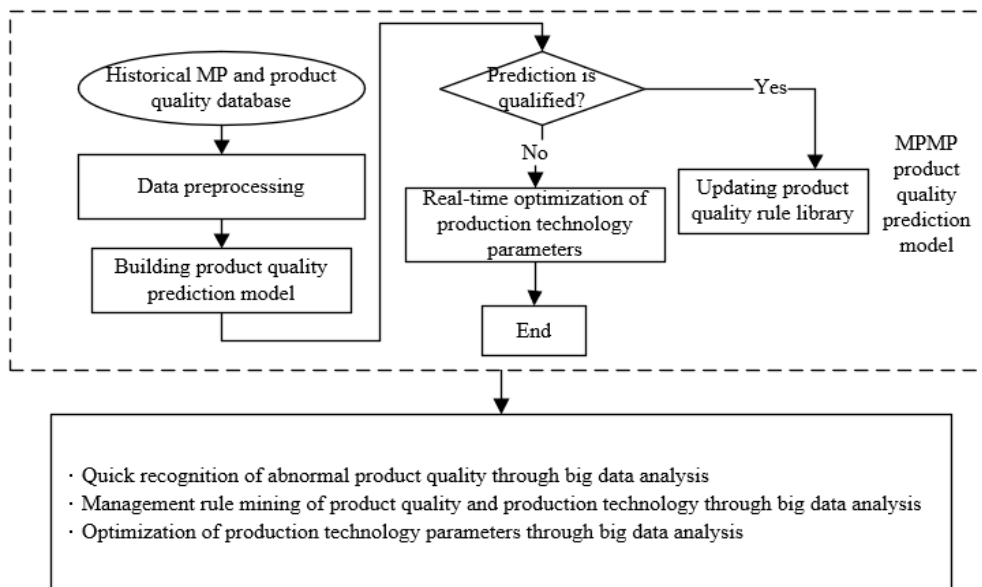


Fig. 2 Flow of MPMP product quality prediction

3. Feature extraction

MPMP product quality data contains a rich information of MP process, and many redundant factors. The variables in the data are strongly correlated, and cannot be directly used to build the MPMP product quality prediction model. To solve the problem, it is necessary to extract low-dimensional features from the data to obtain the most representative data of the MPMP, thereby reducing the modeling difficulty and computing complexity.

The recursive update of principal components was introduced to the PCA based on kernel functions. In this way, the model can be updated without needing overall computing. The model

computing becomes less complex, and satisfies the real-time online requirement of MPMP product quality prediction. Fig. 3 explains the flow of extracting MPMP product quality features.

The kernel-based PCA recursive update algorithm mainly has four steps:

Step 1: The original MPMP product quality data are mapped from low-dimensional feature space to high-dimensional feature space, producing the reconstructed data $\psi(a_i)$.

Step 2: The kernel matrix $L(a_i, a_j) = \{\psi(a_i), \psi(a_j)\}$ is constructed, and the inner product of vectors in the original data space is converted into kernel functions.

Step 3: In the high-dimensional feature space, the kernel functions obtained in the previous steps are subjected to PCA, and the corresponding eigenvalues and eigenvectors are calculated.

Step 4: The MPMP product quality data in the new stage are introduced to the kernel space through recursive solving.

Step 5: The kernel-based PCA model of product quality is updated recursively, and the dynamic PCA features of MP product quality are extracted from the new stage.

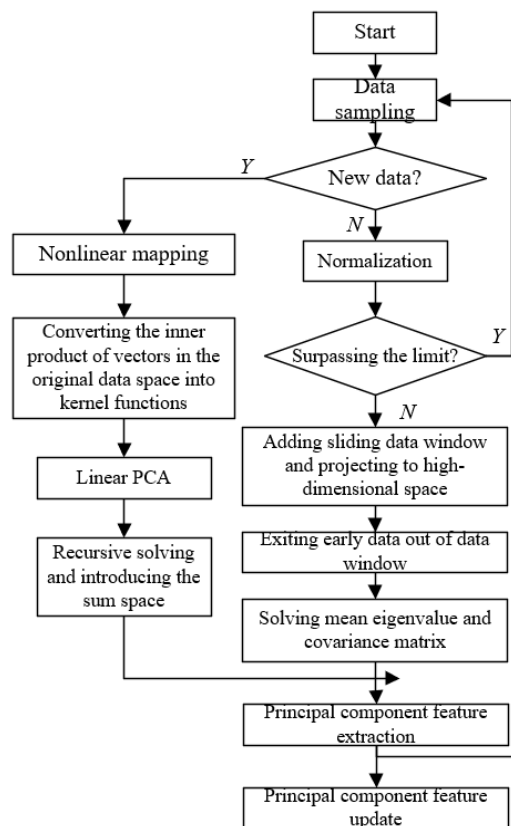


Fig. 3 Flow of MPMP product quality feature extraction

Let a_i be the n -dimensional MPMP product quality variable obtained through m samplings under the normal working condition; E^n be the original MPMP product quality data; G be the high-dimensional feature space; $\psi(a_i) \in G \subseteq E^n$ be the product quality data mapped nonlinearly from E^n to G . Then, we have

$$\psi: E^n \rightarrow G \quad a \rightarrow \psi(a) \tag{1}$$

Let λ_ψ be the mean of the data mapped to space G from the original product quality samples. The covariance matrix D_G of the MP product quality samples in the new stage after the mapping can be calculated by:

$$D_G = \frac{1}{m} \sum_{i=1}^m (\psi(a_i) - \lambda_\psi)(\psi(a_i) - \lambda_\psi)^T = \frac{1}{m} \sum_{i=1}^m \psi(a_i)\psi(a_i)^T \tag{2}$$

where, λ_ψ can be calculated by:

$$\lambda_\psi = (1/m) \sum_{i=1}^m \psi(a_i) \tag{3}$$

Suppose the mapping values of the original product quality samples in space G are zero-centered. Then, λ_ψ is equal to zero. To obtain the corresponding eigenvalue μ and eigenvector U , D_G should go through eigenvalue decomposition in space G :

$$\mu U = D_G U \tag{4}$$

Solving the inner product of each product quality sample, i.e., pre-multiplying Eq. 4 with $\psi(a_l)$, $l = 1, 2, \dots, m$:

$$\mu(\psi(a_l) \cdot U) = (\psi(a_l) \cdot D_G U) \tag{5}$$

According to the reproducing kernel theory, all the eigenvectors U corresponding to nonzero eigenvalues μ are all distributed in the tensor space of $\{\psi(a_1), \psi(a_2), \dots, \psi(a_m)\}$. Then, the coefficient vector $\beta_i (i = 1, 2, \dots, m)$ should satisfy:

$$U = \sum_{i=1}^m \beta_i \psi(a_i) \tag{6}$$

Combining Eqs. 5 and 6:

$$\mu \sum_{i=1}^m \beta_i \langle \psi(a_i), \psi(a_l) \rangle = \frac{1}{m} \sum_{i=1}^m \beta_i \left\langle \psi(a_i) \cdot \sum_{j=1}^n \psi(a_j) \right\rangle \cdot \langle \psi(a_j), \psi(a_l) \rangle \tag{7}$$

Let $L_{ij} = L(a_i, a_j) = \{\psi(a_i), \psi(a_j)\}$ be an $n \times n$ -order kernel matrix. That is, the kernel functions of the two variables in the input space can characterize the inner product between the variables in the feature space. The specific form of ψ should be avoided in the computing process. Substituting L_{ij} into Eq. 7, the characteristic equation can be obtained:

$$m\mu L\beta = L^2\beta \Rightarrow m\mu\beta = L\beta \tag{8}$$

Solving Eq. 8, it is possible to obtain nonzero eigenvalues $\mu_2 (\mu_1 \geq \mu_2 \geq \dots \mu_m)$ and the corresponding eigenvectors $\beta^l (l = 1, 2, \dots, m)$. There exists $(u_l, u_l) = 1$ for normalizing eigenvector U_l . Thus, it can be derived from Eq. 7 that $\mu(\beta^l - \beta^l) = 1$. Then, the l -th principal component p_l mapped from original MPMP product quality sample a to space G can be expressed as:

$$p_l = \langle u_l, \psi(a) \rangle = \sum_{i=1}^m \beta_i^l \langle \psi(a_i) \cdot \psi(a) \rangle = \sum_{i=1}^m \beta_i^l L(a, a_i) \tag{9}$$

The principal component direction of a in space G is the projection of $\psi(a)$ on new eigenvector U . After being added to the data window, the MP data a_{m+1} of a new stage should be mapped to space G . Let $\psi(a_{m+1})$ be the nonlinearly mapped value of a_{m+1} from low-dimensional feature space to high-dimensional feature space. Then, the mapped mean eigenvalue λ'_ψ can be recursively computed by:

$$\lambda'_\psi = \frac{1}{m+1} \psi([A, a_{m+1}]) S_{m+1} = \frac{m}{m+1} \lambda_\psi + \frac{1}{m+1} \psi(a_{m+1}) \tag{10}$$

where, $S = [1, 1, \dots, 1] \in E^{m+1}$. The covariance matrix D'_G can be recursively solved by:

$$\begin{aligned} D'_G &= \frac{1}{m} \overline{\psi}([A, a_{m+1}]) \overline{\psi}([A, a_{m+1}])^T \\ &= \frac{1}{m} \sum_{i=1}^m (\psi(a_i) - \lambda'_\psi)(\psi(a_i) - \lambda'_\psi)^T + \frac{1}{m} \sum_{i=1}^m (\psi(a_{m+1}) - \lambda'_\psi)(\psi(a_{m+1}) - \lambda'_\psi)^T \\ &= \frac{1}{m} \sum_{i=1}^m \left[\psi(a_i) - \lambda_\psi + \frac{1}{m+1} \lambda_\psi + \frac{1}{m+1} \psi(a_{m+1}) \right] \times \left[\psi(a_i) - \lambda_\psi + \frac{1}{m+1} \lambda_\psi + \frac{1}{m+1} \psi(a_{m+1}) \right]^T \\ &\quad + \frac{1}{m} \left[\frac{m}{m+1} \psi(a_{m+1}) - \frac{m}{m+1} \lambda_\psi \right] \times \left[\frac{m}{m+1} \psi(a_{m+1}) - \frac{m}{m+1} \lambda_\psi \right]^T \end{aligned} \tag{11}$$

$$\begin{aligned}
 &= \frac{1}{m} \sum_{i=1}^m (\psi(a_i) - \lambda_\psi)(\psi(a_i) - \lambda_\psi)^T + \frac{1}{m+1} \sum_{i=1}^m (\psi(a_{m+1}) - \lambda_\psi)(\psi(a_{m+1}) - \lambda_\psi)^T \\
 &= \frac{m-1}{m} D_G + \frac{1}{m+1} (\psi(a_{m+1}) - \lambda_\psi)(\psi(a_{m+1}) - \lambda_\psi)^T \\
 &= \frac{m-1}{m} \left[\sqrt{\frac{m-1}{m}} \bar{\psi}(a) \sqrt{\frac{m}{m^2-1}} (\psi(a_{m+1}) - \lambda_\psi) \right] \times \left[\sqrt{\frac{m-1}{m}} \bar{\psi}(a) \sqrt{\frac{m}{m^2-1}} (\psi(a_{m+1}) - \lambda_\psi) \right]^T
 \end{aligned}$$

To complete the eigenvalue decomposition of v'_ψ and D'_G , linear PCA should be employed to extract the principal component features of the MP product quality in the new stage. Therefore, this paper introduces the recursive algorithm to the kernel-based PCA, eliminating the need to compute the entire principal component model again after the input of the MP product quality data of the new stage. In this way, our model can effectively reduce the computing load of real-time prediction.

4. Methodology

4.1 Multidimensional description of quality variables and attention mechanism

Fig. 4 describes MPMP product quality features in multiple dimensions. To illustrate the time-variation of product quality data, this paper evaluates product quality from three dimensions: production technology, product quality, and time. The production technology dimension examines the level of production technology from the accuracy of dimensions, shape, and position. The product quality dimension evaluates product quality from appearance quality, performance index, and life index. The time dimension is generated from the real-time MPMP product quality dataset.

The global decision-making of production control is underpinned by the online detection of key processes of each MP stage, and the information interaction and sharing of the time dimension. This paper extracts the samples from the time series of MPMP product quality, and constructs a multidimensional MPMP product quality prediction model, which is capable of tracing and optimizing the abnormal production technology parameters. Fig. 5 shows the flow of real-time tracking and optimization of abnormal production technology parameters.

Under the different features of production technology parameters, the product quality features of different MP processes are affected to different degrees. To this end, the attention mechanism was innovatively introduced to MPMP product quality prediction. Firstly, the MP product quality of the new stage was analyzed against the quality evaluation criteria. Then, the similarity between product quality features of adjacent stages was calculated. After that, the authors computed the correlation of the product quality features in the current MP stage with the change law of different production technology parameters, and obtained the corresponding similarity score. On this basis, the abnormal technology parameters were valued for the new MP stage, thereby completing the prediction of MPMP product quality.

The core parameters of the attention mechanism include Key, Query, and Value. Among them, Key corresponds to Value, and is used to query for and compute the similarity of product quality features between adjacent stages. Query is the query during the execution of the attention mechanism. Value is the MPMP product quality data receiving attention and being selected. The attention mechanism can be defined by:

$$ATT(Key, Query, Value) = Softmax(SIM(Key, Query)) * Value \tag{12}$$

Let q_i be the output tensor of the upper layer series at position i . If the upper layer is a bidirectional neural network in the model, then the Key at position i can be denoted by u_i :

$$u_i = \tan(\omega q_i + r) \tag{13}$$

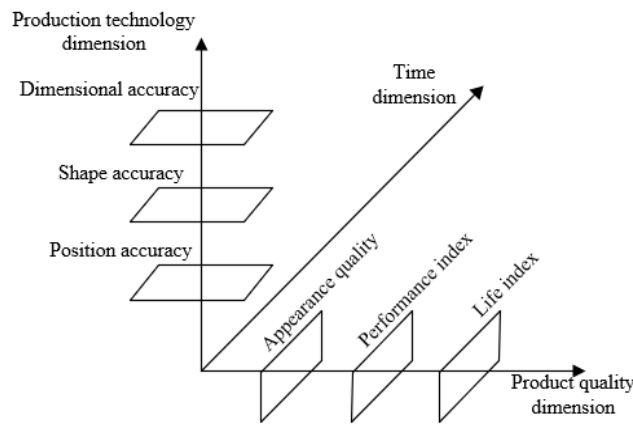


Fig. 4 Multidimensional description of MPMP product quality features

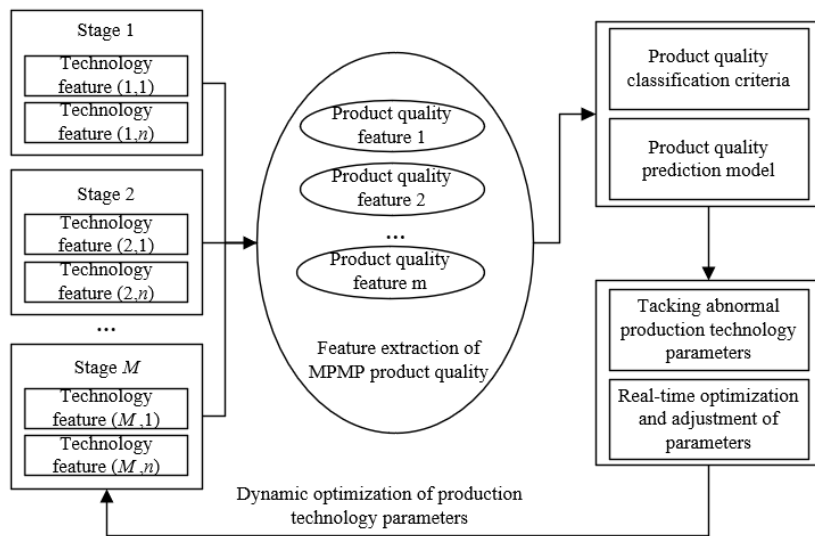


Fig. 5 Real-time tracking and optimization of abnormal production technology parameters

Eq. 13 shows that u_i can be derived from Value via the fully-connected layer. The attention weight β_i can be calculated by:

$$\beta_i = \frac{o^{u_i^T} d}{\sum_i o^{u_i^T} d} \tag{14}$$

The output of the attention layer can be calculated by:

$$SC = \sum_i \beta_i (a) u_i(a) \tag{15}$$

The Query of that attention layer can be adjusted and updated through random initialization and model training:

$$\omega_p(i) = Soft\ max \left(\gamma_p SIM(a_p, N_p(i)) \right) \tag{16}$$

$$\omega_p(i) = Soft\ max \left(\left(\sum_l \omega_p(l) t_p(i+l) \right)^{\alpha_p} \right) \tag{17}$$

The output tensor f_i can be expressed as:

$$q_i = CON(\vec{q}_i, \tilde{q}_i) \tag{18}$$

4.2 Construction of product quality prediction model

The LSTM network, as a variant of recurrent neural network, can prevent the common problems of recurrent neural network: exploding gradients and vanishing gradients. Each LSTM network consists of an input gate SR_p , a forget gate LE_p , an output gate EX_p , and a memory cell d_p . Let A_p be the input vector of stage p ; f_{p-1} be the hidden layer state of stage $p - 1$. Then, the forget gate can be calculated by:

$$A = \left[\frac{A_p}{f_{p-1}} \right] \quad (19)$$

$$LE_p = \varepsilon(\omega_{LE} \cdot [f_{p-1}, A_p] + r_{LE}) \quad (20)$$

The forget gate determines whether the MPMP product quality information should be preserved or discarded. Let D_p^* be the candidate cell state used to determine the new cell state D_p . The input gate can be calculated by:

$$SR_p = \varepsilon(\omega_i \cdot [f_{p-1}, A_p] + r_i) \quad (21)$$

$$D_p^* = \tan(\omega_d \cdot [f_{p-1}, A_p] + r_d) \quad (22)$$

The input gate determines how to update information. The training parameters of our model are configured as follows: the weight of LSTM network, θ ; bias, r ; activation function sigmoid, s ; point-by-point product, \odot . The output gate can be calculated by:

$$D_p = LE_p * D_p + SR_p * D_p^* \quad (23)$$

$$EX_p = \varepsilon(\theta_{EX} \cdot [f_{p-1}, A_p] + r_{EX}) \quad (24)$$

The memory cell can be expressed as:

$$d_p = LE_p \otimes d_{p-1} + SR_p \otimes \tan(\theta_d \cdot A + r_d) \quad (25)$$

The hidden layer state of stage p can be calculated by:

$$f_p = EX_p \otimes \tan(d_p) \quad (26)$$

The activation function can be defined as:

$$\varepsilon(a) = \frac{1}{1 + o^{-a}} \quad (27)$$

$$\tan(a) = \frac{o^a - o^{-a}}{o^a + o^{-a}} \quad (28)$$

The LSTM network can effectively handle product quality data with a strong sequential property and correlations. However, the network is unable to mine the information of future product quality data. This defect can be solved by combining forward LSTM with inverse LSTM into a BiLSTM. Let δ be the length of a data series; ML be the processing of a single LSTM. Then, the BiLSTM can obtain the forward and inverse information of product quality data from input vectors f_p :

$$\vec{f}_p = \vec{ML}(\vec{f}_{p-1}, a_p, d_{p-1}), p \in [1, \delta] \quad (29)$$

$$\tilde{f}_p = \tilde{ML}(\tilde{f}_{p-1}, a_p, d_{p+1}), p \in [1, \delta] \quad (30)$$

The information in the two directions (Eqs. 29 and 30) is combined into the final output of BiLSTM. The output of stage p can be expressed as:

$$b_p = h(\omega_{\vec{f}b} \vec{f}_p + W_{\tilde{f}b} \tilde{f}_p + r_b) \quad (31)$$

Let A_{p-m} and f_{p-m} be the state input and hidden layer output of the previous n MP stages, respectively; A_p be the input of production technology parameters in the current stage; f_p be the output through the hidden layer; A_{p+m} be the input of production technology parameters in the m MP stages in future; f_{p+m} be the hidden layer output. Then, we have:

$$f_p = g(\omega_3 A_p + \omega_4 f_{p-1}) \tag{32}$$

$$f'_p = LE(\omega_1 A_p + \omega_2 f'_{p-1}) \tag{33}$$

$$EX_p = b_p = h(\omega_5 f_p + \omega_6 f'_p) \tag{34}$$

The dynamic memory network capable of retaining time dependence can be established by:

$$f_i^p = h_i^p BiLSTM(d_i, f_{i-1}^p) + (1 - h_i^p) f_{i-1}^p \tag{35}$$

Considering the sequential property and strong correlations between production technology parameters, as well as the dynamic nonlinearity of product quality features, this paper assigns weights to different production technology parameters according to the correlations between the two variables, following the attention mechanism of quality variables, and takes the weighed parameters as the input of BiLSTM.

Firstly, the key parameters that induce the abnormal product quality were identified for each MP stage. Next, a product quality prediction model was established based on BiLSTM. To improve the prediction accuracy, the product quality states of stages $p + 1, \dots, p + m$ were predicted in real time in stage p . Then, the key technology parameters were further optimized.

The production technology parameters of historical MPMP and those Z_{ij} of the current stage were converted into time series stage by stage. Let $Z_{mi}(p - 1)$ be production technology parameter i of MP process m in stage $p - 1$, and $F(p)$ be the corresponding product quality feature. Then, we have:

$$\left[Z_{ij} = \begin{pmatrix} Z_{11}(p - 1) & \dots & Z_{1n}(p) \\ Z_{21}(p - 1) & \dots & Z_{2n}(p) \\ \vdots & \ddots & \vdots \\ Z_{m1}(p - 1) & \dots & Z_{mn}(p) \end{pmatrix} \right] \Rightarrow \begin{bmatrix} F(p) \\ F(p + 1) \\ \vdots \\ F(p + m) \end{bmatrix} \tag{36}$$

Let $\xi_{ij}(l + 1)$ be the observation of stage $l + 1$; ξ_{max} and ξ_{min} be the maximum and minimum of a parameter in that stage, respectively. Then, the normalization can be expressed as:

$$Z_{ij}(l + 1) = \frac{\xi_{ij}(l + 1) - \xi_{max}}{\xi_{min} - \xi_{max}} \tag{37}$$

Let $F^*(l + 1)$ be the prediction for stage $l + 1$; γ_k be the weight of the similarity between the parameter and product quality features; $\chi_k(l + 1)$ be the corresponding attention weight. Then, we have:

$$F^*(l + 1) = \sum_{k=1}^K \chi_k(l + 1) \gamma_k^* a_{ij}(l + 1) \tag{38}$$

The prediction can be expanded as:

$$F^*(l + 1) = LE[F(l), F(l - 1), \dots, F(l - m + 1); Z(l + 1), Z(l), Z(l - n + 1); \sigma(l + 1)] \tag{39}$$

Eq. 39 shows that the output of product quality features in stage $l + 1$ depends on $Z(l + 1)$, $((Z(l), \dots, Z(l - n + 1)), (F(l), F(l - 1), \dots, F(l - m + 1)))$ and an unpredictable error σ . Let F_{i1} and F_{i1}^* be the actual value and predicted value of a quality feature, respectively; $\tau \|\Phi\|^2$ be the regularization term of the loss function. During model training, the loss function of product quality prediction can be expressed as:

$$loss(\Phi) = - \sum_{i=1}^m F_{i1}^* \log(F_{i1}) + F_{i2}^* \log(F_{i2}) + \dots + F_{in}^* \log(F_{in}) + \tau \|\Phi\|^2 \tag{40}$$

The fully-connected layer of the model was activated by Softmax function. The final output of the product quality prediction model can be given by:

$$\hat{b} = Softmax(a_i) = \frac{o^i}{\sum_{n=1}^n o^i} \tag{41}$$

5. Experiments and results analysis

Fig. 6 compares the PCA results before and after the introduction of recursion. In Fig. 6a, the quality samples of 1,200 products were not recursively processed, but statically analyzed. Many PCA results surpassed the control line, indicating that the model could not effectively extract the principal component features of product quality in the latest MP stage. In Fig. 6b, the quality samples of 500 out of the 1,200 samples were recursively processed. It can be observed that the real-time performance of the analysis on samples collected by sliding time windows was effectively enhanced, as the results above the control line were reduced by more than 8 %.

In our prediction model, the MPMP production technology parameters and MPMP product quality variables being collected and stored were preprocessed and normalized, so that the product quality prediction accuracy will not be undermined by dimensional disunity. After that, the product quality variation of stage p was predicted based on the samples of stage $p - 1$. The specific data are given in Tables 1 and 2, where the product quality indices include appearance quality PQ1, performance index PQ2, and life index PQ3. Specifically, PQ1 covers cleanness PQ11, style PQ12, color PQ13, and packaging PQ14; PQ2 covers dimension parameter PQ21, motion parameter PQ22, and power parameter PQ23; PQ3 covers reliability PQ31, failure rate PQ32, and use cycle PQ33.

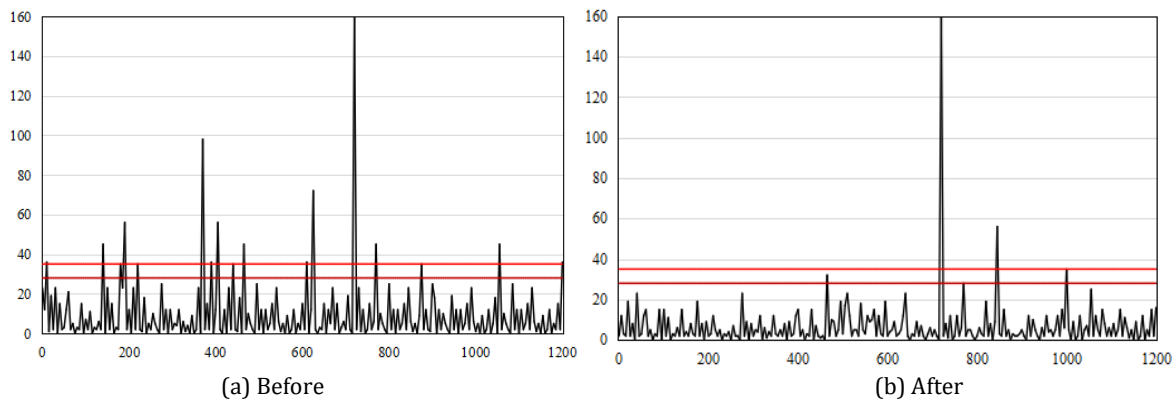


Fig. 6 PCA results before and after the introduction of recursion

Table 1 Normalized values of samples in stage $p - 1$

PQ11	0.9625	0.9657	0.9686	0.9628	0.9639	0.9583	0.9655	0.9662	0.9675
PQ12	0.1658	0.1534	0.1643	0.1725	0.1848	0.1538	0.1342	0.1658	0.1546
PQ13	0.0241	0.0325	0.0521	0.0375	0.0265	0.0164	0.0335	0.0276	0.0215
PQ14	0.9638	0.9254	0.9587	0.9352	0.9583	0.9285	0.9428	0.9647	0.9562
PQ21	0.6521	0.6358	0.6149	0.6823	0.6951	0.6214	0.6725	0.6353	0.6438
PQ22	0.3583	0.3869	0.3763	0.3242	0.3629	0.4233	0.4126	0.3584	0.3217
PQ23	0.5382	0.6353	0.5876	0.6764	0.5372	0.6857	0.5728	0.6241	0.6834
PQ31	0.1574	0.1758	0.1635	0.1634	0.1725	0.1838	0.1524	0.1326	0.1532
PQ32	0.5271	0.3525	0.5241	0.3672	0.4258	0.3581	0.7868	0.5127	0.4136
PQ33	0.3122	0.2174	0.2563	0.3727	0.1631	0.2836	0.2751	0.2675	0.3123

Table 2 Normalized values of samples in stage p

PQ11	0.9584	0.9625	0.9359	0.9433	0.9352	0.9375	0.9537	0.9742	0.9641
PQ12	0.1546	0.1346	0.1738	0.1826	0.1628	0.1435	0.1628	0.1347	0.1527
PQ13	0.0124	0.0135	0.0183	0.0175	0.0163	0.0157	0.0130	0.0175	0.0182
PQ14	0.9258	0.9342	0.9328	0.9626	0.9731	0.9539	0.9582	0.9346	0.9504
PQ21	0.6382	0.6426	0.6375	0.6832	0.6284	0.3505	0.3628	0.3751	0.3624
PQ22	0.3581	0.3684	0.4213	0.3825	0.3862	0.4135	0.4253	0.3926	0.4257
PQ23	0.4968	0.5326	0.4867	0.5315	0.4835	0.5327	0.4932	0.5147	0.4826
PQ31	0.1538	0.1627	0.1628	0.1824	0.1736	0.1524	0.1438	0.1825	0.1926
PQ32	0.2514	0.3012	0.2810	0.2624	0.2519	0.2746	0.2413	0.2534	0.2816
PQ33	0.2386	0.2485	0.2104	0.2517	0.2825	0.2431	0.2042	0.2358	0.2719

This paper adopts two typical ensemble algorithms of machine learning, namely, AdaBoost and XGBoost, as well as our model to predict the product quality in terms of PQ1-3. The prediction results (Table 3) show that our model surpassed the other algorithms in terms of accuracy, mean accuracy, and precision.

Fig. 7 compares the AUCs of PQ1 predicted by AdaBoost, XGBoost, and our model. Our model achieved desirable prediction performance, despite the large difference of MPMP in product quality. Besides, XGBoost algorithm also demonstrated a good classification ability of various product quality features.

XGBoost and our model were separately adopted to predict PQ2 and PQ3 of 60 products with known production technology parameters. The results (Figs. 8 and 9) show that XGBoost incorrectly predicted 5 qualified products as unqualified in terms of PQ2, and incorrectly predicted 2 qualified products as unqualified in terms of PQ3. By contrast, our model successfully predicted all unqualified products. This means our model has a strong ability to predict product quality.

Table 3 Production quality prediction results

Product quality features	Indices	AdaBoost	XGBoost	Our model
PQ1	Accuracy	0.862	0.87	0.89
	Mean accuracy	0.85243	0.884672	0.953281
	Precision	0.842678	0.875689	0.925768
PQ2	Accuracy	0.834	0.846	0.86
	Mean accuracy	0.868457	0.885674	0.896725
	Precision	0.863758	0.883758	0.895235
PQ3	Accuracy	0.814	0.827	0.851
	Mean accuracy	0.823758	0.863074	0.875426
	Precision	0.825712	0.862875	0.886425

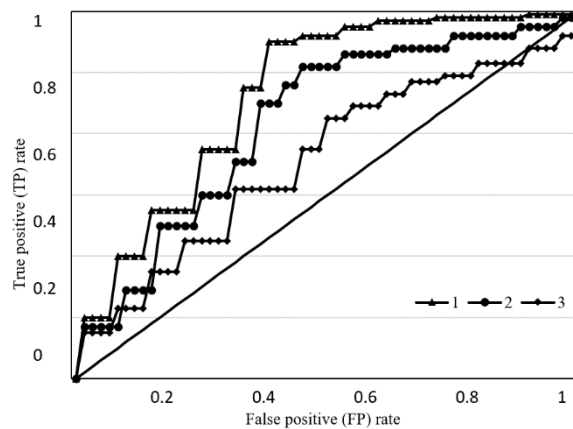


Fig. 7 Area under the curve (AUC) of PQ1

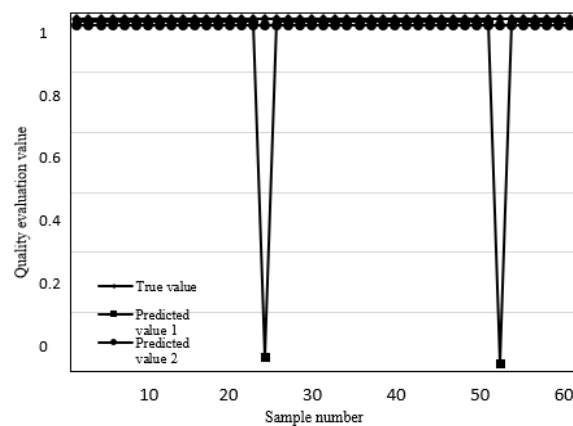


Fig. 8 Predicted PQ2 vs. true PQ2

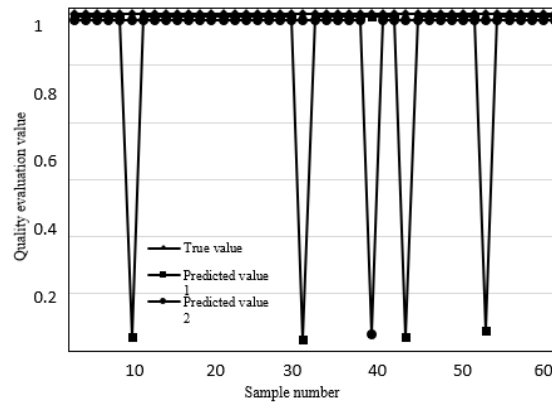


Fig. 9 Predicted PQ3 vs. true PQ3

6. Conclusion

This paper analyzes the MPMP quality prediction and control based on big data analysis. Firstly, the MPMP product quality prediction strategy and flow were detailed, followed by the extraction of MPMP product quality features. Then, the MPMP product quality features were described in multiple dimensions. Next, the attention mechanism was introduced to the prediction process, and a product quality prediction model was established based on BiLSTM. Through experiments, the PCA results before and after the introduction of recursion were compared, revealing the effectiveness of our feature extraction algorithm. After that, our model and several state-of-the-arts were separately adopted to predict product quality in terms of PQ1-3. The results show that our model achieved better accuracy, mean accuracy, and precision of product quality than other algorithms.

This paper innovatively introduces the attention mechanism to establish a quality prediction model. But many details are worthy of further study. For example, the future research could try to optimize the product quality classification rules, and apply reinforcement learning to adaptively optimize various process parameters and the manufacturing quality features collected by sensors. In addition, it is an urgent need to develop a real-time system that can automatically perceive abnormal parameters, and decide on how to optimize these parameters, in the light of the manufacturing state. The product quality prediction model can be embedded into the system to manufacture high-quality products.

References

- [1] Liukkonen, M., Tsai, T.-N. (2016). Toward decentralized intelligence in manufacturing: Recent trends in automatic identification of things, *International Journal of Advanced Manufacturing Technology*, Vol. 87, No. 9, 2509-2531, doi: [10.1007/s00170-016-8628-y](https://doi.org/10.1007/s00170-016-8628-y).
- [2] Nazifa, T.H., Ramachandran, K.K. (2019). Information sharing in supply chain management: A case study between the cooperative partners in manufacturing industry, *Journal of System and Management Sciences*, Vol. 9, No. 1, 19-47, doi: [10.33168/JSMS.2019.0102](https://doi.org/10.33168/JSMS.2019.0102).
- [3] Li, B.-H., Hou, B.-C., Yu, W.-T., Lu, X.-B., Yang, C.-W. (2017). Applications of artificial intelligence in intelligent manufacturing: A review, *Frontiers of Information Technology & Electronic Engineering*, Vol. 18, No. 1, 86-96, doi: [10.1631/FITEE.1601885](https://doi.org/10.1631/FITEE.1601885).
- [4] Istokovic, D., Perinic, M., Vlatkovic, M., Brezocnik, M. (2020). Minimizing total production cost in a hybrid flow shop: A simulation-optimization approach, *International Journal of Simulation Modelling*, Vol. 19, No. 4, 559-570, doi: [10.2507/IJSIMM19-4-525](https://doi.org/10.2507/IJSIMM19-4-525).
- [5] Shafiq, S.I., Sanin, C., Szczerbicki, E., Toro, C. (2017). Towards an experience based collective computational intelligence for manufacturing, *Future Generation Computer Systems*, Vol. 66, 89-99, doi: [10.1016/j.future.2016.04.022](https://doi.org/10.1016/j.future.2016.04.022).
- [6] Wang, C., Yang, B., Wang, H.Q. (2020). Multi-objective master production schedule for balanced production of manufacturers, *International Journal of Simulation Modelling*, Vol. 19, No. 4, 678-688, doi: [10.2507/IJSIMM19-4-C017](https://doi.org/10.2507/IJSIMM19-4-C017).

- [7] Liang, Q. (2020). Production logistics management of industrial enterprises based on wavelet neural network, *Journal Européen des Systèmes Automatisés*, Vol. 53, No. 4, 581-588, [doi: 10.18280/jesa.530418](https://doi.org/10.18280/jesa.530418).
- [8] Stasiak-Betlejewska, R. (2015). Construction product quality improvement with applying production problems analysis, *Manufacturing Technology*, Vol. 15, No. 5, 756-761, [doi: 10.21062/ujep/x.2015/a/1213-2489/MT/15/5/756](https://doi.org/10.21062/ujep/x.2015/a/1213-2489/MT/15/5/756).
- [9] Zhao, Z., Yuan, Q. (2022). Integrated multi-objective optimization of predictive maintenance and production scheduling: perspective from lead time constraints, *Journal of Intelligent Management Decision*, Vol. 1, No. 1, 67-77, [doi: 10.56578/jimd010108](https://doi.org/10.56578/jimd010108).
- [10] Ben-Ammar, O., Bettayeb, B., Dolgui, A. (2020). Integrated production planning and quality control for linear production systems under uncertainties of cycle time and finished product quality, *International Journal of Production Research*, Vol. 58, No. 4, 1144-1160, [doi: 10.1080/00207543.2019.1613580](https://doi.org/10.1080/00207543.2019.1613580).
- [11] Amar, H., Ghodbane, H., Amir, M., Zidane, M.A., Hamouda, C., Rouane, A. (2020). Microstrip sensor for product quality monitoring, *Journal of Computational Electronics*, Vol. 19, 1329-1336, [doi: 10.1007/s10825-020-01517-2](https://doi.org/10.1007/s10825-020-01517-2).
- [12] Schiermeyer, A. (2020). Optimizing product quality in molecular farming, *Current Opinion in Biotechnology*, Vol. 61, 15-20, [doi: 10.1016/j.copbio.2019.08.012](https://doi.org/10.1016/j.copbio.2019.08.012).
- [13] Poth, A., Riel, A. (2020). Quality requirements elicitation by ideation of product quality risks with design thinking, In: *Proceedings of 2020 IEEE 28th International Requirements Engineering Conference (RE)*, Zurich, Switzerland, 238-249, [doi: 10.1109/RE48521.2020.00034](https://doi.org/10.1109/RE48521.2020.00034).
- [14] Hou, Y., Cao, Z.J., Yang, S.L. (2019). Cloud intelligent logistics service selection based on combinatorial optimization algorithm, *Journal Européen des Systèmes Automatisés*, Vol. 52, No. 1, 73-78, [doi: 10.18280/jesa.520110](https://doi.org/10.18280/jesa.520110).
- [15] Xu, M., Cai, H., Liang, S. (2015). Big data and industrial ecology, *Journal of Industrial Ecology*, Vol. 19, No. 2, 205-210, [doi: 10.1111/jiec.12241](https://doi.org/10.1111/jiec.12241).
- [16] Chen, D. (2020). Multiple linear regression of multi-class images in devices of internet of things, *Traitement du Signal*, Vol. 37, No. 6, 965-973, [doi: 10.18280/ts.370609](https://doi.org/10.18280/ts.370609).
- [17] Wang, Y., Jan, M.N., Chu, S., Zhu, Y. (2020). Use of big data tools and industrial internet of things: An overview, *Scientific Programming*, Vol. 2020, Article ID 8810634, [doi: 10.1155/2020/8810634](https://doi.org/10.1155/2020/8810634).
- [18] Song, Y.-J., Lee, J.-K. (2020). A blockchain and internet of things based architecture design for energy transaction, *Journal of System and Management Sciences*, Vol. 10, No. 2, 122-140.
- [19] Yin, B., Wei, X., Wang, J., Xiong, N., Gu, K. (2019). An industrial dynamic skyline based similarity joins for multi-dimensional big data applications, *IEEE Transactions on Industrial Informatics*, Vol. 16, No. 4, 2520-2532, [doi: 10.1109/TII.2019.2933534](https://doi.org/10.1109/TII.2019.2933534).
- [20] Gupta, A.K., Chakraborty, C., Gupta, B. (2019). Monitoring of epileptical patients using cloud-enabled health-IoT system, *Traitement du Signal*, Vol. 36, No. 5, 425-431, [doi: 10.18280/ts.360507](https://doi.org/10.18280/ts.360507).
- [21] Lu, J. (2020). Industrial pollution governance efficiency and big data environmental controlling measures: A case study on Jiangsu province, China, *Nature Environment and Pollution Technology*, Vol. 19, No. 4, 1743-1748, [doi: 10.46488/NEPT.2020.v19i04.046](https://doi.org/10.46488/NEPT.2020.v19i04.046).
- [22] Zhang, X., Ge, Z. (2020). Local parameter optimization of LSSVM for industrial soft sensing with big data and cloud implementation, *IEEE Transactions on Industrial Informatics*, Vol. 16, No. 5, 2917-2928, [doi: 10.1109/TII.2019.2900479](https://doi.org/10.1109/TII.2019.2900479).
- [23] Rosin, F., Forget, P., Lamouri, S., Pellerin, R. (2021). Impact of Industry 4.0 on decision-making in an operational context, *Advances in Production Engineering & Management*, Vol. 16, No. 4, 500-514, [doi: 10.14743/apem2021.4.416](https://doi.org/10.14743/apem2021.4.416).
- [24] Nowakowska, M., Pajeci, M. (2021). Latent class analysis for identification of occupational accident casualty profiles in the selected Polish manufacturing sector, *Advances in Production Engineering & Management*, Vol. 16, No. 4, 485-499, [doi: 10.14743/apem2021.4.415](https://doi.org/10.14743/apem2021.4.415).
- [25] Ren, L., Meng, Z., Wang, X., Zhang, L., Yang, L.T. (2020). A data-driven approach of product quality prediction for complex production systems, *IEEE Transactions on Industrial Informatics*, Vol. 17, No. 9, 6457-6465, [doi: 10.1109/TII.2020.3001054](https://doi.org/10.1109/TII.2020.3001054).
- [26] Chu, F., Peng, C., Jia, R., Chen, T., Lu, N. (2021). Online prediction method of batch process product quality based on multi-scale kernel JYMKPLS transfer model, *CIESC Journal*, Vol. 72, No. 4, 2178-2189, [doi: 10.11949/0438-1157.20200995](https://doi.org/10.11949/0438-1157.20200995).
- [27] Lughofer, E., Zavoianu, A.-C., Pollak, R., Pratama, M., Meyer-Heye, P., Zörrer, H., Eitzinger, C., Radauer, T. (2019). Autonomous supervision and optimization of product quality in a multi-stage manufacturing process based on self-adaptive prediction models, *Journal of Process Control*, Vol. 76, 27-45, [doi: 10.1016/j.jprocont.2019.02.005](https://doi.org/10.1016/j.jprocont.2019.02.005).
- [28] Hao, L., Bian, L., Gebraeel, N., Shi, J. (2016). Residual life prediction of multistage manufacturing processes with interaction between tool wear and product quality degradation, *IEEE Transactions on Automation Science and Engineering*, Vol. 14, No. 2, 1211-1224, [doi: 10.1109/TASE.2015.2513208](https://doi.org/10.1109/TASE.2015.2513208).
- [29] Zheng, R., Pan, F. (2017). Multi-phase support vector regression soft sensor for online product quality prediction in glutamate fermentation process, *American Journal of Biochemistry and Biotechnology*, Vol. 13, No. 2, 90-98, [doi: 10.3844/ajbbbsp.2017.90.98](https://doi.org/10.3844/ajbbbsp.2017.90.98).
- [30] Melhem, M., Ananou, B., Ouladsine, M., Pinaton, J. (2016). Regularized regression models to predict the product quality in multistep manufacturing, In: *Proceedings of 2016 5th International Conference on Systems and Control (ICSC)*, Marrakesh, Morocco, 31-36, [doi: 10.1109/ICoSC.2016.7507067](https://doi.org/10.1109/ICoSC.2016.7507067).

Experimental determination of influences on a gauge block's stack length

Lipus, L.C.^a, Acko, B.^{a,*}, Tompa, J.^a

^aUniversity of Maribor, Faculty of Mechanical Engineering, Slovenia

ABSTRACT

Gauge blocks are an important basis for maintaining traceability in dimensional metrology, used for calibrating length measuring instruments and for adjustments in all branches of manufacturing. Their important feature is that they can be wrung with small dimensional uncertainty. An overview of the factors influencing the accuracy of a stack length, such as the quality of the gauge blocks (grade, wear), surface preparation (cleaning and usage of a lubricant), wringing (way and time, temperature of hands and gloves) is given in the paper. Experiments for determining these influences were performed with a highly precise gauge block comparator. Proper selection of gauge blocks, preparation of their surfaces and oiling improve the accuracy of a stack length. Application of a lubricant, wiped with a dry cloth or paper towel, helps to wring them more easily, but its contribution to the stack length in the experiment was 0.1 µm for oil and 0.2 µm for grease. Temperature changes of gauge blocks were estimated by holding them, and, during wringing in well controlled air conditions, monitoring them to yield the empirical coefficients of their warming up. The results showed that usage of gloves reduces the warming up by approximately half, but still the stack must be stabilised in well controlled conditions for at least one hour if it is used for micrometre-level precise measurements.

ARTICLE INFO

Keywords:
Gauge blocks;
Wringing;
Measurement uncertainty;
Dimensional metrology

**Corresponding author:*
bojan.acko@um.si
(Acko, B.)

Article history:
Received 7 April 2022
Revised 25 September 2022
Accepted 28 September 2022



Content from this work may be used under the terms of the Creative Commons Attribution 4.0 International License (CC BY 4.0). Any further distribution of this work must maintain attribution to the author(s) and the title of the work, journal citation and DOI.

1. Introduction

Gauge blocks (GBs) are one of the most accurate standards of length, an important basis of industrial length measurements, as well as commonly used measurement standards for maintaining traceability in dimensional metrology. They are made of wear-resistant material (hardened steel, ceramics, or tungsten carbide), and their length is defined by two parallel measuring surfaces. An important feature of gauge blocks is that they can be joined together with very little dimensional uncertainty. They are used as a reference, either as single blocks, or two or more joined strongly together by wringing, or wrung onto plates with a similar high-quality surface.

The four grades of GBs available on the market are defined by the Standard SIST EN ISO 3650. The reference standard sets of grade K are calibrated by laser interferometry, performed almost exclusively by national laboratories. Lower-level grade sets are calibrated by mechanical comparison to the reference GBs, performed widely in calibration laboratories throughout the engineering industry. Calibration uncertainty with a comparator is inferior to interferometric calibration, but the instrumentation is less expensive and the procedure much simpler. Generally, GBs of grade zero are used for inspections and calibrations in measurement laboratories, GBs of grade 1 are used for precise adjustments, e.g., for sin bars, GBs of grade 2, having the smallest accuracy, are used for adjusting machine tools.

In micrometre-precise laboratory and production measurements, grade zero is generally used as a reference. Along with length deviation and the uncertainty of GBs, known from their calibration certificate, the uncertainty of wringing film thickness and thermal contributions to the mutual uncertainty of the reference, must be taken into consideration. In the present paper, these uncertainty contributions are analysed and presented by in-situ measurements of different GBs (ceramic, steel; single or wrung), performed with a gauge block comparator and precise temperature sensors in well controlled air conditions.

The experiments were performed in the Laboratory for Production Measurement (University of Maribor, Slovenia). The applied mechanical comparison procedure is accredited, and the calibration and measurement capability (CMC) is included into the key comparison database at BIPM [1, 2]. The laboratory, as a holder of the National Standard for length, is accredited for length-calibrations of standards and measuring equipment, with the primary purpose to assure dimensional traceability in Slovenian industry. For maintaining high level measurement capability, the laboratory develops measurement procedures steadily with novel equipment and laser interferometry, and, periodically, joins international comparisons for their verification [3-6]. Reliable measurement systems are especially important in complex geometrical measurements, as well as in precise machine tool monitoring and verification, in the sense of optimising production processes, and for controlling product quality. The secondary task of the laboratory is focused on the development of sustainable manufacturing systems and advanced automated integration of data, including calibration results, up to the global information level [7, 8].

2. Materials, methods and execution of experiments

2.1 Gauge blocks as a length standard

Standard SIST EN ISO 3650 defines the geometrical characteristics of gauge blocks and tolerances precisely for four grades, at the standard temperature 20 °C. Some are represented here (Fig. 1 and Table 1) for the purpose of interpretation of the experimental results. The limit deviation, t_e , is the maximal permitted deviation of the length from the nominal length l_n at any point of the measuring face. The recommended points to measure are the five points presented in Fig. 1. The tolerance t_v is defined for variation $v = l_{\max} - l_{\min}$. The central deviation is $e_c = l_c - l_n$, while the limit deviations are defined as $f_o = l_{\max} - l_c$ and $f_u = l_c - l_{\min}$.

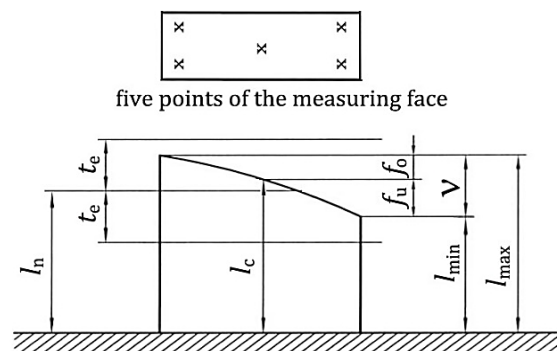


Fig. 1 Geometrical characteristics of GB length

Table 1 Limit deviation, t_e , of the length at any point of the measuring face from the nominal length and tolerance, t_v , for the variation in length

L_n / mm	Grade K		Grade 0		Grade 1		Grade 2	
	$t_e / \mu\text{m}$	$t_v / \mu\text{m}$						
$0.5 \leq L_n \leq 10$	0.2	0.05	0.12	0.1	0.2	0.16	0.45	0.3
$10 < L_n \leq 25$	0.3	0.05	0.14	0.1	0.3	0.16	0.6	0.3
$25 < L_n \leq 50$	0.4	0.06	0.20	0.1	0.4	0.18	0.8	0.3
$50 < L_n \leq 75$	0.5	0.06	0.25	0.12	0.5	0.18	1.0	0.35

Although the materials chosen for producing GBs have very stable crystal structures, on the level of the required reliability (of grade K and 0) the material structure stability is still temporal, even with proper handling and storage. Therefore, periodical calibration of GB sets is recommended, once per year up to three years, depending on the frequency and required dimensional accuracy of their use. The measuring surfaces are polished to such a degree that can be joined easily by sliding, and they can get so strongly adhered that can be separated only by tangential pulling apart. The wringing film is small, with very little dimensional uncertainty, if the gauge blocks are treated properly. Considering the fact that GBs are used either as a single block wrung onto a plate with similar surface quality, or as a stack of blocks, the wringing film is included into the calibration results of the block length, as defined by the ISO 3650 standard (Fig. 1 and Table 1). In the case of calibrating Grade K with laser interferometry, the wringing film on the plate contributes to a length uncertainty of less than 6 nm [9]. The roughness of a well-polished surface varies from 15 nm to 30 nm [10, 11].

The wringing film thickness varies with the surface quality and lubricant fluid used. Blocks are cleaned with alcohol or petrol ether, while steel blocks also need protection against corrosion with special oil wetting. Before usage, the blocks are wiped with a lint-free cloth to make sure they are free from dust. By sliding the blocks air is squeezed out, and the surfaces get adhered together by vacuum and molecular interaction. The strong adherence can be explained by the surface tension of the liquid film (of oil, or water vapour from the air): The cohesive forces between molecules in a liquid and with a solid surface are stronger than those on its surface in contact with the air, therefore, when we try to separate the blocks, the liquid tries to minimise its surface. Fig. 2 presents the high ability of oil to wet the surface of a gauge block. Additionally, the fine roughness observed on the measuring surfaces could enhance the adhesion, due to the phenomenon of liquid bridge splitting, since mobile wetting bridges can naturally migrate to narrower gaps [12].

The stacks should be disassembled after usage, even in daily use. Leaving them together for a few days can cause that they become difficult to separate, or even to get permanently fused.

We need to make sure that the blocks to be wrung are clean, free from dust, nicks and burs. If the surface is not clean, for instance, due to fingerprints, they get wrung more easily, but the uncertainty of the wringing film is higher. The presence of nicks or burs was inspected visually and with an optical flat (Figs. 3a-c). We place the glass on the measuring surface of the block to check for a rainbow by sliding it slightly. If the rainbow disappears when we press harder, it means there are no asperities present. If the rainbow stays in the same place when we slide the glass over the block, it means that the asperity is on the block. If the rainbow moves, the asperity is attached to the glass surface, or too much oil was applied.

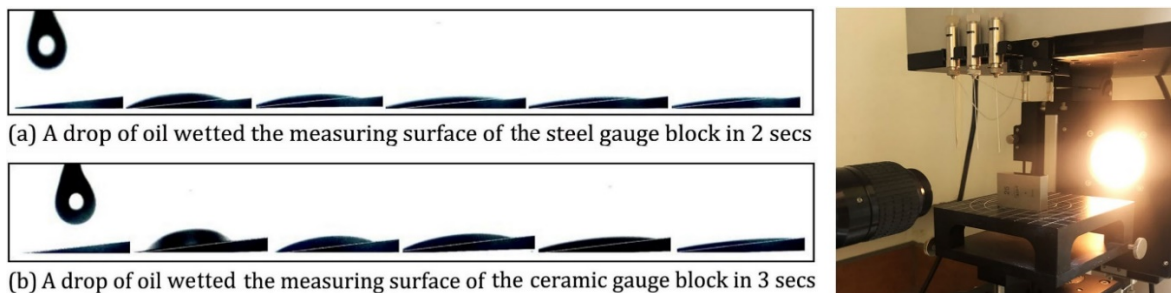


Fig. 2 Wetting of a GB surface with anti-corrosion oil (goniometrical observation of the contact angle)

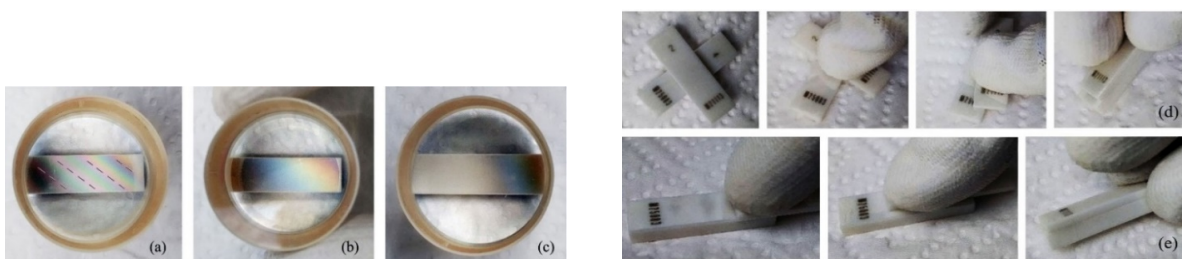


Fig. 3 The surface inspection with plane-parallel glass and wringing of thin blocks

Wringing should be done by sliding without much pressure. Two ways of wringing of thin blocks are presented in Fig. 3. By repeatedly sliding the upper block on the lower at a cross position (with slight pressure of the finger downward at the central point, Fig. 3d), the air is squeezed out and the surfaces stick together. Then, we align the blocks by rotating the upper block (with lateral pressure of another finger keeping the vertical pressure on the centre). Another way is by direct sliding of the upper block along the lower one (with slight pressure of the finger downward, Fig. 3e).

If possible, blocks should be held on their side surfaces, otherwise the measuring surface that has been touched must be cleaned with petroleum ether, either to perform the measurement properly, or to continue with wringing of an additional block. When wringing, excessive force shall not be used, because the contact might be weaker (with greater thickness and variability), also some damage might occur on the edges or scratches on the measuring surfaces. Before storing a steel block, clean it with petroleum ether (or ethanol) and coat it with oil, to protect it from corrosion, especially if it has been touched it with bare hands. When reused, they shall be wiped with a dry cloth or petroleum ether.

As a new block is wrung repeatedly, the film thickness might shrink due to wear of the asperities of surface roughness. If a block becomes worn and scratched, its ability to wring decreases and the film thickness increases, so it is better to replace it with a new one, or to repair it, because even using it as a single may give erratic results. A block with a corroded measuring surface must be replaced immediately, because it will damage any other block it is wrung onto.

In some cases, we can repair a scratched surface with a special stone (Fig. 4). Again, we need to make sure that both surfaces, of the GB and of the stone, are clean and free from dust, before and after polishing. While a scratch remains visible, austerities are removed, and the GB has an improved ability to wring.

Gauge blocks are available in sets enabling them to be stacked to the desired length in a wide range. With GBs from the conventional set presented in Tab. 2, we can make any length up to three decimal places. For instance, 15.63 mm is a combination of four blocks (1.03 + 1.6 + 3 + 10) mm.

We try to assemble the desired length with as few blocks as possible to avoid accumulation of size errors. Single blocks with specific nominal lengths are available for this purpose. There are sets with which we can compose any measure in three decimal places. Depending on the desired minimum number of contacts in the assembly, individual blocks can be purchased, with which the same length can be assembled with one or two blocks less than in the conventional way of assembling. From Table 3, lengths up to 27.50 mm can be assembled only by two blocks, also in regions like (31.00 to 32.50) mm, for instance, 31.11 mm from 30 mm and 1.11 mm, while from Table 2 four blocks would be needed: (1.01 + 1.1 + 9 + 20) mm. In ranges like (27.51 to 29.99) mm we need three blocks from Table 3, for instance 27.51 mm is (1.51 + 1 + 25) mm, and 29.99 mm is (1.49 + 3.5 + 25) mm, a block less than from Table 2.

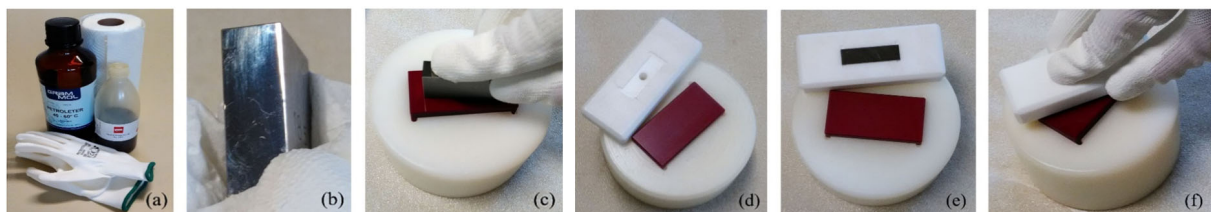


Fig. 4 Polishing with GB stone: (a) Petrol ether for cleaning and anti-corrosion oil, (b) Scratches, (c) Polishing with low pressure along the stone, (d-f) Accessory for a thin GBs

Table 2 Conventional set of gauge blocks (all in mm)

1.001	1.002	1.003	1.004	1.005	1.006	1.007	1.008	1.009
1.01	1.02	1.03	1.04	1.05	1.06	1.07	1.08	1.09
1.1	1.2	1.3	1.4	1.5	1.6	1.7	1.8	19
1	2	3	4	5	6	7	8	9
10	20	30	40	50	60	70	80	90

Table 3 Individual gauge blocks (all in mm)

1.00	1.01	1.02	1.03	1.04	...	1.45	1.46	1.47	1.48	1.49
			1.5	1.6	1.7	1.8	1.9			
2.00	2.01	2.02	2.03	2.04	...	2.45	2.46	2.47	2.48	2.49
			2.5	2.6	2.7	2.8	2.9			
3	3.5	4	4.5	5	...	22.5	23	23.5	24	24.5
25	30	35	40	45	50	60	70	80	90	100

Standard grade blocks are made of a hardened steel alloy, while calibration grade blocks are often made of carbide or ceramic, because they are harder and wear less. The results of measurements should be given at the standard temperature 20 °C, which can be achieved by well-controlled air conditions in measuring rooms or chambers.

When the measuring systems and measurands are made of steel and steel blocks are used, the thermal expansion coefficients of the materials, α , are similar, and the length errors, ΔL , at temperature deviations, ΔT , might be negligible (Eq. 2). The thermal expansion coefficient of steel blocks is approximately $11.5 \cdot 10^{-6} \text{ K}^{-1}$, of ceramic $9.4 \cdot 10^{-6} \text{ K}^{-1}$ and of carbide $4.4 \cdot 10^{-6} \text{ K}^{-1}$. In the case of ceramic or carbide blocks, due to the significant difference of their coefficients compared to steel, it is necessary to pay more attention to the thermal stabilisation and to temperature correction of the measured length.

$$\Delta L = \alpha L \Delta T \tag{1}$$

$$\Delta L = \Delta \alpha L \Delta T \tag{2}$$

Among other influences, a change in a gauge block's temperature may be caused by touching it by hand. Gloves are recommended for handling them, tweezers could also be used to transfer individual gauge blocks, but, when assembling them, the blocks warm up noticeably, even if we manage to wring them in a very short time by using gloves. Therefore, we need to wait some time for the stack to be cooled. The cooling time depends on the required accuracy of measurement for which it is going to be applied.

2.2 Measurement of gauge block stack length

The purpose of the experiments was to determine the time of temperature stabilisation after assembling the blocks, and the repeatability of the residual contact. The deviation was observed with a precision GB comparator (Fig. 5), which is used in our laboratory for calibrating GB sets [1, 2]. The air temperature in the chamber was maintained at $(20 \pm 0.3) \text{ }^\circ\text{C}$ and monitored by a sensor calibrated with a measurement uncertainty of 0.05 K, installed near to the blocks. The GBs' temperature was measured with sensors with a 0.015 K measurement uncertainty (Fig. 6a). Immediately after wringing (Fig. 6b), the stack was inserted under the comparator's probe (Fig. 6c). During its temperature stabilisation, the deviation was measured periodically in comparison with the reference (Figs. 6c-e) until the temperature difference of the assembly and the reference became negligible. The length difference e_c was measured at the central points, and corrected for the length deviation of the reference e_{ref} (taken from the calibration certificate). The measurement uncertainty for the length of 50 mm, evaluated as our CMC in the accredited calibration procedure, is $0.055 \text{ } \mu\text{m}$ for steel and $0.07 \text{ } \mu\text{m}$ for ceramic GBs.

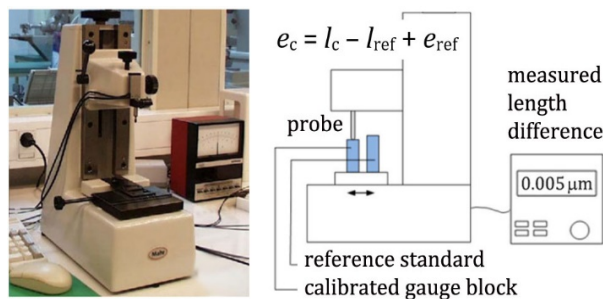


Fig. 5 Mechanical comparator for GB calibration

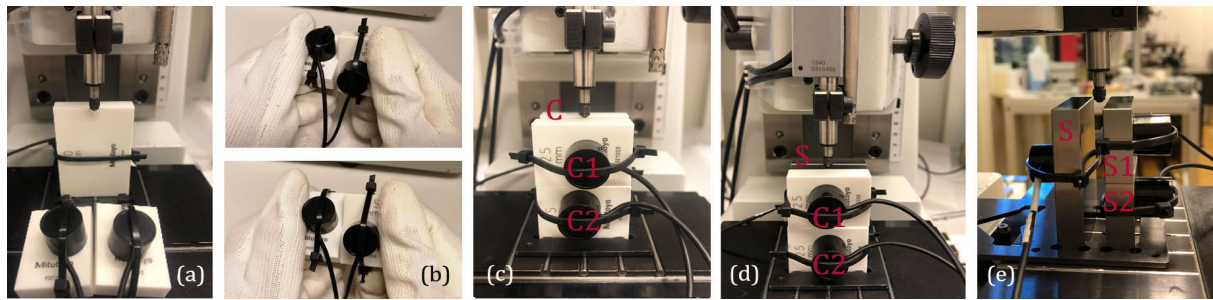


Fig. 6 Measurement of stack length by mechanical comparison: (a) Temperature stabilisation of GBs, (b) Wringing, (c) Comparison of the ceramic stack to the ceramic ref., (d) Ceramic stack to the steel, (e) Steel stack to the steel reference

3. Experimental results and discussion

The measurements were performed for three combinations (presented in Fig. 6). The stack of steel blocks S1 and S2, and the stack of ceramic blocks (C1 and C2) were compared with the (S) steel reference 50 mm from the master set (Grade K). The measurement with the ceramic stack was repeated also in comparison with the (C) ceramic reference 50 mm (Grade 0), in order to eliminate the difference in the thermal expansion coefficient. The blocks used for the wringing test were previously calibrated on the comparator. Their geometrical characteristics, derived from five points (as presented in Fig. 1) are given in Table 4 for five repeated measurements.

Table 4 Geometrical characteristics of the gauge blocks used in the experiments (all in μm)

(C1) ceramic 25 mm (Grade 0)				(S1) steel 25 mm (Grade K)			
e_c	v	f_o	f_u	e_c	v	f_o	f_u
-0.05	0.10	0.10	0.00	0.01	0.02	0.00	0.02
-0.05	0.09	0.09	0.00	0.02	0.02	0.00	0.02
-0.05	0.07	0.07	0.00	0.02	0.03	0.00	0.03
-0.05	0.09	0.08	0.01	0.01	0.02	0.00	0.02
-0.05	0.08	0.08	0.00	0.01	0.02	0.00	0.02

(C2) ceramic 25 mm (Grade 0)				(S2) steel 25 mm (Grade 0)			
e_c	v	f_o	f_u	e_c	v	f_o	f_u
-0.04	0.06	0.06	0.00	0.00	0.04	0.00	0.04
-0.05	0.07	0.07	0.00	0.00	0.04	0.01	0.03
-0.04	0.08	0.08	0.00	-0.01	0.05	0.01	0.04
-0.03	0.06	0.06	0.00	0.00	0.05	0.01	0.04
-0.04	0.08	0.08	0.00	0.00	0.05	0.01	0.04

By precise observation of these characteristics, taking into account that the lower contact layer is already included into the given central deviation e_c for both blocks in the stack, the additional geometrical contribution to the central deviation of the stack can be estimated from the characteristics given for the upper surface of the lower block, and the means of C2 in the ceramic stack and S2 in the steel stack (Fig. 6), respectively. From Table 4, the block S1 has $f_o = 0.00 \mu\text{m}$ and the centre, as the highest level, has the deviation $e_c = 0.014 \mu\text{m}$ (higher than the nominal value 25 mm); the block S2 has $e_c = 0.00 \mu\text{m}$ and $f_o = 0.01 \mu\text{m}$. So, we can estimate the mutual geometrical contribution to be $0.024 \mu\text{m}$. The C1 block has $f_o = 0.084 \mu\text{m}$ (some asperity around the centre, which does not affect the length of the stack, because this block is on the top) and central deviation $e_c = -0.05 \mu\text{m}$ (lower than the nominal value 25 mm). Similarly, C2 has $e_c = -0.04 \mu\text{m}$ and $f_o = 0.07 \mu\text{m}$ (some asperity around the centre, which could affect the length of the stack). So, we can estimate the mutual geometrical contribution to be $-0.02 \mu\text{m}$. Both estimated values are smaller than the measurement accuracy.

To determine the influencing factors, the repeatability of stack length was observed at different conditions, such as temperature of the hand, GB material and the addition of lubricant. Firstly, the single blocks were held in the hand (in a similar way as when assembling them) for 5 min and

then cooled in air in the chamber, to estimate the heat transmission coefficient and time for stabilisation back to a standard temperature. The graphs in Fig. 7 show the heating of 25 mm long blocks, ceramic or steel, with a bare hand or with gloves, respectively (Fig. 7). It should be emphasised here that the general recommendation is to hold the blocks on their side faces. Surfaces touched by bare fingers should be cleaned with alcohol or petroleum ether, and coated with oil before being stored, as contact with the skin promotes corrosion.



Fig. 7 Heating blocks by holding: (a) With gloves, (b) With bare hands, (c) Stabilisation for 45 min

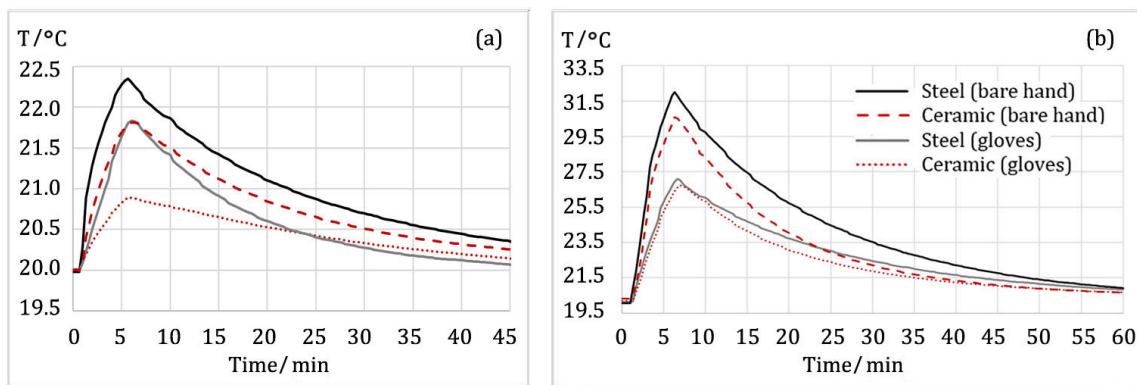


Fig. 8 Heating of 25 mm long blocks: (a) J.T. experimenter with plasticised gloves, (b) M.M. with cotton gloves

Fig. 8 presents the graphs of heating performed by two persons (a J.T. experimenter and an M.M. experimenter). In Fig. 8a the blocks were held with relatively cold hands and plasticised cotton gloves were used, while, in Fig. 8b, held with relatively warm hands and cotton gloves which were not plasticised. We can see that warming up depends strongly on the temperature of the hand (Table 5) and time of holding (Table 6). In the case of the higher temperature of the hand, warming was significantly faster. The heat transfer rates are higher at the beginning, due to the larger temperature differences in the hand-block contact.

Also, the cooling rate was initially higher, depending on the temperature difference between the block and the air. Within one hour, the temperature of the blocks returned to room temperature, regardless of the height of the temperature peak and the material, because the cooling rate depends more on the air convection than on the conductivity of the material.

Table 5 Variation in the hand's temperature during the experimentation (all in °C)

	J.T. experimenter			M.M. experimenter		
Bare hand	20.8	21.5	22.5	29.8	32.5	32.7
With gloves	20.5	21.1	21.8	27.4	30.5	31.0

Table 6 The slope of heating at the first 30 sec (K/10 sec)

	J.T. experimenter		M.M. experimenter	
	First 30 sec	During 5 min	First 30 sec	During 5 min
Steel (bare hand)	0.23	0.08	0.55	0.40
Ceramic (bare hand)	0.13	0.06	0.50	0.34
Steel (gloves)	0.07	0.06	0.37	0.23
Ceramic (gloves)	0.04	0.03	0.25	0.22

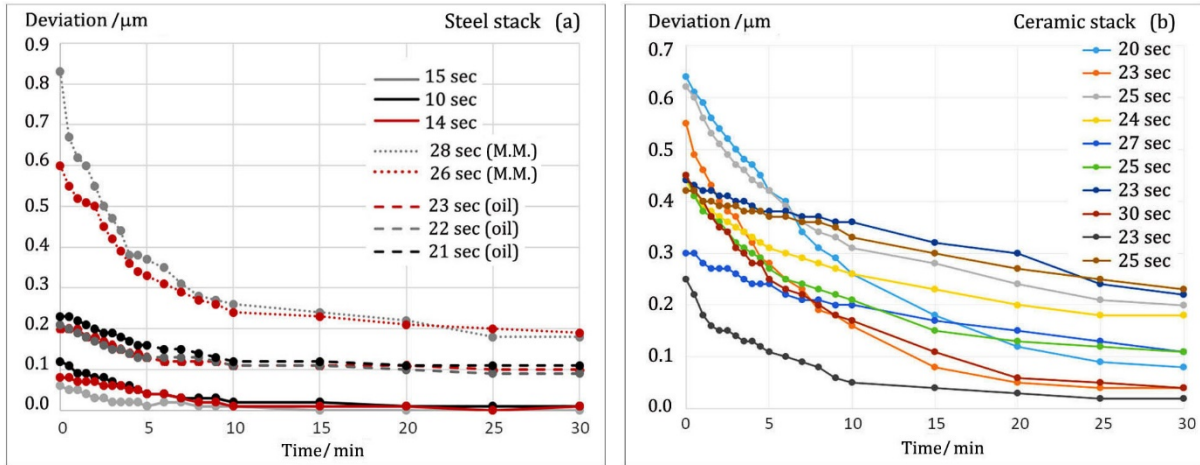


Fig. 9 Deviation of stack length after wringing: (a) Steel stack (J2 + J1) by J.T. with plasticised gloves (at conventional or extra oil application) and M.M. with cotton gloves, (b) Ceramic stack (K2 + K1) by J.T. with plasticised gloves

Some measurements of the stack length were performed on the comparator within 30 seconds of cooling, starting immediately after wringing. The length deviations of the stack in comparison to the reference block are presented in Fig. 9. The time needed for wringing is given in the legend for each repetition. The major cause of the wide range of deviations was the difference in temperature of the hands, time of wringing, while the residual deviations depend on oil application, wear of the gauge blocks and wringing skills. The ceramic blocks were more difficult to wring and easier to separate in comparison to the steel blocks, where traces of oil contributed to stronger adhesion. The major reason for the increased length was warming by hands.

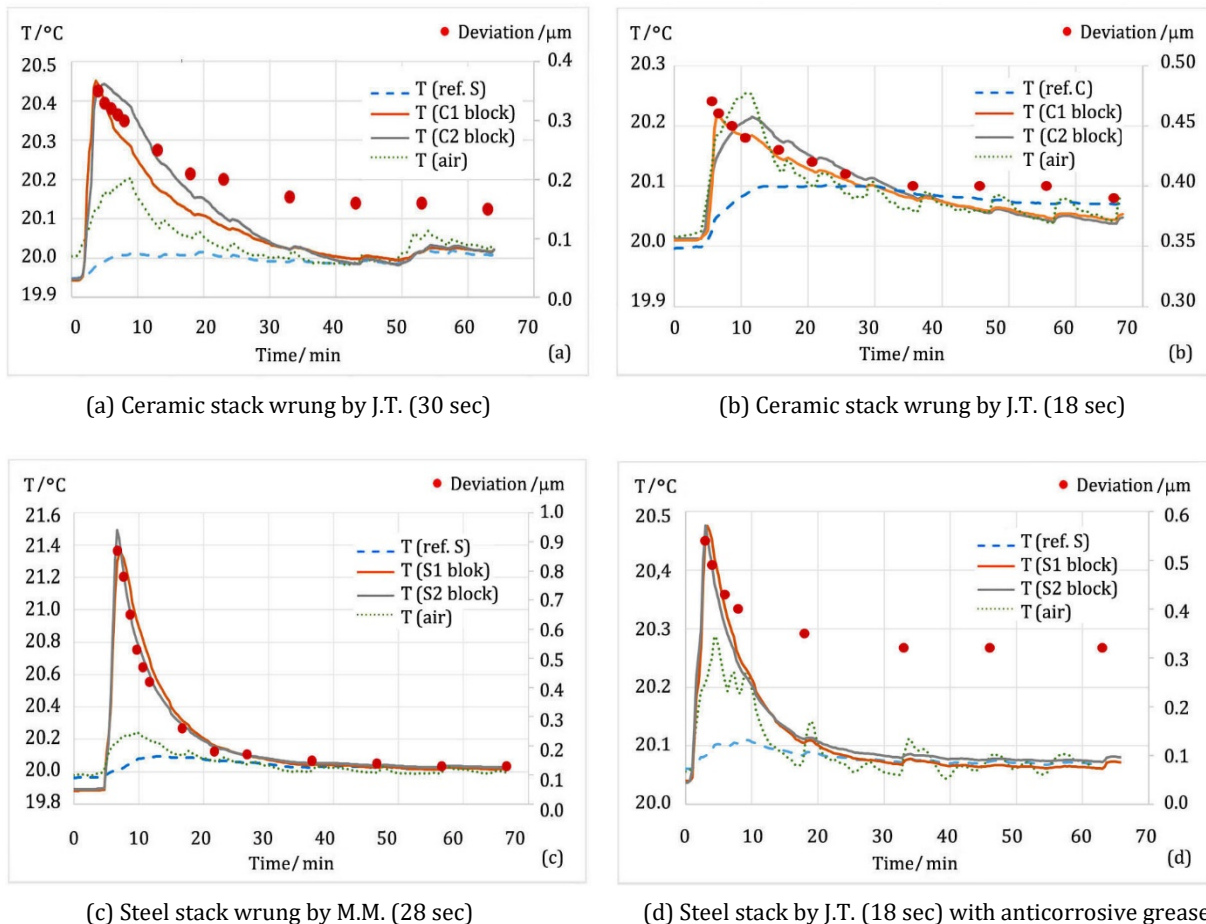


Fig. 10 Temperatures and length deviation of the stacks

Table 7 The residual length deviations (all in μm)

Residual length deviation	After one hour	After 16 hours
Ceramic stack (Fig. 10a)	0.15	0.15
Ceramic stack (Fig. 10b)	0.39	0.40
Steel stack (Fig. 10c)	0.13	0.12
Steel stack with grease (Fig. 10d)	0.32	0.31

The precise observations on the comparator were repeated with the temperature of all blocks and the air monitored in well controlled conditions in the laboratory chamber (Fig. 6). Different cases are collected on Fig. 10. We can see that the temperature of the stack stabilised within one hour. Some fluctuation of the air temperature appeared, due to the experimenter's presence, at the beginning (during wringing and installation of the stack onto the comparator), and periodically during performance of the measurement on the comparator, but this didn't affect the residual deviation of the stack significantly (because both the stack and the reference block had the same temperature of the air at the end), as well it decreased very little the initial length deviation of the stack, maximally 5 % (because the reference block responded slowly, with the quotient between the temperature of refence and the air approximately 0.2).

The residual deviations were checked the next day and remained almost the same (Table 7). The measured deviation is the sum of the residual deviation and the deviation due to the temperature difference between the assembly and the reference block, which can be calculated by Eq. 1.

Taking from Fig. 10 the time of wringing and the initial temperature change, the slope of heating is around 0.55 K/10 sec by the M.M. experimenter, 0.15 K/10 sec for the ceramic and 0.25 K/10 sec for the steel by the J.T. experimenter, which is higher than when the blocks were just held (Table 6), i.e. without active work of the hands. It is known that friction between surfaces can heat the material significantly [13, 14], depending on load, friction coefficient and lubrication [15]. In cases of blocks' wringing, these contributions are rather negligible.

Fig. 11 presents repetitions of the sliding of blocks similarly to the previous wringing (Fig. 10), but in this observation the blocks were held with thick insulation material to prevent the heat transfer from the hands, and the sensors were attached to the side surfaces of the blocks just at the edge, to monitor the temperature close to the sliding surfaces. From the temperature rise for both blocks, corrected for other possible influences from Fig. 11d, the contribution of friction was around 0.03 K/10 sec.

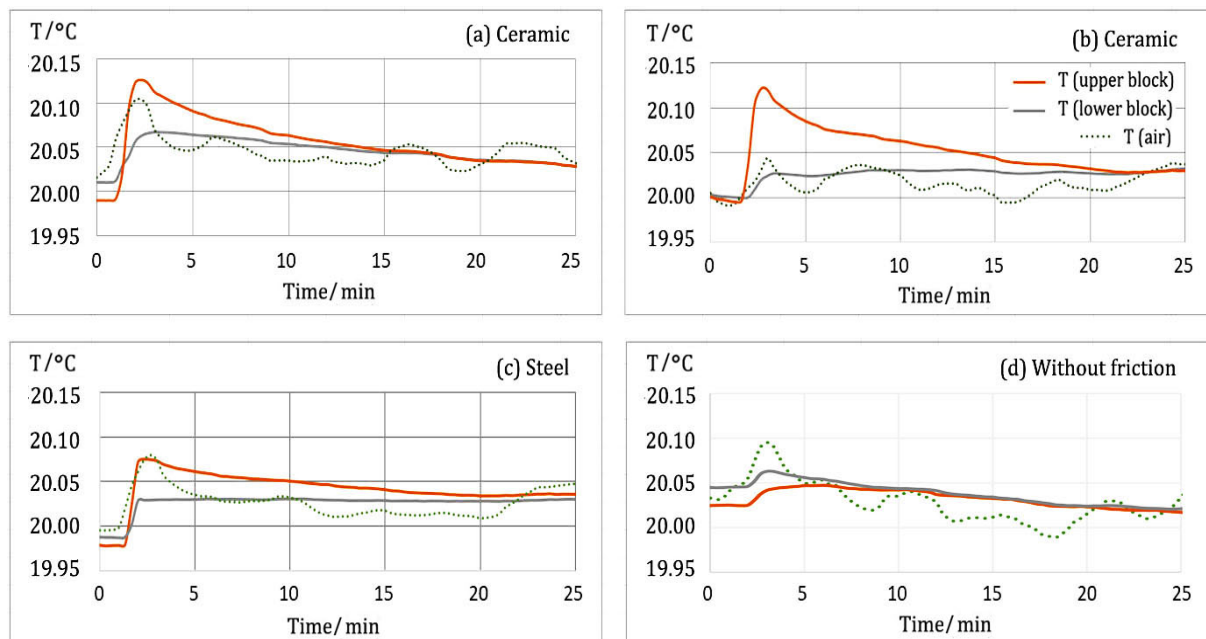


Fig. 11 Temperature rise at the estimated force (perpendicular to the surface) 10 N during 35 sec of sliding

4. Conclusion

Gauge blocks used as a reference, either as single blocks wrung onto a plate or assembled together, have some deviation in length due to inter-surface contact thickness, which depends on many factors: the quality of the blocks (grade, geometric characteristics, roughness, and wear), surface preparation (cleaning and use of a lubricant), the method of assembly, time and wringing skills, hand temperature and insulating protection of gloves.

To determine the quality of blocks, it is recommended to calibrate gauge blocks periodically. In the calibration certificate, the given length of a block already includes the thickness of the contact of the lower measuring surface (when wrung onto an ideal base), and the geometric contribution to the upper contact can be estimated from the given variance of the upper measuring surface. Depending on the length of the gauge blocks and their grade, a tolerance of 0.1 μm variance is allowed up to 25 mm, 0.16 μm for grade 1 and 0.3 μm for grade 2. In our experiment, gauge blocks (grade 0) with such geometric characteristics were selected that the final geometric contribution was negligible compared to the reliability of the measurement procedure on the comparator.

The main contribution in this article are precise insitu measurements with length comparator and temperature sensors in well air controlled laboratory environment to determine the length uncertainty of stacks due to wringing process. The results that initial deviations due to heating by hands are not negligible in comparison to the geometrical deviations (that are determined by quality of blocks used for assembly). They vary with time, way of wringing and temperature of hands. The results in the article are given for the range of cold and extremely warm hands. The use of plasticised gloves is highly recommended to reduce the temperature contribution, as the heating rate was slowed by about half in both cases.

The observations regarding the preparation of blocks' surface showed that in the case of oil traces (after oil application the surface is wiped with petrolether) the adhesion increased, the contact is smaller and with better repeatability. Additional application of oil (wiped just with a dry cloth or paper towel) is useful for lower quality surfaces, this makes the blocks easier to wring, but the contribution of the contact is greater. In our experiments, the oil layer contributed 0.1 μm and the grease 0.2 μm .

After wringing, the stacks shall be allowed to cool to operating temperature before using them, depending on the required reliability of the measurements, where they are use as a reference. Our experiments have shown that one hour is enough at well controlled air conditions. The residual deviations after one hour were the same as after one day of stabilization. The residual value can be estimated from the geometrical quality of used blocks (depending on wear and grade determined from calibration certificate) and slightly varying with application of a lubricant, as was proved in the case of grade 0.

Acknowledgement

The authors acknowledge the financial support from the Slovenian Research Agency (Research Core Funding No. P2-0190), as well as from the Metrology Institute of the Republic of Slovenia (funding of the National Standard of length; Contract No. C3212-10-000072).

References

- [1] Godina, A., Acko, B., Druzovec, M. (2007). New approach to uncertainty evaluation in the calibration of gauge block comparators, *Measurement*, Vol. 40, No. 6, 607-614, doi: [10.1016/j.measurement.2006.09.010](https://doi.org/10.1016/j.measurement.2006.09.010).
- [2] Godina, A., Vuherer, T., Acko, B. (2012). Possibilities for minimizing uncertainty of dissimilar materials gauge blocks calibration by mechanical comparison, *Measurement*, Vol. 45, No. 3, 517-524, doi: [10.1016/j.measurement.2011.10.018](https://doi.org/10.1016/j.measurement.2011.10.018).
- [3] Šafarič, J., Klobučar, R., Ačko, B. (2021). Measurement setup and procedure for precise step gauge calibration, *IEEE Transactions on Instrumentation and Measurement*, Vol. 70, Article No. 1009610, doi: [10.1109/TIM.2021.3115579](https://doi.org/10.1109/TIM.2021.3115579).
- [4] Klobucar, R., McCarthy, M., Acko, B. (2019). Metrological set-up for calibrating 2-dimensional grid plates with sub-micrometre precision, *Measurement*, Vol. 132, 60-67, doi: [10.1016/j.measurement.2018.09.035](https://doi.org/10.1016/j.measurement.2018.09.035).

- [5] Klobucar, R., Acko, B. (2017). Automatic high resolution measurement set-up for calibrating precise line scales, *Advances in Production Engineering & Management*, Vol. 12, No. 1, 88-96, [doi: 10.14743/apem2017.1.242](https://doi.org/10.14743/apem2017.1.242).
- [6] Lipus, L.C., Budzyn, G., Acko, B. (2021). Analysis of laser interferometer measurement uncertainty by simulating error sources, *International Journal of Simulation Modelling*, Vol. 20, No. 2, 339-350, [doi: 10.2507/IJSIMM20-2-563](https://doi.org/10.2507/IJSIMM20-2-563).
- [7] Acko, B., Weber, H., Hutzschenreuter, D., Smith, I. (2020). Communication and validation of metrological smart data in IoT-networks, *Advances in Production Engineering & Management*, Vol. 15, No. 1, 107-117, [doi: 10.14743/apem2020.1.353](https://doi.org/10.14743/apem2020.1.353).
- [8] Ojstersek, R., Acko, B., Buchmeister, B. (2020). Simulation study of a flexible manufacturing system regarding sustainability, *International Journal of Simulation Modelling*, Vol. 19, No. 1, 65-76, [doi: 10.2507/IJSIMM19-1-502](https://doi.org/10.2507/IJSIMM19-1-502).
- [9] Mudronja, V., Katić, M., Šimunović, V. (2014). Realization of the highest level of traceability in Croatian national laboratory for length, *Transactions of Famena*, Vol. 38, No. 1, 37-44.
- [10] Ali, S.H.R., Naeim, I.H. (2014). Surface imperfection and wringing thickness in uncertainty estimation of end standards calibration, *Optics and Lasers in Engineering*, Vol. 60, 25-31, [doi: 10.1016/j.optlaseng.2014.03.012](https://doi.org/10.1016/j.optlaseng.2014.03.012).
- [11] Buchta, Z., Šarbort, M., Čížek, M., Hucl, V., Řeřucha, S., Pikálek, T., Dvořáčková, S., Dvořáček, F., Kůr, J., Konečný, P., Weigl, M., Lazar, J., Číp, O. (2017). System for automatic gauge block length measurement optimized for secondary length metrology, *Precision Engineering*, Vol. 49, 322-331, [doi: 10.1016/j.precisioneng.2017.03.002](https://doi.org/10.1016/j.precisioneng.2017.03.002).
- [12] Butler, M.D., Vella, D. (2022). Liquid bridge splitting enhances normal capillary adhesion and resistance to shear on rough surfaces, *Journal of Colloid and Interface Science*, Vol. 607, Part 1, 514-529, [doi: 10.1016/j.jcis.2021.08.133](https://doi.org/10.1016/j.jcis.2021.08.133).
- [13] Fan, W.G., Zhang, S., Wang, J.D., Wang, X.H., Wang, W.X. (2020). Temperature field of open-structured abrasive belt rail grinding using FEM, *International Journal of Simulation Modelling*, Vol. 19, No. 2, 346-356, [doi: 10.2507/IJSIMM19-2-CO10](https://doi.org/10.2507/IJSIMM19-2-CO10).
- [14] Khawaja, A.H., Jahanzaib, M., Cheema, T.A. (2020). High-speed machining parametric optimization of 15CDV6 HSLA steel under minimum quantity and flood lubrication, *Advances in Production Engineering & Management*, Vol. 15, No. 4, 403-415, [doi: 10.14743/apem2020.4.374](https://doi.org/10.14743/apem2020.4.374).
- [15] Hsu, S.M., Gates, R.S. (2005). Boundary lubricating films: Formation and lubrication mechanism, *Tribology International*, Vol. 38, No. 3, 305-312, [doi: 10.1016/j.triboint.2004.08.021](https://doi.org/10.1016/j.triboint.2004.08.021).

Last-mile delivery optimization considering the demand of market distribution methods: A case studies using Adaptive Large Neighborhood Search algorithm

Huang, Q.L.^{a,b,*}, Wang, W.J.^b, Liang, X.J.^b, Xu, L.^b, Niu, X.Y.^a, Yang, X.Y.^b

^aBeijing Jiaotong University, Shangyuan Village, Haidian District, Beijing, P.R. China

^bChina Academy of Transportation Sciences, Chaoyang District, Beijing, P.R. China

ABSTRACT

Based on the current situation and problems of transportation "last mile" transportation distribution, this paper establishes a path optimization model based on user distribution methods from the perspective of market preference for transportation distribution methods, designs an Adaptive Large Neighborhood Search (ALNS) algorithm, and builds a user portrait based on the solution algorithm and the construction method. Based on the solution algorithm and the user portrait construction method, the solution scenario is established, and the distribution route and transportation distribution method are planned based on five real location data. Through the analysis of the solution scenarios, it can be obtained that after the optimization of the model, the transportation distribution cost of enterprises can be reduced, and the satisfaction of the transportation distribution service quality can be improved. The higher the complaint cost, the lower the total transportation and distribution cost, and the higher the satisfaction rate; the higher the time window penalty cost, the higher the total distribution cost, and the lower the satisfaction rate. Through several model comparisons, it is found that the optimized model has obvious advantages in transportation cost and good performance in transportation service satisfaction. To further strengthen the promotion and application of the distribution path optimization model, countermeasures are proposed in three aspects: establishing a unified end transportation information service platform, increasing the investment in end transportation path optimization, and strengthening the formulation of supporting policies to realize the optimization of end distribution services.

ARTICLE INFO

Keywords:

Transportation;
Last mile;
Adaptive Large Neighborhood Search (ALNS);
Market demand;
Logistics;
Distribution;
Optimization;
Heuristic algorithms

*Corresponding author:

(Huang, Q.L.)
16113127@bjtu.edu.cn

Article history:

Received 19 February 2022

Revised 27 August 2022

Accepted 31 August 2022



Content from this work may be used under the terms of the Creative Commons Attribution 4.0 International License (CC BY 4.0). Any further distribution of this work must maintain attribution to the author(s) and the title of the work, journal citation and DOI.

1. Introduction

In recent years, with the gradual acceleration of China's economic development, people's living standards greatly improved, the demand for all kinds of commodities also gradually increased. With the popularity of the Internet, online shopping, live shopping and other business models have gradually emerged, which has brought new growth points to China's economy and put forward new requirements for the development of China's transportation. With the issuance of the Outline for The Construction of a Transport Power, the development of transport has gradually changed from high-speed development to high-quality development, putting forward higher requirements for the distribution path at the end of the transport logistics supply chain [1]. The distribution path at the end of transportation is the "last mile" link of the development of logistics supply chain in China. It is a direct link between the transportation operator and the har-

vester, and also an important embodiment of the development level of transportation system in cities and regions. It has high requirements for transportation efficiency and service quality. For the development of the transportation industry, optimizing the distribution path of the city transportation terminal and getting through the "last mile" of logistics can further meet the needs of the people. It is an important starting point for the transportation industry to grasp the new development stage, implement the new development concept and construct the new development pattern. For the development of transportation enterprises, scientific and accurate calculation of the optimal distribution path at the end of city transportation can further do a good job in cost control, improve distribution efficiency, enhance the competitiveness of enterprises, and achieve development of enterprises. Pointed in this paper, the proposed path, not just the actual path and distance, but to the goods which are transported to the user in the city or regional distribution site, which is transported from the distribution site to the user to specify locations after submitting orders by the users, and contained in the process of route optimization, cost control, customer satisfaction, etc., by optimizing the path, so as to further meet the needs of user diversity [2].

1.1 Problem definition

In China's city end transportation distribution field, the user's high difficulty in matching the time window has been one of the difficulties of end transportation distribution. User demand is scattered, and the average daily transportation distribution volume of many communities is more than 150 pieces, and there are no less than 500 such communities in each city in China. As China's transportation and distribution platform is gradually bigger, the implementation of city transportation and distribution of goods and cargo types gradually increased, so the diversity of user demand for the end of the goods transportation methods further increased. At present, users for the end distribution mainly includes door-to-door transportation distribution and self-pickup, due to different user needs, the enterprises also need to consider their own costs, so there are often poor communication and coordination between the transporters and users, affecting the consumer experience and satisfaction. The main problems include the following aspects.

Firstly, the distribution path selection and demand mismatch. Due to the diversity of users' demands for transportation distribution modes, sometimes the transportation distribution personnel cannot fully match users' demands when both parties communicate and coordinate, such as the need to wait, etc. Moreover, since the agreed time with the transportation distribution personnel cannot be precise to the minute, and even if users agree to face-to-face transportation distribution, they may be out of the office or in other situations, so they cannot complete the handover and inspection of goods at the first time when the goods arrive. Affecting the efficiency of transportation distribution, sometimes also due to poor communication and coordination between the two sides, resulting in complaints. In the promotion of the use of unmanned intelligent cabinets, as some communities are lack of regular maintenance of some intelligent cabinets leads to a high rate of damage, so it may further lead to transportation distribution personnel and users need to increase the additional transportation distribution distance to complete the transportation distribution.

Secondly, the transportation path selection randomness is strong. From the viewpoint of the implementation status of China's transport enterprises, the implementation path of the "last mile" of urban transportation and distribution is often determined by the subjective experience and awareness of the distribution personnel. In different scenarios, facing different cargo conditions and external environment, the distribution personnel make judgments based on their own subjective experience and determine the final transportation distribution method on their own, even without communicating with users. In addition, influenced by the environment and income treatment, distribution personnel generally have lower education in China, so most of them are "empirical" when choosing the transportation distribution route, which leads to a large randomness of transportation distribution methods and affects the service experience of users is affected.

Thirdly, the depth of the transportation enterprises' awareness of the distribution cost is insufficient. The enterprises' cognition of cost mainly focuses on the cost accounting of labor and

vehicles, ignoring the attention to intangible costs. Since the selection of end distribution mode mainly relies on the experience judgment of distribution personnel, which leads to the distribution personnel always being under pressure in the process of distribution, and when there is a change of distribution time, it may have an impact on the overall distribution time of the distribution personnel on that day. It is difficult for the relevant personnel to choose the best way to deliver through their own decision, and the resulting poor communication and coordination will lead to dissatisfaction and complaints from both sides, which will also affect the experience and satisfaction of the parties concerned with the transportation service.

1.2 Literature review

The end distribution methods include home transportation distribution and goods pickup. The first one is door-to-door distribution, which refers to the transportation distribution method of delivering goods to users on time and at the agreed time and place. Han *et al.* [3] proposed that door-to-door distribution is the transportation distribution of goods to users by short-distance vehicle transportation, and it is one of the most important methods of end transportation. Howe [4] was the first to propose crowdsourcing service, which is the use of "rush order" mode to provide transportation distribution services for users, and this approach has been widely used in end transportation distribution. Bühler *et al.* [5] argued that logistics providers aim at the lowest cost for end transportation distribution, and constructed four new linear mixed integer programming models to portray the service situation of door-to-door transportation distribution. Chen *et al.* [6] constructed the M/D/1 queuing system to portray the specific utility of door-to-door transportation distribution to users, and argued that although door-to-door distribution can bring greater convenience, there are disadvantages such as high cost and low timeliness.

The second one is goods self-pickup, which refers to the transportation distribution method in which goods no longer continue to be delivered door-to-door but are delivered to the user's surrounding logistics terminals and the user picks up the goods by himself, is also the most common way of end logistic supply chain. Guo [7] focused on the end transportation time mismatch problem to alleviate the problem of time conflict between users and distribution personnel. Song *et al.* [8] used the collected end transportation information to study cargo self-pickup, which effectively solved the time mismatch of cargo distribution, and at the same time greatly improved the efficiency of cargo distribution. Zhou *et al.* [9], Li *et al.* [10], and Xu *et al.* [11] analyzed the impact of self-pickup courier services on users' usage, the spatial distribution pattern of cargo self-pickup terminals, and users' willingness to choose self-pickup parcels through example verification. Guo [12] and others summarized cargo font points into different modes, such as: retail stores, subway stations, communities, and 24-hour public smart parcel stations for collection and transportation distribution; cargo self-pickup also includes Jing Dong pickup cabinets, Feng Chao Express provided by SF, CaiNiao post, and ShouHuobao.

In terms of research methods, there are three main algorithms: exact algorithm, traditional metaheuristic algorithm, and ALNS algorithm. Lee *et al.* [13] analyzed the route optimization problem of multiple vehicles and optimized the exact algorithm based on the shortest path search algorithm using the minimum number of vehicles as the optimization goal. Ozbaygin and Savelsberg [14] proposed an iterative branch pricing method based on the solution based on the branch pricing method and used the algorithm to solve the optimization problem of distribution routes. Zhao *et al.* [15] assembled genetic algorithm and forbidden search algorithm to solve a joint optimization scheme for end distribution, taking urban distribution in the core area of Su Ning in Chongqing as an example. Zhou *et al.* [16] portrayed the scenario of multiple users picking up at the same intermediate pickup facility, with the objective of minimizing the total distribution cost. Goeke *et al.* [17] conducted a comparative analysis of the cross-sectional and longitudinal computing performance between the large neighborhood search algorithm and other algorithms through a comparative analysis, and concluded that the large neighborhood search algorithm has higher and better computing efficiency and computing performance. Rohmer *et al.* [18] aimed at cost optimization, and on the basis of fully considering the costs incurred by distribution improved the adaptive large-neighborhood search metaheuristic algorithm with the goal of cost optimization, and verified the effectiveness of the algorithm. Jin *et al.* [19] used heu-

ristic approach to optimize the trucks transportation route to reduce travel cost. In the application of other methods, Ocampo *et al.* [20] constructed an integrated multiple criteria decision-making approach to locate the locations of last-mile delivery facilities. Wang *et al.* [21] discussed optimization model of joint distribution system including warehousing, transportation and logistics business to optimize logistic solution.

2. Model construction and validation

Focusing on the problems faced by "last mile" path of transportation, the fundamental solution lies in understanding the needs of different users and providing exclusive transportation distribution services for users on the basis of good enterprise cost control. Combining the current situation of research and the application of related methods, this paper intends to use the ALNS algorithm to establish a model design to optimize the end transportation path considering users' preferences for transportation distribution methods and users' tendency to complain, and to determine the appropriate strategy to reduce transportation distribution costs and improve users' satisfaction.

2.1 Model construction

Consider the following transportation distribution situation. There is an end distribution terminal which offers service for m users. Every user i has a request q_i and the earliest time window and latest time window E_i, L_i . each user has a preferred transportation distribution method which is represented by p_i . $p_i = 1$ represents user preferred door-to-door transportation distribution, $p_i = 0$ represents user preferred self-pickup transportation distribution. If the vehicle does not deliver according to the user's preference, there may be two results, the user who is easy to complain will complain to the relevant departments, and thus the transportation distribution company has to accept a certain penalty; while another part of the users are more talkative and suffer this result silently, without taking any complaint behavior. Users can be divided into four categories, based on their preferences and complaint behavior, and each category is represented by n ($n = 1, 2, 3, 4$), including preferring door-to-door transportation distribution and easier to complain ($n = 1$), preferring self-pickup transportation distribution and easier to complain ($n = 2$), preferring door-to-door transportation distribution with no complain ($n = 3$), preferring self-pickup transportation distribution with no complain ($n = 4$). The cost of complaint for category n users is p_n^1 . Each user point can be accessed once and only once. The number of vehicles available at the distribution station is k . Each vehicle departs from the distribution station to serve the user point and returns to the station. The capacity of the vehicle is Q_k . The running distance d_{ij} between user points i and j , the running time is t_{ij} , and the running cost is c_{ij} . Vehicles can arrive earlier than the earliest time window of user i or later than the latest time window, but incur a corresponding penalty cost, the size of which is related to the user type and is denoted by p_n^2 . The distribution starts immediately after the vehicle arrives at the user's point i . The service time is s_i (the case of self-pickup applies to loading and unloading time, door-to-door applies to waiting + transportation distribution time) and leaves immediately after serving the point. The vehicles are homogeneous. The model symbols are shown in Table 1.

Constraint Eq. 1 is an objective function with three components: transportation distribution cost, complaint cost, and time window penalty cost. Constraint Eq. 2 limits the number of vehicles used. Constraint Eq. 3 expresses the relationship between and. Constraint Eq. 4 guarantees that each user can be served only once. Constraint Eq. 5 expresses the flow balance. Constraint Eq. 6 expresses that the total demand of user points delivered by a transportation distribution vehicle cannot exceed the capacity of that vehicle. Constraint Eq. 7 expresses the relationship between the starting service moments of two neighboring user points visited by the vehicle. Constraints Eq. 8 to Eq. 9 are the initial values of the vehicle when it stops at the distribution station. Constraints Eq. 10 to Eq. 12 are the decision variable definition fields.

Table 1 End distribution mode model symbol description

Symbol	Instruction
0	Distribution terminal
C	User collection, $C = \{1, 2, \dots, m\}$
V	Terminal collection, $V = C \cup \{0\}$
K	Cars collection, $K = \{1, 2, \dots, k\}$
a_i^n	If the user point i belongs to category n , if so, $a_i^n = 1$; or 0
p_n^1	Cost of complaints for category n users
p_n^2	Cost per unit penalty for violating the time window of n class a user
d_{ij}	Distance between arcs (i, j)
t_{ij}	Operating time between arcs (i, j)
c_{ij}	Operating cost between arcs (i, j)
s_i	Service time of user i
q_i	Demand quantity of user i
e_i, l_i	Time window of user i
Q	Capacity of the vehicle
x_{ijk}	If the car k go through arcs (i, j) , and it is 1; or 0
y_{ik}	If the car k service user i , and it is 1; or 0
z_i	If the distribution method is same with preference of user i , it is 0; or 1
r_{ik}	The starting time of service of the car k to user point i

$$\min \sum_{i \in V} \sum_{j \in V} \sum_{k \in K} c_{ij} x_{ijk} + \sum_{n \in \{1, 2\}} \sum_{i \in C} p_n^1 a_i^n z_i + \sum_{n \in \{1, 2\}} \sum_{k \in K} \sum_{i \in C} p_n^2 a_i^n (1 - z_i) y_{ik} [(E_i - r_{ik})^+ + (r_{ik} - L_i)^+] \quad (1)$$

$$\sum_{k \in K} \sum_{j \in C} x_{0jk} \leq K \quad (2)$$

$$\sum_{i \in V} x_{ijk} = y_{jk} \forall j \in C, k \in K \quad (3)$$

$$\sum_{k \in K} \sum_{j \in C} x_{ijk} = 1 \forall i \in C \quad (4)$$

$$\sum_{i \in V} x_{ijk} = \sum_{i \in V} x_{jik} \forall j \in C, k \in K \quad (5)$$

$$\sum_{i \in C} y_{ik} q_i \leq Q_k \forall k \in K \quad (6)$$

$$r_{ik} + s_i + t_{ij} - r_{jk} \leq M(1 - x_{ijk}) \quad \forall i \in V, j \in V, k \in K \quad (7)$$

$$r_{0k} = 0 \quad (8)$$

$$s_0 = 0 \quad (9)$$

$$x_{ijk} = \{0, 1\} \forall i \in V, j \in V, k \in K \quad (10)$$

$$y_{ik} = \{0, 1\} \quad \forall i \in C, k \in K \quad (11)$$

$$z_i \in \{0, 1\} \quad \forall i \in C \quad (12)$$

To verify the effectiveness of the model proposed in this paper for large-scale cases, we also use this algorithm to solve the Vehicle Routing Problems with Time Windows (VRPTW) problem. Based on numerical examples from Solomon and Desrosiers [22] (100 consumers) and Homberger and Gehring [23] (200 and 400 consumers), the applicability of the proposed algorithm is obtained. Tables 2, 3 and 4 show the 100, 200 and 400 consumer scenarios, respectively. According to the results, the algorithm proposed in this paper has strong adaptability and can solve other similar problems well.

In addition, we also verified the efficiency of the proposed algorithm compared with the genetic algorithm based on the calculation example in this paper, the algorithm effect is shown in Table 5. Compared with the Genetic Algorithm, the proposed algorithm is more efficient, so it can better find the optimal solution, and when the data is larger, the efficiency of the proposed algorithm is higher.

Table 2 Solomon 100 consumers numerical example

Numerical example	HGA (best 6 result)	LNS (best 6 result)
1	828.38	828.38
2	589.86	589.86
3	1210.69	1209.2
4	951.51	956
5	1384.17	1384.17
6	1119.24	1123.17
Total	57196	57259

Table 3 200 consumers numerical example

Numerical example	HGA (best 6 result)	LNS (best 6 result)
1	2718.41	2720.12
2	1831.59	1831.65
3	3613.16	3605.09
4	2929.41	2921.85
5	3180.48	3204.41
6	2536.2	2547.84
Total	168092	168809

Table 4 400 consumers numerical example

Numerical example	HGA (best 6 result)	LNS (best 6 result)
1	7170.47	7188.35
2	3952.95	3877.18
3	8402.57	8538.45
4	6152.92	6238.56
5	7907.14	8145.91
6	5215.21	5233
Total	388013	392214

Table 5 Comparison of algorithm efficiency

Numerical example	Genetic algorithm	LNS	Comparison
100	256.22	254.38	0.7 %
200	292.49	287.66	1.6 %
436	313.57	303.23	3.2 %

2.2 Example adoption and algorithm analysis

Combining the model calculation results, the model of user transportation distribution method preference is further validated and analyzed by using examples.

Example adoption

As shown in Fig. 1, this paper uses five neighborhoods in Haidian District of Beijing as the basis for calculation example analysis, including Gangyan neighborhood, Jiaodajiyuan neighborhood, Mingguangcun neighborhood, Tianzhaojiayuan neighborhood, and Changhewan neighborhood as the community transportation distribution area, and the number of transportation distribution users in each neighborhood is 89, 87, 99, 85, and 75. In order to simplify the analysis and better display the results, the transportation distribution points of users in each district are simplified to 5. According to the actual research of the relevant company, the distribution center is selected at the bottom of Yixi Business Hotel, No. 33, Xueyuannan Road, Haidian District. To get the data of the users in the district, this paper designed questionnaires around basic information, preference of transportation distribution methods and complaint behavior, and the questionnaires were mainly obtained by posting the questionnaire links in the property groups, and 436 valid data were finally collected. Other model calculation parameters are set as follows: $k = 8$, $Q_k = 350$, E_i and L_i are obtained from the questionnaires filled out by users, d_{ij} is calculated from latitude and longitude, $c_{ij} = 10$, s_i and q_i are randomly generated, $p_n^1 = 1$, $p_n^2 = 8$.



Fig. 1 Community distribution district selection figure

Algorithm analysis

Initial setting

Since the objective function is profit maximization, we need to deal with the objective function first. Since $\max f_{netp} = \min (-f_{netp})$, we let the cost of any feasible solution $O(S) = -f_{netp}$. So the initial solution S^0 corresponds to the expression of the temperature function as:

$$T = O(S^0) \times P_{init} \tag{13}$$

Neighborhood structure

Since the distribution method of users who have checked the value-added service will no longer change, we add new removal and insertion policies to improve the feasibility of the path based on the original removal and insertion policies. For the convenience of description, we refer to the users who have checked the value-added service as value users. The basic idea of these two strategies is that the higher the proportion of value users included in a path, the lower the number of solutions generated by adjusting the user distribution method for that path, and the less favorable it is to generate feasible solutions in the early stage of the algorithm. Therefore, our two strategies operate mainly on such paths to ensure the convergence speed of the algorithm.

Path removal strategy

Step1: Count the proportion of each path containing value users in a certain solution S , and then sort them in descending order.

Step2: Remove the paths until the number of removed is n_r .

Distribution method factor insertion strategy

The distribution mode factor insertion strategy is to determine whether the user point is allowed to be inserted based on the distribution mode.

Step1: Calculate the distribution mode correlation between the arc and the user point to be inserted.

Since it is assumed that arc (i, j) is an arc on path p , k is the target insertion point, and $E_i \leq E_k \leq E_j$. Arc (i, j) is associated with the distribution method of the user point k , the calculation method is as follows:

$$\sigma_{ik} = \begin{cases} \max\{L_i - E_k, 0\} & E_i \leq E_k \\ \min\{L_i, L_k\} - E_i & E_k < E_i \leq L_k \\ \max\{L_k - E_i, 0\} & E_i > L_k \end{cases} \tag{14}$$

$$\sigma_{kj} = \begin{cases} \max\{L_k - E_j, 0\} & E_k \leq E_j \\ \min\{L_k, L_j\} - E_k & E_j < E_k \leq L_j \\ \max\{L_j - E_k, 0\} & E_k > L_j \end{cases} \tag{15}$$

$$\sigma_{ij} = \sigma_{ik} + \sigma_{kj} \tag{16}$$

Step2: According to the distribution mode association degree, user point k is inserted into the arc (i, j) with the largest association degree.

By analyzing the distribution mode correlation here, due to the existence of value users in the later stage of the algorithm, the basic constraints such as vehicle capacity can be easily satisfied, but it is more difficult to satisfy the distribution mode constraint, and the penalty cost incurred is larger, which needs to be handled specifically for the distribution method. The increased cost of considering the insertion of arc (i, j) into user point k does not need much consideration. Therefore, we need to recalculate the correlation degree.

3. Case studies: Results and discussion

Combining the model results and the arithmetic results, the optimal path is further analyzed, including the selection of routes and transportation distribution methods, etc., and its sensitivity is further analyzed.

3.1 Optimal path and transportation distribution method

Optimal route

Because of the large number of points in the example, each path is shown separately in this paper to clearly demonstrate the path of the vehicle driving, and the specific vehicle route scheme is shown in Table 6. As can be seen from the Table 6, due to the time window constraints, the transportation distribution paths are not based on the distance to choose aggregated transportation distribution. Most of the vehicles will deliver to 4 or 5 neighborhoods. But in reality, the transportation distribution companies often distribute the cargo to a neighborhood by a special transporter, but after taking into account the cost of time window, user preferences for transportation distribution services and the cost of complaints, the distribution of vehicles will show a more decentralized form.

Table 6 Optimal route display

No.	Path
1	[0,50,115,259,293,309,424,427,436,21,30,142,152,246,264,287,315,347,349,402,8,9,44,71,87,102,110,114,120,136,141,166,169,178,207,209,247,255,279,283,308,321,325,350,385,421,93,155,223,379,387,98,122,180,183,314,274,0]
2	[0,337,390,403,82,83,224,228,268,304,2,15,124,129,131,149,162,168,206,213,225,226,230,328,215,280,281,243,417,46,150,194,273,307,327,352,368,391,404,20,37,184,195,201,222,244,305,330,432,109,116,143,164,277,284,326,419,153,361,19,63,130,170,0]
3	[0,270,285,289,316,324,331,338,346,397,400,426,428,429,431,27,42,57,74,75,112,172,396,58,154,182,62,92,199,359,411,23,101,145,176,250,251,290,317,334,358,383,103,237,261,265,345,348,353,167,375,137,146,212,332,344,418,11,18,81,156,187,231,256,303,398,125,235,16,29,86,105,119,135,138,147,245,249,340,73,0]
4	[0,173,272,298,393,10,77,84,186,288,370,197,39,48,61,89,96,128,157,258,271,323,372,1,41,51,132,214,282,399,433,4,181,216,266,292,364,435,3,36,165,335,177,218,275,286,320,384,388,76,106,161,210,310,378,185,196,200,236,241,252,254,291,311,322,336,339,357,416,99,0]
5	[0,14,204,229,232,28,72,160,260,371,140,238,253,354,413,423,425,5,7,17,22,24,26,31,47,60,64,90,111,123,179,188,198,203,217,221,234,239,257,269,278,297,301,333,366,367,94,97,107,267,318,356,362,373,374,394,409,25,45,49,70,329,377,0]
6	[0,32,38,43,52,56,65,69,78,88,95,104,133,139,190,211,220,242,342,351,360,363,380,386,392,401,406,414,434,53,233,422,34,55,66,68,80,91,117,118,174,208,227,248,276,295,355,365,382,405,67,296,300,306,319,13,144,148,158,313,381,408,59,151,171,412,299,369,0]
7	[0,12,33,35,54,191,193,240,263,40,126,134,189,192,202,205,341,343,395,415,430,302,407,312,100,219,0]
8	[0,79,85,121,127,159,163,175,262,389,6,108,113,294,376,410,420,0]

This section first checks the distribution of users in the different routes and the characteristics of user types.

- Distribution of users in Route 1 and characteristics of user types.

Fig. 2 shows the distribution of users as well as the path. Each point represents the number of users delivered at that point. The users in Route 1 are mainly distributed in Mingguangcun and Tianzhaojiayuan neighborhoods, and a small number of Jiaodajiayuan users. The distance between Mingguangcun and Tianzhaojiayuan neighborhoods is relatively close to each other, so they will deliver together to gain the advantage of distance. In Route 1, the transportation distribution method for Mingguangcun users is mostly door-to-door method, while the transportation distribution method for Tianzhaojiayuan and Jiaodajiayuan users is mostly self-pickup. To satisfy more users within a certain time, the transportation company can intersperse a certain number of self-pickup users among the door-to-door users, so as not to waste waiting time but also to satisfy the needs of self-pickup users.

According to the time window data in Route 1, in order to reduce the waiting time, the distribution company should first transport to users with similar time window together. The time window of users who deliver to Mingguangcun neighborhood in Route 1 are mostly concentrated in the afternoon, and some of them are self-pickup users. Since the time window of self-pickup users are very flexible, they can be satisfied together.



Fig. 2 The user distribution and the route of Route 1

- Distribution of users in Route 2 and characteristics of user types.

Fig. 3 shows the distribution of users in Route 2 and the relevant situation. The distribution of users in Route 2 is similar to Route 1, distributed in Mingguangcun and Tianzhaojiayuan neighborhoods, with the difference that there are also users in Changhewan neighborhood in Route 2. However, the number of users in Changhewan neighborhood is very small, and they are basically self-pickup users, which means that the self-pickup users in Changhewan neighborhood are dispatched by the way because there is still spare capacity in the second vehicle. In route 2, the transportation distribution method of users in Mingguangcun and Tianzhaojiayuan neighborhoods is mostly door-to-door transportation distribution method, while the transportation distribution method of users in Jiaodajiayuan and Changhewan is mostly self-pickup.

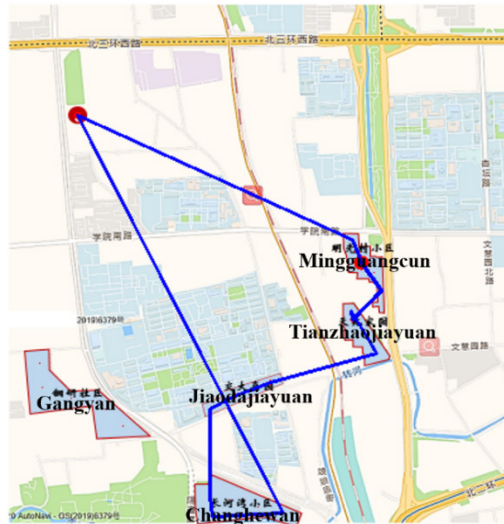


Fig. 3 The user distribution and the route of Route 2

- The distribution of users in Route 3 and the characteristics of user types.

Fig. 4 shows the transportation and distribution of users in Route 3 and the paths. The distribution of users in Route 3 is relatively wide, within all five neighborhoods. However, the number of users in Changhewan and Gangyan neighborhoods are small, and they are basically users of self-pickup method. In Route 3, the transportation distribution methods of users in Mingguangcun, Tianzhaojiayuan, and Jiaodajiayuan neighborhoods are mostly door-to-door method, but the time window of users in Mingguangcun and Tianzhaojiayuan neighborhoods are concentrated in the morning, while the time window of users in Jiaodajiayuan are concentrated in the afternoon. The transportation distribution method for users in Changhewan and Gangyan neighborhoods are mostly self-pickup.

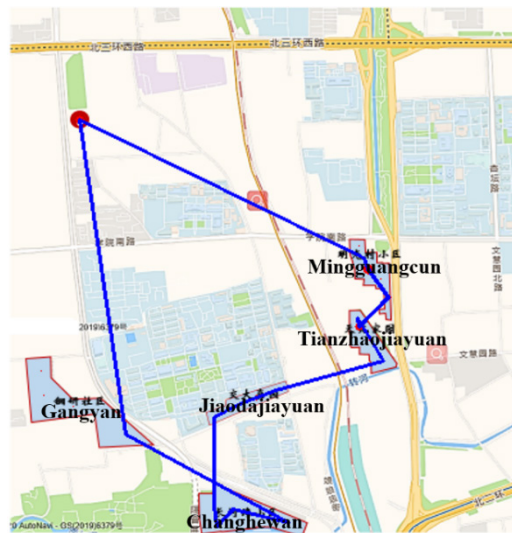


Fig. 4 The user distribution and the route of Route 3

- The distribution of users in Route 4 and the characteristics of user types.

As shown in Fig. 5, in Route 4, the transportation distribution paths are spread across every neighborhood, but users are more concentrated in Tianzhaojiayuan, Jiaodajiayuan, and Changhewan neighborhoods. In route 4, the transportation distribution method of users is door-to-door transportation distribution method. However, the users are more concentrated in Tianzhaojiayuan, Jiaodajiayuan, and Changhewan neighborhoods. The time window of the users in Mingguangcun and Tianzhaojiayuan neighborhoods are concentrated in the morning, while the users in Jiaodajiayuan and Changhewan neighborhoods are concentrated in the afternoon.

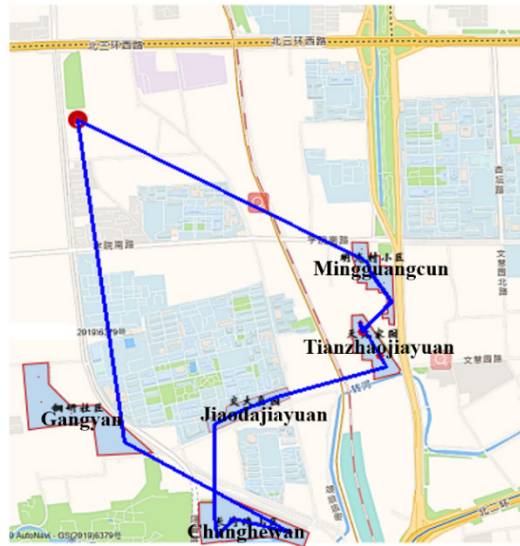


Fig. 5 The user distribution and the route of Route 4

- Distribution of users and the characteristics of user types in Route 5

As shown in Fig. 6, in Route 5, the users are distributed in Tianzhaojiayuan, Jiaodajiayuan, Changhewan, and Gangyan neighborhoods. Among them, the number of users in Changhewan and Gangyan neighborhoods are the largest. In Route 5, the most users' transportation distribution method is door-to-door method. However, there are some self-pickup method users in Changhewan neighborhood. The time window of users in Tianzhaojiayuan and Jiaodajiayuan neighborhoods are concentrated in the morning, while the users in Jiaodajiayuan and Changhewan neighborhoods are concentrated in the afternoon.

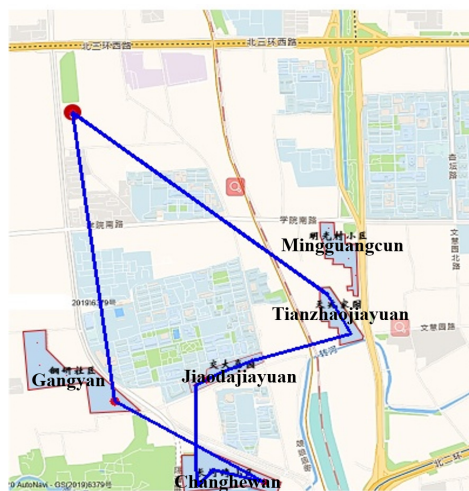


Fig. 6 The user distribution and the route of Route 5

- Distribution of users and the characteristics of user types in Route 6

As shown in Fig. 7, in Route 6, the transportation distribution users are distributed in Jiaodajiayuan, Changhewan, and Gangyan neighborhoods, among which the number of users in Gangyan neighborhood is the largest. In Route 6, the transportation distribution method of users in Jiaodajiayuan and Changhewan neighborhoods are door-to-door distribution method. However, there are more self-pickup method users in Gangyan neighborhood. The time window of users in Jiaodajiayuan and Changhewan neighborhoods are concentrated in the morning, while the users in Gangyan neighborhood are concentrated in the afternoon.

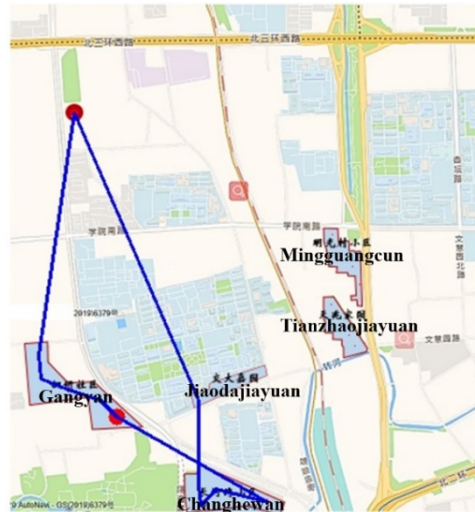


Fig. 7 The user distribution and the route of Route 6

- Distribution of users and the characteristics of user types in Route 7 and 8.

As shown in Fig. 8, in both Route 7 and Route 8, the delivered users are distributed in Gangyan neighborhood. In both Route 7 and Route 8, the transportation distribution method of users is door-to-door transportation distribution method. Among them, the time window of users of Route 7 are all concentrated in the morning, while the time window of users of Route 8 are all concentrated in the afternoon. Therefore, although the Route 7 and 8 have spare capacity, they are not delivered together because the time window of the two paths are so different that it would take a long waiting time if they are delivered together, and it is better to deliver separately.

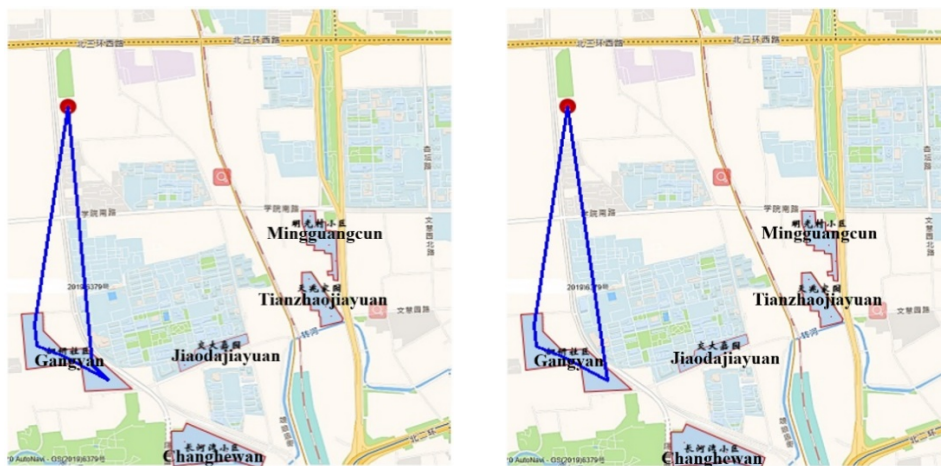


Fig. 8 The user distribution and the route of Route 7 and Route 8

By analyzing the characteristics of the users of each route, it can be found that the users in the same route show the following pattern:

- Type 1: Each path has major distribution cells;
- Type 2: Users in the same neighborhood have relatively close time window;
- Type 3: Self-pickup users are interspersed with door-to-door method users, which can realize interpolated transportation distribution in the gaps of discontinuous time window of two users.

Transportation distribution method

According to the calculation results, the final decision of the transportation distribution method with different user preferences is:

Route 1: 337 390

Route 2: 225 321 250 192

Route 3: 150 58 435 275 47

Route 4: 428 359 157 251 317 395 298 182 28 253 55 300

Route 5: 181 320 235 12 59 85 193 217

Route 6: 267 360 407

Route 7: 117 365 306 219

This section examines the points where transportation distribution methods do not match user preferences, and finds that these user points are characterized by: a lower percentage of Type 1 users changing transportation distribution methods than Type 3 users; fewer users with a large earliest time window changing transportation distribution methods than those with a small earliest time window; a greater tendency for deliverers to concentrate on those users with the same transportation distribution methods; and priority for Type 1 and Type 3 users with smaller earliest time window transportation distribution. This is mainly determined by the complaint cost and time window violation cost, which are analyzed as follows:

- The complaint cost of Type 1 users is higher. Under the condition of the same time window violation cost, compared with Type 3 users, changing the transportation distribution method of Type 1 users will increase the higher complaint cost, while the reduced time window penalty cost is insignificant, therefore, the deliverers will tend to change the transportation distribution method of Type 3 users.
- Users with larger earliest time window are generally placed at the end of the path for transportation distribution, and the arrival time of the deliverer is more likely to be smaller than these users. If the transportation distribution method is changed, not only the complaint cost will increase, but also the arrival time of subsequent user points is advanced, and the time window penalty cost increases accordingly. Therefore, the transportation distribution person prefers not to change the transportation distribution method for this type of users.
- For users whose transportation distribution method is door-to-door method, the transportation distribution method of the dispatcher can choose door-to-door or self-pickup method, which has higher flexibility. The dispatcher can freely adjust the transportation distribution method according to the actual situation to achieve the purpose of reducing the time window penalty cost and thus reducing the total cost.
- If a transportation distribution path has both users who prefer door-to-door and self-pickup methods, the transportation distribution time window of self-pickup users is more relaxed and will not violate the time window of such users. Therefore, the transportation distribution agent will give priority to the door-to-door method users.

Users satisfaction

This section first conducts a comparative study of user satisfaction rates. To show the value of optimizing the user's transportation distribution method, the total cost C_{all} when the satisfaction rate is 100 % (i.e., the transportation distribution is made exactly according to the user's preference for self-pickup and door-to-door transportation distribution) is first calculated. Then, the optimal solution C_{opt} in the example problem of this paper and the number of user points $n_{opt} = 38$, which change the transportation distribution method can be obtained. In reality, the transporters also do not adopt the self-pickup method exactly for the users. Some users' packages are directly delivered to the pickup point, while some users' parcels are delivered to their homes. There is a certain degree of randomness in whether users are delivered by self-pickup or door-to-door transportation distribution, without considering the users' own preferences and complaint behavior. Therefore, 38 users are randomly selected to deliver according to the transportation distribution method opposite to their preferences and get the total cost C'_{opt} . To ana-

lyse the effect of changing the number of users' transportation distribution method preferences by considering the cost, 142 users are also randomly selected to deliver according to the transportation distribution method opposite to their preferences and get the total cost C_{rand} . The cost corresponding to each satisfaction and the parameters are shown in Table 7. As can be seen in Table 7, the higher the satisfaction rate, the greater the transportation distribution cost, meaning that the transportation vehicle needs to drive longer distances to meet the user's transportation distribution method preference. When the satisfaction rate is 100 %, no complaint cost is incurred, but the time window penalty cost is high because one vehicle often has to transport to many users, so it is inevitable that users' time conflicts will occur, but at this time, the transportation distribution mode preference of door-to-door method users cannot be violated, thus the time window of many users will be violated, so the time window penalty cost of users is high.

The total cost $C_{all} = 329.09$, the optimal solution $C_{opt} = 303.23$ is obtained after optimizing the distribution method, which saves 25.86. The number of distribution methods changed after optimization, $n_{opt} = 38$, which has the optimal satisfaction rate which is 91.28 %. Keeping the satisfaction rate constant and randomly violating the user's transportation distribution method preference, the time window violation cost will increase at this time, and the complaint cost will also increase, and the path cost will instead have a small decrease, and the total cost will increase by 17.36. With a satisfaction rate of 67.43 %, the complaint cost is much higher than the complaint cost of the optimal solution, and the time window penalty cost is not much different.

From the overall trend, as the satisfaction rate decreases, the complaint cost increases and the time window penalty cost decreases. However, when the satisfaction rates are the same, the complaint costs will differ, which is mainly determined by the percentage of the first category of users among the user points that change the transportation distribution method. When the satisfaction rates are the same, the complaint cost will be higher for the paths with a high percentage of first category users, so the complaint cost in the optimal solution will be higher than the complaint cost in C'_{opt} . On the other hand, the position of user points in the path that change the transportation distribution method affects the time window penalty cost. When increasing the number of user points that change the transportation distribution method in a small range, the change of the time window penalty cost is unpredictable. When the number of user points to be added to change the transportation distribution method is in a larger range, the time window penalty cost decreases, and the decrease changes according to the location of the user points.

Table 7 Impact of user satisfaction rate on cost

Satisfaction	100 %	91.28 %	91.28 %; $n_{opt} = 38$	67.43 %; $n_{rand} = 142$
Distribution Costs	219.55	184.75	181.37	166.94
Complaint Costs	0	82	94	386
Time window penalty cost	109.54	36.48	45.22	46.43
Total Cost	329.09	303.23	320.59	599.37

3.2 Sensitivity analysis

This section analyses the time window penalty cost. Holding the complaint cost constant, and change the unit time window penalty cost α gradually from 1 to 6 to observe the changes in total cost, complaint cost, transportation cost and time window penalty cost. As seen in Figs. 9 and 10, the total cost rises rapidly and remains constant when $\alpha = 5$, when the penalty factor increases. The complaint cost shows the same trend as the total cost, indicating that the increase in the total cost is mainly caused by the increase in the complaint cost, and the change of α has little effect on the transportation cost and the time window penalty cost.

As seen in Fig. 9, this is mainly because as the time window penalty cost α increases, the transportation distribution personnel choose to put the goods into the self-pickup counter, and the complaint cost increases but reduces the amount of time window violation (time window penalty cost = α * time window violation). At this point, the total cost still increases, but slows down the growth of the total cost. As α continues to increase, the time window violation volume

gradually decreases to 0, and the time window penalty cost will also be 0. No matter how it increases, it has no effect on the time window penalty cost. If we continue to change the transportation distribution method of the first and third category of users, i.e., the goods are put into the self-pickup cabinet, it can only increase the complaint cost and make the total cost not optimal.

Fig. 10 gives the effect of the complaint cost coefficient on the total cost. It can be seen that the larger the complaint cost coefficient is, the lower the total complaint cost is instead, indicating that due to the larger complaint cost, the transport companies choose the way of preference for users to reduce the transportation distribution cost. The higher the complaint cost, instead, the higher the time window penalty cost, because changing the transportation distribution method will require a higher time window, thus increasing the time window penalty cost. In terms of total cost, the complaint cost coefficient can reduce the total cost of the company in general, but it causes a transient increase in total cost because in the first period, it may lead to an increase in time window penalty cost, and the increased penalty cost will be higher than the reduced complaint cost.

The essence of this model lies in the trade-off between the cost of complaints and the cost of time window violation. For users, the unit time window violation cost is the same, but the complaint cost is different, and the heterogeneous and homogeneous costs of users can be transformed by vehicle route planning with the decision of user's transportation distribution method. In the transformation, the cost saving can then be achieved by the route change to form a favorable distribution method for users with high complaint cost.

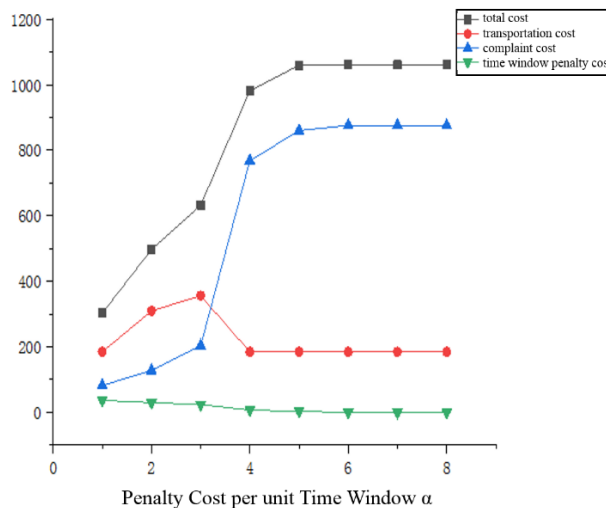


Fig. 9 The effect of penalty cost per unit time window on total cost

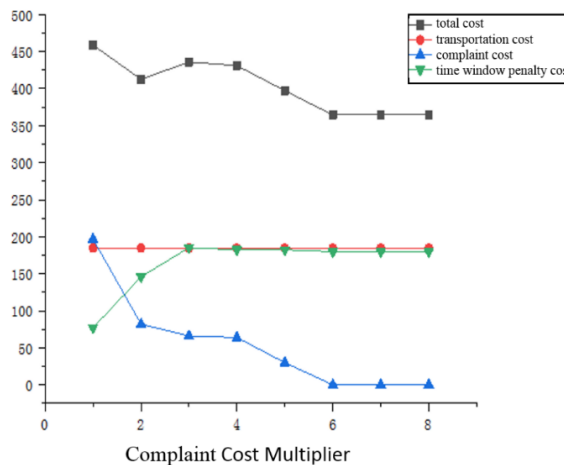


Fig. 10 The influence of complaint cost coefficient on total cost

4. Conclusion remarks and suggestions for policy and measures

In this paper, a path optimization model considering user's transportation distribution mode preference is established to optimize the driving path of end transportation vehicles as well as the transportation distribution methods, and the algorithm of ALNS is designed. Firstly, the initial solution is obtained by greedy algorithm and set as the optimal solution and the current solution, then the current solution is destroyed and repaired to obtain the neighborhood solution S^t . Based on the improved algorithm, the solution scenario is established, and the distribution paths and methods are planned based on the data of five neighborhoods, and the path optimization direction of the distribution methods is clarified. The analysis of the algorithm solution shows that the optimization of the model further satisfies the diversified needs of users for transportation distribution methods, and the satisfaction of the transportation distribution service can be improved while the cost of the terminal transportation distribution enterprises is reduced. The higher the complaint cost is, the total distribution cost first decreases slightly then increases and finally decreases again; the higher the time window penalty cost is, the higher the total distribution cost is. The calculation methods and results can provide some reference for the optimization of transportation end transportation routes based on users' preferences for transportation distribution methods.

In order to ensure the smooth implementation of relevant optimization methods and improve the quality of urban transportation and distribution services, it is necessary to provide policy guarantee and measure guarantee for urban transportation and distribution path optimization from multiple angles and aspects, and strengthen the promotion and application of relevant supporting policies, measures and methods from different levels and angles to achieve high-quality development of urban transportation and distribution market. First, establish a unified terminal transportation information service platform, strengthen the integration of data related to enterprise information, user information and industry information, establish a large database and realize the integration of data resources. Combined with the information on the service scale of distribution enterprises, user demand, and user service feedback, the industry management department further strengthens the research and judgment on the development of the transportation distribution market, forms industry development reports, and evaluates, analyzes and researches the market; enterprises collect information related to the distribution mode preference of users in the end distribution link through the platform, and constantly makes dynamic corrections to the end distribution habit preference characteristics of this user. Thus, the transportation and distribution paths can be further optimized dynamically. Second, increase the investment in the optimization of the end distribution path. Taking policy as a guide, from the height of the industry, guide all places to increase the policy and regulation guarantee for urban transportation and distribution path optimization, so as to realize the scientific and rationalization of end distribution path layout design. To industrial layout optimization, tax relief and other preferential means to guide the relevant enterprises to use scientific and efficient methods to optimize and adjust the path, and open up the transportation distribution "last mile". Enterprises to further increase the investment in path optimization program research, strengthen the science of transport and distribution route selection, control their own costs at the same time, to further meet the diversity of user needs. Third, strengthen the development of supporting policies. At present, urban transportation and distribution "last mile" vehicles are mainly tricycles, motorcycles, often crowding the motorway, sidewalk phenomenon, therefore, it is recommended that through policy guidance, in areas where conditions are ripe to pilot the opening of urban transportation and distribution of special channels, and motorway, non-motorized lanes, sidewalks to distinguish. Further ensure road traffic safety, while improving the efficiency of transportation distribution, and promote the opening of special parking spaces for distribution vehicles to solve the key problem of difficult parking for logistics and distribution vehicles. Establish a negative list in the field of urban transportation and distribution, promote the application of "double random a public" regulatory means, focus on the end of urban transportation and distribution of regulatory priorities, difficulties and weak links, the development of specific regulatory rules to reduce unnecessary costs for enterprises and promote a virtuous cycle of the market.

References

- [1] Liu, Z., Yuan, Q. (2021). Carry forward the spirit of "two roads" towards strong transportation country, *People's Daily*, Vol. 2021, No. 7, doi: [10.28655/n.cnki.nrmrb.2021.012208](https://doi.org/10.28655/n.cnki.nrmrb.2021.012208).
- [2] Sun, H., Gao, H. (2021). Research on the last-mile distribution of rural express logistics based on cost reduction and efficiency enhancement, *Logistics Technology*, Vol. 44, No. 11, 41-44, doi: [10.13714/j.cnki.1002-3100.2021.11.017](https://doi.org/10.13714/j.cnki.1002-3100.2021.11.017).
- [3] Han, S., Zhao, L., Chen, K., Luo, Z.-W., Mishra, D. (2017). Appointment scheduling and routing optimization of attended home delivery system with random customer behavior, *European Journal of Operational Research*, Vol. 262, No. 3, 966-980, doi: [10.1016/j.ejor.2017.03.060](https://doi.org/10.1016/j.ejor.2017.03.060).
- [4] Howe, J. (2006). The rise of crowdsourcing, *Wired Magazine*, Vol. 149, No. 6, 176-183.
- [5] Bühler, D., Klein, R., Neugebauer, M. (2016). Model-based transportation distribution cost approximation in attended home services, *Computers & Industrial Engineering*, Vol. 98, 78-90, doi: [10.1016/j.cie.2016.05.014](https://doi.org/10.1016/j.cie.2016.05.014).
- [6] Chen, Y.Y., Zhang, J., Luo, J.Q., Jian, P. (2020). Impacts of customer bounded rationality on last-mile transportation distribution service systems, *Journal of Systems Management*, Vol. 29, No. 2, 389-399, doi: [10.3969/j.issn.1005-2542.2020.02.020](https://doi.org/10.3969/j.issn.1005-2542.2020.02.020).
- [7] Guo, L. (2021). Research on "last mile" distribution strategy of express transportation distribution industry, *China Storage and Transport*, Vol. 8, 133-134, doi: [10.16301/j.cnki.cn12-1204/f.2021.08.062](https://doi.org/10.16301/j.cnki.cn12-1204/f.2021.08.062).
- [8] Song, L., Cherrett, T., Guan, W. (2011). Implications of collection/delivery points for transport and logistics, *OR Insight*, Vol. 24, 231-255, doi: [10.1057/ori.2011.9](https://doi.org/10.1057/ori.2011.9).
- [9] Zhou, M., Zhao, L., Kong, N., Campy, K.S., Xu, G., Zhu, G., Cao, X., Wang, S. (2020). Understanding consumers' behavior to adopt self-service parcel services for last-mile delivery, *Journal of Retailing and Consumer Services*, Vol. 52, Article No. 101911, doi: [10.1016/j.jretconser.2019.101911](https://doi.org/10.1016/j.jretconser.2019.101911).
- [10] Li, G., Chen, W., Yang, L., Liu, Q., Chen, X. (2019). Spatial pattern and agglomeration mode of parcel collection and delivery points in Wuhan City, *Progress in Geography*, Vol. 38, No. 3, 407-416, doi: [10.18306/dlkxjz.2019.03.010](https://doi.org/10.18306/dlkxjz.2019.03.010).
- [11] Xu, J., Jiang, L., Li, Y. (2014). Research on consumers' willingness to choose self-picked packages based on service driven hypothesis, *Journal of Management*, Vol. 11, No. 12, 1850-1857, doi: [10.3969/j.issn.1672-884x.2014.12.016](https://doi.org/10.3969/j.issn.1672-884x.2014.12.016).
- [12] Guo, L. (2015). Research on the "last mile" problem and new mode of express transportation distribution in colleges and universities – A case study of Fujian commercial college, *Journal of Fujian Commercial College*, Vol. 5, 34-38, doi: [10.19473/j.cnki.1008-4940.2015.05.007](https://doi.org/10.19473/j.cnki.1008-4940.2015.05.007).
- [13] Lee, C.-G., Epelman, M.A., White, C.C., Bozer, Y.A. (2006). A shortest path approach to the multiple-vehicle routing problem with split pick-ups, *Transportation Research Part B*, Vol. 40, No. 4, 265-284, doi: [10.1016/j.trb.2004.11.004](https://doi.org/10.1016/j.trb.2004.11.004).
- [14] Ozbaygin, G., Savelsbergh, M. (2019). An iterative re-optimization framework for the dynamic vehicle routing problem with roaming delivery locations, *Transportation Research Part B: Methodological*, Vol. 128, 207-235, doi: [10.1016/j.trb.2019.08.004](https://doi.org/10.1016/j.trb.2019.08.004).
- [15] Zhao, Q., Zhao, J., Lin, Y. (2017). Research on urban distribution network optimization of large retail enterprises based on O2O, *Chinese Journal of Management Science*, Vol. 25, No. 9, 159-167, doi: [10.16381/j.cnki.issn1003-207x.2017.09.018](https://doi.org/10.16381/j.cnki.issn1003-207x.2017.09.018).
- [16] Zhou, L., Baldacci, R., Vigo, D., Wang, X. (2018). A multi-depot two-echelon vehicle routing problem with transportation distribution options arising in the last mile distribution, *European Journal of Operational Research*, Vol. 265, No. 2, 765-778, doi: [10.1016/j.ejor.2017.08.011](https://doi.org/10.1016/j.ejor.2017.08.011).
- [17] Goeke, D., Roberti, R., Schneider, M. (2019). Exact and heuristic solution of the consistent vehicle-routing problem, *Transportation Science*, Vol. 53, No. 4, 1023-1042, doi: [10.1287/trsc.2018.0864](https://doi.org/10.1287/trsc.2018.0864).
- [18] Rohmer, S.U.K., Claassen, G.D.H., Laporte, G. (2019). A two-echelon inventory routing problem for perishable products, *Computers & Operations Research*, Vol. 107, 156-172, doi: [10.1016/j.cor.2019.03.015](https://doi.org/10.1016/j.cor.2019.03.015).
- [19] Jin, C., Lu, L.J., Min, J.N. (2022). A two-stage construction heuristic approach for vehicle routing problem with split deliveries and pickups: Case studies and performance comparison, *Advances in Production Engineering & Management*, Vol. 17, No. 1, 121-133, doi: [10.14743/apem2022.1.425](https://doi.org/10.14743/apem2022.1.425).
- [20] Ocampo, L.A., Himang, C.M., Kumar, A., Brezocnik, M. (2019). A novel multiple criteria decision-making approach based on fuzzy DEMATEL, fuzzy ANP and fuzzy AHP for mapping collection and distribution centers in reverse logistics, *Advances in Production Engineering & Management*, Vol. 14, No. 3, 297-322, doi: [10.14743/apem2019.3.329](https://doi.org/10.14743/apem2019.3.329).
- [21] Wang, L., Chen, X.Y., Zhang, H. (2021). Joint distribution models in fast-moving consumer goods wholesale enterprise: Comparative analysis and a case study, *Advances in Production Engineering & Management*, Vol. 16, No. 2, 212-222, doi: [10.14743/apem2021.2.395](https://doi.org/10.14743/apem2021.2.395).
- [22] Solomon, M.M., Desrosiers, J. (1988). Survey paper – Time window constrained routing and scheduling problems, *Transportation Science*, Vol. 22, No. 1, 1-13, doi: [10.1287/trsc.22.1.1](https://doi.org/10.1287/trsc.22.1.1).
- [23] Homberger, J., Gehring, H. (1999). Two evolutionary metaheuristics for the vehicle routing problem with time windows, *INFOR: Information Systems and Operational Research*, Vol. 37, No. 3, 297-318, doi: [10.1080/03155986.1999.11732386](https://doi.org/10.1080/03155986.1999.11732386).

Modelling surface roughness in finish turning as a function of cutting tool geometry using the response surface method, Gaussian process regression and decision tree regression

Vukelic, D.^{a,*}, Simunovic, K.^b, Kanovic, Z.^a, Saric, T.^b, Doroslovacki, K.^a, Prica, M.^a, Simunovic, G.^b

^aUniversity of Novi Sad, Faculty of Technical Sciences, Novi Sad, Serbia

^bUniversity of Slavonski Brod, Mechanical Engineering Faculty in Slavonski Brod, Slavonski Brod, Croatia

ABSTRACT

In this study, the modelling of arithmetical mean roughness after turning of C45 steel was performed. Four parameters of cutting tool geometry were varied, i.e.: corner radius r , approach angle κ , rake angle γ and inclination angle λ . After turning, the arithmetical mean roughness Ra was measured. The obtained values of Ra ranged from 0.13 μm to 4.39 μm . The results of the experiments showed that surface roughness improves with increasing corner radius, increasing approach angle, increasing rake angle, and decreasing inclination angle. Based on the experimental results, models were developed to predict the distribution of the arithmetical mean roughness using the response surface method (RSM), Gaussian process regression with two kernel functions, the sequential exponential function (GPR-SE) and Mattern (GPR-Mat), and decision tree regression (DTR). The maximum percentage errors of the developed models were 3.898 %, 1.192 %, 1.364 %, and 0.960 % for DTR, GPR-SE, GPR-Mat, and RSM, respectively. In the worst case, the maximum absolute errors were 0.106 μm , 0.017 μm , 0.019 μm , and 0.011 μm for DTR, GPR-SE, GPR-Mat, and RSM, respectively. The results and the obtained errors show that the developed models can be successfully used for surface roughness prediction.

ARTICLE INFO

Keywords:

Turning;
Tool geometry;
Modelling;
Surface roughness;
Response surface method;
Decision tree regression;
Gaussian process regression

*Corresponding author:

vukelic@uns.ac.rs
(Vukelic, D.)

Article history:

Received 13 June 2022
Revised 19 September 2022
Accepted 21 September 2022



Content from this work may be used under the terms of the Creative Commons Attribution 4.0 International License (CC BY 4.0). Any further distribution of this work must maintain attribution to the author(s) and the title of the work, journal citation and DOI.

1. Introduction

Turning plays an important role in machining. It can be achieved in several ways. The steps that need to be taken must be carefully defined to achieve the desired quality, lower cost and shorter production time. Roughness is an important quality indicator of the machining surface, as it affects the performance of the product, but also the production costs [1]. Numerous factors affect the quality of the machining surface: machining conditions (machine tool rigidity, vibrations, use of cutting fluid, type of cutting fluid, etc.), machining parameters (cutting speed, feed rate and depth of cut), material properties of the workpiece (chemical composition, mechanical properties, physical properties, thermal properties, etc.), and cutting tool parameters (geometry, material, coating, etc.) [2-4]. Cutting tool geometry has a great influence on dimensional accuracy, shape accuracy, tool wear, residual stress, chip shape, cutting force, heat distribution, hardness variation, vibration, and surface roughness.

Various methods have been proposed in the literature that have investigated the effects of tool geometry on surface roughness during turning. For example, Zerti *et al.* [5] studied the effects of corner radius, approach angle, and machining parameters on surface topography. Davoudinejad and Noordin [6] presented the effect of chamfer and honed edge geometry on surface finish. Zhao *et al.* [7] presented the effect of edge radius on surface roughness. Duc *et al.* [8] investigated the effect of cutting edge angle, rake angle, and inclination angle on surface roughness. Neseli *et al.* [9] investigated the influence of corner radius, approach angle and rake angle on surface roughness. Ashish and Loksha [10] presented the effect of rake angle, approach angle, and process parameters on surface roughness. Karim *et al.* [11] studied the effects of different rake angles on surface roughness. Kumar *et al.* [12] determined the effect of corner radius and approach angle, as well as turning parameters on the surface roughness. Cui *et al.* [13] performed an optimization of corner radius, rake angle and approach angle. Sung *et al.* [14] studied the effect of corner radius micro deviation on surface roughness. Ponugoti *et al.* [15] studied the surface roughness after turning with variable cutting speed, feed, depth of cut, corner radius and negative rake angle. Senthilkumar and Tamizharasan [16] analyzed the influence of insert shape, relief angle, and corner radius on surface roughness. Tauhiduzzaman and Veldhuis [17] investigated the role of tool geometry on roughness using a tool with a rounded primary cutting edge and a flat secondary cutting edge. Abainia and Ouelaa [18] studied the effect of rake angle, approach angle, and inclination angle on surface roughness. Mohammad *et al.* [19] studied the effects of approach angle, rake angle, and inclination angle on surface roughness. Hai *et al.* [20] studied the surface quality with different corner radii, cutting speeds, and feeds. Khellaf *et al.* [21] presented a comparison of surface roughness with coated and uncoated mixed ceramics. Ozdemir [22] investigated the influence of turning parameters and corner radius on surface roughness. Kuntoglu *et al.* [23] investigated the influence of turning parameters and approach angle on surface roughness. In addition, some studies compared the machined surface quality of conventional and wiper inserts after turning operations [24, 25]. The results showed that the wiper insert had better surface roughness performance compared to conventional inserts.

In analyzing the previous research in this field, which investigates the effects of tool geometry on surface roughness, experimental research dominates. The results obtained can only be applied to the conditions under which the experiments were conducted, and the associated cost and time cannot be neglected. To streamline this process, it is possible to model it. Response surface methodology, Taguchi method, artificial neural networks and fuzzy logic are most commonly used to model the turning process [26-28]. Most of the previous research dealt with the effects of machining parameters (cutting speed, feed rate, depth of cut) on the output parameters of the process [29-32].

Soft computing methods were predominantly used for modelling the turning process. When the turning process is properly modelled and the errors in predicting surface roughness are within acceptable limits, the cost and time of experimental investigations are reduced and the subjective influence of the technologist on the results obtained is diminished. There is also greater universality and thus the possibility of practical application. The most important question is which method should be used and when, because each of them has advantages, but also disadvantages. Despite some existing guidelines, it is still not possible to define an algorithm for selecting an appropriate method for specific production conditions. The error between the predicted and experimental values must be within acceptable limits for the prediction model to be used in practice. Finally, the results of all surface roughness prediction methods should converge with increasing accuracy, leading to an integration that accounts for all possible variables. All prediction methods require significant resources to achieve the desired goals. Therefore, it is critical to select an appropriate modelling method and formulate a sufficiently accurate model.

In contrast to previous studies, the objective of this study is to evaluate the influence of four cutting tool geometry parameters, which have not been extensively studied in the literature, on surface roughness. The input parameters were the corner radius r , the approach angle κ , the rake angle γ and the inclination angle λ , while the output parameter was the arithmetical mean roughness R_a . For the obtained results, the modelling of the finish turning was performed with DTR, GPR-SE and GPR-Mat, which were also not previously used for modelling the turning process.

2. Materials and methods

The methodological framework used in the research is shown in Fig. 1. The experimental studies were carried out on a DMG Mori CTX 510 Ecoline CNC lathe. Dry external longitudinal turning was performed on a workpiece with dimensions $\varnothing 50 \times 600$ mm. The workpiece was fixed and clamped by means of the chuck and rotating centre.

The tests were carried out on workpieces made of medium-carbon steel C45, whose chemical composition is 0.42-0.50 % C, 0.50-0.80 % Mn, ≤ 0.4 % Si, ≤ 0.045 % P, ≤ 0.045 % S, ≤ 0.4 % Cr, ≤ 0.4 % Ni, ≤ 0.1 % Mo, and ≤ 0.63 % Cr+Mo+Ni. In addition, the mechanical and physical properties were as follows: density 7.87 g/cm³, hardness 163 HB, tensile strength 565 MPa, modulus of elasticity 200 GPa, and Poisson's ratio 0.29.

Turning parameters were set for all tests: cutting speed $v_c = 440$ m/min, feed rate $f = 0.10$ mm/rev, and depth of cut $a_p = 1.5$ mm. The parameters were chosen in accordance with the recommendations of the manufacturers of the turning inserts.

CVD-coated (TiCN+Al₂O₃+TiN) turning inserts were used for the experiments. All inserts had the same parameters: effective cutting edge length 10.34 mm, insert thickness 3.175 mm, inscribed circle diameter 6.35 mm, and clearance angle 7°. A new turning insert was used for each experiment. The geometrical parameters of the inserts varied during the experiments are listed in Table 1.

The study was conducted in accordance with the randomized full factorial experiment, which allows the analysis of all combinations of input quantity levels. A total of $3^4 = 81$ experiments were performed.

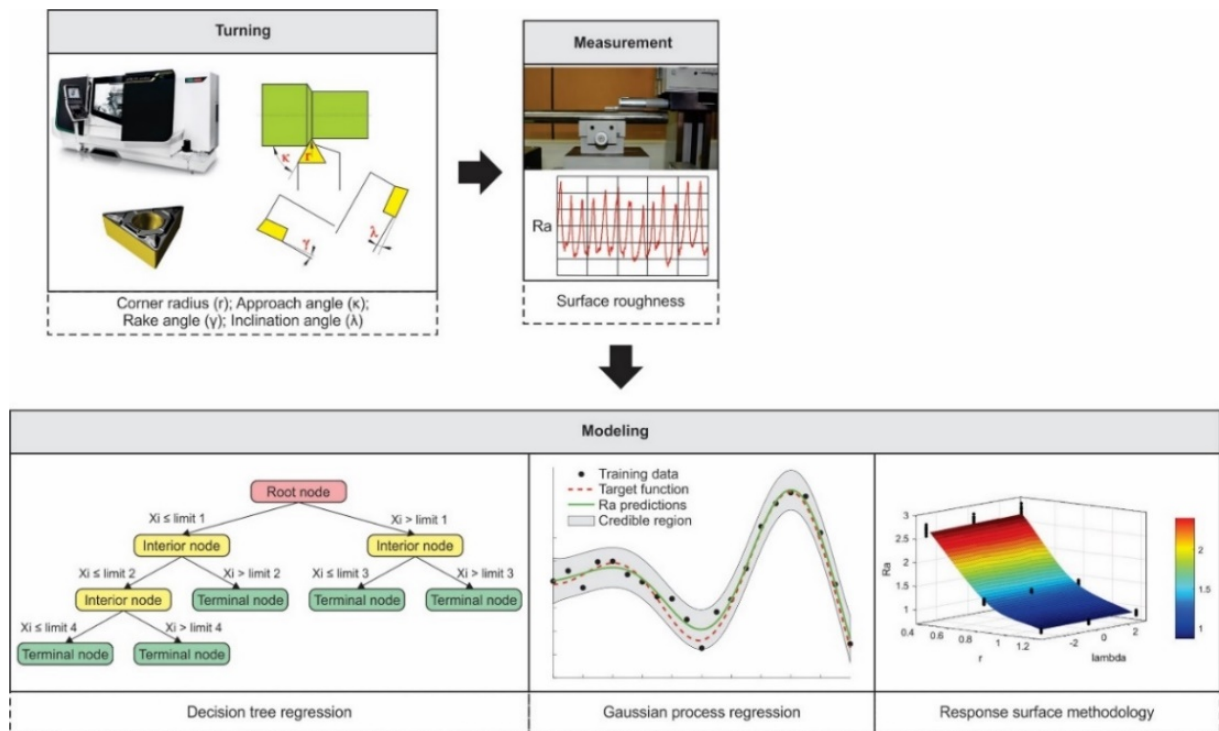


Fig. 1 Methodological framework

Table 1 Turning insert geometry levels (input variables)

Input parameters	Level		
	Low	Medium	High
Corner radius, r (mm)	0.4	0.8	1.2
Approach angle, κ (°)	60	75	90
Rake angle, γ (°)	3	6	9
Inclination angle, λ (°)	-3	0	3

Table 2 Measurement conditions

Parameter	Value
Sampling length	0.8 mm
Cut-off wavelength	0.8 mm
Evaluation length	4 mm
Stylus tip	diamond ball
Stylus radius	2 μ m
Stylus force	1 mN

After each experiment, the surface roughness Ra was measured. The measurement was performed using a Talysurf 6 measuring instrument, under the conditions listed in Table 2. The surface roughness was measured at six evenly spaced locations along the cut length. The average value from these measurements was taken as the mean value of the surface roughness.

After the experiments were conducted, process modelling was performed based on the obtained results, i.e., prediction of surface roughness with: RSM, DTR, GPR-SE and GPR Mat.

3. Results

3.1 Results of experimental research

The results of experimental research, i.e. the measured values of Ra for different combinations of input parameters, are presented in Table 3.

Table 3 Results of experimental research

Run ord.	r (mm)	κ (°)	γ (°)	λ (°)	Ra (µm)	Run ord.	r (mm)	κ (°)	γ (°)	λ (°)	Ra (µm)	Run ord.	r (mm)	κ (°)	γ (°)	λ (°)	Ra (µm)
1	0.8	60	3	-3	1.38	28	0.4	60	6	-3	2.76	55	0.4	60	3	0	2.86
2	0.8	60	6	3	1.39	29	1.2	75	9	0	0.84	56	0.4	75	3	-3	2.74
3	0.4	90	6	3	2.65	30	0.4	60	6	3	2.84	57	1.2	60	9	3	0.88
4	0.4	90	6	-3	2.61	31	1.2	75	9	-3	0.84	58	1.2	75	3	0	0.88
5	1.2	90	9	-3	0.81	32	1.2	90	6	0	0.84	59	0.4	60	6	0	2.80
6	0.8	90	3	3	1.33	33	0.4	90	3	3	2.72	60	0.8	90	9	0	1.27
7	1.2	75	6	0	0.86	34	0.4	90	6	0	2.63	61	0.8	75	9	0	1.30
8	0.8	75	6	0	1.33	35	1.2	90	6	-3	0.83	62	1.2	90	6	3	0.84
9	0.4	90	9	0	2.58	36	0.4	75	6	0	2.71	63	0.8	75	9	3	1.31
10	0.4	60	3	3	2.91	37	1.2	60	9	-3	0.87	64	0.8	75	3	0	1.36
11	0.4	90	9	3	2.60	38	0.8	60	9	-3	1.34	65	1.2	90	9	0	0.82
12	0.4	75	9	-3	2.64	39	1.2	75	6	3	0.87	66	0.8	60	6	0	1.37
13	1.2	75	9	3	0.85	40	1.2	90	3	0	0.86	67	0.8	90	6	0	1.29
14	0.4	90	3	-3	2.68	41	0.8	90	9	-3	1.26	68	1.2	90	3	3	0.86
15	1.2	60	3	0	0.91	42	1.2	60	6	-3	0.87	69	1.2	60	3	3	0.93
16	1.2	60	6	3	0.91	43	1.2	75	3	-3	0.87	70	0.8	90	3	-3	1.31
17	0.4	75	6	-3	2.69	44	0.8	60	6	-3	1.35	71	0.8	60	3	3	1.42
18	0.8	75	9	-3	1.29	45	0.8	90	3	0	1.32	72	1.2	60	9	0	0.87
19	0.8	90	6	-3	1.28	46	0.4	75	9	0	2.66	73	0.8	60	3	0	1.40
20	1.2	90	3	-3	0.85	47	0.8	90	9	3	1.28	74	1.2	90	9	3	0.83
21	0.4	75	3	0	2.77	48	0.8	75	3	3	1.37	75	1.2	60	6	0	0.89
22	0.4	75	3	3	2.80	49	0.8	90	6	3	1.30	76	0.8	75	6	3	1.34
23	0.4	60	9	0	2.75	50	0.4	90	3	0	2.69	77	0.4	60	9	3	2.78
24	1.2	60	3	-3	0.89	51	0.4	75	9	3	2.68	78	0.4	60	3	-3	2.81
25	0.8	60	9	0	1.35	52	0.8	75	6	-3	1.32	79	0.4	90	9	-3	2.56
26	0.8	60	9	3	1.36	53	1.2	75	6	-3	0.85	80	1.2	75	3	3	0.89
27	0.4	75	6	3	2.73	54	0.8	75	3	-3	1.35	81	0.4	60	9	-3	2.72

3.2 Response surface method

The experimental data (Table 3) were statistically processed using Design Expert software (version DX8, 8.0.7.1) and a regression model was derived to predict the surface roughness. Fig. 2 shows the response surface plots of surface roughness resulting from the regression model. Fig. 2 shows that changing the approach angle κ , rake angle γ , and inclination angle λ does not significantly change the surface roughness (Figs. 2a and 2c), while increasing the corner radius r significantly affects the reduction in surface roughness (Figs. 2b and 2d).

Table 4 shows the ANOVA for the reduced quadratic regression model. The nonsignificant interaction terms AD, BC, BD, CD, and the quadratic term A^2 as well as the terms related to interactions between the three factors and higher-order interactions have been removed.

Below is the regression model in terms of the coded (Eq. 1) and the natural (actual) (Eq. 2) input variables.

$$\ln Ra = 0.28 + 0.010 \cdot A - 0.021 \cdot B - 0.031 \cdot C - 0.57 \cdot D - 1.731 \cdot 10^{-3} \cdot A \cdot B - 3.286 \cdot 10^{-3} \cdot A \cdot C + 2.03 \cdot 10^{-3} \cdot B^2 + 2.395 \cdot 10^{-3} \cdot C^2 + 0.14 \cdot D^2 \quad (1)$$

$$\ln Ra = 2.24998 + 0.010042 \cdot \lambda - 9.5811 \cdot 10^{-3} \cdot \gamma - 3.63354 \cdot 10^{-3} \cdot \kappa - 2.82799 \cdot r - 1.92283 \cdot 10^{-4} \cdot \lambda \cdot \gamma - 7.30217 \cdot 10^{-5} \cdot \lambda \cdot \kappa + 2.25531 \cdot 10^{-4} \cdot \gamma^2 + 1.06423 \cdot 10^{-5} \cdot \kappa^2 + 0.87167 \cdot r^2 \quad (2)$$

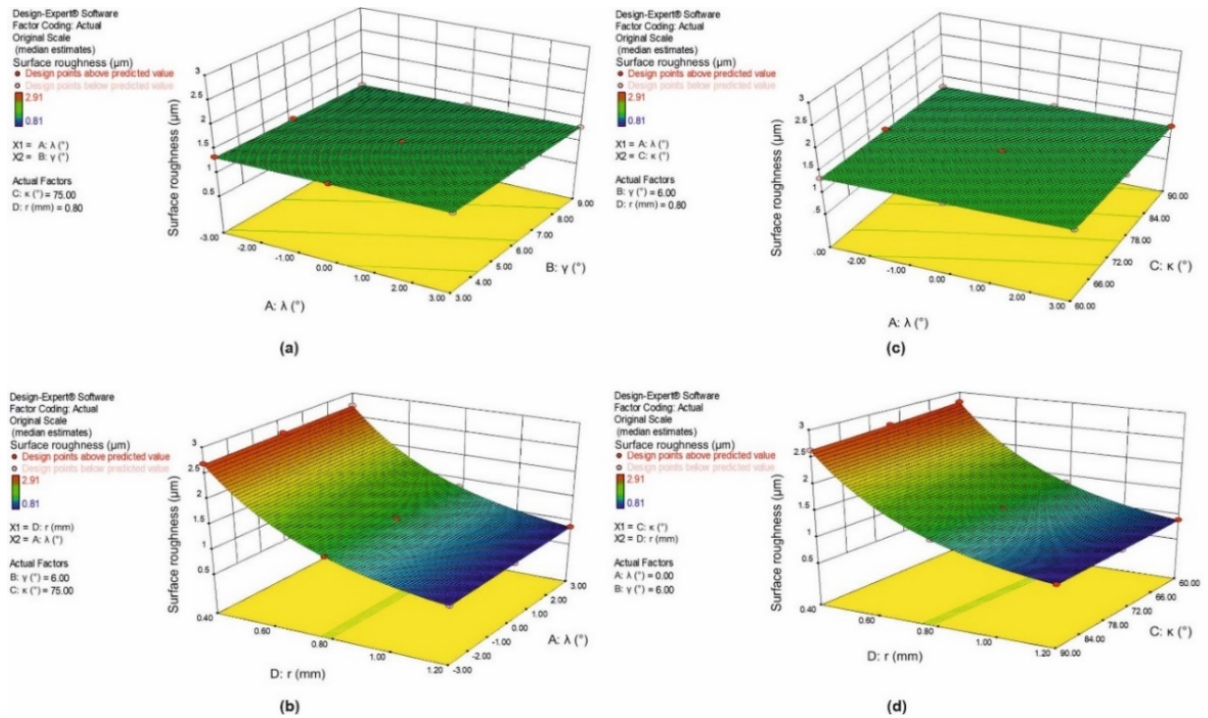


Fig. 2 Response surface plots of surface roughness, a) with approach angle κ and corner radius r at the intermediate levels, b) with rake angle γ and approach angle κ at the intermediate levels, c) with rake angle γ and corner radius r at the intermediate levels, d) with inclination angle λ and rake angle γ at the intermediate levels

Table 4 ANOVA for response surface reduced quadratic model

Source	Sum of Squares	DF	Mean Square	F Value	p-value, Prob > F
Model	18.18	9	2.02	164684.3	< 0.0001
A – inclination angle λ	0.005657	1	0.005657	461.19	< 0.0001
B – rake angle γ	0.023	1	0.023	1872.60	< 0.0001
C – approach angle κ	0.050	1	0.050	4110.92	< 0.0001
D – corner radius r	17.75	1	17.75	1447116	< 0.0001
AB	0.0001078	1	0.0001078	8.79	0.0041
AC	0.0003887	1	0.0003887	31.69	< 0.0001
B ²	7.416 · 10 ⁻⁵	1	7.416 · 10 ⁻⁵	6.05	0.0164
C ²	0.0001032	1	0.0001032	8.41	0.0050
D ²	0.35	1	0.35	28543.75	< 0.0001
Residual	0.0008709	71	1.227 · 10 ⁻⁵		
Cor Total	18.18	80			

Table 5 lists the regression coefficient for each model term, their standard errors, and 95 percent confidence intervals (95 % CI). Confidence intervals are ranges within which the true regression coefficients must fall. In the table, these ranges are low for the intercept, the regression coefficients of A, B, C, D, and D², while they are high for AB, AC, B², and C². However, it is important that the regression coefficients do not span zero, because that would mean that a single regression coefficient can be zero, i.e., that a particular factor has no effect.

Residual analysis follows as an important technique for analyzing regression models. Fig. 3 shows the constructed normal probability plot of the internally studentized residuals to check the assumption of normality of the residuals or errors. From Fig. 3, it can be seen that the error distribution is approximately normal as the graph resembles the straight line. There are small deviations from the straight line at the extremes, but this is not the case for most of the intermediate values. It is also clear that all internally studentized residuals are within ± 3 standard deviations from zero (studentized residuals have unit variance), which means that there are no outliers. This is also evident from Fig. 4, which shows the plot of internally studentized residuals against four

factors. Fig. 4 also shows that for the factor D (corner radius r), there is some rule for the dependence of the residuals on this factor, i.e. some pattern. Although both positive and negative internally studentized residuals occur (which is fine), there is still smaller scatter for the smaller corner radius and larger for the larger corner radius, which means that it is not a completely constant variance. This is mainly affected by only four internally studentized residuals, i.e., for the experiments labelled 5 and 42 (Run ord.) in Table 3 (the internally studentized residuals are -2.59 and -2.53, respectively) and for experiments 37 and 16 (the internally studentized residuals are 2.68 and 2.95, respectively). These samples were rechecked and it was found that there were no possible errors in the measurement or recording of the results.

Table 5 Standard errors and confidence intervals for regression coefficients

Term	Coefficient Estimate	DF	Standard Error	95 % CI Low	95 % CI High
Intercept	0.28	1	$1.030 \cdot 10^{-3}$	0.281	0.285
A – inclination angle (λ)	0.010	1	$4.766 \cdot 10^{-4}$	0.00928	0.011
B – rake angle (γ)	-0.021	1	$4.766 \cdot 10^{-4}$	-0.0216	-0.01967
C – approach angle (κ)	-0.031	1	$4.766 \cdot 10^{-4}$	-0.0315	-0.0296
D – corner radius (r)	-0.57	1	$4.766 \cdot 10^{-4}$	-0.574	-0.572
AB	$-1.731 \cdot 10^{-3}$	1	$5.837 \cdot 10^{-4}$	$-2.89 \cdot 10^{-3}$	$-5.67 \cdot 10^{-4}$
AC	$-3.286 \cdot 10^{-3}$	1	$5.837 \cdot 10^{-4}$	$-4.45 \cdot 10^{-3}$	$-2.12 \cdot 10^{-3}$
B ²	$2.030 \cdot 10^{-3}$	1	$8.255 \cdot 10^{-4}$	$3.84 \cdot 10^{-4}$	$3.68 \cdot 10^{-3}$
C ²	$2.395 \cdot 10^{-3}$	1	$8.255 \cdot 10^{-4}$	$7.485 \cdot 10^{-4}$	$4.04 \cdot 10^{-3}$
D ²	0.14	1	$8.255 \cdot 10^{-4}$	0.138	0.141

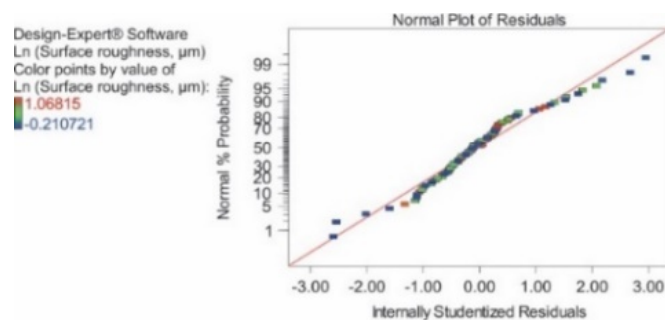


Fig. 3 Normal probability plot of internally studentized residuals

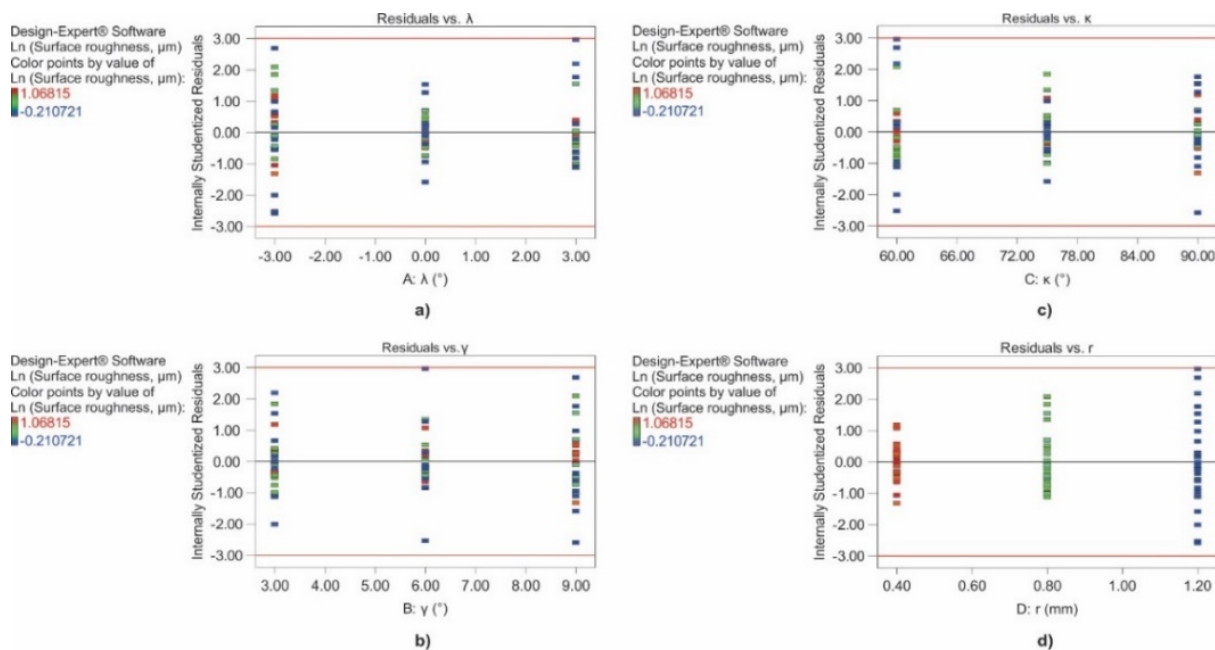


Fig. 4 Residuals versus factors, a) Residuals versus inclination angle λ , b) Residuals versus rake angle γ , c) Residuals versus approach angle κ , d) Residuals versus corner radius r

3.3 Decision tree regression

A decision tree is a machine learning algorithm that can be used for both classification and regression. It is one of the most commonly used practical approaches for supervised learning [33]. In regression, the goal of a decision tree-based model is to predict a continuous output value for a given multivariate input data instance. The model is trained on the given training dataset $\{(x_i, y_i)\}_{i=1}^N \in R^m \times R$, where x_i is an m -dimensional input vector and y_i is the corresponding output value. Based on this dataset, a tree-structured regression model is built, as shown in Fig. 1, which consists of three types of nodes. The root node is the initial node which represents the whole dataset. It is split into additional nodes according to the decision (or division) rules contained in both the root node and all subsequent nodes. The interior nodes represent the features of the dataset, and the branches represent the decision (i.e., division) rules. Finally, the leaf nodes represent terminal parts and provide the output results.

The basic idea is to split the entire dataset into groups of "similar" samples, using decision rules contained in interior nodes, applied to input variables x_i [34]. In the decision tree regression problems, the criterion for dataset splitting is the variance of the output value y_i :

$$var = \frac{1}{n} \sum_{i=1}^n (y_i - \bar{y})^2 \quad (3)$$

where n is the total number of samples in the node and \bar{y} is the mean of the output values of all samples in the node. Each "parent" node is divided into two "child" nodes. All possible ways of splitting the dataset in a given node are considered, and the one that provides the greatest variance reduction defined as follows:

$$VarRed = var(parent) - \sum_{i=1}^2 w_i var(child_i) \quad (4)$$

is adopted. In the Eq. 4, w_i is the ratio between the number of elements in the child node and the total number of elements in the parent node. In other words, we split the dataset each time into two new sets, each containing "similar" data, while at the same time the obtained sets differ as much as possible. The described process of node splitting is performed until the desired depth of the tree is reached, which depends on the complexity of the problem.

Once the tree model is trained, it can be used to obtain the predicted value for each new data sample. Following the division rules for the input values x_i , starting from the root node through all the interior nodes, the data sample can be grouped to one of the terminal nodes. The predicted value for that data sample is calculated as the average value of the output values y_i of all the data samples from the training dataset that were grouped to that particular terminal node.

In this study, the following turning process parameters were used as inputs x_1 to x_4 : corner radius r , approach angle κ , rake angle γ , and inclination angle λ . The value of the surface roughness Ra was taken as the output parameter y . The tree model was built using Matlab and the application Regression learner, which has three variants for the tree depth according to the maximum number of splits: low, medium and fine tree. All variants were tested, and the fine tree variant, which allows a maximum of 100 splits, was adopted based on the mean square error (MSE) value in the 5-fold cross-validation training procedure. The minimum number of samples per node was set at five, which was determined by a trial-and-error procedure. The cross-validation procedure was also used to remove unnecessary branches to avoid overfitting.

3.4 Gaussian process regression

A Gaussian processes regression is a powerful machine learning technique that can be used to solve a wide variety of supervised learning problems, even when only a small amount of training data is available. It is a probability distribution over possible functions matching a set of points, given with the training dataset $\{(x_i, y_i)\}_{i=1}^N \in R^m \times R$, as described previously. The Gaussian process regression is not given in the form of a function, but in a nonparametric form. Thus, instead of computing the probability distribution of the parameters of a specific function, GPR calculates the probability distribution over all admissible functions that fit the data in the dataset.

The regression function modelled by Gaussian process regression has the following form:

$$P(f|X) = \mathcal{N}(f|\mu, K) \tag{5}$$

where $X = [x_1, x_2, \dots, x_N]$, $f = [f(x_1), f(x_2), \dots, f(x_N)]$, $\mu = [m(x_1), m(x_2), \dots, m(x_N)]$ and $K_{ij} = k(x_i, x_j)$. X are the observed input data, m represents the mean function, and K represents a positive definite kernel function, that defines the smoothness of the function, i.e., if the points x_i and x_j are considered similar by the kernel, the function outputs of the two points, $f(x_i)$ and $f(x_j)$ are expected to be similar. Given the points of the training dataset and a mean function f estimated by these points, one can make predictions for each new dataset X_* as $f(X_*)$ with a certain confidence interval depending on the values and distribution of the training dataset. The simple one-dimensional GPR regression is shown in Fig. 1. Based on the training data (black dots), the mean function is determined (green line), and it gives predictions for all new data points X_* with the confidence interval marked in grey.

If we introduce f_* as a prediction for a new dataset X_* , we can express the joint distribution of f and f_* as follows:

$$\begin{bmatrix} f \\ f_* \end{bmatrix} \sim \mathcal{N} \left(\begin{bmatrix} m(X) \\ m(X_*) \end{bmatrix}, \begin{bmatrix} K & K_* \\ K_*^T & K_{**} \end{bmatrix} \right) \tag{6}$$

where $K = K(X, X)$, $K_* = K(X, X_*)$ and $K_{**} = K(X_*, X_*)$. To be able to make a prediction, we need to derive the conditional distribution $P(f_*|f, X, X_*) = \mathcal{N}(f|\mu, K)$. This derivation is given in detail in [35], obtaining:

$$f_*|f, X, X_* \sim \mathcal{N}(K_*^T K f, K_{**} - K_*^T K^{-1} K_*) \tag{7}$$

In real applications, however, we do not need exact function values, but rather the noisy version of the data, $y = f(x) + \varepsilon$, where we assume that ε is an additive independent and identically distributed (i.i.d.) Gaussian noise with a variance σ_n^2 that can be determined from the training dataset. The variance function then becomes $\text{cov}(y) = K + \sigma_n^2 I$, and the joint distribution of the observed points (training dataset) and the function values at new dataset points:

$$\begin{bmatrix} y \\ f_* \end{bmatrix} \sim \mathcal{N} \left(\begin{bmatrix} m(X) \\ m(X_*) \end{bmatrix}, \begin{bmatrix} K + \sigma_n^2 I & K_* \\ K_*^T & K_{**} \end{bmatrix} \right) \tag{8}$$

By deriving the conditional distribution, we get the predictive equations for Gaussian processes regression as follows:

$$\bar{f}_*|y, X, X_* \sim \mathcal{N}(\bar{f}_*, \text{cov}(f_*)) \tag{9}$$

$$\bar{f}_* \triangleq \mathbb{E}[\bar{f}_*|y, X, X_*] = K_*^T [K + \sigma_n^2 I]^{-1} y \quad \text{cov}(f_*) = K_{**} - K_*^T [K + \sigma_n^2 I]^{-1} K_* \tag{10}$$

The practical implementation algorithm for Eqs. 8 to 10 is described in [35]. The best results were obtained with the quadratic exponential kernel (SE) and Matern kernel. The values of kernel parameters were optimized using marginal likelihood as the objective function [35].

3.5 The results of the prediction

Of the total 81 experiments, 72 were used for training and 9 for confirmation. Table 6 shows the results of the training dataset, and Table 7 shows the modelling results of the confirmation dataset. The strength of the modelling, i.e., the deviation between the measured Ra value (Ra_{imv}) and the predicted Ra value (Ra_{ipv}), was estimated by the absolute error (AE) and the percentage error (PE) as follows:

$$AE = |Ra_{ipv} - Ra_{imv}| \tag{11}$$

$$PE = \frac{|Ra_{ipv} - Ra_{imv}|}{Ra_{imv}} \cdot 100 \% \tag{12}$$

Table 6 Modelling results of the training dataset

Run ord.	r (mm)	κ (°)	γ (°)	λ (°)	Ra (μm)				PE (%)				AE (μm)			
					DTR	GPR-SE	GPR-Mat	RSM	DTR	GPR-SE	GPR-Mat	RSM	DTR	GPR-SE	GPR-Mat	RSM
1	0.8	60	3	-3	1.368	1.378	1.380	1.382	0.906	0.139	0.025	0.170	0.013	0.002	0.000	0.002
2	0.8	60	6	3	1.368	1.396	1.395	1.391	1.619	0.464	0.391	0.060	0.023	0.006	0.005	0.001
3	0.4	90	6	3	2.625	2.650	2.650	2.651	0.943	0.001	0.004	0.046	0.025	0.000	0.000	0.001
4	0.4	90	6	-3	2.625	2.612	2.613	2.615	0.575	0.077	0.110	0.177	0.015	0.002	0.003	0.005
5	1.2	90	9	-3	0.832	0.812	0.813	0.817	2.675	0.191	0.318	0.835	0.022	0.002	0.003	0.007
6	0.8	90	3	3	1.294	1.328	1.329	1.332	2.726	0.149	0.084	0.142	0.036	0.002	0.001	0.002
7	1.2	75	6	0	0.866	0.859	0.860	0.860	0.698	0.072	0.047	0.039	0.006	0.001	0.000	0.000
8	0.8	75	6	0	1.335	1.327	1.328	1.328	0.376	0.263	0.185	0.175	0.005	0.003	0.002	0.002
9	0.4	90	9	0	2.625	2.581	2.581	2.584	1.744	0.043	0.049	0.168	0.045	0.001	0.001	0.004
10	0.4	60	3	3	2.804	2.906	2.908	2.907	3.651	0.135	0.061	0.107	0.106	0.004	0.002	0.003
11	0.4	90	9	3	2.625	2.600	2.601	2.598	0.962	0.017	0.039	0.082	0.025	0.000	0.001	0.002
13	1.2	75	9	3	0.832	0.848	0.849	0.852	2.157	0.191	0.120	0.200	0.018	0.002	0.001	0.002
14	0.4	90	3	-3	2.625	2.674	2.675	2.670	2.052	0.224	0.180	0.377	0.055	0.006	0.005	0.010
15	1.2	60	3	0	0.894	0.909	0.908	0.910	1.786	0.117	0.171	0.052	0.016	0.001	0.002	0.000
16	1.2	60	6	3	0.894	0.904	0.905	0.901	1.786	0.628	0.543	0.960	0.016	0.006	0.005	0.009
17	0.4	75	6	-3	2.723	2.686	2.687	2.680	1.208	0.139	0.103	0.354	0.033	0.004	0.003	0.010
19	0.8	90	6	-3	1.294	1.281	1.281	1.282	1.074	0.070	0.047	0.146	0.014	0.001	0.001	0.002
20	1.2	90	3	-3	0.848	0.851	0.851	0.848	0.235	0.116	0.062	0.210	0.002	0.001	0.001	0.002
21	0.4	75	3	0	2.723	2.771	2.769	2.770	1.715	0.023	0.024	0.004	0.047	0.001	0.001	0.000
22	0.4	75	3	3	2.723	2.799	2.799	2.803	2.768	0.025	0.027	0.123	0.077	0.001	0.001	0.003
23	0.4	60	9	0	2.804	2.748	2.749	2.747	1.955	0.064	0.043	0.101	0.054	0.002	0.001	0.003
24	1.2	60	3	-3	0.894	0.888	0.889	0.896	0.421	0.229	0.168	0.648	0.004	0.002	0.001	0.006
25	0.8	60	9	0	1.368	1.349	1.348	1.347	1.296	0.105	0.117	0.231	0.017	0.001	0.002	0.003
26	0.8	60	9	3	1.368	1.364	1.363	1.363	0.551	0.286	0.230	0.210	0.007	0.004	0.003	0.003
27	0.4	75	6	3	2.723	2.735	2.733	2.736	0.275	0.181	0.117	0.217	0.007	0.005	0.003	0.006
28	0.4	60	6	-3	2.804	2.760	2.760	2.761	1.585	0.015	0.008	0.043	0.044	0.000	0.000	0.001
29	1.2	75	9	0	0.832	0.843	0.843	0.844	0.992	0.364	0.307	0.534	0.008	0.003	0.003	0.004
30	0.4	60	6	3	2.804	2.837	2.837	2.837	1.276	0.091	0.111	0.110	0.036	0.003	0.003	0.003
31	1.2	75	9	-3	0.832	0.839	0.838	0.837	0.992	0.144	0.215	0.317	0.008	0.001	0.002	0.003
34	0.4	90	6	0	2.625	2.631	2.631	2.633	0.190	0.032	0.028	0.108	0.005	0.001	0.001	0.003
35	1.2	90	6	-3	0.848	0.828	0.829	0.831	2.169	0.220	0.102	0.078	0.018	0.002	0.001	0.001
36	0.4	75	6	0	2.723	2.710	2.709	2.708	0.461	0.001	0.021	0.072	0.013	0.000	0.001	0.002
38	0.8	60	9	-3	1.368	1.338	1.338	1.331	2.052	0.180	0.139	0.665	0.027	0.002	0.002	0.009
39	1.2	75	6	3	0.866	0.867	0.868	0.869	0.460	0.327	0.214	0.093	0.004	0.003	0.002	0.001
40	1.2	90	3	0	0.848	0.856	0.857	0.856	1.395	0.450	0.300	0.511	0.012	0.004	0.003	0.004
41	0.8	90	9	-3	1.294	1.257	1.256	1.260	2.679	0.223	0.349	0.034	0.034	0.003	0.004	0.000
42	1.2	60	6	-3	0.894	0.873	0.871	0.877	2.730	0.313	0.160	0.830	0.024	0.003	0.001	0.007
43	1.2	75	3	-3	0.866	0.871	0.870	0.870	0.460	0.122	0.024	0.048	0.004	0.001	0.000	0.000
44	0.8	60	6	-3	1.368	1.353	1.353	1.354	1.296	0.188	0.203	0.276	0.017	0.003	0.003	0.004
45	0.8	90	3	0	1.294	1.321	1.321	1.320	1.989	0.086	0.073	0.029	0.026	0.001	0.001	0.000
46	0.4	75	9	0	2.723	2.660	2.660	2.658	2.350	0.004	0.007	0.069	0.063	0.000	0.000	0.002
47	0.8	90	9	3	1.294	1.276	1.276	1.274	1.074	0.318	0.306	0.496	0.014	0.004	0.004	0.006
48	0.8	75	3	3	1.335	1.374	1.374	1.374	2.555	0.278	0.283	0.325	0.035	0.004	0.004	0.004
49	0.8	90	6	3	1.294	1.298	1.299	1.300	0.481	0.172	0.103	0.015	0.006	0.002	0.001	0.000
50	0.4	90	3	0	2.625	2.692	2.692	2.693	2.416	0.067	0.062	0.118	0.065	0.002	0.002	0.003
51	0.4	75	9	3	2.723	2.680	2.680	2.681	1.586	0.009	0.007	0.032	0.043	0.000	0.000	0.001
52	0.8	75	6	-3	1.335	1.317	1.318	1.314	1.136	0.240	0.128	0.443	0.015	0.003	0.002	0.006
53	1.2	75	6	-3	0.866	0.852	0.852	0.852	1.882	0.240	0.181	0.185	0.016	0.002	0.002	0.002
54	0.8	75	3	-3	1.335	1.347	1.347	1.342	1.111	0.229	0.206	0.597	0.015	0.003	0.003	0.008
55	0.4	60	3	0	2.804	2.858	2.857	2.863	1.967	0.079	0.101	0.101	0.056	0.002	0.003	0.003
56	0.4	75	3	-3	2.723	2.743	2.743	2.737	0.639	0.109	0.093	0.104	0.018	0.003	0.003	0.003
57	1.2	60	9	3	0.894	0.880	0.881	0.883	1.562	0.009	0.089	0.356	0.014	0.000	0.001	0.003
58	1.2	75	3	0	0.866	0.880	0.880	0.880	1.591	0.012	0.001	0.005	0.014	0.000	0.000	0.000
60	0.8	90	9	0	1.294	1.266	1.267	1.267	1.870	0.344	0.268	0.234	0.024	0.004	0.003	0.003
61	0.8	75	9	0	1.335	1.303	1.303	1.303	2.692	0.202	0.232	0.248	0.035	0.003	0.003	0.003
62	1.2	90	6	3	0.848	0.844	0.843	0.842	0.952	0.520	0.394	0.271	0.008	0.004	0.003	0.002
63	0.8	75	9	3	1.335	1.311	1.311	1.314	1.908	0.068	0.058	0.332	0.025	0.001	0.001	0.004
64	0.8	75	3	0	1.335	1.359	1.359	1.358	1.838	0.054	0.078	0.140	0.025	0.001	0.001	0.002
65	1.2	90	9	0	0.832	0.822	0.822	0.821	1.423	0.203	0.224	0.126	0.012	0.002	0.002	0.001
66	0.8	60	6	0	1.368	1.373	1.371	1.372	0.182	0.192	0.098	0.157	0.003	0.003	0.001	0.002
68	1.2	90	3	3	0.848	0.861	0.860	0.863	1.395	0.074	0.021	0.357	0.012	0.001	0.000	0.003
69	1.2	60	3	3	0.894	0.932	0.931	0.924	3.898	0.210	0.130	0.698	0.036	0.002	0.001	0.006
70	0.8	90	3	-3	1.294	1.315	1.313	1.309	1.240	0.417	0.255	0.078	0.016	0.005	0.003	0.001
72	1.2	60	9	0	0.894	0.870	0.870	0.873	2.730	0.043	0.015	0.319	0.024	0.000	0.000	0.003
73	0.8	60	3	0	1.368	1.406	1.406	1.404	2.321	0.403	0.399	0.257	0.033	0.006	0.006	0.004
74	1.2	90	9	3	0.832	0.832	0.830	0.825	0.201	0.215	0.012	0.563	0.002	0.002	0.000	0.005
75	1.2	60	6	0	0.894	0.887	0.887	0.889	0.421	0.283	0.284	0.095	0.004	0.003	0.003	0.001
76	0.8	75	6	3	1.335	1.338	1.338	1.341	0.373	0.120	0.134	0.100	0.005	0.002	0.002	0.001
77	0.4	60	9	3	2.804	2.778	2.779	2.780	0.854	0.063	0.037	0.007	0.024	0.002	0.001	0.000
78	0.4	60	3	-3	2.804	2.812	2.811	2.820	0.222	0.063	0.047	0.341	0.006	0.002	0.001	0.010
79	0.4	90	9	-3	2.625	2.563	2.562	2.571	2.539	0.108	0.074	0.425	0.065	0.003	0.002	0.011
81	0.4	60	9	-3	2.804	2.721	2.721	2.715	3.079	0.047	0.041	0.183	0.084	0.001	0.001	0.005

Table 7 Modelling results of the confirmation dataset

Run	r (mm)	κ (°)	γ (°)	λ (°)	Ra (μm)				PE (%)				AE (μm)			
					DTR	GPR-SE	GPR-Mat	RSM	DTR	GPR-SE	GPR-Mat	RSM	DTR	GPR-SE	GPR-Mat	RSM
12	0.4	75	9	-3	2.723	2.642	2.642	2.636	3.125	0.065	0.065	0.165	0.083	0.002	0.002	0.004
18	0.8	75	9	-3	1.335	1.297	1.298	1.292	3.488	0.557	0.581	0.169	0.045	0.007	0.008	0.002
32	1.2	90	6	0	0.848	0.837	0.838	0.836	0.952	0.407	0.244	0.423	0.008	0.003	0.002	0.004
33	0.4	90	3	3	2.625	2.710	2.711	2.717	3.493	0.374	0.325	0.123	0.095	0.010	0.009	0.003
37	1.2	60	9	-3	0.894	0.863	0.863	0.863	2.730	0.749	0.859	0.857	0.024	0.007	0.007	0.007
59	0.4	60	6	0	2.804	2.798	2.797	2.799	0.134	0.082	0.121	0.044	0.004	0.002	0.003	0.001
67	0.8	90	6	0	1.294	1.289	1.290	1.291	0.291	0.100	0.025	0.063	0.004	0.001	0.000	0.001
71	0.8	60	3	3	1.368	1.437	1.439	1.425	3.697	1.192	1.364	0.364	0.053	0.017	0.019	0.005
80	1.2	75	3	3	0.866	0.889	0.888	0.891	2.697	0.097	0.186	0.072	0.024	0.001	0.002	0.001

4. Discussion

The descriptive parameters of surface roughness for the experimental tests performed are listed in Table 8. The surface roughness ranges from 0.81 μm to 2.91 μm , with an average value of 1.64 μm and a standard deviation of 0.795 μm . The lowest roughness value ($Ra = Ra_{min} = 0.81 \mu\text{m}$) was obtained when machining with the largest values for the corner radius ($r = r_{max} = 1.2 \text{ mm}$), the largest approach angle ($\kappa = \kappa_{max} = 90^\circ$), the largest rake angle ($\gamma = \gamma_{max} = 9^\circ$), and the smallest inclination angle ($\lambda = \lambda_{min} = -3^\circ$) of the turning insert. The highest roughness value ($Ra = Ra_{max} = 2.91 \mu\text{m}$) was obtained when machining with the smallest values of corner radius ($r = r_{min} = 0.4 \text{ mm}$), the smallest approach angle ($\kappa = \kappa_{min} = 60^\circ$), the smallest rake angle ($\gamma = \gamma_{min} = 3^\circ$) and the largest inclination angle ($\lambda = \lambda_{max} = 3^\circ$) of the turning insert. The ratio values show that the arithmetical mean roughness changes in a wide range for suitable geometrical parameters, which ensures good process control. In other words, the desired quality of the machined surface can be achieved by a suitable choice of input parameters.

The identified trends of the dependence of Ra on the input variables are consistent with some previous studies. Feed rate and corner radius have the greatest effect on surface roughness. The roughness of the machined surface decreases (improves) in the following cases: with increasing corner radius [5, 11, 12, 16, 20, 21]; with an increase in positive values of the rake angle [8, 11, 18, 19]; with an increase in the approach angle [5, 8-10, 18], and with the reduction of inclination angle [18], although to varying degrees with different combinations. The results are different, but the trend is identical. Some of the studies also reported the opposite. Surface roughness can also deteriorate (increase) under certain experimental conditions with increasing corner radius [9], smaller approach angle [9, 19], with smaller rake angle [10], and with increasing positive values of inclination angle [19]. Under certain machining conditions, roughness first increases and then decreases with increasing inclination angle [8] and in some cases it first decreases and then increases with increasing inclination angle [12].

Table 8 Descriptive parameters of the surface roughness Ra

Parameter	Training Ra (μm)	Confirmation Ra (μm)
Minimum value	0.810	0.848
Maximum value	2.910	2.804
Mean value	1.637	1.639
Standard deviation	0.795	0.834
Ratio	3.593	3.306

The reduction in roughness at a larger corner radius is a result of the lower and shallower peak height and the lower and shallower valley depth of the machined surface. Higher values of approach angle and positive inclination angle result in lower susceptibility to vibration and thus better quality of the machined surface. Increasing the rake angle improves the sharpness of the cutting edge and thus reduces the roughness of the machined surface. When the approach angle decreases, the contact length of the chip increases, the chip thickness decreases and the chip width increases. The cutting forces are distributed over the longer cutting edge and chip breaking is more difficult. Larger approach angles are characterized by an increase in resistance to auxiliary

movements and a decrease in penetration resistance, as well as a lower tendency to vibration. In the present study, increasing the approach angle resulted in a reduction in roughness, mainly due to minimization of vibration. Reducing the cutting forces reduces the possibility of vibration and thus improving the surface roughness. A negative value of the inclination angle directs chips in the direction of workpiece (in the direction of auxiliary motion) and a positive value directs them in the opposite direction (in the direction opposite to the direction of auxiliary motion). A negative inclination angle increases the cutting edge strength, but also the back force of the cutting resistance, which can lead to chattering. In the present study, negative values of the inclination angle improved surface roughness by increasing cutting edge strength (and reducing the occurrence of various wear mechanisms) and did not affect vibration induction. During turning, the tool tip is exposed to high contact pressures and temperatures in the machining zone, which can increase various wear mechanisms. The smaller corner radius is characterized by lower strength and the larger one by higher strength. The poorest surface finish was obtained with the smallest corner radius. This is due to the low strength of the tool tip and the resulting higher wear rate. The shorter contact length between the tool tip and the workpiece results in less heat dissipation from the shear zone and a higher concentration of heat and stress in this zone. This increases the possibility of tool wear and even thermoplastic deformation of the tool tip.

The visual interpretation of the absolute and percentage errors for all experiments performed (for the training dataset and the confirmation dataset) is shown in Fig. 5, and the minimum, maximum, and mean values for both datasets are shown in Table 9.

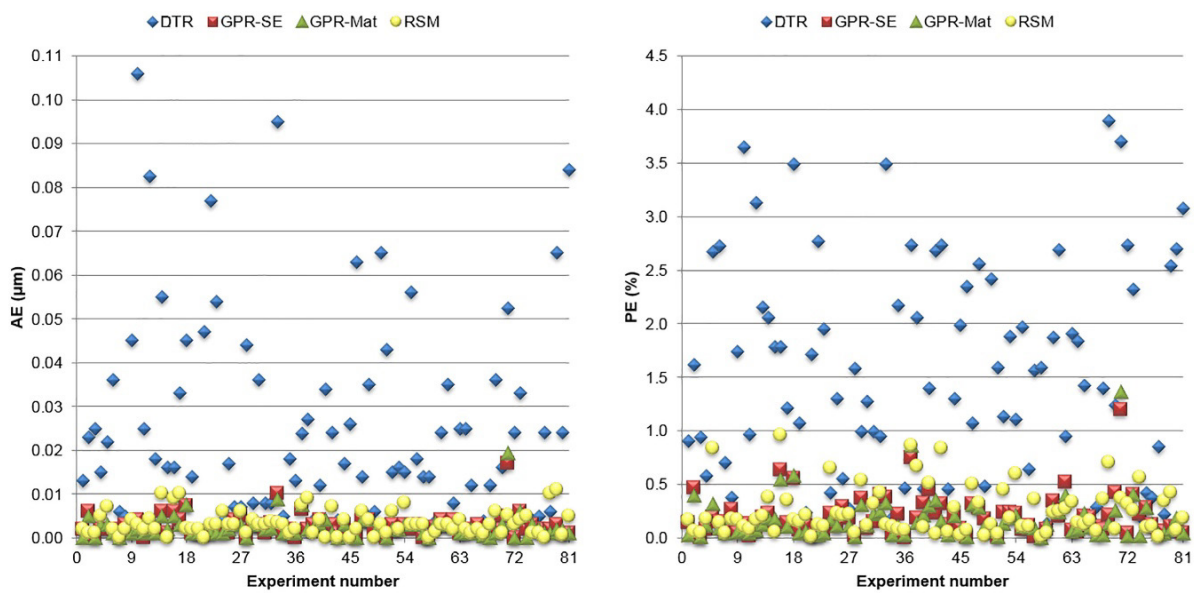


Fig. 5 Visual representation of absolute and percentage errors

Table 9 The percentage and absolute errors of the training and confirmation datasets

Experiment	Value	DTR		GPR-SE		GPR-Mat		RSM	
		PE (%)	AE (µm)	PE (%)	AE (µm)	PE (%)	AE (µm)	PE (%)	AE (µm)
Training	Minimum	0.182	0.002	0.001	0.000	0.001	0.000	0.004	0.000
	Maximum	3.898	0.106	0.628	0.006	0.543	0.006	0.960	0.011
	Mean	1.491	0.025	0.168	0.002	0.137	0.002	0.241	0.003
Confirmation	Minimum	0.134	0.004	0.065	0.001	0.025	0.000	0.044	0.001
	Maximum	3.697	0.095	1.192	0.017	1.364	0.019	0.857	0.007
	Mean	2.290	0.038	0.403	0.006	0.419	0.006	0.253	0.003

Based on Fig. 5 and Table 9, the following can be concluded:

- The DTR model had a PE of less than 1 % for 28 predictions, a PE of between 1% and 2 % for 28 predictions, a PE of between 2 % and 3 % for 18 predictions, and a PE of between 3 % and

4 % for 7 predictions. The absolute error for all predictions except one ($AE_{max} = 0.106 \mu\text{m}$) was less than $0.1 \mu\text{m}$. The maximum error values occur during training. The minimum and mean error values also occur during training.

- The model GPR-SE had a PE of less than 1 % and an AE of less than $0.02 \mu\text{m}$ ($AE_{max} = 0.017 \mu\text{m}$) for all predictions except one ($PE_{max} = 1.192 \%$). The maximum error values occur at confirmation. The minimum and mean error values occur during training.
- The GPR-Mat model had a PE of less than 1 % and an AE of less than $0.02 \mu\text{m}$ ($AE_{max} = 0.019 \mu\text{m}$) for all predictions except one ($PE_{max} = 1.364 \%$). The maximum error values occur at confirmation. The minimum and mean error values occur during training.
- The RSM model had a PE of less than 1 % ($PE_{max} = 0.960 \%$) and an AE of less than $0.02 \mu\text{m}$ ($AE_{max} = 0.011 \mu\text{m}$) for all predictions. The maximum error values occur during training. The minimum and average error values also occur during training.

The GPR-SE, GPR-Mat, and RSM models conditionally gave slightly better results, while the DTR model gave slightly worse results. Moreover, the errors in the confirmation experiments are consistent with those of PE during the training phase, indicating that the modelling was performed correctly. The extremely low values of the maximum PE errors and, most importantly, the correspondingly small values of AE (which give a real deviation from the desired value of the surface roughness) show the real possibilities of practical application of all four models in practice.

5. Conclusion

In this study, the integral influence of four parameters of CVD coated cutting tool geometry (corner radius r , approach angle κ , rake angle γ and inclination angle λ on surface roughness of C45 steel workpiece during finish turning was evaluated. Four models were developed based on the experimental results. Confirmation experiments were conducted to validate the model.

The experimental results show that the surface roughness improves with a simultaneous increase in corner radius r , approach angle κ , and rake angle γ , and a decrease in inclination angle λ . The corner radius r has a dominant effect on roughness, followed by the approach angle κ with less effect on surface roughness, the rake angle γ even less and the inclination angle λ with the least.

Based on the experimental results, the modelling of the finish turning process was performed using DTR, GPR-SE, GPR-Mat and RSM. The maximum percentage errors of the developed models were 3.898 %, 1.192 %, 1.364 % and 0.960 % for DTR, GPR-SE, GPR-Mat and RSM, respectively. In the worst case, the maximum absolute errors were $0.106 \mu\text{m}$, $0.017 \mu\text{m}$, $0.019 \mu\text{m}$, and $0.011 \mu\text{m}$ for DTR, GPR-SE, GPR-Mat, and RSM, respectively. The obtained errors are in the order of tenths and hundredths of micrometers, and in most cases are many times smaller than the allowable processing tolerances in production. Based on the above, all four models can be considered acceptable. Therefore, the developed models can be used in practice as an aid for engineers in selecting the geometrical parameters of the cutting tool during the process planning in order to obtain the required surface roughness.

Future research will focus on studying the influence of various cutting tool geometry factors on surface roughness, inclusion and analysis of other output parameters, and multi-objective optimization of the finish turning process. In addition, future research will consider the other parameters that also affect surface roughness. The integration of a larger number of factors in the model will increase the universality of its application and the accuracy, which is very important in the finish turning, where the influence of all variables is particularly pronounced. One of the future research directions will also be the modelling of surface roughness in finish turning as a function of the geometry of the cutting tool using other methods, as well as the comparison of the results obtained in order to choose the most suitable method for specific machining conditions.

Acknowledgement

This research was funded by the University of Slavonski Brod, Mechanical Engineering Faculty in Slavonski Brod, Republic of Croatia (grant number SV001) and by the Ministry of Education, Science and Technological Development of Republic of Serbia (grant number 451-03-68/2022-14/200156).

References

- [1] Kramar, D., Cica, D. (2021). Modeling and optimization of finish diamond turning of spherical surfaces based on response surface methodology and cuckoo search algorithm, *Advances in Production Engineering & Management*, Vol. 16, No. 3, 326-334, doi: [10.14743/apem2021.3.403](https://doi.org/10.14743/apem2021.3.403).
- [2] Sterpin Valic, G., Cukor, G., Jurkovic, Z., Brezocnik, M. (2019). Multi-criteria optimization of turning of martensitic stainless steel for sustainability, *International Journal of Simulation Modelling*, Vol. 18, No. 4, 632-642, doi: [10.2507/IJSIMM18\(4\)495](https://doi.org/10.2507/IJSIMM18(4)495).
- [3] Ratnam, M.M. (2017). 1.1 Factors affecting surface roughness in finish turning, In: Hashmi, M.S.J. (ed.), *Comprehensive materials finishing*, Elsevier, Oxford, United Kingdom, 1-25, doi: [10.1016/B978-0-12-803581-8.09147-5](https://doi.org/10.1016/B978-0-12-803581-8.09147-5).
- [4] Kang, W.T., Derani, M.N., Ratnam, M.M. (2020). Effect of vibration on surface roughness in finish turning: Simulation study, *International Journal of Simulation Modelling*, Vol. 19, No. 4, 595-606, doi: [10.2507/IJSIMM19-4-531](https://doi.org/10.2507/IJSIMM19-4-531).
- [5] Zerti, O., Yallese, M.A., Khettabi, R., Chaoui, K., Mabrouki, T. (2017). Design optimization for minimum technological parameters when dry turning of AISI D3 steel using Taguchi method, *International Journal of Advanced Manufacturing Technology*, Vol. 89, 1915-1934, doi: [10.1007/s00170-016-9162-7](https://doi.org/10.1007/s00170-016-9162-7).
- [6] Davoudinejad, A., Noordin, M.Y. (2014). Effect of cutting edge preparation on tool performance in hard-turning of DF-3 tool steel with ceramic tools, *Journal of Mechanical Science and Technology*, Vol. 28, 4727-4736, doi: [10.1007/s12206-014-1039-9](https://doi.org/10.1007/s12206-014-1039-9).
- [7] Zhao, T., Zhou, J.M., Bushlya, V., Ståhl, J.E. (2017). Effect of cutting edge radius on surface roughness and tool wear in hard turning of AISI 52100 steel, *International Journal of Advanced Manufacturing Technology*, Vol. 91, 3611-3618, doi: [10.1007/s00170-017-0065-z](https://doi.org/10.1007/s00170-017-0065-z).
- [8] Duc, P.M., Giang, L.H., Dai, M.D., Sy, D.T. (2020). An experimental study on the effect of tool geometry on tool wear and surface roughness in hard turning, *Advances in Mechanical Engineering*, Vol. 12, No. 9, 1-11, doi: [10.1177/1687814020959885](https://doi.org/10.1177/1687814020959885).
- [9] Neşeli, S., Yaldız, S., Türkeş, E. (2011). Optimization of tool geometry parameters for turning operations based on the response surface methodology, *Measurement*, Vol. 44, No. 3, 580-587, doi: [10.1016/j.measurement.2010.11.018](https://doi.org/10.1016/j.measurement.2010.11.018).
- [10] Ashish George, J., Loksha, K. (2019). Optimisation and effect of tool rake and approach angle on surface roughness and cutting tool vibration, *SN Applied Sciences*, Vol. 1, Article No. 1133, doi: [10.1007/s42452-019-1175-z](https://doi.org/10.1007/s42452-019-1175-z).
- [11] Karim, Z., Azuan, S.A.S., Yasir, A. (2013). A study on tool wear and surface finish by applying positive and negative rake angle during machining, *Australian Journal of Basic and Applied Sciences*, Vol. 7, No. 10, 46-51.
- [12] Kumar, S., Singh, D., Kalsi, N.S. (2019). Investigating the effect of approach angle and nose radius on surface quality of Inconel 718, *Journal of The Institution of Engineers (India): Series C*, Vol. 100, 121-128, doi: [10.1007/s40032-017-0411-9](https://doi.org/10.1007/s40032-017-0411-9).
- [13] Cui, X., Guo, J., Zheng, J. (2016). Optimization of geometry parameters for ceramic cutting tools in intermittent turning of hardened steel, *Materials & Design*, Vol. 92, 424-437, doi: [10.1016/j.matdes.2015.12.089](https://doi.org/10.1016/j.matdes.2015.12.089).
- [14] Sung, A.N., Loh, W.P., Ratnam, M.M. (2016). Simulation approach for surface roughness interval prediction in finish turning, *International Journal of Simulation Modelling*, Vol. 15, No. 1, 42-55, doi: [10.2507/IJSIMM15\(1\)4.320](https://doi.org/10.2507/IJSIMM15(1)4.320).
- [15] Ponugoti, U., Dantuluri, R.R., Koka, N.S.S., Bhuvanagiri, R.S. (2020). Experimental investigations on the influence of cutting and tool geometry parameters over the machinability of AISI 52100 steel in hard turning, *International Journal of Modern Manufacturing Technologies*, Vol. 12, No. 1, 144-156.
- [16] Senthilkumar, N., Tamizharasan, T. (2014). Effect of tool geometry in turning AISI 1045 steel: experimental investigation and FEM analysis, *Arabian Journal for Science and Engineering*, Vol. 39, 4963-4975, doi: [10.1007/s13369-014-1054-2](https://doi.org/10.1007/s13369-014-1054-2).
- [17] Tauhiduzzaman, M., Veldhuis, S.C. (2014). Effect of material microstructure and tool geometry on surface generation in single point diamond turning, *Precision Engineering*, Vol. 38, No. 3, 481-491, doi: [10.1016/j.precisioneng.2014.01.002](https://doi.org/10.1016/j.precisioneng.2014.01.002).
- [18] Abainia, S., Ouelaa, N. (2015). Experimental study of the combined influence of the tool geometry parameters on the cutting forces and tool vibrations, *International Journal of Advanced Manufacturing Technology*, Vol. 79, 1127-1138, doi: [10.1007/s00170-015-6885-9](https://doi.org/10.1007/s00170-015-6885-9).
- [19] Mohammad, R., Ariffin, M.K.A.M., Baharuddin, B.T.H.T., Mustapha, F., Aoyama, H. (2017). The effects of single cutting tool geometry on surface roughness, *Journal of Mechanical Engineering*, Vol. 3, No. 1, 45-54.
- [20] Hai, S., Jung, H.-C., Shim, W.-H., Shin, H.-G. (2021). Investigation of surface quality for minor scale diameter of bio-degradable magnesium alloys during the turning process using a different tool nose radius, *Metals*, Vol. 11, No. 8, Article No. 1174, doi: [10.3390/met11081174](https://doi.org/10.3390/met11081174).
- [21] Khellaf, A., Aouici, H., Smaiah, S., Boutabba, S., Yallese, M.A., Elbah, M. (2017). Comparative assessment of two ceramic cutting tools on surface roughness in hard turning of AISI H11 steel: Including 2D and 3D surface topography, *International Journal of Advanced Manufacturing Technology*, Vol. 89, 333-354, doi: [10.1007/s00170-016-9077-3](https://doi.org/10.1007/s00170-016-9077-3).

- [22] Özdemir, M. (2020). Modelling and prediction of effect of machining parameters on surface roughness in turning operations, *Tehnički Vjesnik – Technical Gazette*, Vol. 27, No. 3, 751-760, doi: [10.17559/TV-20190320104114](https://doi.org/10.17559/TV-20190320104114).
- [23] Kuntoğlu, M., Aslan, A., Pimenov, D.Y., Giasin, K., Mikolajczyk, T., Sharma, S. (2020). Modeling of cutting parameters and tool geometry for multi-criteria optimization of surface roughness and vibration via response surface methodology in turning of AISI 5140 steel, *Materials*, Vol. 13, No. 19, Article No. 4242, doi: [10.3390/ma13194242](https://doi.org/10.3390/ma13194242).
- [24] Šarić, T., Vukelić, D., Šimunović, K., Svalina, I., Tadić, B., Prica, M., Šimunović, G. (2020). Modelling and prediction of surface roughness in CNC turning process using neural networks, *Tehnički Vjesnik – Technical Gazette*, Vol. 27, No. 6, 1923-1930, doi: [10.17559/TV-20200818114207](https://doi.org/10.17559/TV-20200818114207).
- [25] Zhang, P., Liu, Z. (2016). Modeling and prediction for 3D surface topography in finish turning with conventional and wiper inserts, *Measurement*, Vol. 94, 37-45, doi: [10.1016/j.measurement.2016.07.080](https://doi.org/10.1016/j.measurement.2016.07.080).
- [26] Benardos, P.G., Vosniakos, G.-C. (2003). Predicting surface roughness in machining: A review, *International Journal of Machine Tools and Manufacture*, Vol. 43, No. 8, 833-844, doi: [10.1016/S0890-6955\(03\)00059-2](https://doi.org/10.1016/S0890-6955(03)00059-2).
- [27] Sousa, V.F.C., Silva, F.J.G. (2020). Recent advances in turning processes using coated tools –A comprehensive review, *Metals*, Vol. 10, No. 2, Article No. 170, doi: [10.3390/met10020170](https://doi.org/10.3390/met10020170).
- [28] Dureja, J.S., Gupta, V.K., Sharma, V.S., Dogra, M., Bhatti, M.S. (2016). A review of empirical modeling techniques to optimize machining parameters for hard turning applications, *Proceedings of the Institution of Mechanical Engineers, Part B: Journal of Engineering Manufacture*, Vol. 230, No. 3, 389-404, doi: [10.1177/0954405414558731](https://doi.org/10.1177/0954405414558731).
- [29] He, C.L., Zong, W.J., Zhang, J.J. (2018). Influencing factors and theoretical modeling methods of surface roughness in turning process: State-of-the-art, *International Journal of Machine Tools and Manufacture*, Vol. 129, 15-26, doi: [10.1016/j.ijmachtools.2018.02.001](https://doi.org/10.1016/j.ijmachtools.2018.02.001).
- [30] Puh, F., Jurkovic, Z., Perinic, M., Brezocnik, M., Buljan, S. (2016). Optimization of machining parameters for turning operation with multiple quality characteristics using Grey relational analysis, *Tehnički Vjesnik – Technical Gazette*, Vol. 23, No. 2, 377-382, doi: [10.17559/TV-20150526131717](https://doi.org/10.17559/TV-20150526131717).
- [31] Trung, D.D., Thinh, H.X. (2021). A multi-criteria decision-making in turning process using the MAIRCA, EAMR, MARCOS and TOPSIS methods: A comparative study, *Advances in Production Engineering & Management*, Vol. 16, No. 4, 443-456, doi: [10.14743/apem2021.4.412](https://doi.org/10.14743/apem2021.4.412).
- [32] Savičević, S., Vukčević, M., Klimentko, S.A., Tanović, L. (2017). Impact of cutting elements on forces and roughness of surface during turning hard steel X160 CrMo V12 with CBN tool, *Tehnički Vjesnik – Technical Gazette*, Vol. 24, No. 4, 1001-1006, doi: [10.17559/TV-20161013100743](https://doi.org/10.17559/TV-20161013100743).
- [33] Ortuño, F.M., Valenzuela, O., Prieto, B., Saez-Lara, M.J., Torres, C., Pomares, H., Rojas, I. (2015). Comparing different machine learning and mathematical regression models to evaluate multiple sequence alignments, *Neurocomputing*, Vol. 164, 123-136, doi: [10.1016/j.neucom.2015.01.080](https://doi.org/10.1016/j.neucom.2015.01.080).
- [34] Breiman, L., Friedman, J., Olshen, R.A., Stone, C.J. (1984). *Classification and regression trees*, First edition, CRC Press, Boca Raton, Florida, USA, doi: [10.1201/9781315139470](https://doi.org/10.1201/9781315139470).
- [35] Rasmussen, C.E., Williams, C.K.I. (2006). *Gaussian processes for machine learning*, MIT Press, Cambridge, United Kingdom, doi: [10.7551/mitpress/3206.001.0001](https://doi.org/10.7551/mitpress/3206.001.0001).

Multi-objective Intuitionistic Fuzzy Linear Programming model for optimization of industrial closed-loop supply chain network

Kousar, S.^a, Batool, M.^a, Kausar, N.^b, Pamucar, D.^c, Ozbilge, E.^{d,*}, Tantay, B.^d

^aInternational Islamic University Islamabad, Department of Mathematics and Statistics, Pakistan

^bYildiz Technical University, Faculty of Arts and Sciences, Department of Mathematics, Istanbul, Turkey

^cUniversity of Belgrade, Faculty of Organizational Sciences, Belgrade, Serbia

^dAmerican University of the Middle East, Department of Mathematics and Statistics, Egaila, Kuwait

ABSTRACT

The urge to remanufacture and address environmental concerns in various industrial processes has drawn the attention of academics as well as practitioners towards Closed-loop Supply Chain Networks (CLSC). Although ever-changing and complex external factors including social and economic ones, adversely impact the sustainable development of closed-loop supply chain networks. The basic aim of the research is to optimize the functioning of CLSC networks. For the above-said, two objective functions are made. The first objective is to minimize the cost of production and assembly expenses of the forward and reverse logistics. Secondly, an endeavour has been made to reduce the fixed costs associated with plants and retailers. For the sake of achieving two objective functions, two methods are employed: triangular fuzzy numbers and triangular intuitionistic fuzzy numbers. Among the two methods, triangular intuitionistic fuzzy numbers achieved the said objectives with greater optimization substantiated by statistics. This method can deal with uncertain external factors without undermining the optimization of the CLSC networks.

ARTICLE INFO

Keywords:

Supply chain;
Closed-loop supply chain;
Multi-objective linear programming;
Modelling;
Optimization;
Fuzzy logic;
Intuitionistic fuzzy numbers

*Corresponding author:

ebru.kahveci@aum.edu.kw
(Ozbilge, E.)

Article history:

Received 7 March 2022

Revised 12 September 2022

Accepted 17 September 2022



Content from this work may be used under the terms of the Creative Commons Attribution 4.0 International Licence (CC BY 4.0). Any further distribution of this work must maintain attribution to the author(s) and the title of the work, journal citation and DOI.

1. Introduction

In human surroundings have a significant impact on daily routines. Environmental policies are associated with sustainable development. Clean environments have positive effects on mental and physical health. Technically and logically, policies are necessary to address environmental challenges. Currently, the reduction of pollution generated by industrial activities is under significant environmental and political pressure [1]. All developed and underdeveloped countries are developing strategies and modifying their plans of action so that their surplus can be recycled. Developing countries face challenges in finding ways out of poverty for their poorest citizens to provide better standards of living for their people. This necessitates providing opportunities for all by increasing industrial output through a series of changes, including the use of by-products

[2]. Most large corporations use their waste materials as raw materials for other processes rather than considering their residues as waste products. Waste management is key in any economy, but as the world shifts toward a more sustainable and circular economy, end-of-life options are being enhanced [3]. The recognition that all wastes are resources and perhaps more appropriately referred to as by-products or non-product outputs is also notable [4].

Excessive return of product flow from consumers to suppliers over a wide range becomes a concern. A supply chain (SC) network is introduced to bring in raw materials and inventory of end products, and transform these materials for the utilisation of retailers. Returns have been viewed as annoyance for manufacturers, suppliers, and distributors. Successful policies and systems for inventory returns result in higher sales, reduced prices, better profitability, and improved consumer service levels [5]. Designing a supply chain network has become a necessity. Owing to government policies and societal appetites for environmental awareness, the supply chain network has acquired enormous importance. With the ongoing pressure to cut prices, environmental issues, high levels of uncertainty, and many other challenges can be successfully controlled by supply chains. The creation of a commodity delivery strategy for supply chain (SC) networks is also a dynamic activity [6]. The primary goal of the supply chain is to reduce costs and improve the efficiency of supply chain enterprises to maximise economic benefits. The traditional supply chain starts with the supplier and ends with users. Closed-loop Supply Chain (CLSC) pattern is divided into two main parts: (a) Forward flow and (b) Reverse Flow.

Integrating forward and reverse logistics delivers strong outcomes such as increasing customer loyalty and boosting revenue through change [7]. Internally, companies analyse logistics services on interest discernment using an appropriate model. Aleksic *et al.* [8] proposed a model which illustrates the failure mode and effects analysis (FMEA) and a case study technique to analyse the productivity of fuzzy logic, and many interdependent challenges related to the reverse supply chain (RSC) were resolved by implementing analysis for long-range production. Many successful organisations have realised that an effective product return strategy significantly enhances costs which is a major aspect of reverse logistics. Reverse logistics covers returns and various other operations pertaining to "backward" products in the supply chain [9]. Many countries have become increasingly aware of the role of handling reverse flows in supply chains along with forward flows. Multi-objective supply chain models are requisite variations of numerous objectives. Optimal supply chain models are essential for the success of industrial network [10]. The stock flow is circular and reversible throughout the closed-loop, and all goods are handled over the entire life cycle [11, 12]. The business environment is continuously changing because the diversification of returned products. This diversification of commodities is related to an increase in operating expenses and a reduction in revenue. Therefore, ensuring the profitability and long-term sustainability of the company, the proper use of returned goods is a key strategic decision [13]. For the competency and proper management of returned products, companies try their best to reduce production costs while keeping customer satisfaction in mind. Sustainable supply chain networks are used to address broad range of economic issues to overcome uncertainty. Fuzzy multi-objective models are ideally suited to solving supply chains [14].

A careful assessment is needed for plants and refurbishing centers that can maintain a CLSC process in a timely manner. Most of the time, supplier strengths and weaknesses vary, which highly affects the closed-loop supply chain process. Many studies on the closed-loop supply chain process have used mathematical programming under uncertain situations owing to societal demands for environmental consciousness [15]. Closed-loop supply chain viability aimed at promoting product circulation flow from production to marketing and then reutilisation and remanufacturing. Duan *et al.* [16] discussed that a large amount of waste material has a considerable impact on production. In pandemic Covid-19 the closed-loop supply chain models lead the entrepreneur to a more valuable and relatively well-balanced economic state. A smooth method of return is better for companies. Thus, returned products are productive for various purposes. In the real world, we deal with vagueness at a certain level, and the uncertainty of the remanufacturing system plays a strategic role in directing a product [17]. Therefore, we deal with such uncertainties using a fuzzy set, which was first introduced by Zadeh [18]. The fuzzy set is defined by the membership degree for all its intactness. The IFS is characterised by a member-

ship function and a non-membership function, such that the sum of both values lies between zero and one. Any model parameter can only be approximately calculated in real-world problems.

Fuzzy models have the ability to model the subjective imagination of a maker as accurately as a decision-maker would describe them. Moreover, fuzzy models help to reduce information costs. The general model for fuzzy linear programming problems includes fuzziness in the coefficients and the accomplishment of the constraints. It is possible to reformulate fuzzy constraints in such a way that they can be solved as a normal linear programming problem. The concept of an intuitionist fuzzy set [19] was explored and introduced in various areas. The intuitionistic fuzzy set/number has also recently been applied in fuzzy optimization, and measures of possibility, precondition, and integrity have a significant role in the optimization of fuzzy theory [20]. Fuzzy linear programming was further examined in decision-making and management problems under uncertain circumstances to obtain an optimal solution [21]. The remaining paper is organised as follows. Section 2 presents all the basic and essential concepts used to develop the optimisation of fuzzy multi-objective linear programming. In Section 3, we formulate the general model of multi-objective fuzzy closed-loop supply chain network, and an interactive fuzzy approach to solve the problem is outlined in Section 4. Finally, concluding remarks and suggestions for further research are presented in Section 5.

2. Preliminaries

2.1 Fuzzy set

According to Zadeh [18], a fuzzy set presents a convenient point for the construction of a logical framework which might be parallel with respect to an ordinary set. In particular, the fuzzy framework provides a natural way to deal with uncertain situations. A fuzzy set μ of X is a function of X in the interval $[0,1]$, that is, for each $x \in X$, $\mu(x)$ is a real number ranging between 0 and 1. Function $\mu(x)$ is a membership function. Mathematically, the fuzzy subset μ of X is expressed as $\mu = \{(x, \mu(x)) : x \in X\}$.

2.2 Triangular fuzzy number

The fuzzy number is a function in which the domain is any specified set, and whose range is the real number lies between 0 and 1, both inclusive. Generally, a triangular fuzzy number [22] is expressed as $TF_{\mu} = (q_1, q_2, q_3)$ with the respective membership function defined as

$$\mu(x) = \begin{cases} \frac{x-q_1}{q_2-q_1} & q_1 \leq x < q_2 \\ 1, & x = q_2 \\ \frac{q_3-x}{q_3-q_2} & q_2 < x \leq q_3 \\ 0, & \text{otherwise.} \end{cases} \quad (1)$$

2.3 Intuitionistic fuzzy set

An intuitionistic fuzzy set [19] (IFS) \mathcal{N} of X can be described in set form as $\mathcal{N} = \{(x, \mu_{\mathcal{N}}(x), \nu_{\mathcal{N}}(x)) : x \in X\}$ where the functions: $\mu_{\mathcal{N}}: X \rightarrow [0,1]$ and $\nu_{\mathcal{N}}: X \rightarrow [0,1]$ represents the degrees of membership and non-membership of each $x \in X$ respectively with

$$0 \leq \mu_{\mathcal{N}}(x) + \nu_{\mathcal{N}}(x) \leq 1.$$

2.4 Triangular intuitionistic fuzzy number

A triangular intuitionistic fuzzy number (TrIFN) [23] \tilde{X}^I is a pair of triplets written as $(x_1, x_2, x_3; x'_1, x'_2, x'_3)$ where $x'_1 \leq x_1 \leq x_2 = x'_2 \leq x_3 \leq x'_3$ having membership and non-membership functions in the following manner:

$$\mu_{\tilde{X}^I}(x) = \begin{cases} \frac{x-x_1}{x_2-x_1} & , x_1 \leq x \leq x_2 \\ 1 & , x = x_2 \\ \frac{x_3-x}{x_3-x_2} & , x_2 \leq x \leq x_3 \\ 0 & , \text{otherwise} \end{cases} \quad \nu_{\tilde{X}^I}(x) = \begin{cases} \frac{x_2-x}{x_2-x_1} & , x_1' \leq x \leq x_2 \\ 0 & , x = x_2 \\ \frac{x-x_2}{x_3'-x_2} & , x_2 \leq x \leq x_3' \\ 1 & , \text{otherwise} \end{cases} \quad (2)$$

As $x_2 = x_2'$ so we can write TrIFN $(x_1, x_2, x_3; x_1', x_2', x_3')$ as $(x_1, x_2, x_3; x_1', x_3')$.

Arithmetic operations on TrIFN

Similar to numbers, several antiemetic operations can be defined on the TrIFNs [24]. Let $\tilde{X}^I = (x_1, x_2, x_3; x_1', x_3')$ and $\tilde{Y}^I = (y_1, y_2, y_3; y_1', y_3')$ be any two TrIFNs and k be a real number. Then

1. $\tilde{X}^I + \tilde{Y}^I = (x_1 + y_1, x_2 + y_2, x_3 + y_3; x_1' + y_1', x_3' + y_3')$.
2. $\tilde{X}^I - \tilde{Y}^I = (x_1 - y_3, x_2 - y_2, x_3 - y_1; x_1' - y_3', x_3' - y_1')$.
3. $k \cdot \tilde{X}^I = k \cdot (x_1, x_2, x_3; x_1', x_3') = (kx_1, kx_2, kx_3; kx_1', kx_3')$ if $k \geq 0$.
4. $k \cdot \tilde{X}^I = k \cdot (x_1, x_2, x_3; x_1', x_3') = (kx_3, kx_2, kx_1; kx_3', kx_1')$ if $k < 0$.
5. $\tilde{X}^I \times \tilde{Y}^I = (x_1y_1, x_2y_2, x_3y_3; x_1'y_1', x_3'y_3')$.

2.5 Linear programming

Linear programming problems [25] include the optimization of real-world problems, in which the quantity of the objective function must be maximized or minimized with some constraints. Constraints are linear equalities or inequalities. It consists of the following parts.

- Decision variables set X ;
- Objective Function: A linear function $f(x)$ is maximized(minimized);
- Constraints: $g_i(x) \leq b_i$.

2.6 Multi-objective linear programming

In multi-objective linear programming [26], we have variations in the objective function as well as in the constraints. The mathematical representation of multi-objective linear programming is as follows:

Maximize

$$f_s(x) = a_{s1} \cdot x_1 + a_{s2} \cdot x_2 + \dots + a_{sn} \cdot x_n \text{ for all } s.$$

such that

$$a_{t1} \cdot x_1 + a_{t2} \cdot x_2 + \dots + a_{tn} \cdot x_n \geq b_t$$

In general, there is no single point $(x) = (x_1, x_2, \dots, x_n)$ which optimizes each objective function individually. Many real-world problems can be modelled as multi-objective linear programming problems. A linear program with more than one objective function is known as a multi-objective linear program (MOLP).

2.7 Fuzzy linear programming

Fuzzy linear programming [27] represented as:

$$\begin{aligned} & \text{Max} \quad \tilde{Z} \cdot x \\ \text{subject to} \quad & \sum_{j=1}^n \tilde{X}_{ij} \cdot x_j \geq \tilde{Y}_i, \quad i = 1, 2, \dots, m \\ & x_j \geq 0, \quad j = 1, 2, \dots, n \end{aligned} \quad (3)$$

where X_{ij} are decision variables in the constraints and x_j are non-negative fuzzy numbers. Fuzzy linear programming problems with decision variables and parameters play an important role in several applications in different areas, such as mathematical modelling, manufacturing and production, environment management, supply chain management, and transportation management. In fuzzy linear programming, fuzziness considers either the objective function or the constraint equations.

2.8 Linear programming with triangular intuitionistic fuzzy number

The linear programming model with triangular intuitionistic fuzzy numbers [21] can be expressed as

$$\begin{aligned} & \text{Minimize} && \sum_{j=1}^n \tilde{Z}_j^l \cdot x_j \\ \text{subject to} &&& \sum_{j=1}^n \tilde{X}_{ij}^l \cdot x_j \geq \tilde{Y}_i^l, \quad i = 1, 2, \dots, m \\ &&& x_j \geq 0, \quad j = 1, 2, \dots, n \end{aligned} \tag{4}$$

where, $\tilde{Z}_j^l = (z_{j,1}, z_{j,2}, z_{j,3}; z'_{j,1}, z'_{j,2}, z'_{j,3})$, $\tilde{Y}_i^l = (y_{i,1}, y_{i,2}, y_{i,3}; y'_{i,1}, y'_{i,2}, y'_{i,3})$ and $\tilde{X}_{ij}^l = (X_{ij,1}, X_{ij,2}, X_{ij,3}; X'_{ij,1}, X'_{ij,2}, X'_{ij,3})$; $i = 1, 2, \dots, m$ and $j = 1, 2, \dots, n$ are TrIFN'S.

3. Model formulation

In a closed-loop supply chain network problem, our main purpose is to minimize overall costs, distribution time, or maximize profit; in general, objectives are usually uncertain due to unpredictable conditions in an evolving environment. In the proposed model, we first consider the raw materials and collect the initial parts. Suppliers send raw materials to the plants; in plants, the number of machines is working for proceeding with the products. These raw forms were further transformed into their final shapes. Retailers rack up commodities from plants and delivered them to customers. Collection centers collect customer previously purchased merchandise and returned goods. Further dispatch of these products to the disassembly center. The model is formulated as follows: after inspection, the reusable and manufacturable products are processed into refurbishing centers, and useless products of bad quality are disposed of. Refurbishing centers sent used parts to the plants to be used in the next period. Consequently, the CLSC problem was contrived, as shown in Fig. 1. The time and cost can be reduced by reducing the overall emissions. End-of-life vehicle (ELV) treatment is an example of a CLSC. Most European countries have had an existing ELV recycling system for decades. Parts of vehicles that are expected to have high re-sale value are first disassembled, and collection centers collect some parts in car accident and others from customers. Metal recycling and other components provide valuable product recovery which fulfils recycling targets at minimal cost [28]. Fig. 1 depicts the closed-loop supply chain network, forward flow from suppliers to plants, plants to retailers, and retailers to customers, and backward flow from customer to collection center, collection center to plant, collection center to disassembly center, disassembly center to refurbishing center, and refurbishing center to plant.

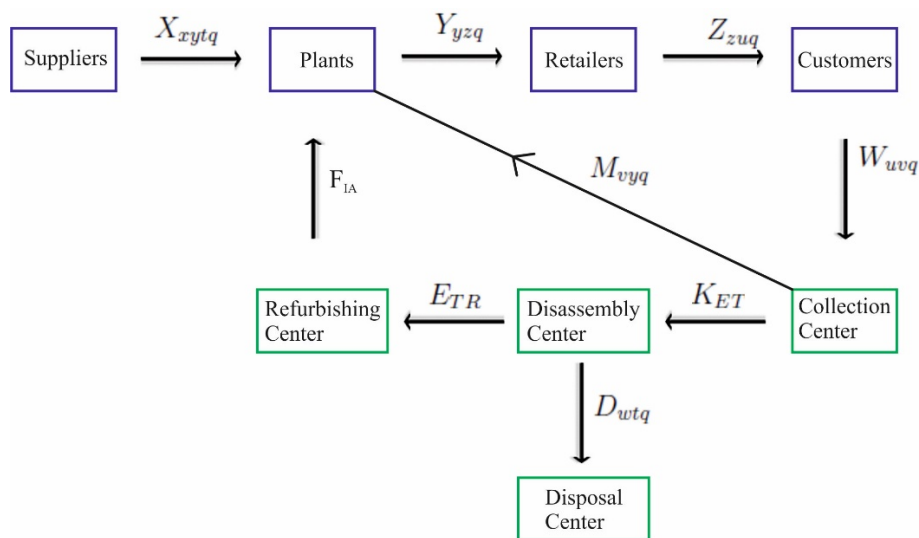


Fig. 1 Closed-loop supply chain network

Index sets

x	suppliers
y	plants
z	retailers
u	customers
v	collection centers
w	disassembly centers
h	refurbishing centers
t	number of parts
q	number of periods

Decision variables

X_{xytq}	supplier x shipped amount to plant y for part t in period q
Y_{yzq}	plant y shipped amount to retailer z for part t in period q
Z_{zuq}	retailer z shipped amount to customer u for part t in period q
W_{uvq}	customer u shipped amount to collection center v for part t in period q
M_{vyq}	collection center v shipped amount to plant y for part t in period q
K_{ET}	collection center v shipped amount to disassembly center w for part t in period q
D_{wtq}	disassembly center w shipped amount to disposal for part t in period q
E_{TR}	disassembly center w shipped amount to refurbishing center h for t in period q
F_{IA}	refurbishing center h shipped amount to plant y for part t in period q
A_{yq}	if plant y is open ,1 ; else 0.
B_{zq}	if retailer z is open ,1 ; else 0.

Parameters

\tilde{l}_{xtq}	fuzzy capacity in supplier x for part t in period q (ton)
\tilde{m}_{yq}	fuzzy capacity in plant y in period q (ton)
\tilde{n}_{zq}	fuzzy capacity in retailer z in period q (ton)
\tilde{p}_{vq}	fuzzy capacity in collection center v in period q (ton)
\tilde{q}_{wtq}	fuzzy capacity in disassembly center w for part t for period q (ton)
\tilde{r}_{htq}	fuzzy capacity in refurbishing center h for part t for period q (ton)
\tilde{o}_{uq}	fuzzy demand of customer u for period q
\tilde{A}_q	maximum availability in plants for period q
\tilde{B}_q	maximum availability in retailers for period q
t	unit cost of shipping
n_t	number of parts for the part t from disassembling one unit of product
l_{xt}	unit cost of purchasing of supplier x for part t
m_{ht}	unit cost of refurbishing of refurbishing center h for part t
μ_{yq}	fixed opening cost for plant y in period q
ν_{zq}	fixed opening cost for retailer z in period q
$\tilde{\alpha}$	demand of fuzzy percentage that is composed by collection centers.
$\tilde{\beta}$	fuzzy percentage for collection of amount that is resent to plants
$\tilde{\theta}$	fuzzy percentage for disassembled amount that is disposed

Distances

d_{xy}	distance in the supplier x to plant y (kilometer)
d_{yz}	distance in the plant y to retailer z (kilometer)
d_{zu}	distance in the retailer z to customer u (kilometer)
d_{uv}	distance in the customer u to collection center v (kilometer)
d_{vy}	distance in the collection center v and plant y (kilometer)
d_{vw}	distance in the collection center v and disassembly center w (kilometer)
d_{wh}	distance in disassembly center w to refurbishing center h (kilometer)
d_{hy}	distance in the refurbishing center h to plant y (kilometer)
d_{sp}	distance between disassembly center w and disposal

3.1 Objective functions

Our main objectives are to minimize the total costs. The first objective is to minimize the cost of production and assembly expenses for forward and reverse logistics, including transport system, buying, and renovation costs. The second goal is to reduce the fixed costs associated with the plants and retailers.

$$\begin{aligned}
 z_1 \cong & t \left(\sum_x \sum_y \sum_t \sum_q \tilde{X}_{xytq}^I \cdot ds_{xy} + \sum_y \sum_z \sum_q \tilde{Y}_{yzq}^I \cdot ds_{yz} + \sum_z \sum_u \sum_q \tilde{Z}_{zuq}^I \cdot ds_{zu} \right. \\
 & + \sum_u \sum_v \sum_q \tilde{W}_{uvq}^I \cdot ds_{uv} + \sum_v \sum_y \sum_q \tilde{M}_{vyq}^I \cdot ds_{vy} + \sum_v \sum_w \sum_q \tilde{K}_{vwq}^I \cdot ds_{vw} \\
 & + \sum_w \sum_t \sum_q \tilde{D}_{wtq}^I \cdot ds_p + \sum_w \sum_h \sum_t \sum_q \tilde{E}_{whtq}^I \cdot ds_{wh} + \sum_h \sum_y \sum_t \sum_q \tilde{F}_{hytq}^I \cdot ds_{hy} \\
 & \left. + \sum_x \sum_y \sum_t \sum_q \tilde{X}_{xytq}^I \cdot l_{xt} + \sum_h \sum_y \sum_t \sum_q \tilde{F}_{hytq}^I \cdot m_{ht} \right) \tag{5}
 \end{aligned}$$

$$z_2 \cong \sum_y \sum_q \tilde{A}_{yq}^I \cdot \mu_{yq} + \sum_z \sum_q \tilde{B}_{zq}^I \cdot \nu_{zq} \tag{6}$$

3.2 Constraints

Supplier constraints

The shipped amount of plant y to supplier x in part t for q is less than or equal to the fuzzy space of supplier x in part t for period q . The supplier constraints converted into fuzzy triangular intuitionistic numbers (see Eq. 7) show that the supplier shipped amount is less than the fuzzy supplier capacities.

$$\begin{aligned}
 \sum_x X_{xytq,1} &\leq \tilde{l}_{xtq,1}, & \sum_x X_{xytq,2} &\leq \tilde{l}_{xtq,2} \\
 \sum_x X_{xytq,3} &\leq \tilde{l}_{xtq,3}, & \sum_x X'_{xytq,1} &\leq \tilde{l}'_{xtq,1} \\
 \sum_x X'_{xytq,2} &\leq \tilde{l}'_{xtq,2}, & \sum_x X'_{xytq,3} &\leq \tilde{l}'_{xtq,3}
 \end{aligned} \tag{7}$$

Plant constraints:

The shipped amount of retailer z to plant y in period q is less than or equal to the fuzzy capacity of plant y in period q (ton). The plant constraints converted into fuzzy triangular intuitionistic numbers (see Eq. 8) show that the shipped amount to the retailer is less than the fuzzy plant capacities.

$$\begin{aligned}
 \sum_z Y_{yzq,1} &\leq \tilde{m}_{yq,1} \cdot A_{yq,1}, & \sum_z Y_{yzq,2} &\leq \tilde{m}_{yq,2} \cdot A_{yq,2} \\
 \sum_z Y_{yzq,3} &\leq \tilde{m}_{yq,3} \cdot A_{yq,3}, & \sum_z Y'_{yzq,1} &\leq \tilde{m}'_{yq,1} \cdot A_{yq,1} \\
 \sum_z Y'_{yzq,2} &\leq \tilde{m}'_{yq,2} \cdot A_{yq,2}, & \sum_z Y'_{yzq,3} &\leq \tilde{m}'_{yq,3} \cdot A_{yq,3}
 \end{aligned} \tag{8}$$

Retailer constraints

The shipped amount of customer u to retailer z in period q is less than or equal to the fuzzy space of retailer z for period q . The retailer constraints converted into fuzzy triangular intuitionistic numbers (see Eq. 9) show that the shipped amount to the customer is less than the fuzzy retailer capacities.

$$\begin{aligned}
 \sum_u Z_{zuq,1} &\leq \tilde{n}_{zq,1} \cdot B_{zq,1}, & \sum_u Z_{zuq,2} &\leq \tilde{n}_{zq,2} \cdot B_{zq,2} \\
 \sum_u Z_{zuq,3} &\leq \tilde{n}_{zq,3} \cdot B_{zq,3}, & \sum_u Z'_{zuq,1} &\leq \tilde{n}'_{zq,1} \cdot B_{zq,1} \\
 \sum_u Z'_{zuq,2} &\leq \tilde{n}'_{zq,2} \cdot B_{zq,2}, & \sum_u Z'_{zuq,3} &\leq \tilde{n}'_{zq,3} \cdot B_{zq,3}
 \end{aligned} \tag{9}$$

Collection center

The shipped amount of plant y and disassembly center w to collection center v for period q is less than or equal to the fuzzy space of collection center v for period q . The collection center constraints converted into fuzzy triangular intuitionistic numbers (see Eq. 10) show that the shipped amount to the plant and disassembly center is less than the fuzzy capacities of the collection center.

$$\begin{aligned}
 \sum_y M_{vyq,1} + \sum_w K_{vwq,1} &\leq \tilde{P}_{vq,1}, \quad \sum_y M_{vyq,2} + \sum_w K_{vwq,2} \leq \tilde{P}_{vq,2} \\
 \sum_y M_{vyq,3} + \sum_w K_{vwq,3} &\leq \tilde{P}_{vq,3}, \quad \sum_y M'_{vyq,1} + \sum_w K_{vwq,1} \leq \tilde{P}'_{vq,1} \\
 \sum_y M'_{vyq,2} + \sum_w K_{vwq,2} &\leq \tilde{P}'_{vq,2}, \quad \sum_y M'_{vyq,3} + \sum_w K_{vwq,3} \leq \tilde{P}'_{vq,3}
 \end{aligned}
 \tag{10}$$

Disassembly center

The shipped amount disposal p to disassembly center w and refurbishing center h of part t for period q is less than or equal to the fuzzy space for disassembly center w of part t in period q . The disassembly center constraints converted into fuzzy triangular intuitionistic numbers (see Eq. 11) show that the shipped amount to the disposal and refurbishing center is less than the fuzzy capacities of disassembly center.

$$\begin{aligned}
 D_{wtq,1} + \sum_h E_{whtq,1} &\leq \tilde{q}_{wtq,1}, \quad D_{wtq,2} + \sum_h E_{whtq,2} \leq \tilde{q}_{wtq,2} \\
 D_{wtq,3} + \sum_h E_{whtq,3} &\leq \tilde{q}_{wtq,3}, \quad D'_{wtq,1} + \sum_h E'_{whtq,1} \leq \tilde{q}'_{wtq,1} \\
 D'_{wtq,2} + \sum_h E'_{whtq,2} &\leq \tilde{q}'_{wtq,2}, \quad D'_{wtq,3} + \sum_h E'_{whtq,3} \leq \tilde{q}'_{wtq,3}
 \end{aligned}
 \tag{11}$$

Refurbishing center

The shipped amount of plant y to refurbishing center h of part t for period q is less than or equal to the fuzzy capacity of refurbishing center h of part t for period q . The refurbishing center constraints converted into fuzzy triangular intuitionistic numbers (see Eq. 12) shows the shipped amount to the plant is less than the fuzzy capacities of the refurbishing center.

$$\begin{aligned}
 \sum_y F_{hytq,1} &\leq \tilde{r}_{htq,1}, \quad \sum_y F_{hytq,2} \leq \tilde{r}_{htq,2} \\
 \sum_y F_{hytq,3} &\leq \tilde{r}_{htq,3}, \quad \sum_y F'_{hytq,1} \leq \tilde{r}'_{htq,1} \\
 \sum_y F'_{hytq,2} &\leq \tilde{r}'_{htq,2}, \quad \sum_y F'_{hytq,3} \leq \tilde{r}'_{htq,3}
 \end{aligned}
 \tag{12}$$

Retailers

The shipped quantity of customer u to retailers z for period q is greater than or equal to the fuzzy demand for customer u of period q . The retailer constraints converted into fuzzy triangular intuitionistic numbers (see Eq. 13) show that the shipped quantity from the retailer is greater than the fuzzy customer demand.

$$\begin{aligned}
 \sum_z Z_{zuq,1} &\geq \tilde{O}_{uq,1}, \quad \sum_z Z_{zuq,2} \geq \tilde{O}_{uq,2} \\
 \sum_z Z_{zuq,3} &\geq \tilde{O}_{uq,3}, \quad \sum_z Z'_{zuq,1} \geq \tilde{O}'_{uq,1} \\
 \sum_z Z'_{zuq,2} &\geq \tilde{O}'_{uq,2}, \quad \sum_z Z'_{zuq,3} \geq \tilde{O}'_{uq,3}
 \end{aligned}
 \tag{13}$$

Plant opening constraints

If plant y is open during period q the value is 1; otherwise, 0 is less than or equal to the maximum available set of plants for period q (see Eq. 14).

$$\begin{aligned}
 \sum_y H_{yq,1} &\leq \tilde{A}_{q,1}, \quad \sum_y H_{yq,2} \leq \tilde{A}_{q,2} \\
 \sum_y H_{yq,3} &\leq \tilde{A}_{q,3}, \quad \sum_y H'_{yq,1} \leq \tilde{A}'_{q,1} \\
 \sum_y H'_{yq,2} &\leq \tilde{A}'_{q,2}, \quad \sum_y H'_{yq,3} \leq \tilde{A}'_{q,3}
 \end{aligned}
 \tag{14}$$

Retailer opening constraints

If retailer z is open during period q the value is 1; otherwise, 0 is less than or equal to the maximum available set of retailers z for period q (see Eq. 15).

$$\begin{aligned}
 \sum_z Z_{zq,1} &\leq \tilde{B}_{q,1}, \quad \sum_z Z_{zq,2} \leq \tilde{B}_{q,2} \\
 \sum_z Z_{zq,3} &\leq \tilde{B}_{q,3}, \quad \sum_z Z'_{zq,1} \leq \tilde{B}'_{q,1} \\
 \sum_z Z'_{zq,2} &\leq \tilde{B}'_{q,2}, \quad \sum_z Z'_{zq,3} \leq \tilde{B}'_{q,3}
 \end{aligned}
 \tag{15}$$

Balance equations

Balance equations (see Eqs. 16 to 61) show that the shipped amounts that enter these capacities must be equal to the number of products that leave the places for forward and reverse flow, and Eq. 62 incites the non-negativity of the decision variables.

$$\begin{aligned}
 \sum_x X_{xytq,1} + \sum_n F_{hyt(q-1),1} + n_t \sum_v M_{vy(q-1),1} - n_t \sum_z Y_{yzq,1} &= 0 \tag{16} \\
 \sum_x X_{xytq,2} + \sum_n F_{hyt(q-1),2} + n_t \sum_v M_{vy(q-1),2} - n_t \sum_z Y_{yzq,2} &= 0 \tag{17}
 \end{aligned}$$

$$\sum_x X_{xytq,3} + \sum_n F_{hyt(q-1),3} + n_t \sum_v M_{vy(q-1),3} - n_t \sum_z Y_{yzq,3} = 0 \tag{18}$$

$$\sum_x X_{xytq,1} + \sum_n F_{hyt(q-1),1} + n_t \sum_v M_{vy(q-1),1} - n_t \sum_z Y_{yzq,1} = 0 \tag{19}$$

$$\sum_x X_{xytq,2} + \sum_n F_{hyt(q-1),2} + n_t \sum_v M_{vy(q-1),2} - n_t \sum_z Y_{yzq,2} = 0 \tag{20}$$

$$\sum_x X_{xytq,3} + \sum_n F_{hyt(q-1),3} + n_t \sum_v M_{vy(q-1),3} - n_t \sum_z Y_{yzq,3} = 0 \tag{21}$$

$$\sum_y Y_{yzq,1} - \sum_u Z_{zuq,1} = 0, \quad \sum_y Y_{yzq,2} - \sum_u Z_{zuq,2} = 0 \tag{22}$$

$$\sum_y Y_{yzq,3} - \sum_u Z_{zuq,3} = 0, \quad \sum_y Y'_{yzq,1} - \sum_u Z'_{zuq,1} = 0 \tag{23}$$

$$\sum_y Y'_{yzq,2} - \sum_u Z'_{zuq,2} = 0 \tag{24}$$

$$\sum_y Y'_{yzq,3} - \sum_u Z'_{zuq,3} = 0 \tag{25}$$

$$\tilde{\alpha} \sum_z Z_{zuq,1} - \sum_v W_{uvq,1} = 0 \tag{26}$$

$$\tilde{\alpha} \sum_z Z_{zuq,2} - \sum_v W_{uvq,2} = 0 \tag{27}$$

$$\tilde{\alpha} \sum_z Z_{zuq,3} - \sum_v W_{uvq,3} = 0 \tag{28}$$

$$\tilde{\alpha} \sum_z Z'_{zuq,1} - \sum_v W'_{uvq,1} = 0 \tag{29}$$

$$\tilde{\alpha} \sum_z Z'_{zuq,2} - \sum_v W'_{uvq,2} = 0 \tag{30}$$

$$\tilde{\alpha} \sum_z Z'_{zuq,3} - \sum_v W'_{uvq,3} = 0 \tag{31}$$

$$\tilde{\beta} \sum_u W_{uvq,1} - \sum_y M_{vyq,1} = 0 \tag{32}$$

$$\tilde{\beta} \sum_u W_{uvq,2} - \sum_y M_{vyq,2} = 0 \tag{33}$$

$$\tilde{\beta} \sum_u W_{uvq,3} - \sum_y M_{vyq,3} = 0 \tag{34}$$

$$\tilde{\beta} \sum_u W'_{uvq,1} - \sum_y M'_{vyq,1} = 0 \tag{35}$$

$$\tilde{\beta} \sum_u W'_{uvq,2} - \sum_y M'_{vyq,2} = 0 \tag{36}$$

$$\tilde{\beta} \sum_u W'_{uvq,3} - \sum_y M'_{vyq,3} = 0 \tag{37}$$

$$(1 - \tilde{\beta}) \sum_u W_{uvq,1} - \sum_w K_{vwq,1} = 0 \tag{38}$$

$$(1 - \tilde{\beta}) \sum_u W_{uvq,2} - \sum_w K_{vwq,2} = 0 \tag{39}$$

$$(1 - \tilde{\beta}) \sum_u W_{uvq,3} - \sum_w K_{vwq,3} = 0 \tag{40}$$

$$(1 - \tilde{\beta}) \sum_u W'_{uvq,1} - \sum_w K'_{vwq,1} = 0 \tag{41}$$

$$(1 - \tilde{\beta}) \sum_u W'_{uvq,2} - \sum_w K'_{vwq,2} = 0 \tag{42}$$

$$(1 - \tilde{\beta}) \sum_u W'_{uvq,3} - \sum_w K'_{vwq,3} = 0 \tag{43}$$

$$n_t(\tilde{\theta}) \sum_v K_{vwq,1} - D_{wtq,1} = 0 \tag{44}$$

$$n_t(\tilde{\theta}) \sum_v K_{vwq,2} - D_{wtq,2} = 0 \tag{45}$$

$$n_t(\tilde{\theta}) \sum_v K_{vwq,3} - D_{wtq,3} = 0 \tag{46}$$

$$n_t(\tilde{\theta}) \sum_v K'_{vwq,1} - D'_{wtq,1} = 0 \tag{47}$$

$$n_t(\tilde{\theta}) \sum_v K'_{vwq,2} - D'_{wtq,2} = 0 \tag{48}$$

$$n_t(\tilde{\theta}) \sum_v K'_{vwq,3} - D'_{wtq,3} = 0 \tag{49}$$

$$n_t(1 - \tilde{\theta}) \sum_v K_{vwq,1} - \sum_h E_{wtq,1} = 0 \tag{50}$$

$$n_t(1 - \tilde{\theta}) \sum_v K_{vwq,2} - \sum_h E_{wtq,2} = 0 \tag{51}$$

$$n_t(1 - \tilde{\theta}) \sum_v K_{vwq,3} - \sum_h E_{wtq,3} = 0 \tag{52}$$

$$n_t(1 - \tilde{\theta}) \sum_v K'_{vwq,1} - \sum_h E'_{wtq,1} = 0 \tag{53}$$

$$n_t(1 - \tilde{\theta}) \sum_v K'_{vwq,2} - \sum_h E'_{wtq,2} = 0 \tag{54}$$

$$n_t(1 - \tilde{\theta}) \sum_v K'_{vwq,3} - \sum_h E'_{wtq,3} = 0 \tag{55}$$

$$\sum_w E_{whtq,1} - \sum_y F_{hytq,1} = 0 \tag{56}$$

$$\sum_w E_{whtq,2} - \sum_y F_{hytq,2} = 0 \tag{57}$$

$$\sum_w E_{whtq,3} - \sum_y F_{hytq,3} = 0 \tag{58}$$

$$\sum_w E'_{whtq,1} - \sum_y F'_{hytq,1} = 0 \tag{59}$$

$$\sum_w E'_{whtq,2} - \sum_y F'_{hytq,2} = 0 \tag{60}$$

$$\sum_w E'_{whtq,3} - \sum_y F'_{hytq,3} = 0 \tag{61}$$

$$X_{xytq}, Y_{yzq}, Z_{zuq}, W_{uvq}, M_{vyq}, K_{vwq}, D_{wtq}, E_{whtq}, F_{hytq} \geq 0. \tag{62}$$

Binary variables

If plant y and retailer z in period q are open 1, then the binary variables \tilde{A}_{yq}^I and \tilde{B}_{zq}^I are 1; otherwise 0.

4. Application: Results and discussion

Closed-loop supply chain networks are primarily expressed as forward and reverse logistics. In this study the forward flow of the industrial CLSC contains five suppliers, four plants, four retailers, and five customers, as shown in Fig. 2. It is assumed that each supplier has three different components for the six periods, and each component has different rates depending upon its quality and demand.

In this study, reverse flow incorporates two collection centers which collect used products from customers. Two disassembly centers assemble the returned products, whether they are further recycled. If the product cannot be recycled, it is sent to one disposal center to be discarded, and the remaining items are further forwarded into two refurbishing centers, as shown in reverse logistic Fig. 3.

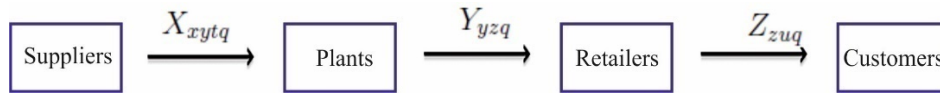


Fig. 2 Forward flow in closed-loop supply chain network

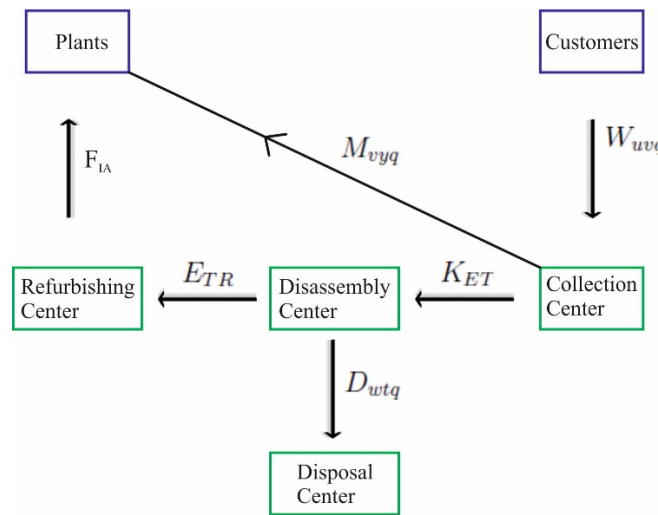


Fig. 3 Reverse flow in closed-loop supply chain network

Transportation cost t per unit is taken as 4.21 USD of one tonne goods over a distance of one kilometer for general loading vehicle. Purchasing and refurbishing unit costs named as l_{xt} and m_{ht} for all the three components are set as 15 USD per ton and 10 USD per ton respectively. Fixed cost for each plant μ_{yq} and retailer ν_{zq} taken as 500 USD and 300 USD respectively for all the six periods. Maximum available plants A_{yq} and retailers B_{zq} both are four. The multi objective closed-loop supply chain model is used for transportation plan to control the expenses and maximize the profit. For optimising the model in fuzzy scenario, we apply the hypothetical values in proposed model in Section 3. The proposed model of closed-loop supply chain centralizes the envision to minimize total and fixed distribution cost on available capacities.

Now we generate some scenarios to get the optimum result. Consider the hypothetical values for amount shipped from one stage to the next and capacities according to the storage of products. Firstly, convert the data into triangular intuitionistic fuzzy numbers to maximize the profit in industrial closed-loop supply chain. Maximization of profit by using triangular intuitionistic fuzzy numbers is highly dependent upon the constraints and objective function. In this research we convert our constraints into fuzzy constraint by using weighted average method which minimize the total and fixed cost. For instance, the supplier constraints in Eq. 7 are modified as:

$$\begin{aligned}
 \sum_x X_{xytq,1} &\leq w_1 \cdot \tilde{l}_{xtq,1}, & \sum_x X_{xytq,2} &\leq w_2 \cdot \tilde{l}_{xtq,2} \\
 \sum_x X_{xytq,3} &\leq w_3 \cdot \tilde{l}_{xtq,3}, & \sum_x X'_{xytq,1} &\leq w_4 \cdot \tilde{l}'_{xtq,1} \\
 \sum_x X'_{xytq,2} &\leq w_5 \cdot \tilde{l}'_{xtq,2}, & \sum_x X'_{xytq,3} &\leq w_6 \cdot \tilde{l}'_{xtq,3}
 \end{aligned}
 \tag{63}$$

where $w_1 = 0.16, w_2 = 0.18, w_3 = 0.16, w_4 = 0.16, w_5 = 0.18, w_6 = 0.16$ with $w_1 + w_2 + w_3 + w_4 + w_5 + w_6 = 1$. For the application of presented model hypothetical numeric values are taken in Tables 1-5. The Table 4 and 5 shows the converted values in triangular intuitionistic fuzzy number by weighted sum method which provides the significant finding. Due to recognition of ecological challenges, authorizing legislation closed-loop supply chain is highly adoptable for industrial production. However, results from complex projects show that the proposed model can find an effective, adaptable, and suitable method for industrial closed-loop supply chain network. The formulated problem is solved through MATLAB2018a fuzzy technique gives the optimality result of total cost 2020800, in which the fuzziness and ambiguity of data is absorbed by using triangular fuzzy number. Second scenario generated by using triangular intuitionistic fuzzy concept and the modelling yields more accurate and flexible result 1012400, which depicts the cost is minimized with the noticeable difference of 1008400. Therefore, the triangular intuitionistic method is much appropriate for given closed-loop supply chain problem.

Table 1 Distance from suppliers to plants, plants to retailers and collection centers in km

Stages	Plant 1	Plant 2
1st supplier	150	200
2nd supplier	150	150
3rd supplier	160	110
1st Retailer	80	90
2nd Retailer	150	100
3rd Retailer	70	90
1st collection center	40	55
2nd collection center	70	50
3rd collection center	50	70

Table 2 Distance from retailers to customers and customers to collection centers in km

Stage	Customer A	Customer B	Customer C	Customer D
1st Retailer	100	60	150	80
2nd Retailer	150	90	90	60
3rd Retailer	100	80	80	30
1st collection center	150	60	30	90
2nd collection center	70	50	35	80
3rd collection center	30	80	40	50

Table 3 Distance from collection centers to disassembly centers and disassembly centers to refurbishing centers in km

Disassembly center	Collection center 1	Collection center 2	Collection center 3	Disposal	Refurbishing center 1	Refurbishing center 2	Refurbishing center 3
1	90	60	50	70	40	70	50
2	100	95	30	50	50	60	90
3	150	80	40	80	40	30	70

Table 4 Triangular intuitionistic fuzzy supplier capacity

Supplier	a_1	a_2	a_3	a'_1	a'_3	a_1	a_2	a_3	a'_1	a'_3	a_1	a_2	a_3	a'_1	a'_3	a_1	a_2	a_3	a'_1	a'_3	a_1	a_2	a_3	a'_1	a'_3					
	Period 1					Period 2					Period 3					Period 4					Period 5					Period 6				
Component 1																														
1	90	110	120	80	150	160	170	180	150	200	240	250	260	210	270	130	140	160	110	180	100	130	150	80	180	160	180	200	130	210
2	70	80	90	60	100	180	200	210	160	230	220	230	240	200	250	60	90	130	40	150	120	140	180	100	200	220	230	240	200	250
3	70	75	80	60	90	170	180	200	140	210	210	230	240	180	300	60	70	100	30	110	90	100	120	70	150	210	200	220	180	240
Component 2																														
1	160	180	190	140	210	250	210	280	210	300	280	290	300	270	310	110	130	150	100	170	200	220	250	190	270	210	230	240	200	280
2	150	170	180	90	200	210	220	230	200	250	305	310	320	300	330	160	170	180	150	200	160	180	190	150	200	250	270	280	230	290
3	110	120	130	90	150	160	170	180	130	200	210	280	290	260	300	110	120	130	100	150	200	210	230	160	250	150	170	180	140	200
Component 3																														
1	210	230	250	200	300	80	90	100	60	120	160	180	200	140	210	200	210	220	180	230	260	280	290	240	300	120	130	140	100	150
2	150	170	190	120	200	70	80	90	50	100	150	160	170	130	180	110	150	200	100	210	270	290	300	250	310	130	150	170	120	180
3	180	200	220	160	250	100	110	130	70	150	120	130	150	110	90	120	130	150	90	180	220	250	270	200	280	140	150	160	115	170

Table 5 Triangular intuitionistic fuzzy capacity

TIFNC	a_1	a_2	a_3	a'_1	a'_3	a_1	a_2	a_3	a'_1	a'_3	a_1	a_2	a_3	a'_1	a'_3
Stage	Period 1					Period 2					Period 3				
Plant1	150	160	170	130	180	310	320	350	300	380	270	280	290	250	300
Plant2	160	170	180	150	200	300	310	380	350	400	250	260	270	230	280
	Period 4					Period 5					Period 6				
Plant1	100	110	120	90	130	120	130	140	100	150	370	380	390	360	400
Plant2	140	150	170	130	180	150	170	180	140	190	410	420	430	400	450
	Period 1					Period 2					Period 3				
Retailer1	160	170	180	150	190	140	160	170	130	180	350	370	380	330	390
Retailer2	150	160	170	130	180	80	900	100	70	110	270	280	290	260	300
Retailer3	120	130	140	110	150	100	110	130	80	150	250	260	280	220	290
	Period 4					Period 5					Period 6				
Retailer1	250	260	270	240	280	230	270	280	200	300	230	260	270	210	280
Retailer2	160	170	180	130	190	190	200	210	180	220	220	230	240	200	250
Retailer3	200	220	230	180	250	210	220	230	200	240	260	280	300	240	310
	Period 1					Period 2					Period 3				
Customer1	200	210	220	190	230	260	270	280	250	290	370	380	400	350	410
Customer2	170	180	190	160	200	210	220	230	200	240	400	410	420	380	440
Customer3	120	130	140	110	150	270	280	290	250	300	370	380	390	360	400
Customer4	120	140	150	100	170	310	330	340	300	360	220	230	250	200	290
	Period 4					Period 5					Period 6				
Customer1	260	270	280	230	290	340	350	360	330	370	230	240	250	220	300
Customer2	210	240	250	200	260	350	370	380	340	390	200	220	230	200	250
Customer3	150	170	200	220	210	360	370	380	350	400	240	250	260	230	270
Customer4	230	240	250	210	280	420	430	440	410	450	230	240	250	210	260

5. Conclusion

Developing countries are striving to fight poverty and achieve sustainable development goals to improve the masses. In the current era, effective management of supply chain networks is imperative for reducing costs and maximizing optimization, thus contributing to the achievement of human capital development. This study chooses closed-loop supply chain (CLSC) networks for various industrial processes, as it integrates forward and backward logistics. The study relies on the triangular intuitionistic fuzzy number model to improve the output of CLSC networks in terms of reduced costs. This study contributes to the existing literature by using the chosen closed-loop supply chain model that comprehensively discusses forward and backward logistics in a systematic manner to address pricing issues more effectively under uncertain circumstances. Second, the employed method of triangular intuitionistic fuzzy numbers helped us to deal with a large dataset in a systematic and coordinated fashion, thus producing the desired results. Accounting for the catastrophes of Covid-19, and the ongoing financial turmoil in developing countries, the usage and implementation of CLSC networks alongside the employment of triangular intuitionistic fuzzy numbers for optimization of the linear programming model will effectively improve the efficiency of various supply chain networks, thus adding to human evolution. Moreover, the enhancement in software solutions would lead to more sustainable and efficient findings for further research.

References

- [1] Zhang, H., Ren, Y., Sui, Y., Qi, J., Wei, F. (2020). Recycle of industrial waste: A new method of applying the paint residue to supercapacitors, *Journal of Materials Science: Materials in Electronics*, Vol. 31, 274-285, doi: [10.1007/s10854-019-02488-2](https://doi.org/10.1007/s10854-019-02488-2).
- [2] Rubinos, D.A., Spagnoli, G. (2018). Utilization of waste products as alternative landfill liner and cover materials– A critical review, *Critical Reviews in Environmental Science and Technology*, Vol. 48, No. 4, 376-438, doi: [10.1080/10643389.2018.1461495](https://doi.org/10.1080/10643389.2018.1461495).
- [3] Wu, J., Zhu, Q., Chu, J., Liang, L. (2015). Two-stage network structures with undesirable intermediate outputs reused: A DEA based approach, *Computational Economics*, Vol. 46, 455-477, doi: [10.1007/s10614-015-9498-3](https://doi.org/10.1007/s10614-015-9498-3).
- [4] Sarkar, B., Ullah, M., Sarkar, M. (2022). Environmental and economic sustainability through innovative green products by remanufacturing, *Journal of Cleaner Production*, Vol. 332, Article No. 129813, doi: [10.1016/j.jclepro.2021.129813](https://doi.org/10.1016/j.jclepro.2021.129813).
- [5] Savaskan, R.C., Bhattacharya, S., Van Wassenhove, L.N. (2004). Closed-loop supply chain models with product remanufacturing, *Management Science*, Vol. 50, No. 2, 239-252, doi: [10.1287/mnsc.1030.0186](https://doi.org/10.1287/mnsc.1030.0186).

- [5] Hugos, M. (2018). *Essentials of supply chain management*, Fourth edition, John Wiley & Sons, Hoboken, New Jersey, USA, doi: [10.1002/9781119464495](https://doi.org/10.1002/9781119464495).
- [7] Özceylan, E., Paksoy, T. (2013). A mixed integer programming model for a closed-loop supply-chain network, *International Journal of Production Research*, Vol. 5, No. 3, 718-734, doi: [10.1080/00207543.2012.661090](https://doi.org/10.1080/00207543.2012.661090).
- [8] Aleksić, A., Runić Ristić, M., Komatina, N., Tadić, D. (2019). Advanced risk assessment in reverse supply chain processes: A case study in Republic of Serbia, *Advances in Production Engineering & Management*, Vol. 14, No. 4, 421-434, doi: [10.14743/apem2019.4.338](https://doi.org/10.14743/apem2019.4.338).
- [9] Jindal, A., Sangwan, K.S. (2014). Closed loop supply chain network design and optimisation using fuzzy mixed integer linear programming model, *International Journal of Production Research*, Vol. 52, No. 14, 4156-4173, doi: [10.1080/00207543.2013.861948](https://doi.org/10.1080/00207543.2013.861948).
- [10] Garcia, D.J., You, F. (2015). Supply chain design and optimization: Challenges and opportunities, *Computers & Chemical Engineering*, Vol. 81, 153-170, doi: [10.1016/j.compchemeng.2015.03.015](https://doi.org/10.1016/j.compchemeng.2015.03.015).
- [11] Fang, I.W., Lin, W.-T. (2021). A multi-objective optimal decision model for a green closed-loop supply chain under uncertainty: A real industrial case study, *Advances in Production Engineering & Management*, Vol. 16, No. 2, 161-172, doi: [10.14743/apem2021.2.391](https://doi.org/10.14743/apem2021.2.391).
- [12] Özceylan, E., Paksoy, T. (2013). Fuzzy multi-objective linear programming approach for optimising a closed-loop supply chain network, *International Journal of Production Research*, Vol. 51, No. 8, 2443-2461, doi: [10.1080/00207543.2012.740579](https://doi.org/10.1080/00207543.2012.740579).
- [13] Liu, Z., Li, K.W., Li, B.-Y., Huang, J., Tang, J. (2019). Impact of product-design strategies on the operations of a closed-loop supply chain, *Transportation Research Part E: Logistics and Transportation Review*, Vol. 124, 75-91, doi: [10.1016/j.tre.2019.02.007](https://doi.org/10.1016/j.tre.2019.02.007).
- [14] Tsao, Y.-C., Thanh, V.-V., Lu, J.-C., Yu, V. (2018). Designing sustainable supply chain networks under uncertain environments: Fuzzy multi-objective programming, *Journal of Cleaner Production*, Vol. 174, 1550-1565, doi: [10.1016/j.jclepro.2017.10.272](https://doi.org/10.1016/j.jclepro.2017.10.272).
- [15] Govindan, K., Darbari, J.D., Agarwal, V., Jha, P.C. (2017). Fuzzy multi-objective approach for optimal selection of suppliers and transportation decisions in an eco-efficient closed loop supply chain network, *Journal of Cleaner Production*, Vol. 165, 1598-1619, doi: [10.1016/j.jclepro.2017.06.180](https://doi.org/10.1016/j.jclepro.2017.06.180).
- [16] Duan, W., Ma, H., Xu, D.S. (2021). Analysis of the impact of COVID-19 on the coupling of the material flow and capital flow in a closed-loop supply chain, *Advances in Production Engineering & Management*, Vol. 16, No. 1, 5-22, doi: [10.14743/apem2021.1.381](https://doi.org/10.14743/apem2021.1.381).
- [17] Zhou, L., Xie, J., Gu, X., Lin, Y., Ieromonachou, P., Zhang, X. (2016). Forecasting return of used products for remanufacturing using Graphical Evaluation and Review Technique (GERT), *International Journal of Production Economics*, Vol. 181, Part B, 315-324, doi: [10.1016/j.ijpe.2016.04.016](https://doi.org/10.1016/j.ijpe.2016.04.016).
- [18] Zadeh, L.A. (1965). Fuzzy sets, *Information and Control*, Vol. 8, No. 3, 338-353, doi: [10.1016/S0019-9958\(65\)90241-X](https://doi.org/10.1016/S0019-9958(65)90241-X).
- [19] Atanassov, K.T. (1986). Intuitionistic fuzzy sets, *Fuzzy Sets and Systems*, Vol. 20, No. 1, 87-96, doi: [10.1016/S0165-0114\(86\)80034-3](https://doi.org/10.1016/S0165-0114(86)80034-3).
- [20] Zimmermann, H.-J. (1975). Description and optimization of fuzzy systems, *International Journal of General Systems*, Vol. 2, No. 1, 209-215, doi: [10.1080/03081077508960870](https://doi.org/10.1080/03081077508960870).
- [21] Ghanbari, R., Ghorbani-Moghadam, K., Mahdavi-Amiri, N., De Baets, B. (2020). Fuzzy linear programming problems: Models and solutions, *Soft Computing*, Vol. 24, 10043-10073, doi: [10.1007/s00500-019-04519-w](https://doi.org/10.1007/s00500-019-04519-w).
- [22] Seikh, M.R., Nayak, P.K., Pal, M. (2012). Generalized triangular fuzzy numbers in intuitionistic fuzzy environment, *International Journal of Engineering Research and Development*, Vol. 5, No. 1, 8-13.
- [23] Fullér, R. (1991). On product-sum of triangular fuzzy number, *Fuzzy Sets and Systems*, Vol. 41, No. 1, 83-87, doi: [10.1016/0165-0114\(91\)90158-M](https://doi.org/10.1016/0165-0114(91)90158-M).
- [24] Shaw, A.K., Roy, T.K. (2012). Some arithmetic operations on triangular intuitionistic fuzzy number and its application on reliability evaluation, *International Journal of Fuzzy Mathematics and Systems*, Vol. 2, No. 4, 363-382.
- [25] Eiselt, H.A., Sandblom, C.-L. (2007). *Linear programming and its applications*, Springer-Verlag, Berlin, Germany, doi: [10.1007/978-3-540-73671-4](https://doi.org/10.1007/978-3-540-73671-4).
- [26] Chanas, S. (1989). Fuzzy programming in multiobjective linear programming – A parametric approach, *Fuzzy Sets and Systems*, Vol. 29, No. 3, 303-313, doi: [10.1016/0165-0114\(89\)90042-0](https://doi.org/10.1016/0165-0114(89)90042-0).
- [27] Zimmermann, H.-J. (1978). Fuzzy programming and linear programming with several objective functions, *Fuzzy Sets and Systems*, Vol. 1, No. 1, 45-55, doi: [10.1016/0165-0114\(78\)90031-3](https://doi.org/10.1016/0165-0114(78)90031-3).
- [28] Schultmann, F., Zumkeller, M., Rentz, O. (2006). Modeling reverse logistic tasks within closed-loop supply chains: An example from the automotive industry, *European Journal of Operational Research*, Vol. 171, No. 3, 1033-1050, doi: [10.1016/j.ejor.2005.01.016](https://doi.org/10.1016/j.ejor.2005.01.016).

Appendix A

List of abbreviations

SC	Supply chain
RSC	Reverse supply chain
CLSC	Closed-loop supply chain
IFS	Intuitionistic fuzzy set
ELV	End of life vehicle
IFS	Intuitionistic fuzzy

Calendar of events

- 16th International Conference on Micromachining Technology, October 17-18, 2022, Dubai, United Arab Emirates.
- 36th Annual European Simulation and Modelling Conference, October 26-28, 2022, Porto, Portugal.
- 33rd DAAAM International Symposium, Virtual Online Edition, hosted by Vienna University of Technology, October 27-28, 2022, Vienna, Austria.
- 7th International Conference of Computational Methods in Engineering Science, November 24-26, 2022, Zamosc, Poland.
- 14th International Conference on Mechatronics and Manufacturing, February 10-12, 2023, Royal Princess Larn Luang, Bangkok, Thailand.
- 7th International Conference on Material Engineering and Manufacturing, April 7-10, 2023, Chiba University, Japan.
- 51th North American Manufacturing Research Conference, June 12-16, 2023, Rutgers University, New Brunswick, New Jersey, USA.

Notes for contributors

General

Articles submitted to the *APEM journal* should be original and unpublished contributions and should not be under consideration for any other publication at the same time. Manuscript should be written in English. Responsibility for the contents of the paper rests upon the authors and not upon the editors or the publisher. The content from published paper in the *APEM journal* may be used under the terms of the Creative Commons Attribution 4.0 International Licence (CC BY 4.0). For most up-to-date information please see the APEM journal homepage apem-journal.org.

Submission of papers

A submission must include the corresponding author's complete name, affiliation, address, phone and fax numbers, and e-mail address. All papers for consideration by *Advances in Production Engineering & Management* should be submitted by e-mail to the journal Editor-in-Chief:

Miran Brezocnik, Editor-in-Chief
UNIVERSITY OF MARIBOR
Faculty of Mechanical Engineering
Chair of Production Engineering
Smetanova ulica 17, SI – 2000 Maribor
Slovenia, European Union
E-mail: editor@apem-journal.org

Manuscript preparation

Manuscript should be prepared in *Microsoft Word 2010* (or higher version) word processor. *Word .docx* format is required. Papers on A4 format, single-spaced, typed in one column, using body text font size of 11 pt, should not exceed 12 pages, including abstract, keywords, body text, figures, tables, acknowledgements (if any), references, and appendices (if any). The title of the paper, authors' names, affiliations and headings of the body text should be in *Calibri* font. Body text, figures and tables captions have to be written in *Cambria* font. Mathematical equations and expressions must be set in *Microsoft Word Equation Editor* and written in *Cambria Math* font. For detail instructions on manuscript preparation please see instruction for authors in the *APEM journal* homepage apem-journal.org.

The review process

Every manuscript submitted for possible publication in the *APEM journal* is first briefly reviewed by the editor for general suitability for the journal. Notification of successful submission is sent. After initial screening, and checking by a special plagiarism detection tool, the manuscript is passed on to at least two referees. A double-blind peer review process ensures the content's validity and relevance. Optionally, authors are invited to suggest up to three well-respected experts in the field discussed in the article who might act as reviewers. The review process can take up to eight weeks on average. Based on the comments of the referees, the editor will take a decision about the paper. The following decisions can be made: accepting the paper, reconsidering the paper after changes, or rejecting the paper. Accepted papers may not be offered elsewhere for publication. The editor may, in some circumstances, vary this process at his discretion.

Proofs

Proofs will be sent to the corresponding author and should be returned within 3 days of receipt. Corrections should be restricted to typesetting errors and minor changes.

Offprints

An e-offprint, i.e., a PDF version of the published article, will be sent by e-mail to the corresponding author. Additionally, one complete copy of the journal will be sent free of charge to the corresponding author of the published article.

APEM

journal

Advances in Production Engineering & Management

Chair of Production Engineering (CPE)
University of Maribor
APEM homepage: apem-journal.org

Volume 17 | Number 3 | September 2022 | pp 259-396

Contents

Scope and topics	262
Financing and information sharing in capital-constrained supply chain Duan, H.W.; Wang, M.T.; Ye, Y.S.	263
Effect of printing parameters on the mechanical behaviour of the thermoplastic polymer processed by FDM technique: A research review Tripathy, C.R.; Sharma, R.K.; Rattan, V.K.	279
Evolutionary game analysis of company collaborative strategy in cloud manufacturing platform environment Xiao, M.; Tian, Z.Y.	295
Development of a flexible tooling system for sheet metal bending Stefanovska, E.; Pepelnjak, T.	311
A new approach for quality prediction and control of multistage production and manufacturing process based on Big Data analysis and Neural Networks Tian, S.; Zhang, Z.; Xie, X.; Yu, C.	326
Experimental determination of influences on a gauge block's stack length Lipus, L.C.; Acko, B.; Tompa, J.	339
Last-mile delivery optimization considering the demand of market distribution methods: A case studies using Adaptive Large Neighborhood Search algorithm Huang, Q.L.; Wang, W.J.; Liang, X.J.; Xu, L.; Niu, X.Y.; Yang, X.Y.	350
Modelling surface roughness in finish turning as a function of cutting tool geometry using the response surface method, Gaussian process regression and decision tree regression Vukelic, D.; Simunovic, K.; Kanovic, Z.; Saric, T.; Doroslovacki, K.; Prica, M.; Simunovic, G.	367
Multi-objective Intuitionistic Fuzzy Linear Programming model for optimization of industrial closed-loop supply chain network Kousar, S.; Batool, M.; Kausar, N.; Pamucar, D.; Ozbilge, E.; Tantay, B.	381
Calendar of events	394
Notes for contributors	395

Published by CPE, University of Maribor



apem-journal.org